PROCESS, STRUCTURE AND ELECTROCHEMICAL PROPERTIES OF CARBON NANOTUBE CONTAINING FILMS AND FIBERS

A PhD Thesis
Presented to
The Academic Faculty

by

Sudhakar Jagannathan

In Partial Fulfillment
of the Requirements for the Degree
Doctor of Philosophy in the
School of Polymer Textile and Fiber Engineering

Georgia Institute of Technology
August 2009

PROCESS, STRUCTURE AND ELECTROCHEMICAL PROPERTIES OF CARBON NANOTUBE CONTAINING FILMS AND FIBERS

Approved by:

Dr. Satish Kumar, Advisor
School of Polymer, Textile and Fiber Engineering
Georgia Institute of Technology

Dr. Lawrence A. Bottomley
School of Chemistry and Biochemistry
Georgia Institute of Technology

Dr. W. Brent Carter
School of Materials Science and Engineering
Georgia Institute of Technology

Dr. Fred L. Cook
School of Polymer, Textile and Fiber Engineering
Georgia Institute of Technology

Dr. Gleb Yushin
School of Materials Science and Engineering
Georgia Institute of Technology

Date approved: April 30, 2009

Dedicated to

Lord Venkateswara

Hindu Temple of Atlanta
Riverdale, GA

ACKNOWLEDGEMENTS

The author wishes to express sincere gratitude to his advisor, Prof. Satish Kumar for his continuous encouragement, support, and guidance throughout the course of this project. The opportunity to access good research facilities in the group, to collaborate and participate in projects outside thesis, to publish research, review articles and theses, and involvement in writing proposal helped towards becoming an independent researcher. The gratitude is also extended to his committee advisors Professors Lawrence A. Bottomley, W. Brent Carter, Fred L. Cook, and Gleb Yushin for serving on the committee.

The author feels extremely blessed and grateful to be part of a wonderful academic family. The author thanks Dr. Chongfu Zhou and Dr. Tong Wang for teaching the basics of electrochemical capacitor project. The author also thanks Dr. Tao Liu and BeomJin Yoon for helpful discussions and input. The author is indebted to his colleagues Dr. HanGi Chae, Rahul Jain and YoungHo Choi for fiber spinning, Dr. Huina Guo for help with film preparation during initial stages, Dr. Marilyn Minus for transmission electron microscopy as well as for her comments on the thesis and Dr. Dhriti Nepal for critical reading of the thesis. Special thanks to Dr. Geon-woong Lee for involving him in polypropylene/carbon nanotube project and for sharing his knowledge on the subject. The author also wishes to thank his past and current group members Dr. Jing Liu, Dr. Asif Rasheed, Dr. Shanju Zhang, Dr. Jong Beom Baek, Hong Shen, Chandana Kolluru, Yaodong Liu, Ericka NJ Ford and Ian Winters, for their help and support at different stages of the project. The author thanks Prof. Z L Wang and Yolande Berta for use of electron microscopes, Prof. Meilin Liu's group for use of impedance spectrometer, and

Prof. Mohan Srinivasarao's group for use of optical microscope and Raman spectroscopy. This project submitted as thesis work for Doctor of Philosophy diploma was funded in part by Air force office of scientific research (AFOSR), Office of naval research (ONR) and Carbon Nanotechnologies Inc(CNI). The author thanks Dr. Charles Lee of AFOSR for his input.

The author thanks the staff of School of Polymer, Textile and Fiber Engineering, Angie Abbott, Michael Boyett, Dan Brooks, James Gallman, Hope Payne, Linda Roberson and others for their help throughout the project. Assistance from all professors, research staff and students of School of Polymer, Textile and Fiber engineering in completing this PhD work is gratefully acknowledged. The author also thanks his roommates and friends, Siva Venkatachalam, Vijayaraj Alagaraj, Narashiman Swaminathan, Wei Zhang, Murari Lal Gupta, Yi Liu, and Dinesh Bansal for their understanding during the stay in Atlanta, GA. Finally, the author wishes to thank his parents and sisters, for their patience and support during this study.

TABLE OF CONTENTS

LIST OF TABLES

LIST OF FIGURES

LIST OF SYMBOLS

Wh/Kg	Watt hour per kilogram
W/Kg	Watt per kilogram
Å	Angstrom
C	Capacitance
A	Area of plane capacitor plates
d	Distance between capacitor plates
ε	Dielectric medium
C_{sp}	Specific capacitance
C_{dl}	Double layer capacitance
C_{Φ}	Pseudocapacitance
I	Discharging current
V	Discharging voltage
t	Discharging time
m_A, m_B	Mass of electrodes
ED	Energy density
PD	Power density
CC	Constant current
CV	Cyclic voltammetry
ED_{max}	Maximum energy density
Δq	Extent of charge stored
ΔV	Change in potential
F/g	Farad per gram
V	Volts

mV/s	Milli volts per second
m^2/g	Square meter per gram
J/g	Joules per gram
$\mu F/cm^2$	Micro farad per square centimeter
mA	Milli amphere
mHz	Milli hertz
kHz	Kilo hertz
G, G', and D	Raman bands of carbon nanotubes
nm	Nanometer
μm	Micrometer
M	Molarity
Na	Sodium
K	Potassium
N_2	Nitrogen
C	Carbon

LIST OF ABBREVIATIONS

RuO_2	Ruthenium oxide
IrO_2	Iridium oxide
MnO_2	Manganese dioxide
CO_2	Carbon di oxide
KOH	Potassium hydroxide
HNO_3	Nitric acid
Fl	Fluorine
NH_3	Ammonia
RTIL	Room temperature ionic liquid
$BMIMBF_4$	1-butyl-3-methylimidazolium tetrafluoroborate
$BMIMPF_6$	1-butyl-3-methylimidazolium hexafluoro - phosphate
BMIMCl	1-butyl-3-methylimidazolium chloride
$EMIBF_4$	1-ethyl-3-methylimidazolium tetrafluoroborate
$TEABF_4$ or Et_4NBF_4	Tetraethylammonium tetrafluoroborate
AN	Acetonitrile
EC	Ethylene carbonate
PC	Propylene carbonate
NaOH	Sodium hydroxide
$ZnCl_2$	Zinc chloride
DMF	N, N- dimethylformamide
DMAc	N, N- dimethylacetamide
$LiClO_4$	Lithium perchlorate

H_2SO_4	Sulphuric acid
AgCl	Silver chloride
H_3PO_4	Phosphoric acid
NH_4Cl	Ammonium chloride
$FeCl_3$	Ferric chloride
$AlCl_3$	Aluminum chloride
$(NH_4)_2HPO_4$	Diammonium hydrogen phosphate
HCl	Hydrochloric acid
PAN	Polyacrylonitrile
SAN	Styrene-acrylonitrile
PMMA	Poly (methyl methacrylate)
Ppy	Polypyrrole
PTFE	Poly(tetrafluoroethylene)
PVDF	Poly (vinylidene fluoride)
RBM	Radial breathing mode
CNT	Carbon Nanotube
SWNT	Single Wall Carbon Nanotube
MWNT	Multi Wall Carbon Nanotube
SEM	Scanning Electron Microscopy
TEM	Transmission Electron Microscopy
DMA	Dynamic Mechanical Analysis
FT-IR	Fourier transform infrared spectroscopy
EDS	Energy dispersive system

WAXD	Wide-angle X-ray diffraction
SAXS	Small angle X-ray scattering
FWHM	Full width at half maximum of peak
BET	Brunauer, Emmett and Teller
DFT	Density Functional Theory
IUPAC	International union of pure and applied chemistry
SCFH	Standard cubic feet per hour

SUMMARY

The objective of this thesis is to study the effect of process conditions on structure and electrochemical properties of polyacrylonitrile (PAN)/carbon nanotube (CNT) composite film based electrodes developed for electrochemical capacitors. The process parameters like activation temperature, CNT loading in the composite films are varied to determine optimum process conditions for physical (CO_2) and chemical (KOH) activation methods. Films prepared by solution casting, fibers spun by solution spinning, and gel spinning and buckypapers made from SWNT and MWNT were used in this study. The PAN/CNT precursors are stabilized in air, carbonized in inert atmosphere (argon), and activated by physical (CO_2) and chemical (KOH) methods. The physical activation process is carried out by heat treating the carbon precursors in CO_2 atmosphere at activation temperatures. In the chemical activation process, stabilized carbon precursors are immersed in aqueous solutions of activating media (KOH), dried, and subsequently heat treated in an inert atmosphere at the activation temperature. The structure and morphology are probed using scanning electron microscopy, x-ray diffraction, and fourier transform infrared spectroscopy. The specific capacitance, power and energy density of the activated electrodes are evaluated with aqueous electrolytes (KOH) as well as organic electrolyte (ionic liquid in acetonitrile) in Cell Test. The surface area and pore size distribution of the activated composite electrodes are evaluated using nitrogen absorption. Specific capacitance dependence on factors such as surface area and pore size distribution are studied.

Carbon nanotube containing electrode is developed with high specific capacitance, energy density and power density. The process conditions for physical and chemical activation processes were varied and conditions for achieving superior electrochemical properties, surface area and controlled pore size were determined. A maximum specific capacitance of 300 F/g in KOH electrolyte and maximum energy density of 22 wh/kg in ionic liquid has been achieved. BET surface areas in excess of 2500 m^2/g with controlled pore sizes in 1 - 5 nm range has been attained in this work. The specific capacitances of physically and chemically activated samples have direct positive correlation to micropore volume.

Chapter 1

INTRODUCTION

1.1 History of Electrochemical capacitors

The ancient Greeks observed that pieces of amber attracted lighter objects when rubbed against each other due to static electric charge. The first device to store this static electric charge was the *Leyden jar* invented by a Dutch scientist, Pieter van Musschenbroek in 1745[1]. The original version of the Leyden jar called “condensor” used glass phial as a dielectric medium with acidic electrolyte as a conductor contacted by metal coating on either side of the glass as electrodes. Since then, the performance of a capacitor has progressed through generations of technological improvement with vital contributions from Luigi Galvani, Alessandro Volta, Michael Faraday and Joseph John Thompson in understanding the science behind the electrochemical charge storage device[1].

Batteries are another set of energy storage devices using chemical reactions at the electrodes to generate electric energy. The invention of a battery is attributed to Alessandro Volta in 1800[2]. He demonstrated an assembly with two dissimilar metal plates separated by a paper soaked in an aqueous solution that support transportation of ions. Further improvement in battery technology included use of multiple stacks of the cells, different combinations of electrodes, electrolytes, and separators[2].

The devices which store energy within the electrochemical double-layer at the electrode - electrolyte interface are known as “electrochemical double layer capacitors”, “supercapacitors” or “ultracapacitors”. The first claim for a practical use of

electrochemical capacitor was made by H. E. Becker of General Electric Corporation in 1957[3]. The patent granted to him described use of high surface area porous carbon electrode with an aqueous electrolyte (Figure 1.1). Though the electrochemical capacitor developed showed an exceptionally high capacitance, the mechanism of charge storage was not well understood at that time. The first commercial electrochemical charge storage device was patented by R. Rightmire of the Standard Oil Company, Cleveland in 1966[4]. This patent used porous carbon electrode in combination with non-aqueous electrolyte to achieve a wider operating voltage due to improved decomposition voltage of tetraalkyl ammonium salts.

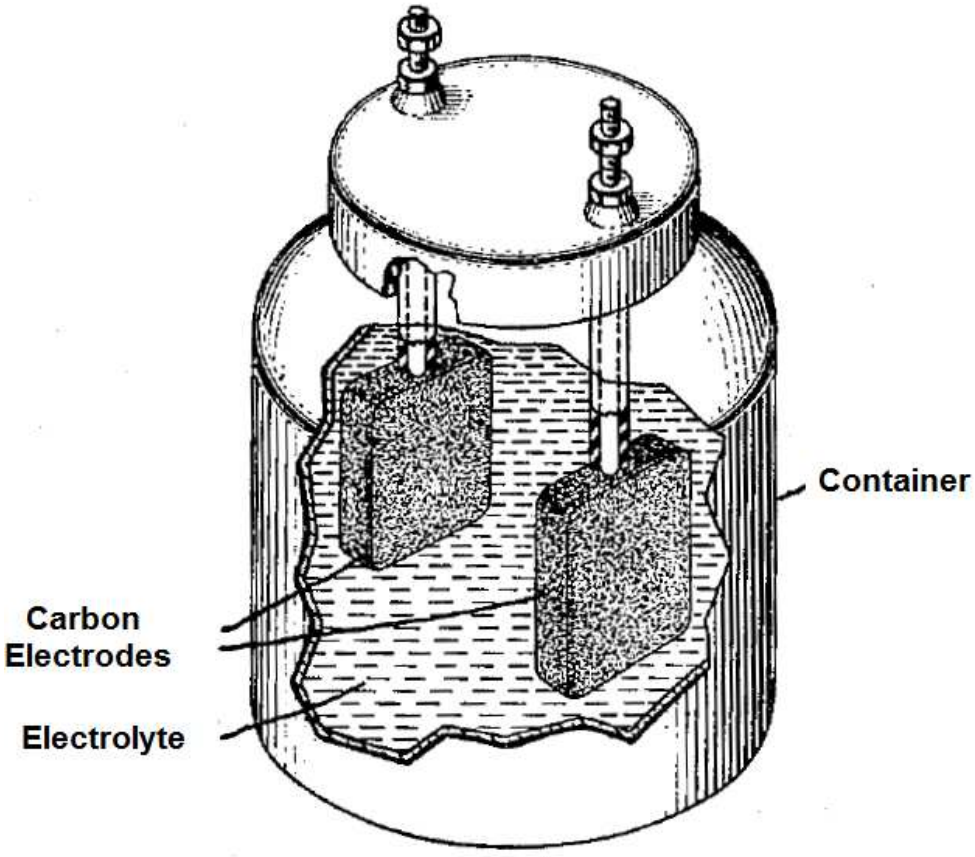

Figure 1.1. The first electrochemical capacitor patented by General Electric (from reference[3]).

The first non-carbon electrode material, ruthenium dioxide proposed by S. Trasatti[5] lead to understanding of the concept of "pseudocapacitance" by later researchers. The continuous oxidation or reduction of Ru_2O coupled with double layer capacitance resulted in high capacitance values. The voltage dependence of the electrochemical reaction of transition metal oxides like Ru_2O, TiO_2 and IrO_2 are further explored by Conway et al.[6, 7]. The high surface area carbon (1000 – 2000 m^2/g) based electrodes or the solid state transition metal oxide led to the commercialization of the energy storage devices by Matsushita Electric Industrial Co. (Japan) called power capacitors with power densities 200 – 300 W/Kg in 1980's[1]. The US Department of Energy initiated an ultracapacitor development program in 1989, where short (2003) as well as long term goals of 5 and 15 Wh/Kg of specific energy and 500 and 1600 W/Kg of specific power respectively were defined for further improvement in the field[8]. Maxwell Laboratories in cooperation with Auburn University developed carbon fiber based composite electrodes with high electrical conductivity in 1991. Maxwell continued active research in advanced electrochemical capacitors for electric vehicle with projected energy density of 5.5 Wh/Kg and power density of 20 W/Kg in 1991. Tanahashi (1991) described direct use of carbon fibers for electrode of electrochemical capacitor by plasma spraying of aluminum current collector onto surface of compacted fiber matrix[9]. The companies that are actively involved in developing electrochemical capacitors around the world for applications such as electric and fuel cell vehicles for improving acceleration and recovering braking energy, backup power supply for memories, microcomputers, system boards, and others are given in Table 1.1.

Table 1.1. The current (as of January 2009) companies that are actively involved in electrochemical energy storage device design and manufacture [1, 10-12].*

	United States/Canada		Japan
1	Evans Capacitor Company (www.evanscap.com)	15	Nippon Chemi-con Corporation (NCC) (www.chemi-con.co.jp)
2	Maxwell Technologies Inc (www.maxwell.com)	16	Shizuki Electric Co. (www.shizuki.co.jp)
3	Cooper Bussman Electronic Technologies(CET) (www.bussmann.com)	17	Japan Radio Co. (www.jrc.co.jp)
4	Axion Power International (API) (www.axionpower.com)	18	Power Systems Co. Ltd (www.powersystems.co.jp)
5	AVX Corporation (www.avx.com)	19	NEC – Tokin Corporation (www.nec-tokin.com)
6	Kanthal Globar (www.globar.com)	20	Advanced Capacitor Technologies Inc (www.act.jp)
7	Intertechpira (www.intertechpira.com)	21	Asahi Glass Company/Elna Capacitors (www.agc.co.jp)
8	Redox Engineering LLC (www.supercapseminar.com)	22	Matsushita Electric Industrial Co. Ltd (www.panasonic.net)
9	Kold Ban International, Ltd (www.koldban.com)		
10	Tavrima Canada Ltd (www.tavrima.com)		
	Europe/Russia		**Korea**
11	ESMA Company (Russia) (www.esma-cap.com)	23	Nesscap Co. Ltd (www.nesscap.com)
12	Elit Co (Russia) (www.elit-cap.com)		
13	EPCOS (Germany) (www.epcos.com)		**Australia**
14	Skeleton Technologies AG (Switzerland) (www.skeletonnanolab.com)	24	CAP – XX Inc. (www.cap-xx.com)

*Individual websites accessed on 01/20/2009.

1.2 Definitions, Principle and working of electrochemical capacitors

Electrochemical capacitors or supercapacitors store the energy within the electrochemical double-layer at the electrode-electrolyte interface[1, 8]. The performance of an energy storage device is defined by two most important parameters. The first is *energy density*, which characterizes the energy that can be stored by unit weight or per unit volume of the device, and the second is *power density*, the rate at which the energy is delivered for a unit weight or unit volume of the electrochemical device. Electrochemical capacitors have higher energy density than the regular capacitors and higher power density than the conventional batteries. In addition, since little or no redox reaction occurs on the electrode of a carbon based supercapacitor, the cycle life for a supercapacitor can be greater than 10^5 compared to battery's cycle life of 10 to 1000[13]. Hence, electrochemical capacitors combine the advantages of both regular capacitors and batteries without compromising the cycle life of energy storage device as given in Figure 1.2.

A schematic of electrochemical double layer capacitor is given in Figure 1.3[14]. The energy is stored within the electrochemical double-layer at the electrode-electrolyte interface using the charge separation mechanism. The electrochemical capacitor has two electrodes made from porous, high surface area materials immersed in an electrolyte and separated by a semi permeable separator which permeable to only ions in electrolyte. When voltage is applied, there will be a charge on the electrode and electrolyte due to excess or deficiency of electrons. This charge resides in a very thin layer (<0.1 Å) on the surface. The charge in solution is an excess of either cations or anions near the

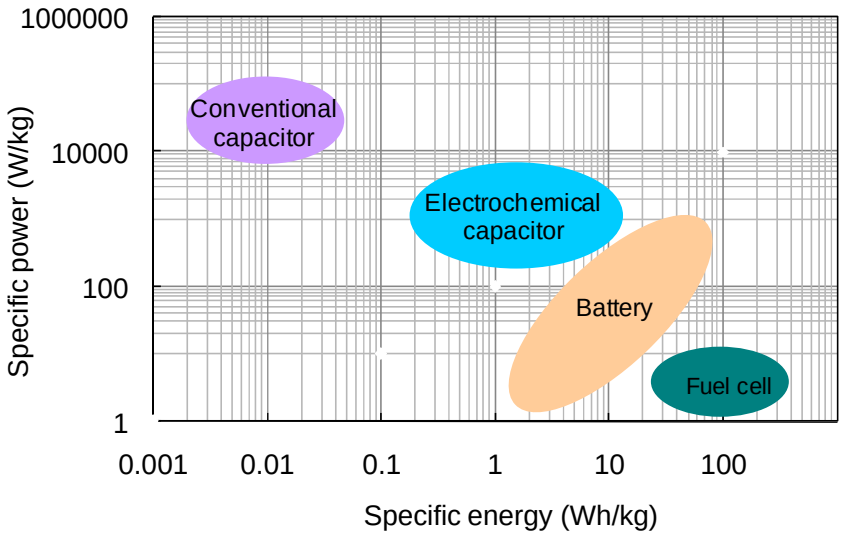

Figure 1.2 A comparison of important properties for a typical fuel cell, battery, capacitors and electrochemical capacitor[15].

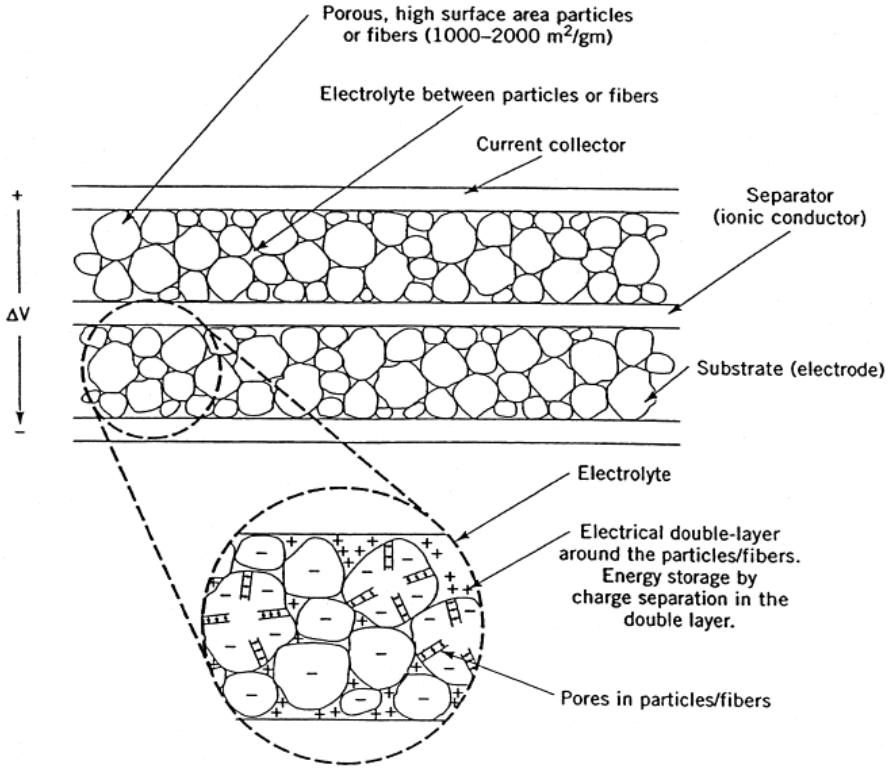

Figure 1.3 Schematic of electrochemical double layer capacitor and mechanism of charge storage[14].

electrode surface. A whole array of oppositely charged ions exists at the electrode-electrolyte interface and hence the electrochemical capacitor is also called double layer capacitor.

The capacitance (C) in a plane capacitor with a pair of plates of equal area, *A*, in parallel configuration and separated by a distance *d*, with dielectric constant of the medium, ε, is given by equation 1.1[1]

$$C = \frac{A\varepsilon}{4\pi d} \qquad (1.1)$$

The specific capacitance (C_{sp}) (capacitance per unit mass of a single electrode) from the electrochemical double layer capacitor was calculated as a function of discharging voltage using the formula[1, 8, 16] in equation 1.2

$$C_{sp} = \frac{I}{dV(t)/dt}\left(\frac{1}{m_A} + \frac{1}{m_B}\right) \qquad (1.2)$$

Where, m_A and m_B are the masses of the two electrodes and *I*, *V*(*t*), and *t* are the discharging current, voltage and time respectively. The energy density (ED) and the power density (PD) delivered by the electrodes of the supercapacitor testing cell at time t are calculated by the following equations:

$$ED = \int_{t=t_1}^{t} IV(t)dt \qquad (1.3)$$

$$PD = IV(t) \qquad (1.4)$$

The energy storage mechanism in electrical double layer capacitor is due to charge accumulation in the electric double layer at the interface between the surface of a conductor and an electrolyte solution. It creates two separate layers of capacitive storage with the maximum energy density stored in the capacitor given by equation 1.5 [1].

$$ED_{\max} = \frac{1}{2} C_{sp} V^2 \qquad (1.5)$$

where C_{sp} is the specific capacitance, and V is voltage.

The capacitance value measured from the electrochemical capacitor can have contributions from (1) the separation of charge in the double layer, and from (2) capacitance associated with chemical reactions on the surface. There is no definitive method available at this time to quantify the contribution of double layer capacitance and capacitance due to chemical reactions to overall specific capacitance. The capacitance from the faradaic process (or redox chemical reactions) is referred to as pseudocapacitance. The pseudocapacitance can be calculated by using the extent of charge stored (Δq) and the change of the potential (ΔV) using the relationship given by equation 1.6.

$$C = \frac{\partial(\Delta q)}{\partial(\Delta V)} \qquad (1.6)$$

1.3 Electrochemical capacitor construction and design

The construction of supercapacitor is similar to a battery with two electrodes made from porous high surface area materials immersed in an electrolyte and separated by a semi permeable separator. For superior electrochemical capacitor performance, the electrode should have high electrical conductivity, high surface area for charge accumulation, sufficiently large pore diameter, and good pore connectivity for the electrolyte wetting and rapid ionic motion[17]. A variety of electrode materials and designs have been studied for electrochemical capacitors. The commonly used electrode materials, electrolytes, and electrochemical capacitor designs are briefly discussed below.

1.3.1 Electrode materials

1.3.1.1 Metal oxides

Conducting metal oxides like RuO_2[5, 7], IrO_2[18, 19], and MnO_2[20, 21] are used as electrode materials in electrochemical capacitors due to high specific capacitance (up to 720 F/g) in combination with low resistance. The cyclic voltammograms of RuO_2 or IrO_2 show reversible rectangular shape with higher specific capacitance due to a series of reversible electrochemical reactions[22].

Several modifications of metal oxides were studied with an aim to reduce cost of electrode. Miller[23] used chemical vapor impregnation of ruthenium into carbon aerogel to increase specific capacitance from 95 F/g for untreated aerogel to 200 F/g for ruthenium coated sample. Similar coating was performed on carbon nanotubes[24], TiO_2[25] and other materials to increase specific capacitance. Another approach was partial substitution of ruthenium in an oxide structure like perovskites ($ARuO_3$) to exhibit pseudocapacitance behavior[26]. Other forms of metal compounds such as nitrides and carbides were also investigated for electrochemical capacitors [27, 28]. The main disadvantages of this kind of electrochemical capacitor are its cost and restriction to aqueous electrolytes with a maximum cell voltage of 1 V. Considerable research on these materials has been conducted in military and other applications where cost is a lesser concern than performance. Even with minimal use of metal oxide in other electrode materials, they are far from being used commercially.

1.3.1.2 Conducting polymers

Conducting polymer electrodes including polyaniline[29, 30], polypyrrole[31-35], and polythiophene[36, 37] with high energy density and power density have also been

reported. The electrode material undergoes doping/de-doping process to deliver charge. The charge storage occurs by the doping process where ions in the electrolyte are transferred to the polymer backbone. The ions are released back into the solution during the de-doping process. This charge storage in bulk volume of sample can result in capability to store high specific capacitances. However, long-term performance and dimensional stability has been an issue with this class of electrode materials. The electrochemical properties of conducting polymer based electrodes aniline, chloro-aniline, and aryl suphonic acid treated CNTs were evaluated and are presented in Appendix A.

1.3.1.3 Carbon

Different forms of carbon material have been extensively studied for use as the supercapacitor electrode material due to their high surface area, easy processability, and high chemical stability. The commonly used precursors for activated carbon include polyacrylonitrile[38-42], phenolic resin[42, 43], petroleum coke[44, 45], anthracite[46, 47], pitch[48], coal[49-52], carbon nanotube/nanofiber[53, 54], and other natural fibers/shells[55-58]. High surface area and porous carbon electrodes can be achieved by carbonization, physical (using steam, CO_2) and chemical (using KOH, HNO_3, Fl, NH_3) activation, phase separation, gelation, or replication using templates[1, 35, 59-61]. Further discussion on carbon based electrodes from PAN and CNT precursors are presented in section 1.3.4.

1.3.2 Electrolytes

The choice of electrolyte is important in determining the operating voltage of electrochemical devices. Energy density of a material, which is dependant on the voltage,

is determined by the type of electrolyte used. Power density of devices is dependent on the electrical conductivity of electrolyte used. Hence, choice of electrolyte used is an important factor in the resulting electrochemical properties. A wide range of electrolytes are used for electrochemical capacitors. The aqueous alkali/acid electrolytes like potassium hydroxide[62] and aqueous sulphuric acid[63] are commonly used in applications requiring voltage less than one volt. With room temperature ionic liquid (RTIL) electrolytes a high charging voltage (up to about 3V) can be used, which subsequently increases the energy density of the capacitor [64-66]. However, the mobility of the electrolyte ions in ionic liquid are restricted due to large ionic radii. For example, the ionic liquid used in this thesis, 1-butyl-3-methylimidazolium tetrafluoroborate ($BMIMBF_4$) have larger ionic radius ($BMIM^+$ - 3.39 Å and BF_4 - 2.29 Å)[67, 68] than aqueous KOH (ionic radius – K^+ - 1.38 Å and OH^- - 1.33 Å)[68]. The mobility of ionic liquids is improved when used as an electrolyte by dissolving in a non-aqueous solvent. Typical non-aqueous electrolyte consist of a quaternary ammonium salts and tetra alkyl imidazolium salts in non-aqueous solvents like acetonitrile (AN), ethylene carbonate (EC), and propylene carbonate (PC)[65, 66]. All solid electrochemical double layer capacitors using poly(vinyl alcohol) or polyethylene oxide electrodes were also investigated to eliminate flammability issues with organic electrolytes and for easier handling[69, 70].

1.3.3 Cell design

The cell configuration is an important factor in electrochemical capacitor to determine the performance of the active electrode material. For the same active electrode material and inactive component, the difference in design may result in different power density and

energy density for a packaged supercapacitor. The commercial electrochemical capacitors can have single/multi cell electrodes, monoblock[71, 72] and spiral-wound[73, 74] designs of multi-cell electrodes. In monoblock design as given in Figure 1.4, each cell consists of many positive and negative electrodes in parallel to increase the effective cross-sectional area of the electrode to greater than the geometric area of one electrode. The current collected from the multi-electrode plates is of primary concern in achieving a low cell resistance. In the spiral-wound design, the stacked electrode strips are rolled up in a cylindrical structure.

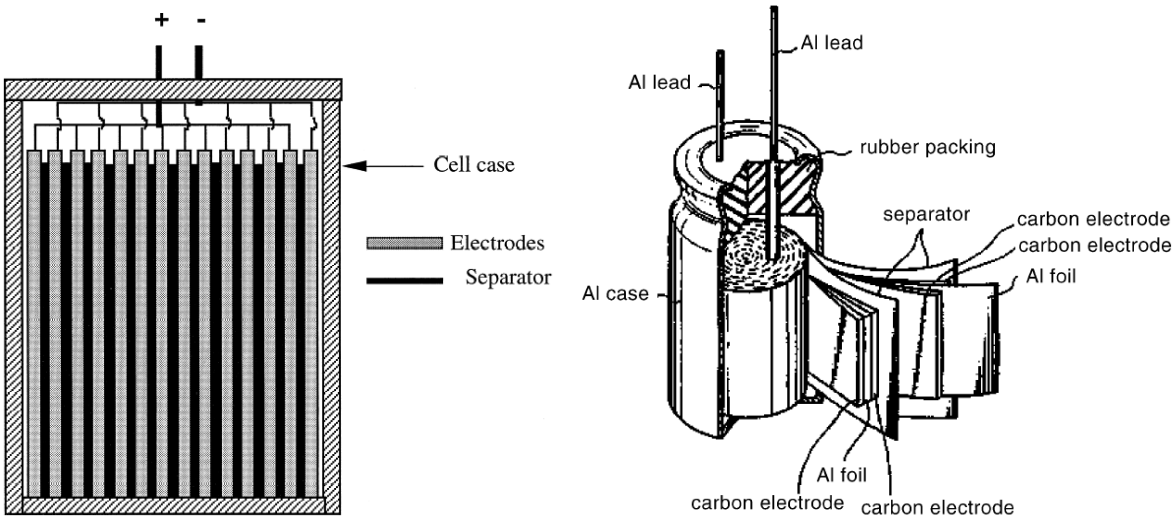

Figure 1.4. Schematic for mono-block and spiral wound electrochemical capacitor assembly[71, 73].

1.3.4 Polyacrylonitrile based electrodes

Polyacrylonitrile (PAN) based activated carbon materials are generally amorphous graphitic carbon consisting of mainly sp^2 hybridized carbon layers with different pore sizes resulting in high surface area and adsorption capacity. The production of activated carbon material involves three stages: (1) thermo-oxidative stabilization of PAN precursor in air or other oxidizing atmosphere, (2) carbonization of stabilized PAN

in an inert atmosphere, and (3) activation using gasifying agents or chemicals. The different reactions occurring during stabilization process include cyclization, dehydrogenation, aromatization, oxidation and cross-linking which can result in the formation of the conjugated ladder structure[75, 76]. The stabilized PAN precursor is heat treated in the process of carbonization in an inert atmosphere to achieve typically 95% carbon content. In carbonization process, the hydrogen groups present in PAN structure are mostly eliminated in the form of byproducts along with a little carbon to result in a graphite like carbon structure consisting of mainly pore sizes less than 2 nm (micro pores according to IUPAC classification). These micropores are widened during the activation process using gases (physical) or chemical activating agents. The activation processes are explained in detail in section 1.4.1.

Currently, most commercial high strength carbon fibers and porous activated carbon fibers use PAN as the precursor material. PAN having good interaction with CNTs is preferred precursor for carbon nanotube containing composites[77-80]. A number of studies has been reported on PAN/CNT films and fibers for variety of applications[16, 77-79, 81-88]. Fibers have been spun by conventional solution spinning[77, 78], gel spinning[79], as well as by electrospinning[82-84, 86]. PAN/CNT based carbon fiber containing 1 wt% CNT with respect to the weight of the polymer, can have 50% higher tensile strength than a carbon fiber processed without CNT[89]. These studies clearly suggest the potential of PAN/CNT system for making both structural as well as porous carbon materials for a variety of applications.

The literature summary of activation conditions and capacitance performance for PAN based precursors is given in Table 1.2. Physical activation of PAN/SWNT

Table 1.2. Summary of process conditions and properties for physical and chemical activation of PAN based precursor from literature as well as this work.

A. Physical activation

Report	Activation Temperature (°C)	Precursor	Activation Agent	BET Surface Area (m^2/g)	Specific Capacitance (F/g)
Kim[93]	800	PAN electrospun fiber	Steam	~ 1160	133
Frackowiak[95]	800	Templated PAN	CO_2	~800	160
Ryu[94]	860	PAN based carbon fiber	Steam	~ 860	-
Wang[92]	900	PAN/SAN film	CO_2	~730	~ 165
Wang[92]	900	PAN electrospun fiber	CO_2	~306	~ 210
Zhou[91]	900	PAN/SAN/ SWNT films	CO_2	~130	~ 110
Liu[16]	700	PAN/SWNT 60/40 films	CO_2	-	~ 380

B. Chemical activation

Report	M:C Ratio*/ Molarity/%	Precursor	Activation Agent	BET Surface Area (m^2/g)	Specific Capacitance (F/g)
Lee[96]	1-3:1	PAN fibers	KOH	~ 2500	-
Yue[42]	2:1	PAN coated fiber	$ZnCl_2$	~ 1600	-
Moon[97]	2 M	PAN fibers	KOH/ NaOH	~ 1200/750	-
Lee[39]	1-3 M	PAN fibers	KOH	~ 2300	~ 180
Kim[98]	1- 3 %	Electrospun PAN fiber mat	$ZnCl_2$	~ 550	~ 140
Im[99]	2-6/4-8 M	Electrospun PAN fiber mat	$ZnCl_2$/ KOH	~ 950/2400	-
Xu[100]	4:1	PAN fibers	NaOH	3291	371

* M is K, Na, Zn etc and C is carbon

composite film and electrospun fiber based electrochemical capacitor electrodes have been explored by our research group over the past decade [16, 90-92]. PAN/SWNT film containing 40 wt% SWNT formed bundled structure of porous carbon over SWNTs during CO_2 activation. This composite sample exhibited lower shrinkage than PAN during heat treatment, improved electrical conductivity and specific capacitance was as high as 380 F/g[16]. A sacrificial component of SAN (styrene-co-acrylonitrile) was introduced into PAN/SWNT film to form a ternary composite. On heat treatment in an inert atmosphere, SAN domains are removed to form pores with size ranging from 1-200 nm and the double layer capacity of 205 $\mu F/cm^2$ in aqueous KOH electrolyte[91]. PAN/SAN and PAN/SAN/SWNT composites were electospun into precursor fibers with diameters 100 - 400 nm for electrochemical capacitors. A specific capacitance value greater than 200 F/g with energy density up to 2.4 Wh/Kg and power density of 850 W/Kg was achieved[92].

Literature studies from other research groups on physically activated PAN based precursors report surface area of 800 – 1000 m^2/g and specific capacitance of 100 – 200 F/g consistent with results from our group. Kim et al.[93] and Ryu et al.[94] explored physical activation of electrospun PAN fibers using steam for producing activated carbon. A maximum surface area of 1160 m^2/g resulted in specific capacitance of 113 F/g. The physical activation being diffusion controlled process, results in larger pore size distributions with wider pores on the surface and smaller pores in the bulk. A pore size distribution of 2 – 100 nm for films and nano fibers was consistently reported for physically activated PAN based carbon.

For chemically activated samples, surface area approaching 2500 m^2/g is often reported. Y. J. Lee et al.[96] studied the effect of the amount of activating agent and heat treatment temperature on carbon yield, surface area and microstructure of activated PAN-based carbon fibers using KOH activating agent. Activation of PAN fibers at 800 ºC with K:C ratio of 1:1 showed a carbon yield of 36% with specific surface area of 2545 m^2/g. However, further increase in activation temperature or K:C ratio led to abrupt decrease in surface area.

S. Y. Moon et al.[97] developed PAN based activated carbon fibers for iodine adsorption. The samples activated using KOH/NaOH resulted in BET surface area of 2244 m^2/g with KOH and 1786 m^2/g with NaOH. Z. Yue et al.[42] reported the effect of activation temperature and $ZnCl_2$:C ratio for PAN based fibrous porous materials. A maximum specific capacitance of 371 F/g and BET surface area of 3271 m^2/g has been achieved for partially carbonized PAN fibers activated using NaOH[100]. However, to the best of our knowledge, there are no previous literature reports on chemical activation of solution spun PAN/CNT composites.

Kim et al.[101] used electrospun PAN/$ZnCl_2$ precursor based activated carbon for electrochemical capacitor. PAN and $ZnCl_2$ were directly dissolved in DMF to electrospin fibers from 200 to 350 nm diameter. Increase of salt concentration from 1 to 5 wt % increased the specific capacitance from 120 to 140 F/g[101]. Im[102] activated electrospun PAN fibers using $ZnCl_2$ and KOH salts for hydrogen storage. $ZnCl_2$ was directly added to PAN/DMF solution while KOH was incorporated into PAN nanofibers by the immersion method[102]. The surface area, pore volume and hydrogen adsorption capacity increased with increase of molarity of both the salts. KOH immersion method

showed higher surface area and pore volume than direct addition of $ZnCl_2$. However, nanofibers activated with 6M $ZnCl_2$ displayed higher hydrogen storage capability than samples activated with 8M KOH. The surface area differences between the physically and chemically activated current set of samples is consistent with the literature reports.

Attempts have been made to correlate the pore sizes in activated carbon to size of electrolyte ions. Extensive studies on the capacitance performance of porous electrodes show that electrolyte access to the smaller pores is limited by a cut-off pore size up to several nanometers (with typical aqueous electrolyte ion sizes less than 2 Å), depending on the electrolyte concentration and the applied voltage[39, 103, 104]. Only those pores larger than the cut-off pore size can be accessed by the electrolyte to form an electrical double layer. Table 1.3 summarizes capacitance data for other carbon materials with different pore size ranges. The smaller size pores thus lose their capacitance contribution at higher current density, resulting in lower capacitance. Pores with sizes (2-50 nm) were conventionally believed to impart maximum specific capacitance. However, there is a recent report of anomalous increase in specific capacitance for sub-nanometer pore size[105]. There is no systematic study in literature to understand the effect of pore sizes on electrochemical properties. This necessitates development of electrodes with controlled pore sizes at different ranges to comprehend the correlation between size of electrolyte ions to pore sizes in electrodes.

Table 1.3. Surface area and electrochemical capacitance performance of various other carbon materials with pore size in subnanometer, micro and meso pore range.

Report	Pore size	Carbon precursor	Electrolyte	BET Surface Area (m^2/g)	Specific Capacitance (F/g)
Chmiola[105]	< 1 nm	Chlorinated of carbide derived carbon	H_2SO_4	~ 1300	~ 140
Yamada[106]	< 2nm	Phenol formaldehyde based activated carbon	$LiClO_4$	~ 1302	~ 104
Lee[39]	< 2nm	PAN based carbon	KOH	~ 2312	~ 113
Fuertes[107]	2 – 10 nm	Polyfurfuryl alcohol based carbon	KOH	~ 1880	~ 200
Yamada[106]	2 – 50 nm	Phenol formaldehyde based activated carbon	LiClO4	~ 1455	~ 119
Morishita[108]	2 - 30 nm	Polyvinyl alcohol based activated carbon with magnesium acetate/citrate	H_2SO_4	~ 1900	> 300

1.3.5 Carbon nanotube based electrodes

CNTs have generated significant interest in energy storage applications due to hollow tubular and interconnected porous structures required for ion transport/storage, lower electrical resistance, high chemical stability, and possibility of controlling the structure at nano-scale. The carbon nanotubes are added with an aim to increase the rate of discharge by increasing the power density. Literature reports on CNT based electrodes for electrochemical capacitors show a specific capacitance of 15 – 55 F/g for untreated CNT buckypapers in aqueous electrolytes [35, 90, 109, 110] and 25 – 75 F/g in organic electrolytes [110-112] (Table 1.4). The CNTs were treated with NH_3 plasma[109], HNO_3[113, 114], HCl[112, 115] or functionalized with aryl sulphonic acid[35, 90] to increase the specific capacitance to 100 – 365 F/g by increasing the pseudocapacitance of the electrodes.

Sodium hydroxide and potassium hydroxide, among all chemical activating agents, are the widely reported for activation of CNT electrodes[116-118]. Jiang et

al.[118] reported increase in specific capacitance of carbon nanotubes from 25 to 50 F/g when activated with KOH at 850 ºC for 1 h with increase in specific capacitance and pore volume. Jiang et al.[117] also measured the effect of nitrogen flow rate on specific capacitance of KOH activated carbon nanotubes. The experiment with nitrogen flow rates varying form 0 – 1400 ml/min showed a maximum capacitance of 45 F/g for flow rate maintained at 400 ml/min. Similar observation was reported by Frackowiak et al. [116] where the specific capacitance increased from 10-15 F/g for untreated sample in 6M KOH, 1M H_2SO_4 and 1.4 M $TEABF_4$ in acetonitrile to 90 F/g in KOH, and up to 95 F/g

Table 1.4. Surface area and electrochemical capacitance performance of various other carbon materials with pore sizes in subnanometer, micro and meso pore range.

Report	CNT type	Carbon nanotube treatment	Electrolyte	BET Surface Area (m^2/g)	Specific Capacitance (F/g)
Yoon[109]	MWNT	As synthesized/NH_3 plasma treated	KOH	~ 10/87	~ 39/207
Zhang[110]	MWNT	Aligned/Entangled	$EMIBF_4$*	~ 111/283	~ 25/15
Shiraishi[115]	MWNT	As synthesized/HCl treated	Et_4NBF_4 **	~ 222/382	~ 24/15
Niu[113]	MWNT	HNO_3 treated	H_2SO_4	~ 430	113
Chen[114]	MWNT	HNO_3 treated	H_2SO_4	-	~ 365
Pan[119]	MWNT	Tube in Tube structure***	H_2SO_4	~ 500	~ 203
Futaba[111]	SWNT	Densely packed SWNT	Et_4NBF_4**	~ 1000	< 15
Shiraishi[112]	SWNT	HCl treated/Thermal oxidation at 225 ºC/5h	$LiClO_4$	~ 780	~ 60
Liu[120]	SWNT	Electrochemical treated with KOH	KOH	~ 110	~ 56
Zhou[35, 90]	SWNT	Untreated buckypaper	KOH	~ 540	~ 55
Zhou[35, 90]	SWNT	Untreated buckypaper	$BMIMBF_4$****	~ 540	~ 75
Zhou[35, 90]	SWNT	Aryl sulponic acid functionalized	$BMIMBF_4$****	~ 300	~ 105
Barisci[121]	SWNT	Untreated/ Annealed upto 1050 ºC	Ag/AgCl	~ 173/247	~ 36/14

* $EMIBF_4$ – 1-ethyl-3-methylimidazolium tetrafluoroborate
** Et_4NBF_4 -Tetraethylammonium tetrafluoroborate in propylene carbonate
*** Tube in tube structure – Templated MWNTs (300 nm) were pyrolysed in ethylene at 900 ºC to create tubular structures (30nm) inside CNTs.
**** $BMIMBF_4$ - 1-butyl-3-methylimidazolium tetrafluoroborate in Acetonitrile (1:1 ratio)

in H_2SO_4, 65 F/g in $TEABF_4$ on activation of MWNTs with 4:1 chemical ratio KOH at 800 ºC in nitrogen atmosphere.

The surface area and pore volumes achieved by CNT based electrodes are lower than other carbon based electrodes due to limited accessible pore volume in undamaged tubes and tube interstices. Even though the specific capacitances of pristine CNT electrodes are lower than 100 F/g to date, researchers continue to investigate their potential due to their excellent electrical conductivity increasing the power density and the possibility of storing higher energy in their hollow tubular structures.

1.4 Process methods

1.4.1 Carbon activation process

Activated carbon materials are widely used for different applications, including liquid/gas phase adsorptions[103, 122-124], gas, water or element purification[45, 56, 97], catalyst support[125-127], energy storage[1, 39, 43, 54, 57, 104, 128] and many other applications due to high surface area, pore structure and adsorption capacity[129-131]. The pore structure of activated carbon depends on the type of precursor, the kind of activating agent and process conditions. There are two general approaches utilized by researchers to modify micro porous carbon material to increase surface area and adsorption capacity: physical and chemical activation processes.

1.4.1.1 Physical activation process

The physical activation process usually involves three step processes: stabilization, carbonization, and activation as discussed for PAN based carbon precursors in section 1.3.4. Activation is an important step in creating porosity and modifying surface chemistry of the activated carbon. After activation, porous carbon with surface area as

high as 1000~3000 m^2/g can be obtained. The first approach is to make use of gasifying agents like CO_2 or water vapor (reactions given below). The process of these endothermic reactions occurring entirely in gas phase is known as thermal or physical activation.

$$C + CO_2 \rightarrow 2CO \qquad (1.7)$$

$$C + H_2O \rightarrow CO + H_2 \qquad (1.8)$$

The physical activation being diffusion controlled process, results in wide pore size distributions with wider pores on the surface and narrow pores in the bulk. A pore size distribution of 2 – 100 nm for films and nano fibers was consistently reported for physically activated PAN based activated carbons. The physical activation process is discussed in detail in previous theses from our research group[90, 92].

1.4.1.2 Chemical activation process

The chemical activation method using hydroxides, halides and acids is another approach. The chemical reaction between the activating agents like hydroxides and carbon play an important role in the development of porosity in activated carbon. Depletion of carbon molecules from the charred carbon network leads to increase of micro and meso pores. Several researchers have studied the interactions between alkaline hydroxide MOH (M- alkali groups like K, Na) with carbon material and proposed three possible chemical reactions.

$$6MOH + 2C \rightarrow 2M + 3H_2 + 2M_2CO_3 \qquad (1.9)$$

$$4MOH + 2CO_2 \rightarrow 2M_2CO_3 + 2H_2O \qquad (1.10)$$

$$4MOH + C \rightarrow 4M + CO_2 + 2H_2O \qquad (1.11)$$

Pore generation by gasification reactions listed above is one of the reasons for the high surface areas and porosities of activated carbons. An additional mechanism is proposed by the researchers to justify the development of highly porous structure. S. Y. Moon et al.[97] presume that the M^+ ions present in MOH intercalates between carbon layers causing the interlayer spacing to increase during chemical activation process. MOH changes into intermediate M_2O at the activation temperature and subsequently to metallic M^+ ions. The metallic M^+ ions intercalated into carbon layers are changed into M^+ vapors causing expansion of different layers in carbon fibers[52, 97, 132]. This random process of intercalation of metal ions and high temperature activation results in a porous structure and develops the high surface area required for the material in these applications. After washing the samples, excess M is eliminated leaving free interlayer space that contributes to the porosity of the product.

The commonly used chemically activating agents include KOH[41, 46, 53, 54, 97] , NaOH[46, 48, 53, 97, 133], $ZnCl_2$[42, 130, 134, 135], and H_3PO_4[55, 56, 136] with limited research on activation using NH_4Cl, $FeCl_3$, and $AlCl_3$[55, 129, 130, 137]. The chemical activation presents itself with different advantages reported in literature including higher carbon yield, lower activation time and temperature, and controlled pore size distribution compared to physical activation process. The studies on chemical activation of PAN based carbon fibers are limited because of higher cost of activating agents (due to high activating agent to carbon ratio, typically 4:1 to 8:1) compared to CO_2 or steam. An additional washing step is also involved in the chemical activation process. The corrosive nature of the activating agents is another important factor limiting usage of chemical activation process[48, 52, 97].

The development of controlled pore structure by chemical activation requires careful selection of method to incorporate the activation agent into carbon precursor, depth of penetration/ intercalation efficiency, process conditions for activation, and removal of excess chemical groups present after activation. Several researchers impregnated the activating agents by immersion of stabilized or pre-carbonized precursors in solutions containing required quantity of impregnates[43, 47, 97, 123, 136]. A temperature of up to 60 ºC and subsequent stirring were also employed to improve impregnation efficiency. S. Y. Moon et al.[97] impregnated stabilized PAN fibers in 0.5-2.0M KOH or NaOH for 24 hours, dried at 90 ºC for 24 hours before activation. Similar approach was followed by M. Wu et al.[41] for PAN-based pre-oxidized cloth and carbonized cloth, where the samples were soaked for 2 hours followed by drying at 150 ºC for 4 hour before activation. The physical mixing of carbon precursor with the activating agent in dry state in a agate mortar or ball mill [44, 45, 48, 53, 54] were also reported for other pre-stabilized/pre-carbonized carbon precursors.

Direct additions of alkali hydroxide like KOH or NaOH activating agents are seldom reported in literature due to degradation or chain scission of PAN precursor[138, 139]. However, the activating agents like $ZnCl_2$, NH_4Cl, NH_4Cl, $FeCl_3$, and $(NH_4)_2HPO_4$ were directly incorporated into virgin PAN precursors. J. Sun et al.[140-142] impregnated PAN hollow fiber ammonium di basic phosphate solution (4 wt%) for 30 minutes, oxidized at 230 ºC in air for different times before carbonization and activation. S. H. Cho et al.[143] spun PAN fibers by dry-jet wet spinning from a spinning dope containing 13 wt% PAN/DMF with 0.02 mol $ZnCl_2$ per mol of acrylonitrile units. Z. Yue et al.[42] used different approaches to prepare fibrous porous material by coating $ZnCl_2$

impregnated PAN on fiber glass mat. PAN was first dissolved in DMF at 70 ºC, then $ZnCl_2$ was dissolved in solution at ambient temperature to give viscous mixture with 3.2 wt% PAN and 6.4 wt% $ZnCl_2$. The fiber mat is dip-coated, passed through 5 wt% $ZnCl_2$ solution to remove excess DMF and better coagulate PAN. Additional method involves dissolving PAN in 66 wt% $ZnCl_2$ solution at 90 ºC to give high $ZnCl_2$: PAN ratio (PAN:DMF:$ZnCl_2$ = 1:23.61:X, where X varied from 1-5). S. Mah et al.[135] photo-polymerized acrylonitrile from a concentrated solution containing $ZnCl_2$ in water. These techniques to incorporate activating agents into PAN precursors can be a potential route to produce chemically activated carbon materials.

1.4.2 Process, structure properties of chemically activated PAN

The main advantages offered by the chemical activation process over physical activation are (1) lower processing temperature, (2) high carbon yield and (3) controlled pore size distribution. The development of controlled pore structure by chemical activation requires good understanding of selection of precursor/activating agent, optimum process conditions for activation, and an efficient post treatment process for removal of excess chemical groups present. Y. J. Lee et al.[96] studied the effect of the amount of activating agent and heat treatment temperature on carbon yield, surface area and microstructure of activated PAN-based carbon fibers using KOH activating agent. Activation of PAN fibers at 800 ºC with K:C ratio of 1:1 showed carbon yield of 36% with specific surface area of 2545 m^2/g as given in Figure 1.5. However, further increase in activation temperature or K:C ratio led to abrupt decrease in surface area.

S. Y. Moon et al.[97] developed PAN based activated carbon fibers for iodine adsorption. The samples were impregnated in 2.0M KOH/NaOH at 800 ºC in nitrogen

atmosphere to achieve a BET surface area of 2244 m^2/g with KOH and 1786 m^2/g with NaOH. The amount of iodine absorbed by these samples were 1202 and 972 mg/g respectively. Z. Yue et al.[42] reported the effect of activation temperature and $ZnCl_2$:C ratio for PAN based fibrous porous materials. The activation temperature range of 350 - 650 ºC is recommended for achieving high surface area from PAN/$ZnCl_2$ system. The BET surface area also increased with the chemical ratio of 1:1 to 4/5:1 as given in Figure 1.6.

Several researchers reported that the ratio of activating agent to carbon precursors significantly affect the pore development during activation process[49, 52, 134, 144].

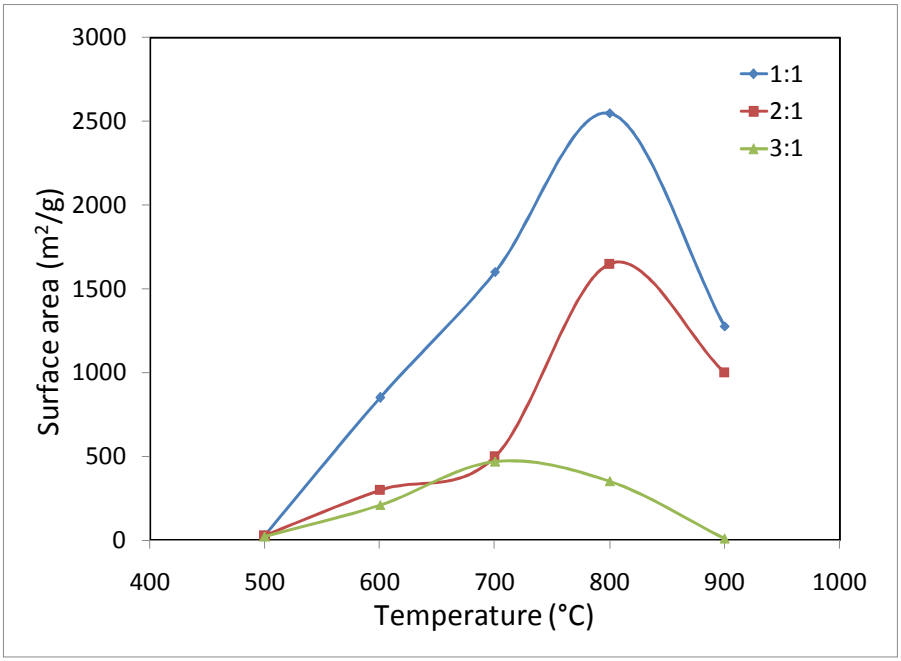

Figure 1.5 Effects of amount of KOH and heat treatment temperature on carbon yield and BET surface area; weight ratio of KOH and stabilized PAN fibers (adopted from reference [96]).

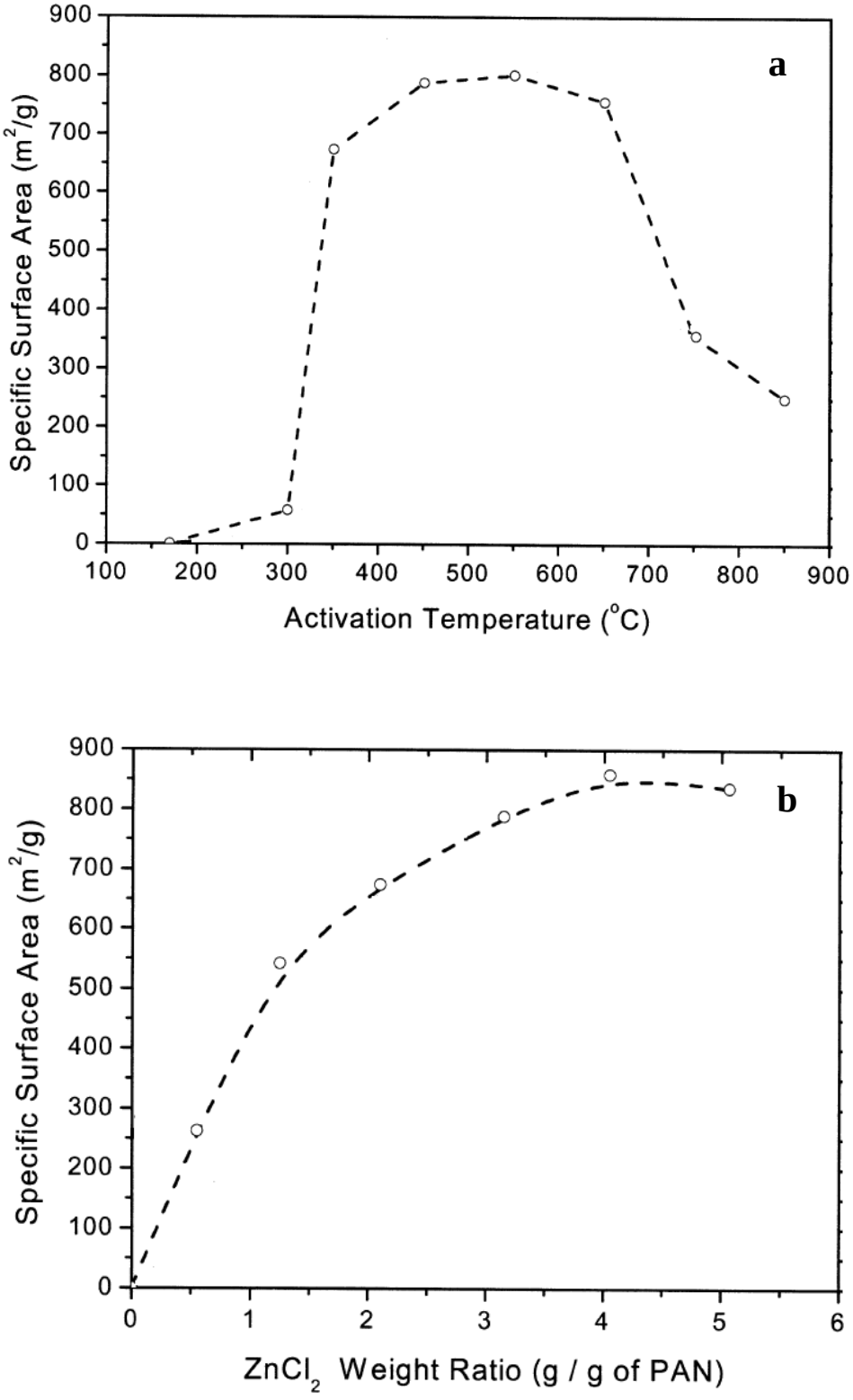

Figure 1.6 Effects of amount of $ZnCl_2$ (at 350 °C) and heat treatment temperature on BET surface area for PAN based fibrous porous materials[42].

A chemical ratio of 1-3:1 for KOH and 1-5:1 for $ZnCl_2$ has been reported for chemical activation of PAN based precursors [54, 94, 96, 97, 145] while a chemical ratio of 1-8:1 has been reported for non-PAN based carbon precursors using different chemical activating agents[46, 47, 49, 52, 116, 134, 144]. The usage of larger quantities of activating agents not only makes the chemical activation process expensive but also complicates the removal of activating agents from activated carbon before final use. Also, the chemical ratios quoted in literature represents ratio of the starting materials and not the amount of activating agents impregnated into the carbon precursors.

1.4.3 Process methods for polyacrylonitrile/carbon nanotubes based precursors

The physical properties of polymer nanotube composites depend on the degree of polymer molecular orientation, degree of exfoliation and orientation of carbon nanotubes. The carbon nanotubes (CNT) tend to aggregate to form ropes or bundles due to the strong van der Waals interaction between tubes[146]. The CNT ropes entangle together in the solid state to produce a highly dense, complex network structure that is extremely resistant to wetting. The carbon nanotubes in pristine form do not have any surface functional groups that can react with matrix to enhance dispersion. Achieving uniform dispersion or exfoliation of nanotubes in the solvent or polymer matrix is important for achieving uniform composite properties. A combination of sonication and shear mixing has been used in earlier studies to achieve uniform dispersion of nanotubes in dispersing solvent as well as in polymer[16, 90, 147]. Polymer carbon nanotube films typically have randomly oriented polymer chains and carbon nanotubes while fibers have polymer

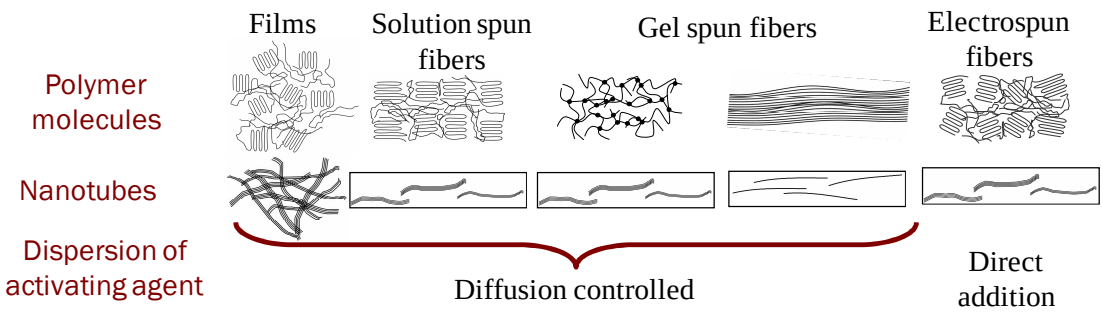

Figure 1.7 Representation of polymer molecular orientation, CNT orientation and degree of exfoliation and methods of incorporation of chemical activating agent.

chains oriented along the direction of spinning (Figure 1.7). Fully drawn gel spun fiber is reported to have exfoliated SWNTs[79]. The method of incorporation of activating agents was also varied from immersion of stabilized or pre-carbonized carbon precursors in solutions containing required quantity of impregnates[43, 47, 97, 123, 136] to direct addition of activating agent to precursors in solution stage[140-142].

For PAN/CNT films, a well dispersed composite solution mixture is cast onto a glass substrate maintained at required temperature and under vacuum to prepare films of uniform thickness. The use of activated carbon fibers results in higher surface area over activated carbon films. In the dry-jet wet spinning process used for fiber spinning, the solution of polymer or spinning dope is extruded from a die through one or more liquid baths containing various amounts of the solvent used in the dope and a non-solvent, such as water. The amount of solvent to non-solvent ratio decreases from first to last bath. In the last coagulating bath, the solvent is removed from the dope to form the fiber. Tension is maintained on the fiber through coagulation to improve the orientation of polymer molecules along the direction of fiber[78, 148]. Activated carbon fibers produced by

these processes were used for iodine adsorption[96, 97], water purification and other similar applications[130, 149].

If the individual nanotubes are completely exfoliated in PAN/SWNT composites, there is a possibility of utilizing maximum surface area of exfoliated CNTs for energy storage. The PAN/SWNT composite fibers spun by gel spinning process and drawn to a draw ratio of 51 is reported to have fully exfoliated SWNTs[79]. The gel spinning process was developed to produce ultra high strength fibers from high molecular weight polyethylene. This process involves transformation of polymer solution into a gel, gel spinning and subsequent solvent removal, and drawing to orient the polymer chains. The as-spun fibers from gel spinning will retain most of the solvent to form a gel of polymer and solvent. These fibers on annealing can form additional pores due to solvent evaporation. These drawn gel spun fibers/as-spun fibers can be activated using the chemical methods to achieve high performance electrochemical capacitor electrodes.

The polymer fibers that are traditionally produced by spinning from solution, melt, liquid crystalline state, or gel state were reported to have diameters ranging from 10 to 500 μm[150]. Attempts have been made to produce fibers with diameter of sub-micron size to increase the surface area for different applications[151-157]. Unlike conventional fiber spinning techniques, electrospinning is a process that is capable of producing polymer fibers in the nanometer diameter range. This electrospinning process uses a high voltage electric field to produce fibers of nano scale diameter from a polymer melt or solution. The significance of these nanofibers is their small diameters, their large surface area per unit mass, and small pore sizes between fibers. The electrospinning of two different polymers (nylon 6,6 and poly(trimethyl hexamethylene terephthalamide) in

formic acid) together were also reported to achieve intermediate properties of the two polymers[158]. A wide range of properties can be achieved by varying the type of polymer spun.

An interesting application of the electrospinning process proposed is the possibility of incorporating chemical activating agents like $ZnCl_2$ into carbonizing polymers like PAN at the solution preparation stage. When PAN/$ZnCl_2$ solution is spun from a common solvent using this method, there is possibility of phase separation between PAN and $ZnCl_2$ like any other method used to produce polymer fibers. However, the rapid evaporation of the solvent may prevent phase separation; making this method suitable to produce a homogenous phase for almost any activating agent/ carbonizing polymer system that cannot be achieved from diffusion controlled impregnation, if they can be dissolved in a common solvent. The homogenous mixture can be annealed to allow phase separation to occur which can result in very fine nano-scale morphology, depending on annealing conditions. This activating agent impregnated polymer can be further heat treated at higher temperature to achieve activated carbon with optimum pore size distribution. The concept of dispersing activating agent $ZnCl_2$ in PAN/DMF solution, electrospinning the mixed solution, heat treatment at activation temperatures, and measurement of electrochemical properties are presented in Appendix B.

1.5 Characterization methods

The performance of electrochemical capacitors depends on its electrochemical parameters like specific capacitance, energy density, power density, and surface properties like pore size, pore volume, and surface area. These properties must be

evaluated quantitatively to make comparisons between different materials and their corresponding processes to develop these materials, and also to establish suitability of these materials and processes for a specific application. The commonly used method to evaluate electrochemical properties are galvanostatic test (or constant current test), cyclic voltammetry, and impedance spectroscopy. The surface area and pore size analysis at the molecular level is made using an inert gas adsorption, usually nitrogen[159].

1.5.1 Galvanostatic test

The galvanostatic test is one of the chronopotentiometric method (voltage measured as a function of time), where the electrochemical electrodes are applied with a constant current source (called galvanostat) and change in voltage is recorded as a function of time[59]. The charging cycle can be followed by a discharge cycle by reversing the current at switch over voltage immediately or after a specific hold time. The presence of resistance component (equivalent series resistance (ESR)) in electrochemical capacitor can be detected using the ohmic drop in the charge-discharge curves. The voltage jump at charge – discharge curves given in Figure 1.8, is due to the presence of distributed resistance in electrodes. The results of galvanostatic test is often given in the form of ragaone plot which is a plot between energy and power densities of the electrode.

The ragone plot represent an electrochemical capacitor's energy storage capabilities at different power levels. The electrochemical device shows a cut off value observed by a rapid decrease in energy density at a particular power level. The ragone plot of electrodes made with SWNT buckypaper, carbonized PAN/SWNT and CO_2 activated PAN/SWNT films are presented in Figure 1.9. The knee shaped characteristic observed in ragone plots represent energy densities rapidly decreasing at a critical power

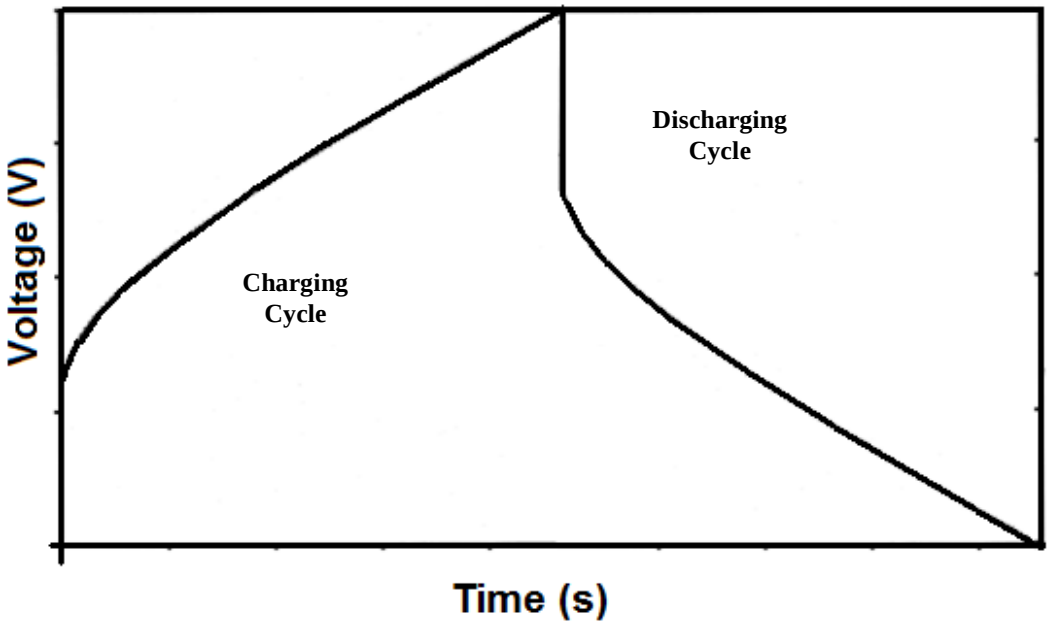

Figure 1.8 Typical charge discharge curve for an electrochemical capacitor electrode.

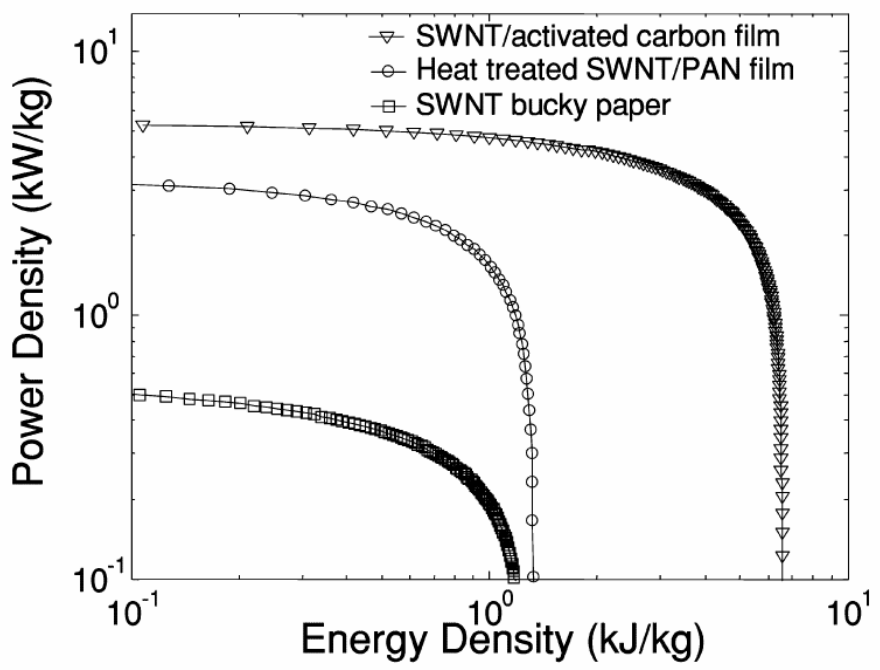

Figure 1.9 Energy versus power density (Ragone plot) for SWNT buckypaper, carbonized PAN/SWNT and CO_2 activated PAN/SWNT films[16].

level. We find the energy and power densities of PAN/SWNT films are significantly higher than that for the buckypaper electrodes[16].

1.5.2 Cyclic voltammetry

Cyclic voltammetry is a technique that is used to measure charge response of a electrochemical electrode with change in voltage. The experimental procedure involves applying a constant sweep rate (dV/dt) between two voltages suitable for a given electrolyte and measuring the response current. The specific capacitance is calculated using the equation 1.2 in earlier section 1.2 using the current I, scan rate (dv/dt), and mass of the two electrodes. The shape of cyclic voltammograms is often used to determine occurrence of any faradaic reactions in the operating voltage range. An ideal double layer capacitance behavior is denoted by the rectangular shape shown in Figure 1.10. The charge storage phenomenon is purely electrostatic in this case. When an electrochemical capacitors are associated with a resistive component, the measured current varies linearly depending on the contribution from the resistive component. When the electrode material undergoes a redox reaction in the operating voltage window, the charge measured is a continuously changing function of the potential V. The contribution from this capacitance is called a faradaic or pseudo capacitance. An example of material pseudocapacitance properties is illustrated using a conducting polymer composite electrode polyphenylene/carbon nanotube, as well as metal oxide (MnO_2)/carbon nanotube electrodes in Figure 1.11[160]. The deviation from parallelogram shape and presence of prominent peaks are evidence for pseudo capacitance behavior.

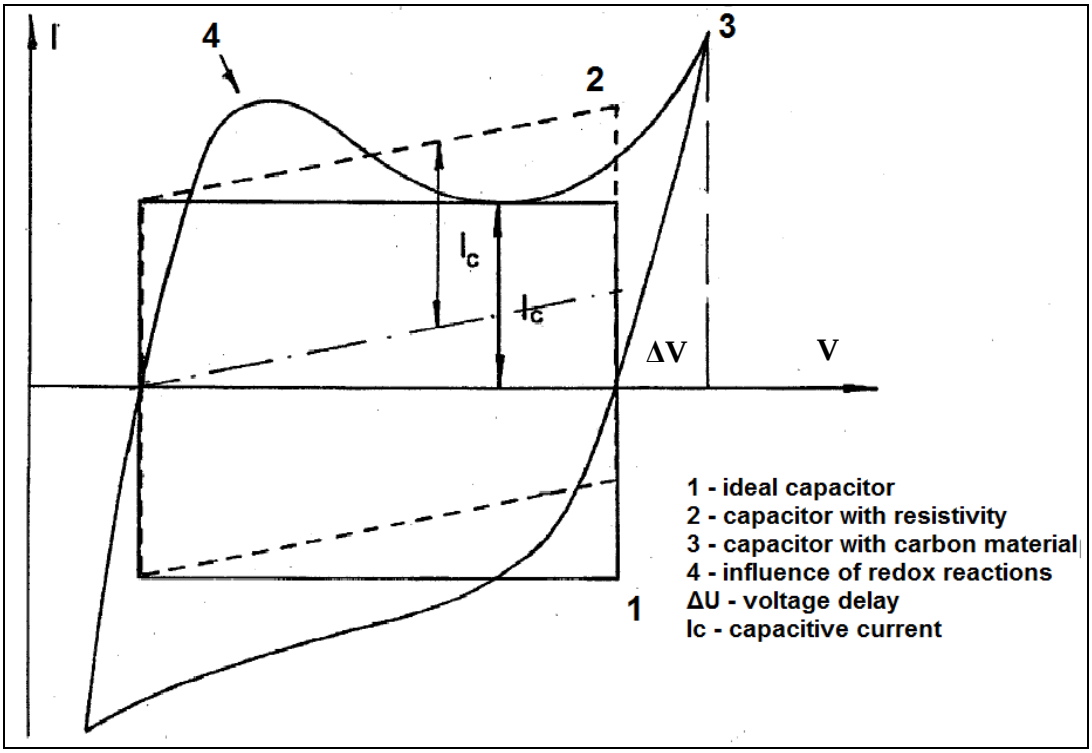

Figure 1.10 Typical cyclic voltammetry characteristics of electrochemical capacitors[161].

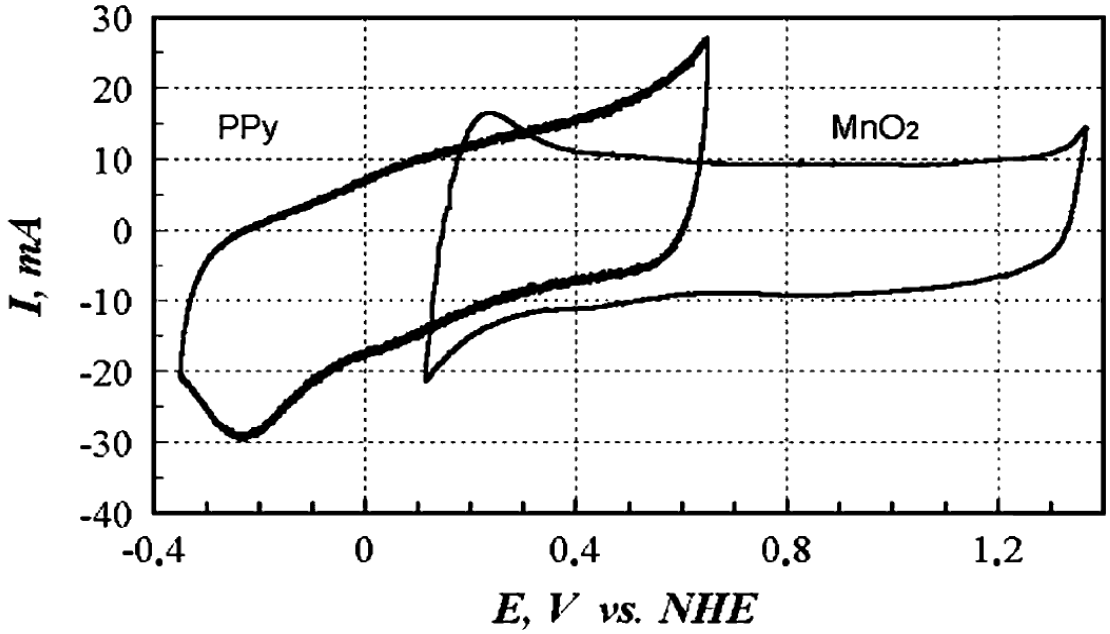

Figure 1.11 Cyclic voltammetry for PPy/nanotube and MnO2/nanotube composites measured in 2 mol/L KNO_3 at scan rate of 10 mV/s[160].

Cyclic voltammetry can also provide information about degree of reversibility of these redox reactions. A mirror image of charging and discharging profiles represents a reversible reaction while a reaction in which electrode material is consumed is represented by difference in charging and discharging curves.

1.5.3 Impedance spectroscopy

Impedance spectroscopy is a technique where impedance of electrode materials are evaluated at different frequency domains. The real and imaginary parts of impedance are represented by a nyquist plot Figure 1.12. The nyquist plots are characterized by a semi circle at high frequency domain and a straight line at low frequency region. The semi circle intersects the (–Z')-axis at two distinct points. The left intersect of the semi-circle to the real axis indicates the resistance of the electrolyte and the right intersect shows the resistance caused by the Faradic reactions. The knee frequency, transition point

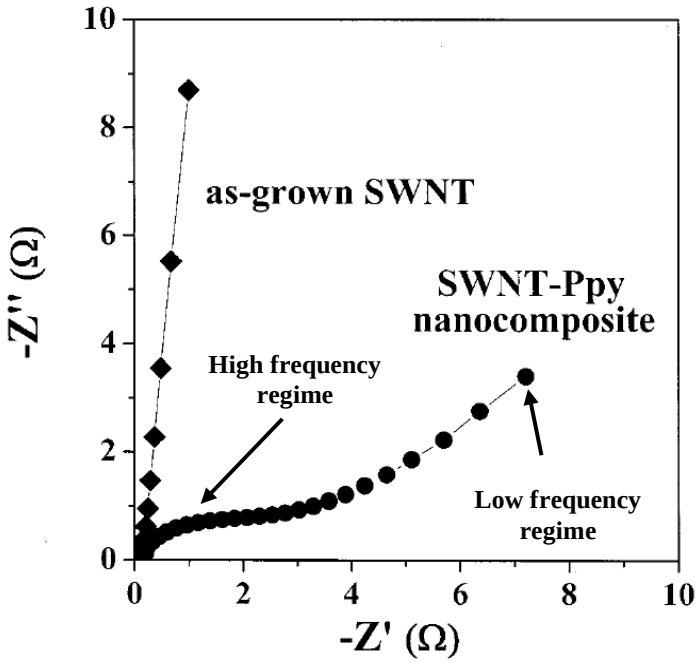

Figure 1.12 The complex-plane impedance plots at ac amplitude of 5 mV for as-grown SWNTs and SWNT-Polypyrrole nanocomposite electrodes[31].

between kinetics controlled high-frequency impedance and migration controlled low-frequency impedance, is a measure of electrical and ionic conductivity of the cell. The impedance results for as grown SWNT electrodes show negligible resistance due to faradaic reactions while SWNT/polyphenylene composites show significant faradaic resistance in Figure 1.12[31].

1.5.4 Surface area and pore size analysis

The surface area and pore size analysis are generally measured using gas adsorption studies. The surface area measurements at the molecular level require the sample to free from moisture or any surface vapors[159]. The instrument removes moisture by application of heat and either evacuation or purging with a non-adsorbent gas, usually helium. Then the sample temperature is reduced to that of liquid nitrogen (most common), liquid argon, or another coolant appropriate for gas to be adsorbed. The adsorbing gas (usually nitrogen) is then admitted in incremental doses at different partial pressures to probe the pore structure of the material. The amount of gas quantity adsorbed vs gas pressure is plotted to generate an *adsorption isotherm,* which can reveal the structure of the adsorbing material (called adsorbent) from the shape of isotherm. The classical adsorption theory assumes that gas molecules (called *adsorbate*) form a layer one molecule thick (monolayer) on the surface before beginning a second layer. The techniques used to calculate the surface area uses the dimensions of gas molecule and number of molecules of gas fed at a partial pressure to calculate the area covered. The adsorption of gas molecule in an adsorbent with pore dimensions considerably larger than the gas molecule is characterized by a hysteresis loop at higher partial pressures due to difference in adsorption and desorption rates. The adsorption isotherms generally follow

one of the six forms, five of which were originally assigned by Brunauer in1940[162] as given in Figure 1.13. Based on the IUPAC classification, Type I isotherms are observed for microporous solids having relatively small external surfaces, the limiting uptake being governed by the accessible micropore volume rather than by the internal surface area. The reversible Type II isotherm is the normal form of isotherm observed for a non-porous or macroporous adsorbent with unrestricted monolayer-multilayer adsorption. Point B in figure 1.13 (a) II, the beginning of the almost linear middle section of the isotherm, is often taken to indicate the stage at which monolayer coverage is complete and multilayer adsorption about to begin. Types III and V arise under conditions where gas molecules have more affinity for one another than for the adsorbent. Type VI isotherm that is rarely observed, indicates non porous samples with completely uniform surface[159, 163, 164].

The Type IV isotherms are characterized by hysteresis loop which is associated with capillary condensation at mesopores limiting uptake to a high partial pressure. Although the effect of various factors on adsorption hysteresis is not fully understood, the shapes of hysteresis loops have often been used to identify the specific pore structures. Hysteresis loops observed at higher partial pressures of adsorption isotherm are associated with capillary condensation in mesopore structures. H1 type loop has two branches are almost vertical and nearly parallel over an appreciable range of gas uptake.

On the other hand, the branches remain nearly horizontal and parallel over a wide range for H4 loop. Types H2 and H3 are regarded as intermediate between these two extremes. The steep region of the desorption branch leading to the lower closure point

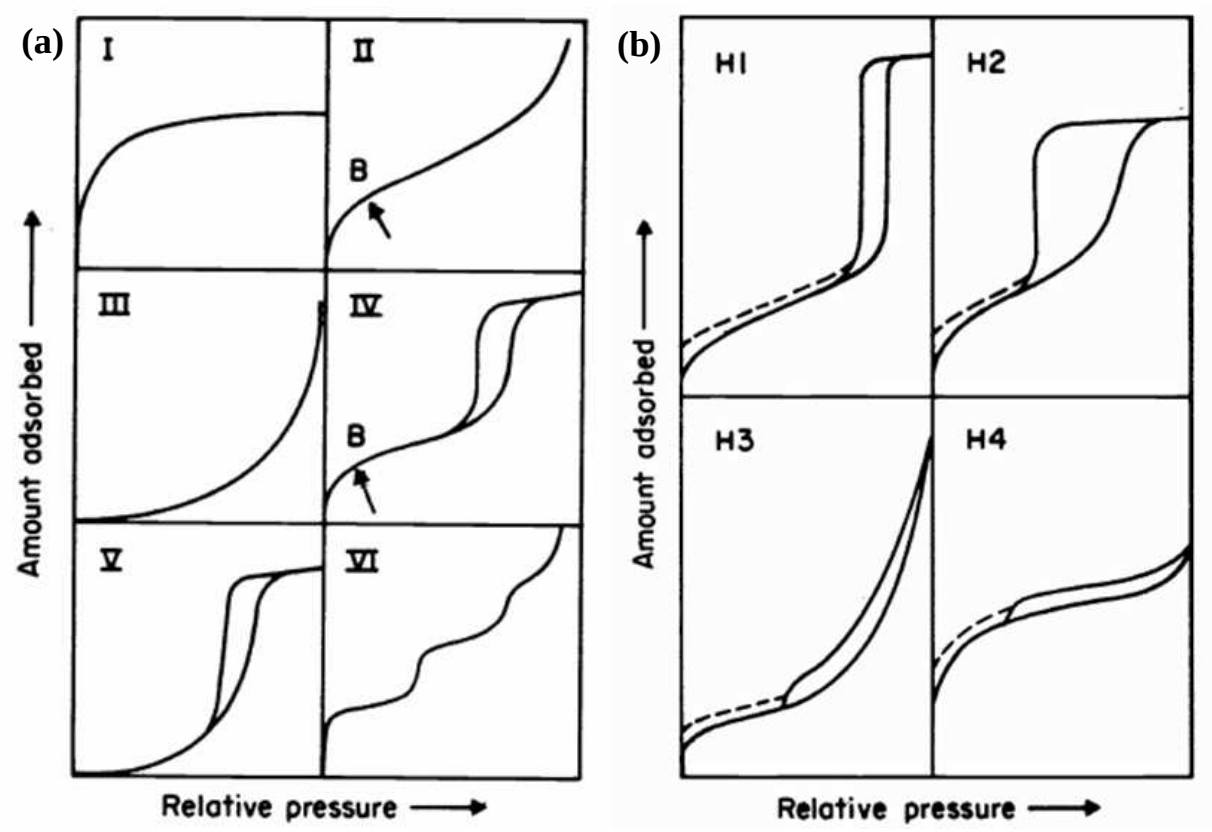

Figure 1.13 (a) Basic types of physical adsorption isotherms and (b) types of hysteresis loops[164]. Graphs are not drawn to scale and are representations of shape of each isotherm (see text for details).

occurs at a relative pressure depending on adsorbate (for Nitrogen, p/p° - 0.42) and is almost independent of the nature of the porous adsorbent.

According to IUPAC[164], Type H1 represents porous materials consisting of agglomerates or compacts of approximately uniform spheres and narrow distributions of pore size. Type H2 loops represent a wide distribution of pore size and shape is not well-defined and at times were attributed to a difference in mechanism between condensation and evaporation processes occurring in pores with narrow necks and wide bodies ('ink bottle' pores). The Type H3 loop observed with aggregates of plate-like particles giving

rise to slit-shaped pores. Similarly, the Type H4 loop is often associated with narrow slit-like pores with significant microporosity.

1.5.5 Other characterization techniques

The wide-angle X-ray diffraction (WAXD) is used to determine the extent of stabilization process in PAN precursor samples. WAXD integrated patterns of unstabilized PAN precursors show a strong peak at $2\theta \sim 17°$ corresponding to reflections from (110) and (200) planes. The intensity of this peak reduces considerably due to changes in structure during the stabilization process and has been used to determine the extent of stabilization for PAN precursors[165, 166].

The FTIR studies[44, 46, 167, 168] are commonly used to understand the chemical reactions involved in the chemical activation process. The FTIR spectrums of as-prepared and activated PAN, CNT or composite precursors are compared to determine the formation of any functional groups during the activation process. The changes in characteristic carbon bands of $–CH_{1-3}$ (reduction in alkyl groups ~ 2900 cm^{-1} peak), C-O-C or C-O (stretching or bending of phenolic or carboxylic functional groups ~ 1200 cm^{-1}), C=O (increase in surface oxygen complexes by stretching vibration at 1700 cm^{-1}), O-H (development of hydroxyl functional groups ~ 3500 cm^{-1}), and C=C (stretching at 1600 cm^{-1}) were investigated to understand the chemical reactions involved in the activation process. The spectra are characterized by the disappearance of adsorption band at 2240 cm^{-1} for stabilized as well as activated samples representing changes to nitrile groups. An intense absorption peak assigned to conjugated –C=N- and –C=C- structures, appears in the 1600 cm^{-1} range for activated samples indicating presence of structures similar to polypyridine rings[145].

The Raman spectrum of SWNTs show peaks corresponding to radial breathing mode (RBM) (200-500 cm^{-1}), G band (1500 to 1605 cm^{-1}), D band(1250-1450 cm^{-1}), and G' band (overtone of D* band) (2500-2900 cm^{-1})[169]. The intensities in most cases are normalized to the intensity of the G band for comparison. The disorder induced D band appears at ~1300 cm^{-1} due to the presence of disordered carbon, and SWNTs with incomplete or modified wall structure[170, 171]. The intensity of this peak is referred to understand the degree of disorder in CNTs.

The quality of nanotube dispersion in polymer matrices or solvents and structure of CNT can be examined using optical microscopy, scanning electron microscopy (SEM), and transmission electron microscopy (TEM).

1.6 Motivation for this study

As discussed in section 1.3, three different categories of materials are generally used as electrodes for electrochemical capacitors - metal oxides (RuO_2, IrO_2), conducting polymers (polyaniline, polypyrrole), and porous carbon. The current electrochemical capacitor electrodes from conducting metal oxides have a limitation of operation in only aqueous electrolytes restricting the operating voltage to 1 V. Conducting polymers undergo electrochemical reaction to exhibit high energy and power densities. Hence, long term performance and dimensional stability of these electrode materials (metal oxides and conducting polymers) are always a cause of concern. The carbon-carbon composite electrodes are becoming popular for electrochemical application due to lower cost, high surface area, ease of availability and established electrode production methods.

The lower energy density has been a limiting factor for carbon based electrochemical capacitors to date. Different approaches have been used to increase the energy density of carbon based electrochemical capacitors without affecting the high power performance. One approach has been to use non-aqueous electrolytes to increase the operating voltage to about 3 V. This will result in an increase in stored energy. The second approach for increasing the energy density of electrochemical capacitors has been to use a conducting polymer or metal oxide material along with carbon electrodes to make use of contribution from pseudocapacitance to overall energy density. The challenge in electrochemical capacitor industry is to produce long lifetime, low self discharging electrochemical capacitor with optimum specific capacitance, energy density and power density with wide operating voltage/temperature range that can be useful for wide range of applications.

A great deal of research on carbon based electrochemical capacitors deals with optimizing energy density and long term cyclability of the electrode material. Limited isolated studies on PAN/CNT composites prove them promising material for energy storage applications. However, there has been no systematic study on effect of varying activation process conditions on electrochemical properties. There is no definite correlation established between the measured specific capacitance (C_{sp}) , electrolyte ion size, wettability and electrode pore distribution to determine real accessible/chargeable surface area per gram. The contribution of double layer capacitance (C_{dl}) and pseudocapacitance (C_{Φ}) to overall capacitance is not clearly understood. The contribution of surface functionalities to pseudocapacitance (C_{Φ}), the influence of resistance from the electrolyte, and internal resistance from micro/mesopores also needs further

investigation. More attention on establishing methods for carbon preparation, surface chemistry and pretreatment conditions for electrodes is also required[1].

1.7 Thesis objectives

The key objectives of this study are:

- To develop carbon nanotube containing electrochemical capacitor material with high specific capacitance, energy density and power density.
- To investigate the effect of process parameters of physical and chemical activation process for PAN/CNT precursor films on electrochemical properties and porosity of activated carbon.
- To develop activated carbon with controlled pore size distribution.
- To study the dependence of specific capacitance on factors such as surface area, pore size and pore size distribution.

1.8. References:

[1] Conway BE. Electrochemical supercapacitors : scientific fundamentals and technological applications Plenum Press, New York. 1999:xxviii, 698 p.

[2] Scherson DA, Palencsar A. Batteries and electrochemical capacitors. Electrochemical Society Interface. 2006;15(1):17-22.

[3] Becker HE. Low voltage eletrolytic capacitors. US Patent 2800616. 1957.

[4] Rightmire R. Electrical energy storage apparatus. US patent 3288641. 1966.

[5] Trasatti S, Buzzanca G. Ruthenium dioxide: A new interesting electrode material. Solid state structure and electrochemical behaviour. Journal of Electroanalytical Chemistry. 1971;29(2):A1-A5.

[6] Conway BE, Angerstein-Kozlowska H. The electrochemical study of multiple-state adsorption in monolayers. Acc Chem Res. 1981;14(2):49-56.

[7] Hadzi-Jordanov S, Angerstein-Kozlowska H, Conway BE. Surface oxidation and H deposition at ruthenium electrodes: Resolution of component processes in potential-sweep experiments. Journal of Electroanalytical Chemistry. 1975;60(3):359-62.

[8] Kotz R, Carlen M. Principles and applications of electrochemical capacitors. Electrochimica Acta. 2000;45(15-16):2483-98.

[9] Tanahashi I, Yoshida A, Nishino A. The effect of heat-treatment on the properties of activated carbon fibre cloth polarizable electrodes. Journal of Applied Electrochemistry. 1991;21(1):28-31.

[10] Burke AF. Batteries and Ultracapacitors for Electric, Hybrid, and Fuel Cell Vehicles. Proceedings of the IEEE. 2007;95(4):806-20.

[11] Burke A. The present and projected performance and cost of double-layer pseudo-capacitive ultracapacitors for hybrid vehicle applications. Vehicle Power and Propulsion, 2005 IEEE Conference; 2005; 2005. p. 11 pp.

[12] Pandolfo AG, Hollenkamp AF. Carbon properties and their role in supercapacitors. Journal of Power Sources. 2006;157(1):11-27.

[13] Dell RM. Aqueous Electrolyte Batteries. Philosophical Transactions: Mathematical, Physical and Engineering Sciences. 1996;354(1712):1515-27.

[14] Burke A. Ultracapacitors: why, how, and where is the technology. Journal of Power Sources. 2000;91(1):37-50.

[15] Supercapacitors chart. [cited 2006 September]; Available from: www.maxwell.com/ultracapacitors/index.html

[16] Liu T, Sreekumar TV, Kumar S, Hauge RH, Smalley RE. SWNT/PAN composite film-based supercapacitors. Carbon. 2003;41(12):2440-2.

[17] Vix-Guterl C, Saadallah S, Jurewicz K, Frackowiak E, Reda M, Parmentier J, et al. Supercapacitor electrodes from new ordered porous carbon materials obtained by a templating procedure. Materials Science and Engineering B. 2004;108(1-2):148-55.

[18] Grupioni AAF, Arashiro E, Lassali TAF. Voltammetric characterization of an iridium oxide-based system: the pseudocapacitive nature of the Ir0.3Mn0.7O2 electrode. Electrochimica Acta. 2002 Dec;48(4):407-18.

[19] Grupioni AAF, Lassali TAF. Effect of the Co3O4 introduction in the pseudocapacitive behavior of IrO2-based electrode. Journal of The Electrochemical Society. 2001 Sep;148(9):A1015-A22.

[20] Chang J-K, Tsai W-T. Material Characterization and Electrochemical Performance of Hydrous Manganese Oxide Electrodes for Use in Electrochemical Pseudocapacitors. Journal of The Electrochemical Society. 2003;150(10):A1333-A8.

[21] Xu C, Li B, Du H, Kang F, Zeng Y. Supercapacitive studies on amorphous MnO2 in mild solutions. Journal of Power Sources. 2008;184(2):691-4.

[22] Hadzi-Jordanov S, Angerstein-Kozlowska H, Vukovic M, Conway BE. Reversibility and Growth Behavior of Surface Oxide Films at Ruthenium Electrodes. Journal of The Electrochemical Society. 1978;125(9):1471-80.

[23] Miller JM, Dunn B, Tran TD, Pekala RW. Deposition of ruthenium nanoparticles on carbon aerogels for high energy density supercapacitor electrodes. Journal of The Electrochemical Society. 1997 Dec;144(12):L309-L11.

[24] Xie XF, Gao L. Characterization of a manganese dioxide/carbon nanotube composite fabricated using an in situ coating method. Carbon. 2007 Oct;45(12):2365-73.

[25] Panic VV, Vidakovic TR, Dekanski AB, Miskovic-Stankovic VB, Nikolic BZ. Capacitive properties of RuO2-coated titanium electrodes prepared by the alkoxide ink procedure. Journal of Electroanalytical Chemistry. 2007 Nov;609(2):120-8.

[26] Wohlfahrt-Mehrens M, Schenk J, Wilde PM, Abdelmula E, Axmann P, Garche J. New materials for supercapacitors. Journal of Power Sources. 2002;105(2):182-8.

[27] Liu TC, Pell WG, Conway BE, Roberson SL. Behavior of Molybdenum Nitrides as Materials for Electrochemical Capacitors. Journal of The Electrochemical Society. 1998;145(6):1882-8.

[28] Choi D, Blomgren GE, Kumta PN. Fast and Reversible Surface Redox Reaction in Nanocrystalline Vanadium Nitride Supercapacitors. Advanced Materials. 2006;18(9):1178-82.

[29] Sivaraman P, Rath SK, Hande VR, Thakur AP, Patri M, Samui AB. All-solid-supercapacitor based on polyaniline and sulfonated polymers. Synthetic Metals. 2006;156(16-17):1057-64.

[30] Park JH, Park OO. Hybrid electrochemical capacitors based on polyaniline and activated carbon electrodes. Journal of Power Sources. 2002;111(1):185-90.

[31] An KH, Jeon KK, Heo JK, Lim SC, Bae DJ, Lee YH. High-Capacitance Supercapacitor Using a Nanocomposite Electrode of Single-Walled Carbon Nanotube and Polypyrrole. Journal of the Electrochemical Society. 2002;149:A1058-A62.

[32] Fan L-Z, Maier J. High-performance polypyrrole electrode materials for redox supercapacitors. Electrochemistry Communications. 2006;8(6):937-40.

[33] Hughes M, Chen GZ, Shaffer MSP, Fray DJ, Windle AH. Electrochemical Capacitance of a Nanoporous Composite of Carbon Nanotubes and Polypyrrole. Chem Mater. 2002 April 15, 2002;14(4):1610-3.

[34] Jurewicz K, Delpeux S, Bertagna V, Béguin F, Frackowiak E. Supercapacitors from nanotubes/polypyrrole composites. Chemical Physics Letters. 2001;347(1-3):36-40.

[35] Zhou C, Kumar S, Doyle CD, Tour JM. Functionalized Single Wall Carbon Nanotubes Treated with Pyrrole for Electrochemical Supercapacitor Membranes. Chem Mater. 2005;17(8):1997-2002.

[36] Laforgue A, Simon P, Sarrazin C, Fauvarque J-F. Polythiophene-based supercapacitors. Journal of Power Sources. 1999;80(1-2):142-8.

[37] Gallegos AKC, Rincon ME. Carbon nanofiber and PEDOT-PSS bilayer systems as electrodes for symmetric and asymmetric electrochemical capacitor cells. Journal of Power Sources. 2006 Nov;162(1):743-7.

[38] Fitzer E, Muller DJ. The influence of oxygen on the chemical reactions during stabilization of pan as carbon fiber precursor. Carbon. 1975;13(1):63-9.

[39] Lee J-G, Kim J-Y, Kim S-H. Effects of microporosity on the specific capacitance of polyacrylonitrile-based activated carbon fiber. Journal of Power Sources. 2006;160(2):1495-500.

[40] Rahaman MSA, Ismail AF, Mustafa A. A review of heat treatment on polyacrylonitrile fiber. Polymer Degradation and Stability. 2007;92(8):1421-32.

[41] Wu M, Zha Q, Qiu J, Guo Y, Shang H, Yuan A. Preparation and characterization of porous carbons from PAN-based preoxidized cloth by KOH activation. Carbon. 2004;42(1):205-10.

[42] Yue Z, Mangun CL, Economy J. Preparation of fibrous porous materials by chemical activation: 1. ZnCl2 activation of polymer-coated fibers. Carbon. 2002;40(8):1181-91.

[43] Teng H, Chang Y-J, Hsieh C-T. Performance of electric double-layer capacitors using carbons prepared from phenol-formaldehyde resins by KOH etching. Carbon. 2001;39(13):1981-7.

[44] Chunlan L, Shaoping X, Yixiong G, Shuqin L, Changhou L. Effect of pre-carbonization of petroleum cokes on chemical activation process with KOH. Carbon. 2005;43(11):2295-301.

[45] Otowa T, Nojima Y, Miyazaki T. Development of KOH activated high surface area carbon and its application to drinking water purification. Carbon. 1997;35(9):1315-9.

[46] Lillo-Rodenas MA, Cazorla-Amoros D, Linares-Solano A. Understanding chemical reactions between carbons and NaOH and KOH: An insight into the chemical activation mechanism. Carbon. 2003;41(2):267-75.

[47] Lozano-Castello D, Lillo-Rodenas MA, Cazorla-Amoros D, Linares-Solano A. Preparation of activated carbons from Spanish anthracite: I. Activation by KOH. Carbon. 2001;39(5):741-9.

[48] Macia-Agullo JA, Moore BC, Cazorla-Amoros D, Linares-Solano A. Activation of coal tar pitch carbon fibres: Physical activation vs. chemical activation. Carbon. 2004;42(7):1367-70.

[49] Ahmadpour A, Do DD. The preparation of active carbons from coal by chemical and physical activation. Carbon. 1996;34(4):471-9.

[50] Ehrburger P, Addoun A, Addoun F, Donnet J-B. Carbonization of coals in the presence of alkaline hydroxides and carbonates: Formation of activated carbons. Fuel. 1986;65(10):1447-9.

[51] Illan-Gomez MJ, Garcia-Garcia A, Salinas-Martinez de Lecea C, Linares-Solano A. Activated Carbons from Spanish Coals. 2. Chemical Activation. Energy Fuels. 1996;10(5):1108-14.

[52] Teng H, Hsu LY. High-Porosity Carbons Prepared from Bituminous Coal with Potassium Hydroxide Activation. Ind Eng Chem Res. 1999;38(8):2947-53.

[53] Raymundo-Pinero E, Azais P, Cacciaguerra T, Cazorla-Amoros D, Linares-Solano A, Beguin F. KOH and NaOH activation mechanisms of multiwalled carbon nanotubes with different structural organisation. Carbon. 2005;43(4):786-95.

[54] Yoon S-H, Lim S, Song Y, Ota Y, Qiao W, Tanaka A, et al. KOH activation of carbon nanofibers. Carbon. 2004;42(8-9):1723-9.

[55] Huidobro A, Pastor AC, Rodriguez-Reinoso F. Preparation of activated carbon cloth from viscous rayon: Part IV. Chemical activation. Carbon. 2001;39(3):389-98.

[56] Phan NH, Rio S, Faur C, Le Coq L, Le Cloirec P, Nguyen TH. Production of fibrous activated carbons from natural cellulose (jute, coconut) fibers for water treatment applications. Carbon. 2006;44(12):2569-77.

[57] Subramanian V, Luo C, Stephan AM, Nahm KS, Thomas S, Wei B. Supercapacitors from Activated Carbon Derived from Banana Fibers. J Phys Chem C. 2007;111(20):7527-31.

[58] Yang T, Lua AC. Textural and chemical properties of zinc chloride activated carbons prepared from pistachio-nut shells. Materials Chemistry and Physics. 2006;100(2-3):438-44.

[59] Bard AJ, Faulkner LR. Electrochemical methods : fundamentals and applications Wiley, New York. 2001:xviii, 718 p.

[60] Frackowiak E, Beguin F. Carbon materials for the electrochemical storage of energy in capacitors. Carbon. 2001;39(6):937-50.

[61] Teng H, Wang S-C. Preparation of porous carbons from phenol-formaldehyde resins with chemical and physical activation. Carbon. 2000;38(6):817-24.

[62] Raymundo-Pinero E, Kierzek K, Machnikowski J, Beguin F. Relationship between the nanoporous texture of activated carbons and their capacitance properties in different electrolytes. Carbon. 2006;44(12):2498-507.

[63] Toupin M, Belanger D, Hill IR, Quinn D. Performance of experimental carbon blacks in aqueous supercapacitors. Journal of Power Sources. 2005;140(1):203-10.

[64] Frackowiak E. Supercapacitors Based on Carbon Materials and Ionic Liquids. J Braz Chem Soc. 2006;17(6):1074-82.

[65] Galinski M, Lewandowski A, Stepniak I. Ionic liquids as electrolytes. Electrochimica Acta. 2006;51(26):5567-80.

[66] Lewandowski A, Galinski M. Carbon-ionic liquid double-layer capacitors. Journal of Physics and Chemistry of Solids. 2004;65(2-3):281-6.

[67] Arzhantsev S, Jin H, Baker GA, Maroncelli M. Measurements of the Complete Solvation Response in Ionic Liquids. The Journal of Physical Chemistry B. 2007;111(18):4978-89.

[68] Huang J, Sumpter Bobby G, Meunier V. A Universal Model for Nanoporous Carbon Supercapacitors Applicable to Diverse Pore Regimes, Carbon Materials, and Electrolytes. Chemistry - A European Journal. 2008;14(22):6614-26.

[69] Lewandowski A, Zajder M, Frackowiak E, Beguin F. Supercapacitor based on activated carbon and polyethylene oxide-KOH-H2O polymer electrolyte. Electrochimica Acta. 2001;46(18):2777-80.

[70] Liu X, Osaka T. All-Solid-State Electric Double-Layer Capacitor with Isotropic High-Density Graphite Electrode and Polyethylene Oxide/LiClO[sub 4] Polymer Electrolyte. Journal of The Electrochemical Society. 1996;143(12):3982-6.

[71] Bonnefoi L, Simon P, Fauvarque JF, Sarrazin C, Sarrau JF, Lailler P. Multi electrode prismatic power prototype carbon/carbon supercapacitors. Journal of Power Sources. 1999;83(1-2):162-9.

[72] Peter K, Ottmar S. Bipolar electrode-electrolyte unit. United States Patent 5,955,215. 1999.

[73] Zheng JP, Jiang ZN. Resistance distribution in electrochemical capacitors with spiral-wound structure. Journal of Power Sources. 2006;156(2):748-54.

[74] Michel G, Marc B, Herve M. Method of manufacturing a multilayer electrochemical assembly comprising an electrolyte between two electrodes, and an assembly made thereby United States Patent 5,593,462. 1997.

[75] Bashir Z. A critical review of the stabilisation of polyacrylonitrile. Carbon. 1991;29(8):1081-90.

[76] Dalton S, Heatley F, Budd PM. Thermal stabilization of polyacrylonitrile fibres. Polymer. 1999;40(20):5531-43.

[77] Sreekumar TV, Liu T, Min BG, Guo H, Kumar S, Hauge RH, et al. Polyacrylonitrile Single-Walled Carbon Nanotube Composite Fibers. Advanced Materials. 2004;16(1):58-61.

[78] Chae HG, Sreekumar TV, Uchida T, Kumar S. A comparison of reinforcement efficiency of various types of carbon nanotubes in polyacrylonitrile fiber. Polymer. 2005;46(24):10925-35.

[79] Chae HG, Minus ML, Kumar S. Oriented and exfoliated single wall carbon nanotubes in polyacrylonitrile. Polymer. 2006;47(10):3494-504.

[80] Uchida T, Kumar S. Single wall carbon nanotube dispersion and exfoliation in polymers. Journal of Applied Polymer Science. 2005;98(3):985-9.

[81] Sreekumar TV, Kumar S. Macroscopic fiber comprising single-wall carbon nanotubes and acrylonitrile-based polymer and process for making the same US Patent 6,852,410 2005.

[82] Ko F, Gogotsi Y, Ali A, Naguib N, Ye H, Yang GL, et al. Electrospinning of Continuous Carbon Nanotube-Filled Nanofiber Yarns. Advanced Materials. 2003;15(14):1161-5.

[83] Ye H, Lam H, Titchenal N, Gogotsi Y, Ko F. Reinforcement and rupture behavior of carbon nanotubes--polymer nanofibers. Applied Physics Letters. 2004;85(10):1775-7.

[84] Prilutsky S, Zussman E, Cohen Y. The effect of embedded carbon nanotubes on the morphological evolution during the carbonization of poly(acrylonitrile) nanofibers. Nanotechnology. 2008;19(16):165603.

[85] Vaisman L, Wachtel E, Wagner HD, Marom G. Polymer-nanoinclusion interactions in carbon nanotube based polyacrylonitrile extruded and electrospun fibers. Polymer. 2007;48(23):6843-54.

[86] Kim D-K, Park SH, Kim BC, Chin BD, Jo SM, Kim DY. Electrospun Polyacrylonitrile-Based Carbon Nanofibers and Their Hydrogen Storages. Macromolecular Research. 2005;13(6):521-8.

[87] Béguin F, Szostak K, Lota G, Frackowiak E. A Self-Supporting Electrode for Supercapacitors Prepared by One-Step Pyrolysis of Carbon Nanotube/Polyacrylonitrile Blends. Advanced Materials. 2005;17(19):2380-4.

[88] Hou H, Ge JJ, Zeng J, Li Q, Reneker DH, Greiner A, et al. Electrospun Polyacrylonitrile Nanofibers Containing a High Concentration of Well-Aligned Multiwall Carbon Nanotubes. Chem Mater. 2005;17(5):967-73.

[89] Chae HG, Minus ML, Rasheed A, Kumar S. Stabilization and carbonization of gel spun polyacrylonitrile/single wall carbon nanotube composite fibers. Polymer. 2007;48(13):3781-9.

[90] Zhou C. Carbon nanotube based electrochemical supercapacitors. PhD Thesis, Georgia Institute of Technology. 2006:42.

[91] Zhou C, Liu T, Wang T, Kumar S. PAN/SAN/SWNT ternary composite: Pore size control and electrochemical supercapacitor behavior. Polymer. 2006;47(16):5831-7.

[92] Wang T. Electrospun Carbon Nanofibers for Electrochemical Capacitor Electrodes. PhD Thesis, Georgia Institute of Technology. 2007.

[93] Kim C, Kap-Seung Y, Wan-Jin L. The Use of Carbon Nanofiber Electrodes Prepared by Electrospinning for Electrochemical Supercapacitors. Electrochemical and Solid-State Letters. 2004;7(11):A397-A9.

[94] Ryu Z, Rong H, Zheng J, Wang M, Zhang B. Microstructure and chemical analysis of PAN-based activated carbon fibers prepared by different activation methods. Carbon. 2002;40(7):1144-7.

[95] Frackowiak E, Lota G, Machnikowski J, Vix-Guterl C, Beguin F. Optimisation of supercapacitors using carbons with controlled nanotexture and nitrogen content. Electrochimica Acta. 2006;51(11):2209-14.

[96] Lee Y-J, Kim J-H, Kim J, Lee DB, Lee J-C, Chung Y-J, et al. Fabrication of activated carbon fibers from stabilized PAN-based fibers by KOH. Materials Science forum. 2004;449-452:217-20.

[97] Moon SY, Kim M-s, Hahm H-S, Lim Y-S. Preparation of activated carbon fibers by chemical activation method with hydroxides. Material Science Forum. 2006;510-511:750-3.

[98] C. Kim, Ngoc BTN, Yang KS, Kojima M, Kim YA, Kim YJ, et al. Self-Sustained Thin Webs Consisting of Porous Carbon Nanofibers for Supercapacitors via the Electrospinning of Polyacrylonitrile Solutions Containing Zinc Chloride. Advanced Materials. 2007;19(17):2341-6.

[99] Im JS, Park S-J, Lee Y-S. Preparation and characteristics of electrospun activated carbon materials having meso- and macropores. Journal of Colloid and Interface Science. 2007;314(1):32-7.

[100] Xu B, Wu F, Chen R, Cao G, Chen S, Zhou Z, et al. Highly mesoporous and high surface area carbon: A high capacitance electrode material for EDLCs with various electrolytes. Electrochemistry Communications. 2008;10(5):795-7.

[101] Kim C, Yang K-S, Lee W-J. The Use of Carbon Nanofiber Electrodes Prepared by Electrospinning for Electrochemical Supercapacitors. Electrochemical and Solid-State Letters. 2004;7(11):A397-A9.

[102] Im JS, Park S-J, Kim TJ, Kim YH, Lee Y-S. The study of controlling pore size on electrospun carbon nanofibers for hydrogen adsorption. Journal of Colloid and Interface Science. 2008;318(1):42-9.

[103] Lozano-Castello D, Cazorla-Amoros D, Linares-Solano A, Quinn DF. Influence of pore size distribution on methane storage at relatively low pressure: preparation of activated carbon with optimum pore size. Carbon. 2002;40(7):989-1002.

[104] Wu F-C, Tseng R-L, Hu C-C, Wang C-C. Effects of pore structure and electrolyte on the capacitive characteristics of steam- and KOH-activated carbons for supercapacitors. Journal of Power Sources. 2005;144(1):302-9.

[105] Chmiola J, Yushin G, Gogotsi Y, Portet C, Simon P, Taberna PL. Anomalous Increase in Carbon Capacitance at Pore Sizes Less Than 1 Nanometer. Science. 2006 September 22, 2006;313(5794):1760-3.

[106] Yamada H, Moriguchi I, Kudo T. Electric double layer capacitance on hierarchical porous carbons in an organic electrolyte. Journal of Power Sources. 2008;175(1):651-6.

[107] Fuertes AB, Lota G, Centeno TA, Frackowiak E. Templated mesoporous carbons for supercapacitor application. Electrochimica Acta. 2005;50(14):2799-805.

[108] Morishita T, Soneda Y, Tsumura T, Inagaki M. Preparation of porous carbons from thermoplastic precursors and their performance for electric double layer capacitors. Carbon. 2006;44(12):2360-7.

[109] Yoon B-J, Jeong S-H, Lee K-H, Seok Kim H, Gyung Park C, Hun Han J. Electrical properties of electrical double layer capacitors with integrated carbon nanotube electrodes. Chemical Physics Letters. 2004;388(1-3):170-4.

[110] Zhang H, Cao G, Yang Y, Gu Z. Comparison Between Electrochemical Properties of Aligned Carbon Nanotube Array and Entangled Carbon Nanotube Electrodes. Journal of The Electrochemical Society. 2008;155(2):K19-K22.

[111] Futaba DN, Hata K, Yamada T, Hiraoka T, Hayamizu Y, Kakudate Y, et al. Shape-engineerable and highly densely packed single-walled carbon nanotubes and their application as super-capacitor electrodes. Nat Mater. 2006;5(12):987-94.

[112] Shiraishi S, Kurihara H, Okabe K, Hulicova D, Oya A. Electric double layer capacitance of highly pure single-walled carbon nanotubes (HiPco(TM) Buckytubes(TM)) in propylene carbonate electrolytes. Electrochemistry Communications. 2002;4(7):593-8.

[113] Niu C, Sichel EK, Hoch R, Moy D, Tennent H. High power electrochemical capacitors based on carbon nanotube electrodes. Applied Physics Letters. 1997;70(11):1480.

[114] Chen Q-L, Xue K-H, Shen W, Tao F-F, Yin S-Y, Xu W. Fabrication and electrochemical properties of carbon nanotube array electrode for supercapacitors. Electrochimica Acta. 2004;49(24):4157-61.

[115] Shiraishi S, Kibe M, Yokoyama T, Kurihara H, Patel N, Oya A, et al. Electric double layer capacitance of multi-walled carbon nanotubes and B-doping effect. Applied Physics A: Materials Science & Processing. 2006;82(4):585-91.

[116] Frackowiak E, Delpeux S, Jurewicz K, Szostak K, Cazorla-Amoros D, Beguin F. Enhanced capacitance of carbon nanotubes through chemical activation. Chemical Physics Letters. 2002;361(1-2):35-41.

[117] Jiang Q, Lu XY, Zhao Y. Effects of protection gas flow rate on the electrochemical capacitance of activated carbon nanotubes. Materials Chemistry and Physics. 2006;99(2-3):314-7.

[118] Jiang Q, Qu MZ, Zhou GM, Zhang BL, Yu ZL. A study of activated carbon nanotubes as electrochemical super capacitors electrode materials. Materials Letters. 2002;57(4):988-91.

[119] Pan H, Poh CK, Feng YP, Lin J. Supercapacitor Electrodes from Tubes-in-Tube Carbon Nanostructures. Chem Mater. 2007;19(25):6120-5.

[120] Liu CG, Fang HT, Li F, Liu M, Cheng HM. Single-walled carbon nanotubes modified by electrochemical treatment for application in electrochemical capacitors. Journal of Power Sources. 2006;160(1):758-61.

[121] Barisci JN, Wallace GG, Chattopadhyay D, Papadimitrakopoulos F, Baughman RH. Electrochemical Properties of Single-Wall Carbon Nanotube Electrodes. Journal of The Electrochemical Society. 2003;150(9):E409-E15.

[122] Ahmadpour A, King BA, Do DD. Comparison of Equilibria and Kinetics of High Surface Area Activated Carbon Produced from Different Precursors and by Different Chemical Treatments. Ind Eng Chem Res. 1998;37(4):1329-34.

[123] Hu Z, Srinivasan MP, Ni Y. Novel activation process for preparing highly microporous and mesoporous activated carbons. Carbon. 2001;39(6):877-86.

[124] Hattori Y, Noguchi N, Okino F, Touhara H, Nakahigashi Y, Utsumi S, et al. Defluorination-enhanced hydrogen adsorptivity of activated carbon fibers. Carbon. 2007;45(7):1391-5.

[125] Fan M, Zhang P. Activated Carbon Supported K2CO3 Catalysts for Transesterification of Dimethyl Carbonate with Propyl Alcohol. Energy Fuels. 2007;21(2):633-5.

[126] Guha A, Lu W, Zawodzinski Jr TA, Schiraldi DA. Surface-modified carbons as platinum catalyst support for PEM fuel cells. Carbon. 2007;45(7):1506-17.

[127] Tien PD, Satoh T, Miura M, Nomura M. Continuous Hydrogen Evolution from Tetrahydronaphthalene over Palladium Catalysts Supported on Activated Carbon Fibers. Energy Fuels. 2005;19(5):2110-3.

[128] Wu F-C, Tseng R-L, Hu C-C, Wang C-C. The capacitive characteristics of activated carbons--comparisons of the activation methods on the pore structure and effects of the pore structure and electrolyte on the capacitive performance. Journal of Power Sources. 2006;159(2):1532-42.

[129] Bansal RC, Donnet J-B, Stoeckli F. Active carbon Marcel Dekker, Inc New York. 1988.

[130] Donnet J-B, Bansal RC. Carbon fibers. Marcel Dekker, Inc New York. 1984.

[131] Marsh H, Rodriguez-Reinoso F. Activation Processes (Chemical). *Activated Carbon*. Oxford: Elsevier Science Ltd 2006:322-65.

[132] Stavropoulos GG. Precursor materials suitability for super activated carbons production. Fuel Processing Technology. 2005;86(11):1165-73.

[133] Lozano-Castello D, Macia-Agullo JA, Cazorla-Amoros D, Linares-Solano A, Muller M, Burghammer M, et al. Isotropic and anisotropic microporosity development upon chemical activation of carbon fibers, revealed by microbeam small-angle X-ray scattering. Carbon. 2006;44(7):1121-9.

[134] Caturla F, Molina-Sabio M, Rodriguez-Reinoso F. Preparation of activated carbon by chemical activation with ZnCl2. Carbon. 1991;29(7):999-1007.

[135] Mah S, Park S, Nam H, Seoul C. Photopolymerization of acrylonitrile in concentrated aqueous zinc halide solutions. Journal of Applied Polymer Science. 2000;77(12):2588-94.

[136] Nakagawa Y, Molina-Sabio M, Rodriguez-Reinoso F. Modification of the porous structure along the preparation of activated carbon monoliths with H3PO4 and ZnCl2. Microporous and Mesoporous Materials. 2007;103(1-3):29-34.

[137] Marsh H, Rodriguez-Reinoso F. Activated carbon 2006.

[138] Batty NS, Guthrie JT. Degradation of polyacrylonitrile in solution by alkali. Polymer. 1978;19(10):1145-8.

[139] Batty NS, Gradwell AJ, Guthrie JT, Greig D, Hardy ND, Jakeways R, et al. Structural order in alkali-degraded PAN as seen in studies of low-temperature thermal conductivity. Polymer. 1983;24(3):258-62.

[140] Junfen Sun CHSZQW. Effects of oxidation time on the structure and properties of polyacrylonitrile-based activated carbon hollow fiber. Journal of Applied Polymer Science. 2007;106(1):470-4.

[141] Junfen Sun LWQW. Comparison about the structure and properties of PAN-based activated carbon hollow fibers pretreated with different compounds containing phosphorus. Journal of Applied Polymer Science. 2005;96(2):294-300.

[142] Junfen Sun QW. Effects of the oxidation temperature on the structure and properties of polyacrylonitrile-based activated carbon hollow fiber. Journal of Applied Polymer Science. 2005;98(1):203-7.

[143] Seo Hyun Cho JSPSMJIJC. Influence of ZnCl2 on the structure and mechanical properties of polyacrylonitrile fibers. Polymer International. 1994;34(3):333-7.

[144] Teng H, Yeh TS. Preparation of Activated Carbons from Bituminous Coals with Zinc Chloride Activation. Ind Eng Chem Res. 1998;37(1):58-65.

[145] Yue Z, Benak KR, Wang J, Mangun CL, Economy J. Elucidating the porous and chemical structures of ZnCl2-activated polyacrylonitrile on a fiberglass substrate. Journal of Materials Chemistry. 2005;15(30):3142-8.

[146] Girifalco LA, Hodak M, Lee RS. Carbon nanotubes, buckyballs, ropes, and a universal graphitic potential. Physical Review B. 2000 Nov 15;62(19):13104-10.

[147] Guo H, Sreekumar TV, Liu T, Minus M, Kumar S. Structure and properties of polyacrylonitrile/single wall carbon nanotube composite films. Polymer. 2005;46(9):3001-5.

[148] Veedu S, Kumar S. Macroscopic fiber comprising single-wall carbon nanotubes and acrylonitrile-based polymer and process for making the same US Patent 6,852,410. 2005.

[149] Marsh H, Rodriguez-Reinoso F. Oxford: Activated Carbon, Elsevier Science Ltd 2006:322-65.

[150] Vaidya AA. Production of synthetic fibers. New Delhi, Prentice Hall. 1988.

[151] Larrondo L, John Manley RS. Electrostatic fiber spinning from Polymer melts. I. Experimental observations on fiber formation and properties. Journal of polymer science: Part B: Polymer physics. 1981;19:909 – 20.

[152] Reneker DH, Chun I. Nanometre diameter fibers of polymer, produced by electrospinning. Nanotechnology. 1996;7:216 – 23.

[153] Jaeger R, Bergshoel MM, Batlle CMI, Shonherr H, Vancso GJ. Electrospinning of ultra thin polymer fibers. Macromolecular symposia. 1998;127:141 – 50.

[154] Fong H, Chun I, Reneker D. Beaded nanofibers formed during electrospinning. Polymer. 1999;40:4585.

[155] Deitzel JM, Kleinmeyer J, Harris D, Beck Tan NC. The effect of processing variables on the morphology of electrospun nano fibers and textiles. Polymer 2001;42:261 - 72.

[156] Gibson P, Gibson HS, Rivin D. Transport properties of porous membranes based on electrospun nanofibers. Colloids and surfaces A: Physicochemical and Engineering Aspects. 2001;187-188:469-81.

[157] Demir MM, Yilgor I, Yilgor E, Erman B. Electrospinning of polyurethane fibers. Polymer. 2002;43:3003-309.

[158] Jagannathan S. Process-structure-property relationships of electrospun nanofibers. MS Thesis, University of Tennessee, Knoxville. 2003.

[159] Webb PA, Orr C. Analytical methods in fine particle technology. Micromeritics Instruments Corp , Norcross, Georgia. 1997.

[160] Frackowiak E. Carbon materials for supercapacitor application. Physical Chemistry Chemical Physics. 2007;9(15):1774-85.

[161] Frackowiak E, Béguin F. Carbon materials for the electrochemical storage of energy in capacitors. Carbon. 2001;39(6):937-50.

[162] Brunauer S, Deming LS, Deming WE, Teller E. On a Theory of the van der Waals Adsorption of Gases. Journal of the American Chemical Society. 1940;62(7):1723-32.

[163] Lowell S, Shields JE, Thomas MA, Thommes M. Characterization of porous solids and powders: Surface area, pore size and density. Kluwer Academic Publishers, Dordrecht/Boston/London. 2004.

[164] Sing KSW, Everett DH, Haul RAW, Moscou L, Pierotti RA, Rouquerol J, et al. Reporting physisorption data for gas/solid systems with special reference to the determination of surface area and porosity. Pure & Appl Chem. 1985;57(4):603.

[165] Jagannathan S, Chae HG, Jain R, Kumar S. Structure and electrochemical properties of activated polyacrylonitrile based carbon fibers containing carbon nanotubes. Journal of Power Sources. 2008;185(2):676-84.

[166] Yu M-J, Bai Y-J, Wang C-G, Xu Y, Guo P-Z. A new method for the evaluation of stabilization index of polyacrylonitrile fibers. Materials Letters. 2007;61(11-12):2292-4.

[167] Yu M-J, Wang C-G, Bai Y-J, Ji M-X, Xu Y. SEM and OM Study on the Microstructure of Oxidative Stabilized Polyacrylonitrile Fibers. Polymer Bulletin. 2007;58(5):933-40.

[168] Lu C, Xu S, Wang M, Wei L, Liu S, Liu C. Effect of pre-oxidation on the development of porosity in activated carbons from petroleum coke. Carbon. 2007;45(1):206-9.

[169] Dresselhaus MS, Dresselhaus G, Jorio A, Souza AG, Saito R. Raman spectroscopy on isolated single wall carbon nanotubes. Carbon. 2002;40(12):2043-61.

[170] Duesberg GS, Loa I, Burghard M, Syassen K, Roth S. Polarized Raman spectroscopy on isolated single-wall carbon nanotubes. Physical Review Letters. 2000 Dec 18;85(25):5436-9.

[171] Zhang MF, Yudasaka M, Koshio A, Iijima S. Thermogravimetric analysis of single-wall carbon nanotubes ultrasonicated in monochlorobenzene. Chemical Physics Letters. 2002 Oct 4;364(3-4):420-6.

Chapter 2

MATERIALS AND EXPERIMENTAL METHODS

2.1 Materials

Polyacrylonitrile (PAN) used to prepare films and solution spun fibers, is a copolymer with molecular weight of ~ 100,000 g/mol containing 6.7 mol% methylacrylate, was obtained from Exlan, Co. (Japan). Poly(acrylonitrile) with viscosity average molecular weight ~ 250,000 g/mol from same supplier was used for preparing gel spun fibers. The solvents, dimethyl formamide (DMF) and dimethyl Acetamide (DMAc) purchased from Sigma-Aldrich were used as received.

Carbon nanotubes (CNT) (Grade XO12UA ~ 1% metal impurity) received from Carbon Nanotechnologies Inc., Houston, TX was used in films used for CO_2 activation. A comparable diameter and purity CNTs (XO671UA ~ 1% catalytic impurity) obtained from the same supplier was used to prepare films for KOH activation and CNT buckypapers. SWNTs (Grade P0247, 2.4% catalytic impurity) and SWNTs (Grade XO1PPP, 2.4% catalytic impurity) also from Carbon Nanotechnologies Inc. were used for solution spun and gel spun fibers respectively. MWNTs from Iljin Nanotech, Co. (Korea) (2.5% catalytic impurity) were used in solution spun fibers, gel spun fibers as well as MWNT buckypapers. The SEM images, TEM images and Raman spectra of various CNTs used in this thesis are given in Figures 2.1 - 2.3 respectively. Complete descriptions of samples used in this thesis are presented in Table 2.1.

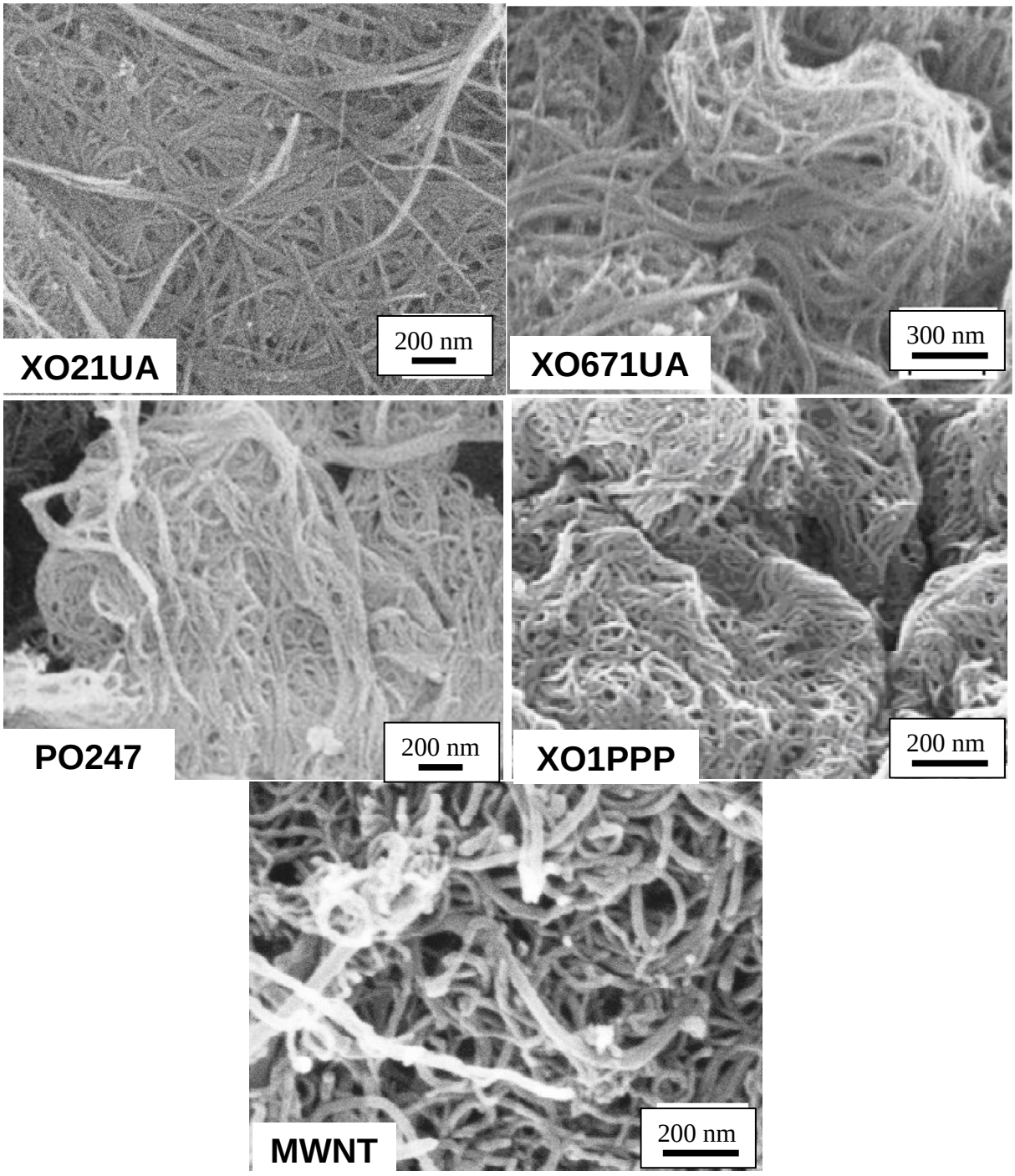

Figure 2.1 SEM images of various CNTs used in this thesis.

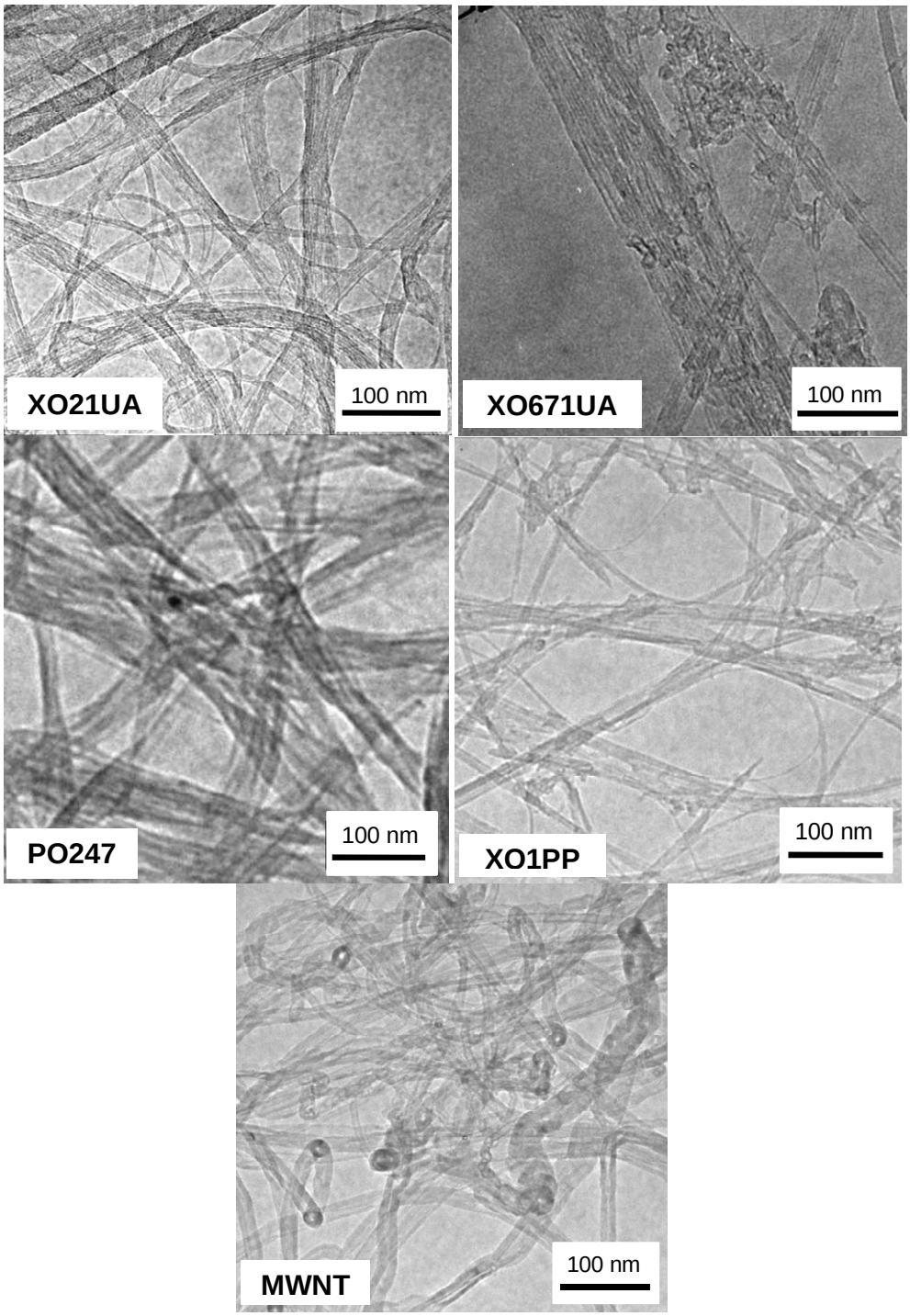

Figure 2.2 TEM images of various CNTs used in this thesis.

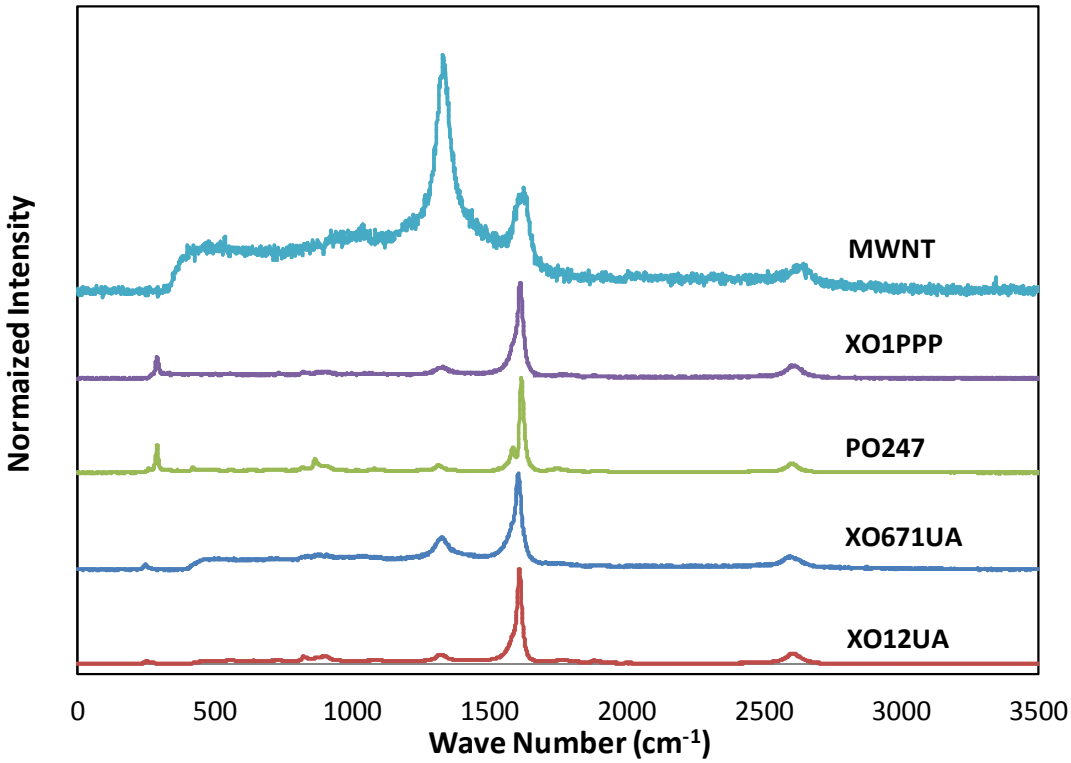

Figure 2.3 Raman spectra normalized to G band intensity for various CNTs used in this thesis.

2.2 Precursor Sample preparation

2.2.1 PAN/CNT films

As-received CNTs (XO21UA and XO671UA) were dispersed in DMF solvent at concentration of 100 mg/L (in batches of 30 mg CNT in 300 ml DMF) by bath sonication (Branson sonicator model #: 3510K-MT, output frequency: 42 kHz ± 6 %) for 48 hours at room temperature. For sample with 80:20 PAN /CNT ratio 60 mg of CNT (2 batches of 30 mg) were sonicated for 48 hours. PAN/CNT solution mixture was prepared by adding solution of PAN dissolved in DMF at ~100 ºC (240 mg PAN in 160 ml DMF for PAN/CNT 80/20 films (FK.82.8.6M and FC.82.9.3), same ratio maintained for other

Table 2.1 Description of samples used in this thesis.

Label	Sample	PAN molecular weight	CNT type (Impurity %)	Thickness /Diameter (μm)	Activation temperature (°C)	Activation time (min)	Molarity
Films (KOH activated)							
FK.00.8.6M	PAN	100 K	-	25	800	60	6M
FK.91.8.6M	PAN/CNT (90/10)	100 K	XO671UA (1%)	25	800	60	6M
FK.82.8.6M	PAN/CNT (80/20)	100 K	XO671UA (1%)	25	800	60	6M
FK.64.8.6M	PAN/CNT (60/40)	100 K	XO671UA (1%)	25	800	60	6M
FK.46.8.6M	PAN/CNT (40/60)	100 K	XO671UA (1%)	25	800	60	6M
BS.00.8.6M	CNT	-	XO671UA (1%)	50	800	60	6M
FK.82.8.1M	PAN/CNT (80/20)	100 K	XO671UA (1%)	25	800	60	1M
FK.82.8.3M	PAN/CNT (80/20)	100 K	XO671UA (1%)	25	800	60	3M
FK.82.8.10M	PAN/CNT (80/20)	100 K	XO671UA (1%)	25	800	60	10M
FK.82.7.6M	PAN/CNT (80/20)	100 K	XO671UA (1%)	25	700	60	6M
FK.82.9.6M	PAN/CNT (80/20)	100 K	XO671UA (1%)	25	900	60	6M
Films (CO_2 activated)							
FC.82.9.3	PAN/CNT (80/20)	100 K	XO21UA (1%)	25	900	30	-
FC.73.9.3	PAN/CNT (70/30)	100 K	XO21UA (1%)	25	900	30	-
FC.64.9.3	PAN/CNT (60/40)	100 K	XO21UA (1%)	25	900	30	-
FC.82.7.3	PAN/CNT (80/20)	100 K	XO21UA (1%)	25	700	30	-
FC.82.8.3	PAN/CNT (80/20)	100 K	XO21UA (1%)	25	800	30	-
FC.82.9.6	PAN/CNT (80/20)	100 K	XO21UA (1%)	25	900	60	-
FC.82.9.9	PAN/CNT (80/20)	100 K	XO21UA (1%)	25	900	90	-
Solution spun fibers (KOH Activated)							
SSK.8.6M	PAN	100 K	-	55	800	60	6M
SSKM.8.6M	PAN/MWNT (95/5)	100 K	Iljin (2.5%)	86	800	60	6M
SSKS.8.6M	PAN/SWNT (95/5)	100 K	P0247 (2.4%)	70	800	60	6M
Solution spun fibers (CO_2 activated)							
SSC.9.6	PAN	100 K	-	55	900	60	-
SSCM.9.6	PAN/MWNT (95/5)	100 K	Iljin (2.5%)	86	900	60	-
SSCS.9.6	PAN/SWNT (95/5)	100 K	P0247 (2.4%)	70	900	60	-
Gel spun as-spun fibers (KOH Activated)							
GSASK.8.6M	PAN DR - 4	250 K	-	58	800	60	6M
GSASKM.8.6M	PAN/MWNT (99/1) DR - 3	250 K	Iljin (2.5%)	49	800	60	6M
GSASKS.8.6M	PAN/SWNT (99/1) DR - 3	250 K	XO1PPP (2.4%	26	800	60	6M
Gel spun drawn fibers (KOH Activated)							
GSDRK.8.6M	PAN DR - 42	250 K	-	28	800	60	6M
GSDRKM.8.6M	PAN/MWNT (99/1) DR - 45	250 K	Iljin (2.5%)	14	800	60	6M
GSDRKS.8.6M	PAN/SWNT (99/1) DR - 45	250 K	XO1PPP (2.4%	19	800	60	6M
Buckypaper (KOH Activated)							
BM.00.8.6M	MWNT	-	Iljin (2.5%)	100	800	60	6M
BS.00.8.6M	SWNT	-	XO671UA (1%)	50	800	60	6M

concentrations) to the sonicated solution and by continuous mechanical stirring (Caframo high shear mixer, model# BDC1850) at ~100 ºC for 24 hours.

The optical homogeneity of the solution was verified by Leica DMRX Optical Microscope (Leica Microsystems, Gemany) equipped with a Sony Digital Photo Camera DKC-5000. Homogeneous solution was further heated at same temperature, while continuously stirred and evaporated solvent was collected in a cold trap until the solid content reduced to 12 g/L. The partially evaporated solution was then casted on to a glass substrate and subsequently placed in a vacuum oven at 85 ºC and 15 psi vacuum for 12 hours. The PAN/CNT composite films (thickness ~ 25 µm, FK series and FC series in Table 2.1) obtained were peeled off from the glass substrate and further dried under vacuum at 85 ºC for 48 hours.

2.2.2 Solution spun fibers

The PAN, PAN/SWNT (P0247) and PAN/MWNT fibers containing 5 wt% CNT were solution spun using dry-jet-wet spinning by H.G. Chae and R. Jain[1]. CNTs were dispersed in DMF at a concentration of 40 mg/L using 24 h bath sonication at room temperature. PAN (15 g) was dried in vacuum at 100 ºC and dissolved in DMF (100 mL) at 80 ºC. Optically homogeneous CNT/DMAc dispersion was added to the PAN/DMAc solution. The PAN/CNT/DMAc solutions were spun at room temperature by dry-jet-wet spinning using the small scale spinning system manufactured by Bradford University Research Ltd. The air gap between spinneret (single hole, 500 µm diameter) and the coagulation media was about 2 cm. DMAc/water volumetric ratios in the coagulation baths (baths 1 and 2) and drawing bath (bath 3) were 60/40, 10/90, and 0/100 respectively, while the two coagulation baths were maintained at 30 ºC and the drawing

bath at 100 ºC[1]. The control (SSK.8.6M and SSC.9.6) and composite fibers (PAN/SWNT and PAN/MWNT - SSKS.8.6M, SSCS.9.6 and SSKM.8.6M, SSCM.9.6) are drawn to a draw ratio of 6 and 10 respectively [1, 2]. Diameter of the solution spun fibers was in the range of 60 to 80 µm.

2.2.3 Gel-spun fiber

The as-spun and drawn PAN(GSASK.8.6M and GSDRK.8.6M), PAN/SWNT (GSASKS.8.6M and GSDRKS.8.6M), and PAN/MWNT(GSASKM.8.6M and GSDRKM.8.6M) gel-spun fibers containing 1 wt% CNT were processed using gel spinning process by H.G. Chae and H.Y. Choi[3]. CNTs were dispersed in DMF at a concentration of 40 mg/L using 24 h bath sonication at room temperature. PAN (15 g) was dried in vacuum at 100 ºC and dissolved in DMF (100 mL) at 80 ºC. Optically homogeneous CNT/DMF dispersion was added to the PAN/DMF solution. The excess amount of solvent was evaporated by vacuum distillation at 80 ºC, while stirring, to obtain the desired solution concentration (15 g solids (PAN + CNT)/100 mL solvent). The PAN/DMF and PAN/CNT/DMF solutions were spun at 31.4 m/min using a 500 µm diameter single hole spinneret (250 µm diameter spinneret was used for PAN/SWNT as-spun fiber) at 110 ºC into a methanol bath maintained at -50 ºC. The air gap between spinneret and the methanol bath was about 2 cm. The as-spun fibers were taken up at 100 m/min and were kept immersed in methanol bath (maintained between -20 and -40 ºC) for 1 week, to ensure gelation. As a result, the as-spun fiber draw ratio was between 3 - 4. The gel fiber was further drawn (draw ratio in the range of 7–16) at 160 ºC in glycerol bath followed by washing in ethanol and vacuum drying at 40 ºC for 3 days.

2.2.4 Buckypapers

CNTs (BS.00.8.6M) and MWNTs (BM.00.8.6M) are dispersed in DMF by bath sonication for 24 h at concentration of 30 mg in 300 ml. These suspensions of CNTs are filtered (poly(tetrafluoroethylene) (PTFE) filter paper - 1.0 μm pore size, Pall Gelman Laboratory, East Hills, NY) to form buckypaper. The film was washed with excess distilled water. After drying, the nanotube paper (buckypaper) was removed from supporting filter membrane and vacuum dried at 85 ºC for 48 hours.

2.3 Heat treatment and activation conditions

2.3.1. KOH Activated films

Solution cast films (FK series) were stabilized by heating in air at 1 ºC/min to 285 ºC and by holding at that temperature for 2, 4, 8, and 16 hours respectively. To verify the completion of stabilization process, the samples were examined by WAXD to confirm the disappearance of peak at 2θ ~ 17° due to (110) and (200) PAN reflections[4]. The films stabilized at 16 h show complete disappearance of WAXD peak at 2θ ~ 17° denoting completion of stabilization process. The sample with 80:20 PAN/CNT ratio (FK.82 series) was used to determine effect of activation temperature on KOH activation of composite films. The activation temperatures used were 700, 800, and 900 ºC at a fixed activation time of 30 minutes. 1M, 3M, 6M and 10M KOH were used to impregnated stabilized PAN/CNT films (FK.82 series) to understand the effect of molarity on electrochemical properties. Films with PAN/CNT ratios 100:0, 90:10, 80:20, 60:40, 40:60, and 0:100 (FK.00.8.6M to BS.00.8.6M in Table 2.1) were prepared to understand the effect of composition on chemical activation process.

2.3.2 CO_2 Activated films

Solution cast films (PAN/CNT 80/20, FC.82 series) were carbonized in an inert atmosphere (argon flow rate fixed at 20 SCFH (standard cubic feet per hour)) in a box furnace (51668-HR box furnace 1200C, Blue M Electric, Asheville, NC) by ramping from room temperature to 700 °C at 5 °C/min and holding at that temperature for 30 minutes. The activation temperatures used were 700, 800, and 900 °C at a fixed activation time of 30 minutes and for activation time variation study, 30, 60, and 90 minutes were used at a constant temperature of 900 °C. For activation, the films carbonized at 700 °C were further heated to required activation temperature at the rate of 5 °C/min. When the temperature reached 900 °C argon flow was switched off and CO_2 was introduced in the box furnace at a fixed flow rate of 20 SCFH. The solutions with PAN/CNT ratios of 70/30 (210:90 mg - FC.73.9.3) and 60/40 (180:120 mg - FC.64.9.3) were prepared to understand the effect of composition on physical activation. These samples were activated at 900 °C for 30 minutes.

2.3.3 Solution spun fibers

Solution spun fibers (SSK and SSC series) were stabilized without tension in a ceramic crucible in air by heating at 1 ºC/min to 285 ºC and by holding at that temperature for 2, 4, 8 and 16 hours. To study the extent of stabilization, these samples were treated in dimethyl formamide (DMF) at 150 ºC for 6 hours to remove unstabilized PAN, and were examined by scanning electron microscopy as well as by WAXD. On determining optimum stabilization temperature to be 16 hours, PAN, PAN/SWNT, and PAN/MWNT fibers (SSK and SSC series) used for carbonization and activation were stabilized for 16 hours.

Samples stabilized for 16 h were carbonized by heating them from room temperature to 700 ºC at 5 ºC/min, and then holding for one hour at 700 ºC in argon in a box furnace. These carbonized samples were activated at 900 ºC in CO_2 for one hour in the same furnace (SSC series). For chemical activation (SSK series), 16 hour stabilized samples were immersed in 6 M KOH for 24 hours at room temperature. KOH impregnated fibers were dried at 90 ºC for 24 hours in vacuum. With KOH impregnation, fiber weight increased by about a factor of two, and resulted in increased diameter. KOH impregnated fibers were heated at 5 ºC/min to 800 ºC and held at that temperature for one hour in argon. KOH activated samples were cooled to room temperature and repeatedly washed with hot distilled water to remove excess KOH. Therefore it should be noted that CO_2 activated samples were first carbonized and then activated, while the samples activated by KOH went from stabilization to activation, without the separate carbonization step. The activation temperature of 900 ºC for CO_2 and 800 ºC for KOH were chosen based on the literature reports as well as our own preliminary work [5-7].

2.3.4 Gel-spun fibers

Gel-spun fibers (GSASK and GSDRK series) were stabilized without tension in a ceramic crucible in air by heating at 1 ºC/min to 285 ºC and by holding at that temperature for 10 hours followed by heating up to 330 ºC at a heating rate of 1 ºC/min and held at 330 ºC for 3 h. These process conditions were optimized by H. Chae et al.[8] used for preparing carbon fibers. The extent of stabilization was verified using WAXD as explained in section 2.3.2

For chemical activation, all fibers (GSASK and GSDRK series) were immersed in 6 M KOH for 24 hours at room temperature. KOH impregnated fibers were dried at 90 ºC

for 24 hours in vacuum. With KOH impregnation, fiber weight increased by about a factor of two. Dried fibers were heated at 5 ºC/min to 800 ºC and held at that temperature for one hour in argon. KOH activated samples were cooled to room temperature and repeatedly washed with hot distilled water to remove excess KOH.

2.3.5 Buckypapers

For chemical activation, SWNT (BS.00.8.6M) and MWNT (BM.00.8.6M) buckypapers were immersed in 6 M KOH for 24 hours at room temperature. KOH impregnated nanotube films were dried at 90 ºC for 24 hours in vacuum. With KOH impregnation, weight of SWNT and MWNT buckypapers increased by about a factor of two and three, respectively. Dried films were heated at 5 ºC/min to 800 ºC and held at that temperature for one hour in argon. KOH activated samples were cooled to room temperature and repeatedly washed with hot distilled water to remove excess KOH.

2.4 Electrochemical measurements

The specific capacitance of the activated samples was evaluated by using a two-electrode cell. Two film electrodes (diameter = 0.8 cm) separated by a thin microporous membrane (Celgard 3400, Celgard Inc., Charlotte, NC) were sandwiched between nickel current collectors, and 6 M KOH aqueous solution as electrolyte. Constant current charging and discharging (CC) and cyclic voltammetry measurements (CV) were carried out on Solartron 1470 Cell Test (Solartron Analytical, Houston, TX) at room temperature for capacitance evaluation. In CC measurements, the cell was charged and discharged in 0 to 0.8 V range at a current of 0.5, 1, 2, 3, and 5 mA. In CV measurements, scanning rates of 5, 10, 20, 30, and 40 mV/s were used. The specific capacitance, energy density

(ED) and the power density (PD) delivered by the electrodes of the supercapacitor testing cell were calculated using the equations 1.2 – 1.4 given in chapter 1.

For KOH activated films (FK series), solution spun fibers (SSC and SSK series), gel-spun fibers (GSASK and GSDRK series), and buckypapers (BS.00.8.6M and BM.00.8.6M) both aqueous 6M KOH (ionic radius – K^+ - 1.38 Å and OH^- - 1.33 Å)[9] as well as ionic liquid/organic electrolyte mixture of 1-Butyl-3-methylimidazolium tetrafluoroborate ($BMIMBF_4$ – structure below):acetonitrile (1:2 ratio) (ionic radius – $BMIM^+$ - 3.39 Å and BF_4 – 2.29 Å)[9, 10] were used as electrolyte.

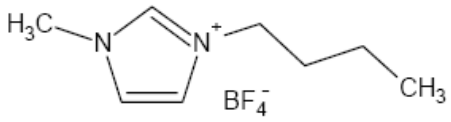

In the galvanostatic measurements, the cell was charged and discharged from 0 to 3 V for ionic liquid, at constant current values of 0.1, 0.2, 0.5, 1, 2 and 5 mA. In CV measurements, scan rates of 5, 10, 20, 30, and 40 mV/s were used similar to 6M KOH [11-13].

For activated samples that cannot form a uniform film preferred for measurement of electrochemical properties (KOH activated PAN films (FK.00.8.6M), solution (SSC and SSK series), and gel-spun fibers (GSASK and GSDRK series), the samples were crushed in mortar with a pestle and mixed with 20 wt% polyvinylidene difluoride (–CH_2 – CF_2 –) binder (80:20, carbon:PVDF). The electrodes were prepared by compression molding the activated carbon/binder mixture at 140 ºC, under ~ 0.6 GPa stress for 1 hour. Only the mass of the carbon electrodes was used in the calculations and the mass of the binder was excluded. The electrode thickness varied between 100-300 µm, and the electrode diameter was about 0.5 cm. The impedance spectroscopy was performed on

Potentiostat/Galvanostat (EG&G PAR Model 273A) in the frequency range of 100 mHz to 100 kHz using a two electrode cell.

2.5 Gas adsorption and other characterization techniques

The isothermal N_2 gas adsorption and desorption at 77 K were carried out on surface area and porosity analyzer (Model: ASAP 2020, Micromeritics Inc.), on samples degassed at 90 °C for 16 h. The specific surface area, pore size, and pore size distribution were determined using Brunauer, Emmet, Teller (BET) and density functional theory (DFT) methods [14-16]. WAXD studies were performed on a Rigaku Micromax-002 WAXS/SAXS system operated at 45 kV and 0.66 mA equipped with a Rigaku R-axis IV++ 2-D detection system. Scanning electron microscope (Leo 1530, Osaka, Japan) was used to characterize the morphology of the SWNT/PAN composite films and their heat-treated products. Before imaging, all the samples were sputter coated with gold for 90 seconds using Edwards Scancoat Six Sputter Coater. The dispersion of potassium in stabilized solution spun fibers was characterized using the energy dispersive system (EDS) in LEO SEM 1530. Raman spectroscopy was performed on Holoprobe Research 785 Raman Microscope using 785 nm incident laser wavelength with polarizer and analyzer parallel to each other. Infrared spectroscopy was conducted on the buckypapers using Perkin Elmer FT-IR microscope and by collecting 1028 scans at a resolution of 1 cm^{-1}.

2.6. References

[1] Chae HG, Sreekumar TV, Uchida T, Kumar S. A comparison of reinforcement efficiency of various types of carbon nanotubes in polyacrylonitrile fiber. Polymer. 2005;46(24):10925-35.

[2] Sreekumar TV, Liu T, Min BG, Guo H, Kumar S, Hauge RH, et al. Polyacrylonitrile Single-Walled Carbon Nanotube Composite Fibers. Advanced Materials. 2004;16(1):58-61.

[3] Chae HG, Minus ML, Kumar S. Oriented and exfoliated single wall carbon nanotubes in polyacrylonitrile. Polymer. 2006;47(10):3494-504.

[4] Yu M-J, Bai Y-J, Wang C-G, Xu Y, Guo P-Z. A new method for the evaluation of stabilization index of polyacrylonitrile fibers. Materials Letters. 2007;61(11-12):2292-4.

[5] Lee J, Kim J, Kim S. Microtexture and electrical properties of PAN-ACF. Journal of Materials Science. 2007;42(7):2486-91.

[6] Lee J-G, Kim J-Y, Kim S-H. Effects of microporosity on the specific capacitance of polyacrylonitrile-based activated carbon fiber. Journal of Power Sources. 2006;160(2):1495-500.

[7] Moon SY, Kim M-s, Hahm H-S, Lim Y-S. Preparation of activated carbon fibers by chemical activation method with hydroxides. Material Science Forum. 2006;510-511:750-3.

[8] Chae HG, Minus ML, Rasheed A, Kumar S. Stabilization and carbonization of gel spun polyacrylonitrile/single wall carbon nanotube composite fibers. Polymer. 2007:1-9.

[9] Huang J, Sumpter Bobby G, Meunier V. A Universal Model for Nanoporous Carbon Supercapacitors Applicable to Diverse Pore Regimes, Carbon Materials, and Electrolytes. Chemistry - A European Journal. 2008;14(22):6614-26.

[10] Arzhantsev S, Jin H, Baker GA, Maroncelli M. Measurements of the Complete Solvation Response in Ionic Liquids. The Journal of Physical Chemistry B. 2007;111(18):4978-89.

[11] Liu T, Sreekumar TV, Kumar S, Hauge RH, Smalley RE. SWNT/PAN composite film-based supercapacitors. Carbon. 2003;41(12):2440-2.

[12] Zhou C, Liu T, Wang T, Kumar S. PAN/SAN/SWNT ternary composite: Pore size control and electrochemical supercapacitor behavior. Polymer. 2006;47(16):5831-7.

[13] Zhou C, Kumar S, Doyle CD, Tour JM. Functionalized Single Wall Carbon Nanotubes Treated with Pyrrole for Electrochemical Supercapacitor Membranes. Chem Mater. 2005;17(8):1997-2002.

[14] Lowell S, Shields JE, Thomas MA, Thommes M. Characterization of porous solids and powders: Surface area, pore size and density. Kluwer Academic Publishers, Dordrecht/Boston/London. 2004.

[15] Sing KSW, Everett DH, Haul RAW, Moscou L, Pierotti RA, Rouquerol J, et al. Reporting physisorption data for gas/solid systems with special reference to the determination of surface area and porosity. Pure & Appl Chem. 1985;57(4):603.

[16] Webb PA, Orr C. Analytical methods in fine particle technology. Micromeritics Instruments Corp , Norcross, Georgia. 1997.

Chapter 3

ELECTROCHEMICAL CAPACITOR BEHAVIOR OF CHEMICALLY ACTIVATED POLYACRYLONITRILE - CARBON NANOTUBE FILMS

3.1 Introduction

The chemical activation method using hydroxides, halides, and acids was explored for producing activated carbon due to the advantages reported including higher carbon yield, lower activation time and temperature, and controlled pore size distribution[1-8]. Earlier studies on PAN based systems for making porous carbon materials using chemical activation process resulted in higher surface area with narrow pore size distribution compared to physically activated samples [4, 9, 10]. Specific capacitance as high as 371 F/g has been achieved for partially carbonized PAN fibers activated using NaOH[11]. However, to the best of our knowledge, there are no previous literature reports on chemical activation of solution spun PAN/CNT composites.

The effect of process variables on chemically activated carbon has been previously explored for Bituminous coal precursor. Experiences from Lozano-Castello group[12], Teng group [7, 13] and Ahmadpour group[1] on chemical activation of coal has been used in this study to optimize the process conditions for PAN/CNT system. KOH activation yielded higher pore volume compared to NaOH and $ZnCl_2$ activation and a temperature range of 700 - 800 ºC for KOH activation of carbon has been recommended by most researchers[3, 4, 14] with optimum K:C ratio of 4:1. The performances of supercapacitor based on PAN/CNT composite films (FK series in Table 2.1) activated at different conditions are explored in this chapter. The effect of activation

temperature, molarity of impregnating agent and composition of precursor films are investigated.

3.2 Experimental

CNTs were obtained from Carbon Nanotechnologies, Inc (Houston, TX) (Grade XO671UA, 1% catalytic impurity). PAN used in this study, poly(acrylonitrile-co-methylacrylate) containing 6.7 mol% methylacrylate, was obtained from Exlan, Co. (Japan). DMF purchased from Sigma-Aldrich was used as received. Detailed description of film preparation method, heat treatment conditions as well as characterization methods are given in chapter 2.

3.3 Results and Discussion

3.3.1 Stabilization studies

PAN/CNT films (FK series) of different composition were stabilized for 16 h at 285 ºC in air to form a ladder structure stable enough for further heat treatment at higher temperatures[15, 16]. The completion of stabilization process is verified by examining the WAXD peak to confirm the disappearance of peak at 2θ ~ 17° due to (110) and (200) PAN reflections as shown for PAN/CNT (80/20) samples (FK.82 series) in Figure 3.1[17]. Stabilized PAN/CNT (80/20) samples (FK.82 series) were impregnated in 6M KOH for 24 hours, dried and activated at temperatures 700 – 900 ºC.

3.3.2 Structure and morphology

The SEM images of the samples activated at different times and temperature are given in Figure 3.2. The diameter of as-received CNT bundles were 17 ± 2 nm measured by averaging randomly selected 30 bundles from high resolution SEMs while the diameter

of CNT bundles after activation at all activation temperatures and compositions varied from 30 to 50 nm. This increase in diameter of CNT bundles after activation is due to PAN wrapping CNT bundles. The fibril structure observed for KOH activated PAN fibers reported by S. Y. Moon[4] and Y. J. Lee[18] was not seen for PAN films (FK.00.8.6M) activated at same activation temperature of 800 ºC.

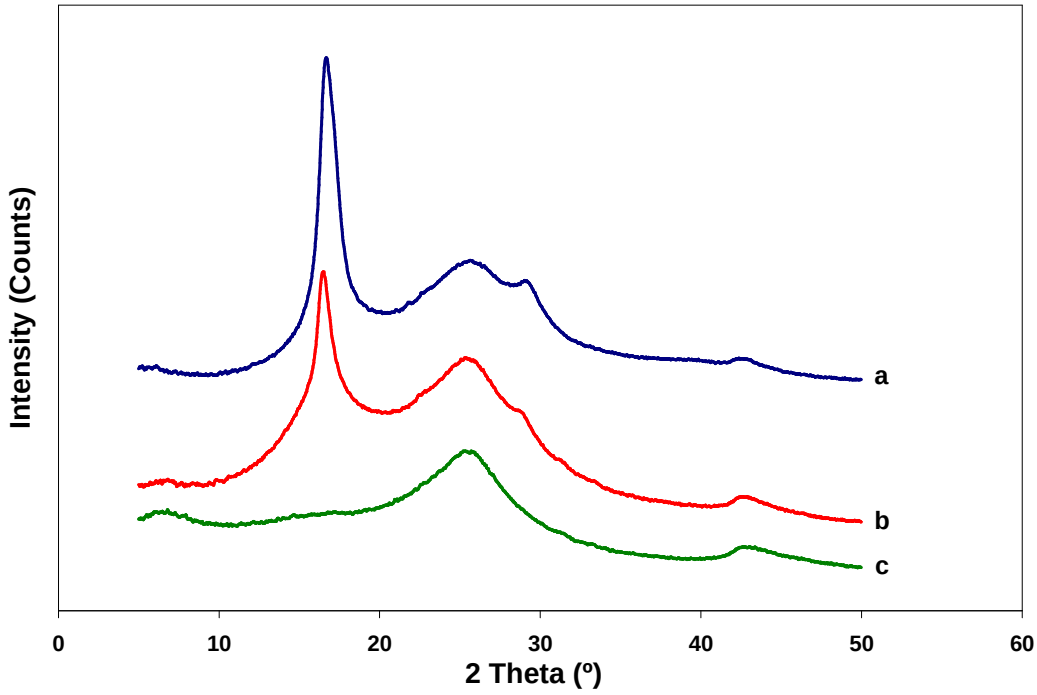

Figure 3.1 WAXD scans for unstabilized and stabilized PAN/CNT 80/20 films (for FK.82 series). Stabilization time (a) 0 h, (b) 8 h, and (c) 16 h.

3.3.3 Effect of molarity of impregnating agent

The amount of KOH impregnated into stabilized PAN/CNT (80/20) samples (FK.82.8 series) was controlled by varying the molarities of aqueous KOH (1M, 3M, 6M and 10M KOH immersed for up to 24 hours). The amount of KOH pick up from each solution at 2, 8 and 24 hours is given in Figure 3.3.

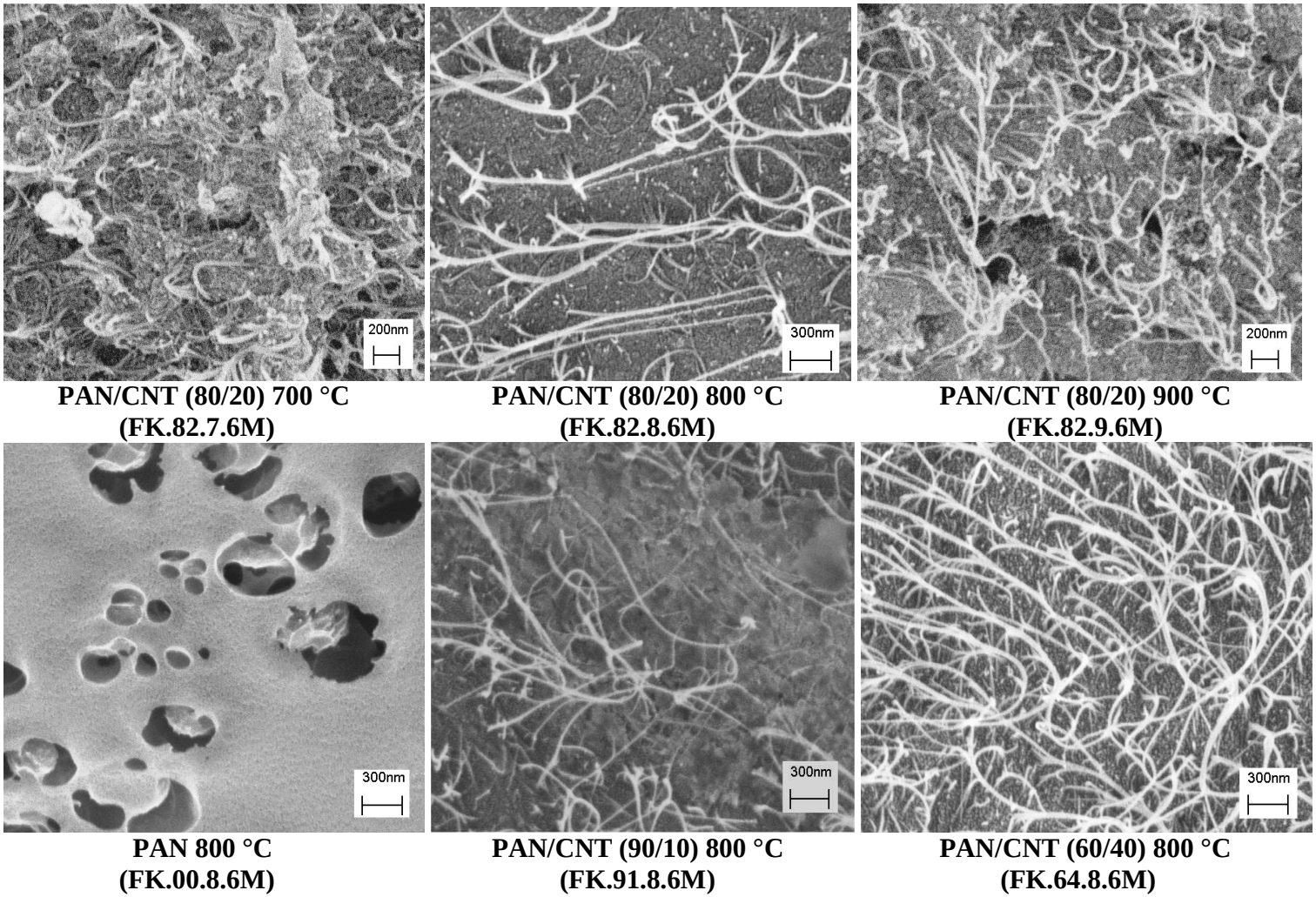

Figure 3.2 Scanning electron micrographs of activated PAN and PAN/CNT (FK series) films with different activation temperatures and compositions activated using 6M KOH.

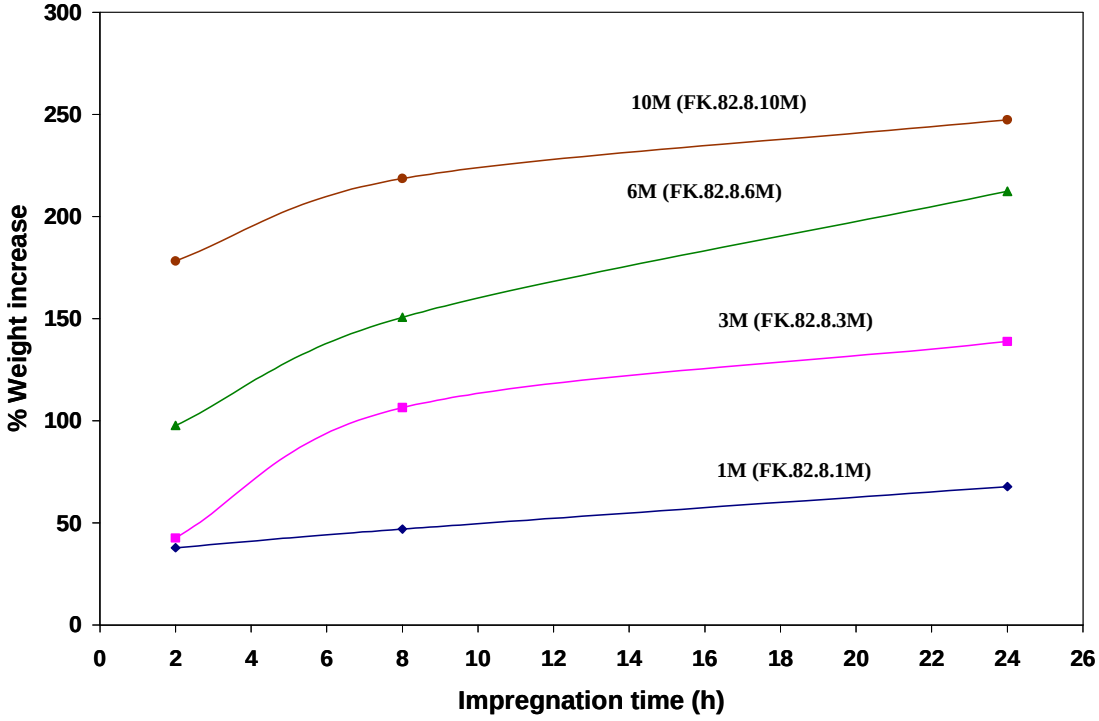

Figure 3.3 Amount of KOH pick up by PAN/CNT 80/20 film (FK.82 series) during immersion in 1, 3, 6 and 10M KOH for 2, 8 and 24 h. The samples were dried at 90 °C for 24 hours before weighing.

An increasing trend in amount of KOH pick up has been observed with increasing molarity as well as impregnation time. Hence, by controlling the impregnation time or molarity of the activation agent, the degree of chemical activation can be controlled. The samples impregnated in 1M and 3M KOH for 24 hours were dried and activated at 800 ºC. The pore size distribution and BET surface area show an increasing trend with increase in molarity.

The BET surface area of 538, and 1170 m^2/g for 1 and 3M (FK.82.8.1M and FK.82.8.3M) increases to 1740 and 1480 m^2/g for 6 and 10M samples (FK.82.8.6M and FK.82.8.10M). The specific capacitance, energy density and power density of 6 and 10M

samples were significantly higher than 1M and 3M samples as expected (Figure 3.4b and 3.5b). Comparable specific capacitances were obtained by constant current test as well as cyclic voltammetry as shown for 6M KOH activated sample (Figure 3.4b).

3.3.4 Effect of activation temperature

The surface area and electrochemical properties were evaluated to determine the optimum process conditions. The sample activated at 700 ºC (FK.82.7.6M) showed pores in the range of 1 - 2.5 nm while samples activated at 800 ºC (FK.82.8.6M) show increased pore size distribution from 1 - 5 nm (Figure 3.6). The BET surface area for various samples are given in Table 3.l. The lower surface area values for PAN/CNT (80/20) samples activated at 700 ºC compared to 800 ºC can be due to lower degree of conversion to carbon which is consistent with literature for carbon-carbon composites[19]. Further increase in activation temperature to 900 ºC (FK.82.9.6M) did not change the pore size distribution and BET surface area (1700 m^2/g) significantly (Figure 3.6 and Table 3.1). Similar increase in surface area and nitrogen absorption was reported by Teng[7] for activated bituminous coal based porous carbon from 500 – 800 ºC due to continuous removal of amorphous carbon as volatiles. Above 800 ºC, the nitrogen absorption decreased with increased temperature due to collapsed pore structure upon thermal treatment. Surface areas of PAN/CNT films of samples heat treated at 800 and 900 ºC were comparable due to possible collapse of additional pores created above 800 ºC. Similar study conducted by Moon[4] on PAN based carbon fibers at activation temperature range of 700 – 900 ºC showed that highest surface area was obtained at 800 ºC. Hence, 800 ºC is concluded as optimum activation temperature resulting in maximum values of surface area and pore volume. This is used as activation temperature for

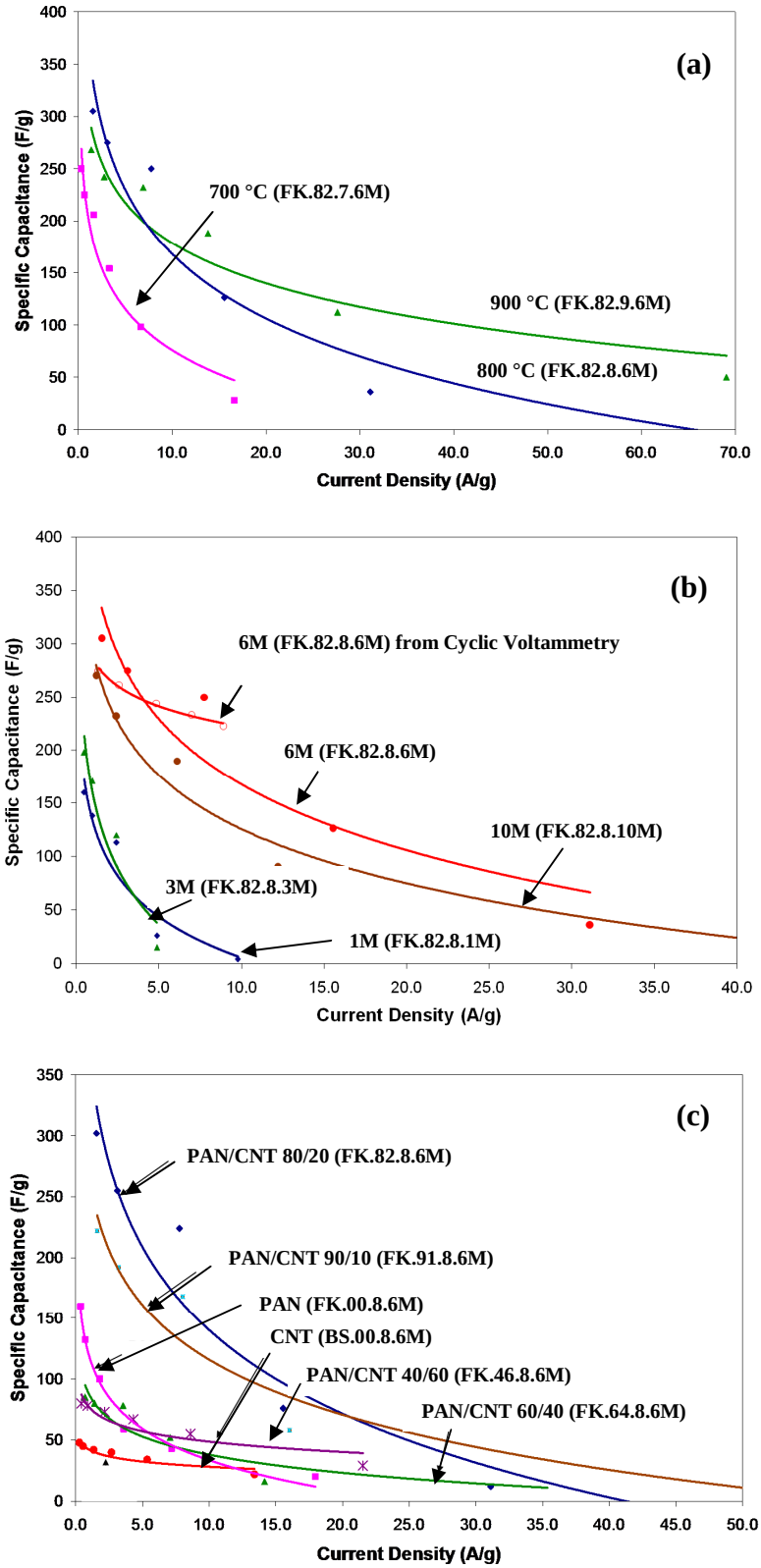

Figure 3.4 Specific capacitance as a function of current density measured in 6M KOH electrolyte for PAN/CNT films. The effect of (a) activation temperature, (b) molarities of impregnating activating agent, and (c) composition of PAN/CNT film.

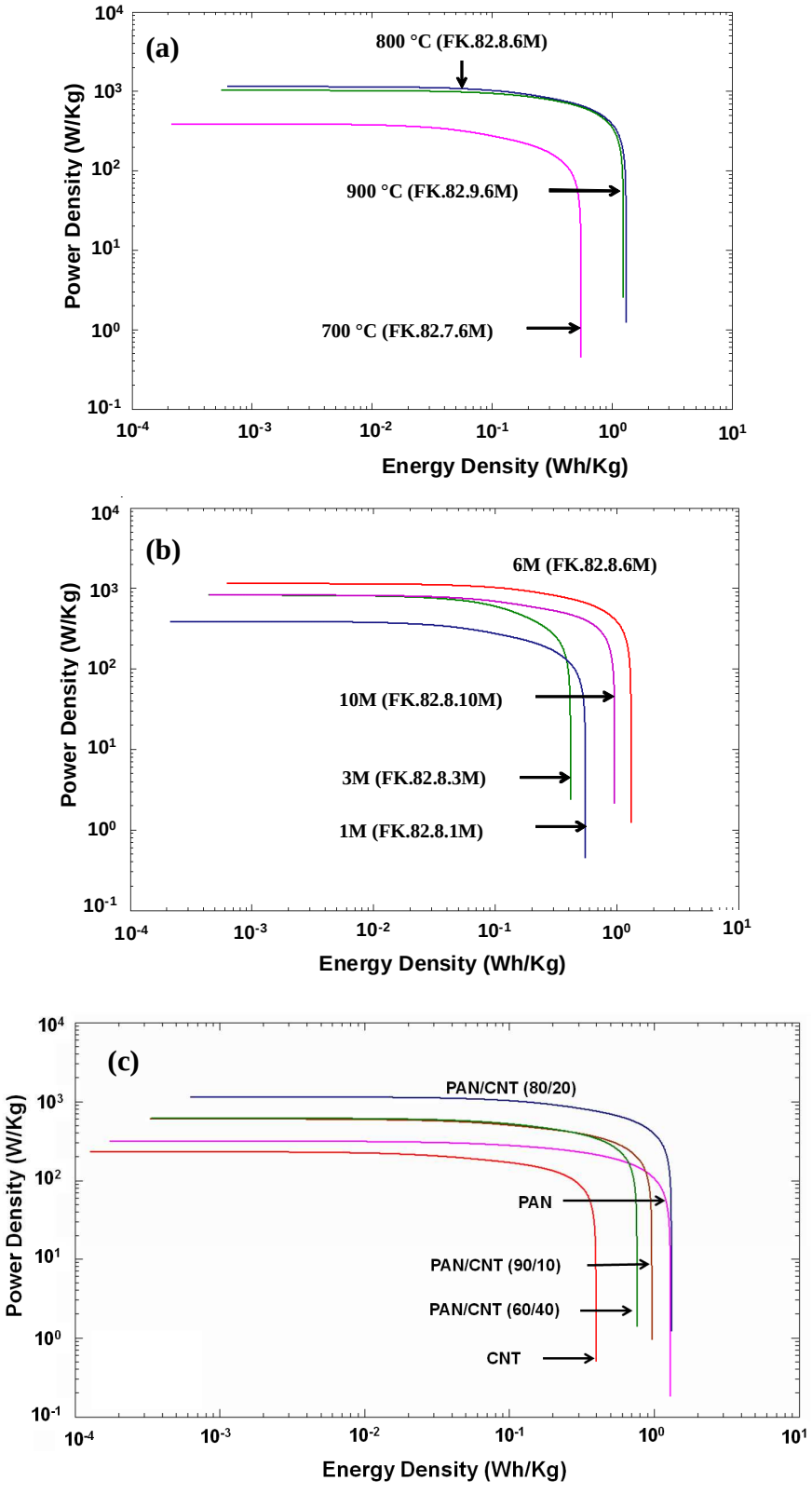

Figure 3.5 Power density and Energy density measured at 0.5 mA galvanostatic test measured in 6M KOH electrolyte for PAN/CNT films. The effect of (a) activation temperature, (b) molarities of impregnating activating agent, and (c) composition of PAN/CNT film.

Table 3.1 Specific capacitance, surface area, porosity and double layer capacity for KOH activated PAN/CNT films.

Label	Sample	Specific capacitance (F/g) (0.1 mA constant current		Surface Area (m^2/g)		Average pore size	Energy Density*	Power Density*	Double layer capacitance (μF/cm^2)**		Pore volume (cm^3/g)
		6M KOH	BMIMBF$_4$:AC (1:2)	BET	DFT	(nm)	(Wh/Kg)	(W/Kg)	BET	DFT	
Effect of Activation temperature (PAN/CNT 80/20, 6M KOH Activation)											
FK.82.7.6M	700 ºC	250	109	750	254	2.1	0.55	310	33	98	0.17
FK.82.8.6M	800 ºC	302	184	1740	715	2.2	1.32	1350	17	42	0.66
FK.82.9.6M	900 ºC	268	180	1700	668	2.4	1.26	1320	16	40	0.67
Effect of Molarity (PAN/CNT 80/20, 800 ºC)											
FK.82.8.1M	1 M KOH	160	60	538	172	2.0	0.55	390	30	93	0.32
FK.82.8.3M	3 M KOH	198	120	1170	404	2.1	0.43	820	17	49	0.29
FK.82.8.6M	6M KOH	302	184	1740	715	2.2	1.32	1350	16	38	0.66
FK.82.8.10M	10M KOH	270	184	1479	643	2.7	0.97	825	18	42	0.78
Effect of composition (PAN/CNT 800 ºC, 6M KOH Activation)											
FK.00.8.6M	PAN	167	150	880	273	2.4	1.30	315	19	61	0.26
FK.91.8.6M	PAN/CNT (90/10)	206	190	1120	410	2.3	0.97	600	18	50	0.39
FK.82.8.6M	PAN/CNT (80/20)	302	184	1740	715	2.2	1.32	1350	17	42	0.66
FK.64.8.6M	PAN/CNT (60/40)	83	90	820	349	3.1	0.76	615	10	24	0.49
FK.46.8.6M	PAN/CNT (40/60)	90	68	830	349	3.2	1.10	410	11	26	0.49
BS.00.8.6M	CNT	45	68	625	272	5.8	0.40	230	7	17	0.77

*Energy density and Power density measured at galvanostatic test at 0.5 mA using KOH electrolyte.
**Double layer capacitance reported for 6M KOH electrolyte.

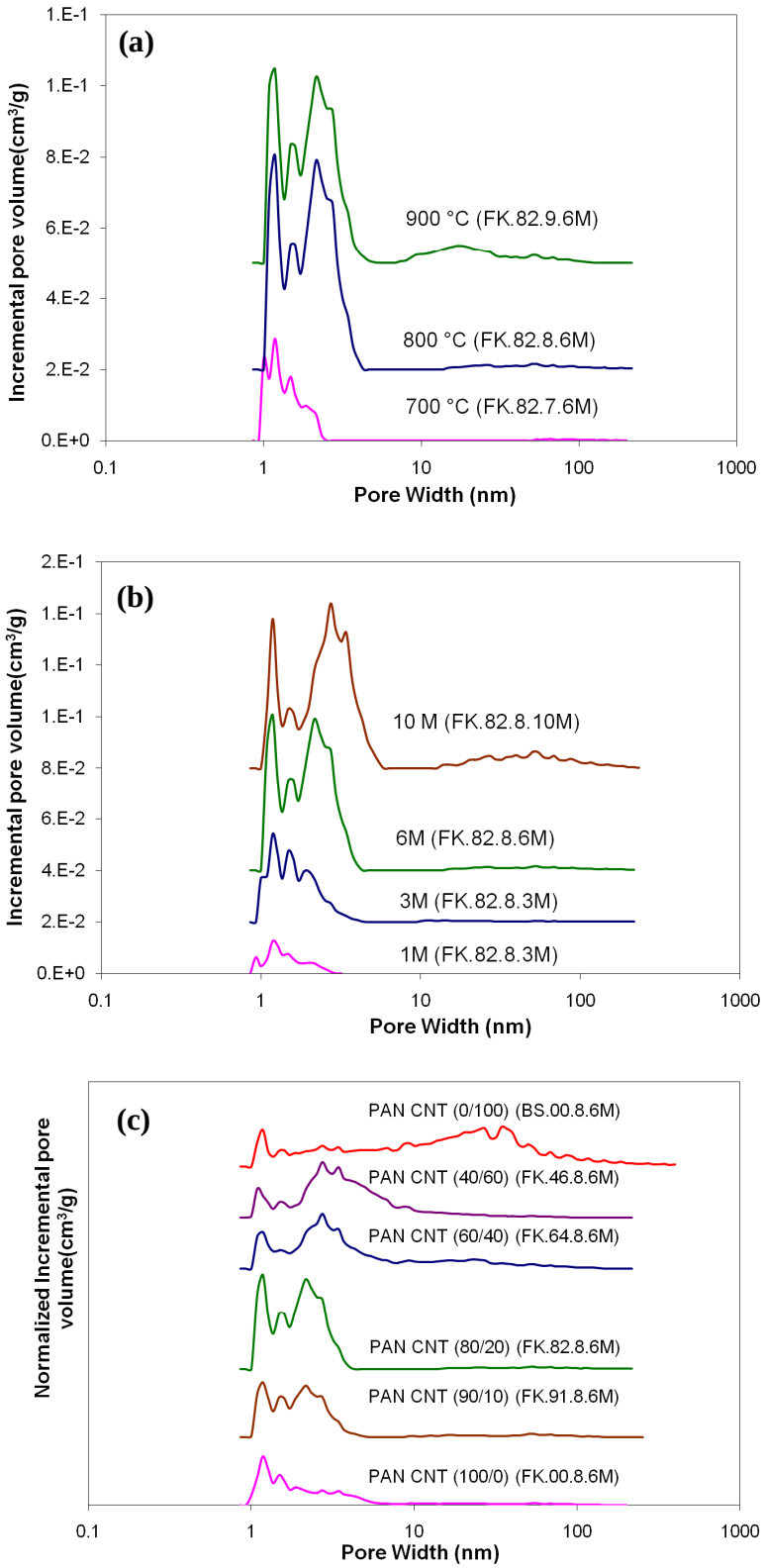

Figure 3.6 Pore volume distributions for PAN/CNT films (FK series) activated at different processing conditions to understand the effect of (a) activation temperature, (b) molarities of impregnating activating agent, and (c) composition of PAN/CNT film.

optimizing other process conditions, namely, molarity and composition. The specific capacitance for samples activated at different temperatures reported in Figure 3.4a shows a trend similar to that of the surface areas. The lower values of specific capacitance for samples activated at 700 ºC (FK.82.7.6M) due to lower surface area achieved by lower degree of carbonization is similar to the observation made for physically activated samples[20, 21]. The specific capacitance of 250 F/g observed for samples activated at 700 ºC can possibly have contributions from both pseudocapacitance as well as double layer capacitance. This value is ~ 302 F/g for 800 ºC activated sample and 268 F/g for 900 ºC samples. An increase of energy and power density was also observed for samples activated at 800 and 900 ºC compared to 700 ºC samples as expected (Figure 3.5a).

3.3.5 Effect of composition of PAN/CNT films

The CNT loading in PAN/CNT films was varied to study the influence of composition on pore size distribution and specific capacitance of activated films. The BET surface area increased from ~ 880 m^2/g for PAN films (FK.00.8.6M) to 1120 m^2/g for 90/10 films (FK.91.8.6M), and to a maximum of ~ 1740 m^2/g for 80/20 films (FK.82.8.6M). The values then decreased to ~ 820 m^2/g for 60/40, 40/60 films and ~ 625 m^2/g for activated CNT buckypaper (FK.64.8.6M, FK.46.8.6M and BS.00.8.6M). An important observation made in this study is that the pore size distribution increased to a wider range with increase in nanotube content as given in Figure 3.6c. The average pore size of ~ 2 nm in 0-20 % CNT samples increased to ~ 3 nm for 40-60 % sample and ~ 6 nm for activated CNT buckypaper (Table 3.1). All samples show pores predominantly in the 1-5 nm range, with two prominent peaks at 1.2 and 2.5-2.7 nm range. The first peak is more prominent for PAN films while the pore size distribution becomes wider with CNT

content, as noted by the increase in intensity of second peak. The specific capacitance as well as energy and power densities correlate to the BET surface areas measured for all compositions (Figure 3.4c and 3.5c). The power densities, expected to increase with CNT content, did not show a clear trend with change in PAN/CNT composition. The power density of CNT buckypaper electrode were lower than that for the PAN films, similar to the results reported by Liu[22]. Even though the contact resistance of overlapping tubes could be a possible reason for drop in power density, there is no clear understanding of this behavior at this point.

3.3.6 Correlation between pore size and specific capacitance

The specific capacitance values measured by varying activation time, molarity as well as composition of the films (FK series) are plotted with micro, meso, and macro pore volumes in Figure 3.7. In all cases, micro pores appear to have direct correlation with specific capacitance, and contribute to its increase. While no definite correlation has been established between specific capacitance, electrolyte ion size and pore sizes of electrodes in literature, micropores seem to contribute to higher specific capacitance in these chemically activated PAN/CNT films (FK series) when tested in 6M KOH (ionic radius – K^+ - 1.38 Å and OH^- - 1.33 Å)[23].

3.3.7 Cycle life study

The cyclic voltammetry test has been performed for 10,000 cycles to determine the life cycle activated PAN/CNT films with different compositions (Figure 3.8). The specific capacitance and energy density of activated CNT buckypaper films remained fairly constant for 10,000 cycles while activated PAN film (FK.00.8.6M) with initial

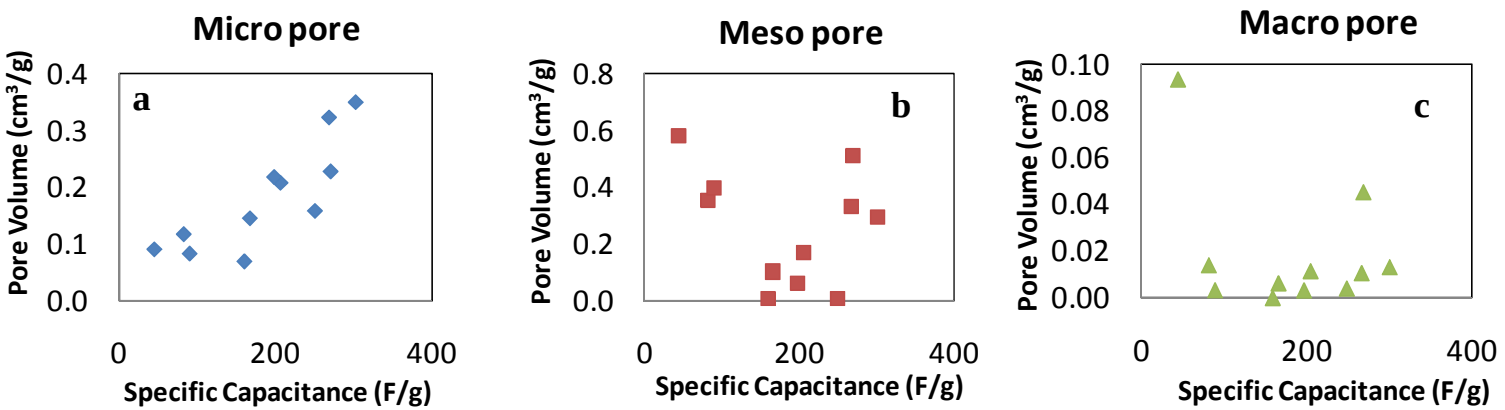

Figure 3.7. Correlation between specific capacitance measured in 6M KOH electrolyte and pore sizes for PAN/CNT films (FK series) activated at different processing conditions (a) micropore, (b) mesopores, and (c) macropore. All conditions from Table 3.1 are included.

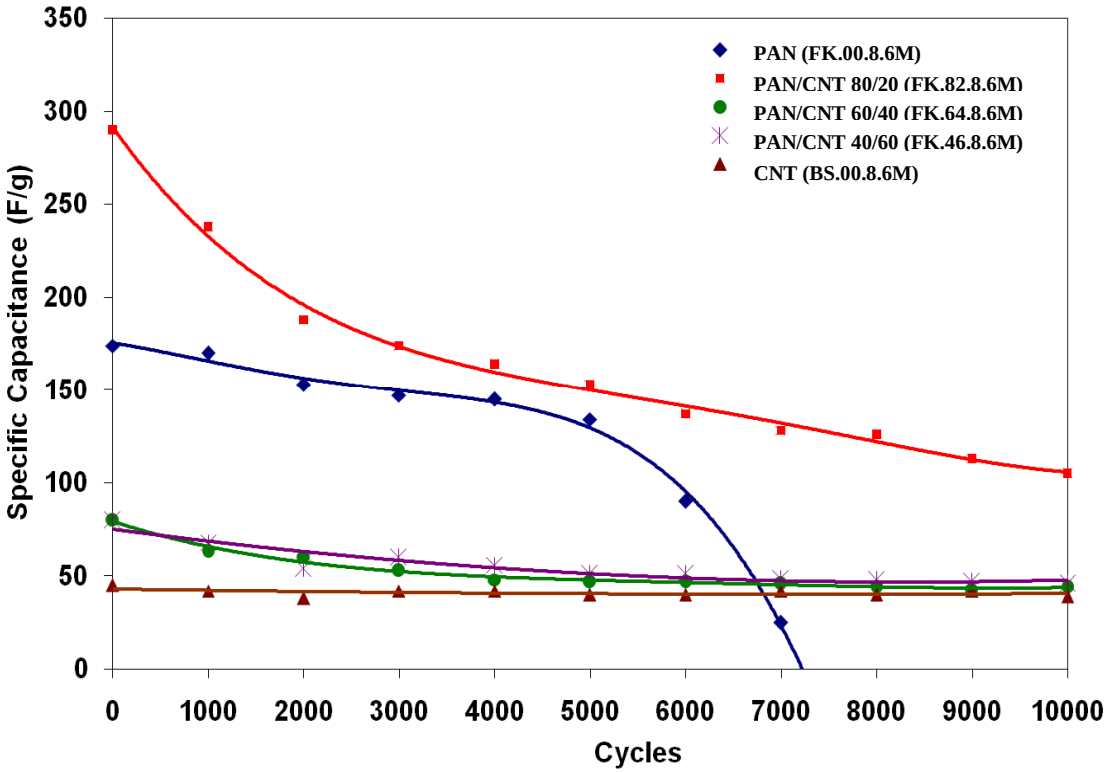

Figure 3.8. Changes in specific capacitance for PAN/CNT films with different compositions measured at 100 mV/s scan rate cyclic voltammetry test in 6M KOH electrolyte for 10,000 cycles. Data points were collected at 5 mV/s scan rate after every 1000 cycles.

specific capacitance of ~ 175 F/g initially looses its capacitance to lower than 20 F/g above 7000 cycles. The PAN/CNT film looses its capacitance to 55-60 % of its initial value after 10000 cycles for 60/40 and 40/60 compositions (FK.64.8.6M and FK.46.8.6M) while the capacitance of 80/20 films (FK.82.8.6M) decreased to 39 % of initial value. Hence, the cycle life of activated PAN/CNT films improves with increase in the CNT content due to increase in concentration of electrochemically stable CNTs.

3.3.8 Ionic liquid electrolyte

Ionic liquids as electrolyte offer a greater operating voltage window, and high thermal stability as compared to aqueous electrolytes. The decomposition voltage of ionic liquids can be between 3-4 V depending on the type of anion as well as cation while the aqueous

electrolytes are limited to a decomposition voltage of 1.2 V. This distinct advantage of ionic liquids can be made use in supercapacitors to approach and even match the energy densities of batteries and fuel cells. Zhou[24] evaluated 1-butyl-3-methylimidazolium tetrafluoroborate ($BMIMBF_4$), 1-butyl-3-methylimidazolium hexafluoro - phosphate($BMIMPF_6$), 1-butyl-3-methylimidazolium chloride (BMIMCl), and a mixture of ionic liquid/acetonitrile (AN) electrolytes with PAN/CNT film and SWNT buckypaper electrodes. The electrolyte with $BMIMBF_4$/AN (1:2) ratio resulted in better wetting of electrodes than pure $BMIMBF_4$ as measured by contact angle. For a given electrode, higher specific capacitance is obtained for BMIMBF4 than $BMIMPF_6$ as well as BMIMCl systems. Hence, $BMIMBF_4$/AC (1:2) is chosen for this study on PAN/CNT films (FK series). The specific capacitance of PAN/CNT (80/20) film (FK.82.8.6M) activated at 800 °C decreased from ~ 302 F/g to ~ 184 F/g when tested with $BMIMBF_4$/AC system (Figure 3.9a). However, huge increase of energy density from ~ 2 Wh/Kg in 6M KOH to ~ 22 Wh/Kg in $BMIMBF_4$/AC was achieved at 0.1mA constant current by increasing the operating voltage from 0.8 to 3.0 V respectively (Figure 3.9c).

The specific capacitance reduced to half (120 F/g at 0.1 mA galvanostatic test) for samples activated at 700 ºC (FK.82.7.6M) when $BMIMBF_4$/AC electrolyte was used in place of 6M KOH due to larger size ($BMIM^+$ - 3.39 Å compared to K^+ - 1.38 Å) and lower mobility of electrolyte ions. This value increases to ~ 184 F/g for 800 ºC activated sample and 180 F/g for 900 ºC samples (FK.82.9.6M) (Figure 3.10a) due to increased pore volume.

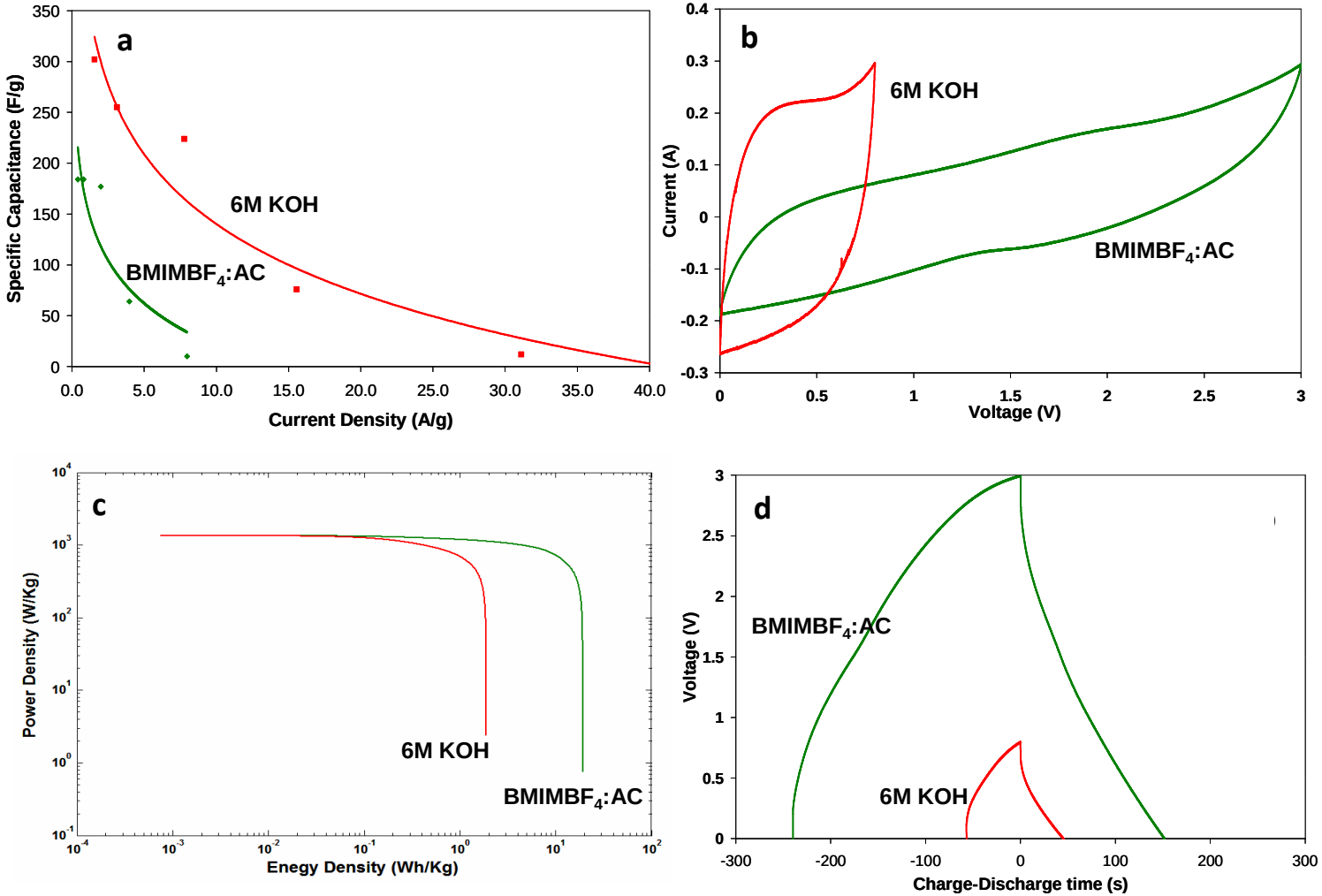

Figure 3.9 Effect of electrolytes (6M KOH and $BMIMBF_4$:Acetonitrile (1:2 ratio)) on electrochemical properties for PAN/CNT (80/20) films (FK.82.8.6M) (a) Specific capacitance as a function of current density, (b) cyclic voltammogram measured at 5mV/s scan rate (c) energy density and power density, and (d) charge-discharge curves both measured at 0.5 mA galvanostatic test.

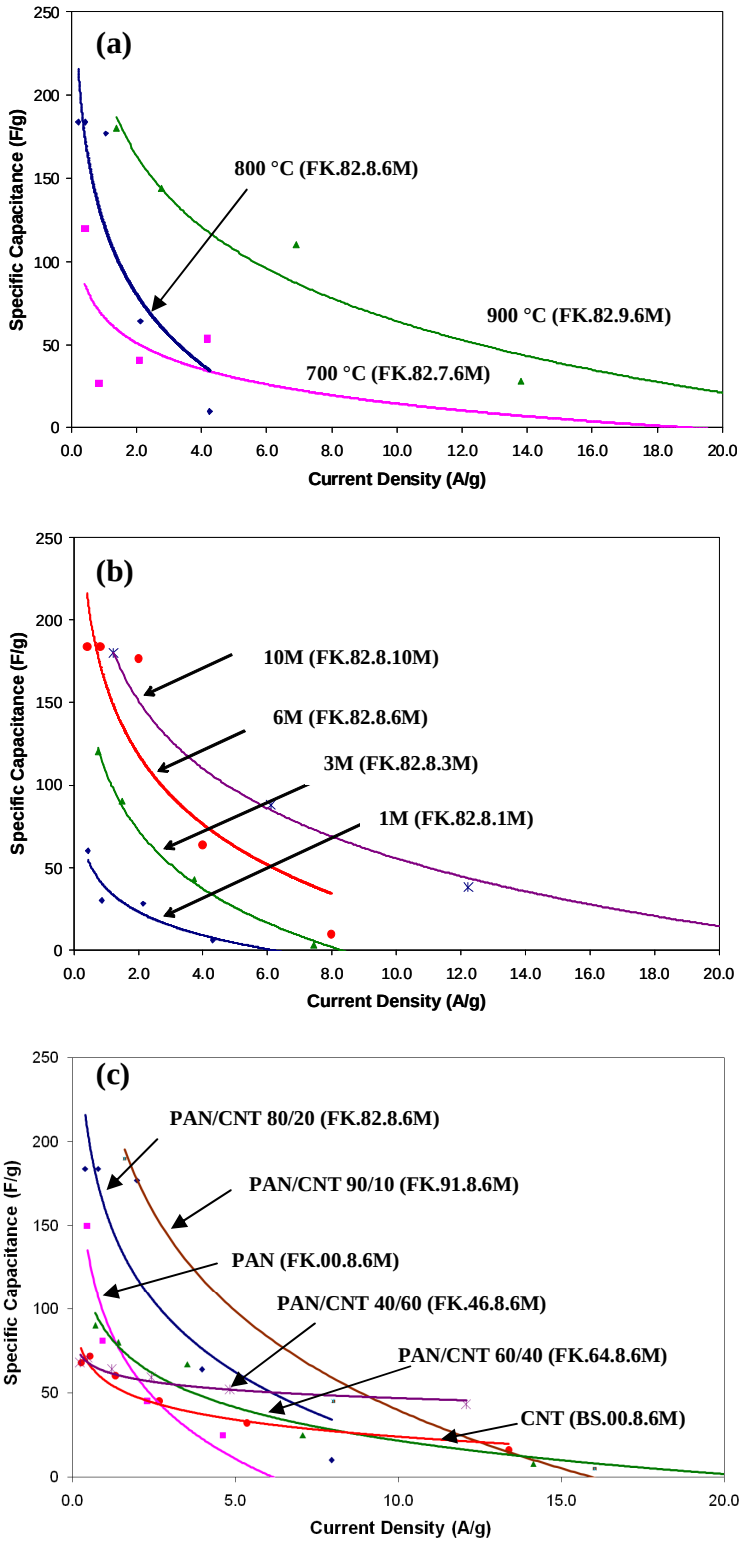

Figure 3.10 Specific capacitance as a function of current density measured in BMIMBF4/AN(1:2) electrolyte for PAN/CNT films (FK series) activated at different processing conditions to understand the effect of (a) activation temperature, (b) molarities of impregnating activating agent, and (c) composition of PAN/CNT film.

When the molarity of impregnating agent is varied (1, 3, 6, and 10M – FK.82.8 series), an increase of specific capacitance was observed (60, 120, 184, and 184 F/g respectively) (Figure 3.10b). The specific capacitance of PAN/CNT sample (FK.82 series) with 0-20 wt % CNT content were more than 150 F/g in $BMIMBF_4$/AC while the values decreased to ~ 90 F/g for 40 % and 68 F/g for 60% and higher CNT sample (Figure 3.10c). Similar to results from 6M KOH electrolyte, micro pores have direct correlation with specific capacitance in $BMIMBF_4$/AC also, and meso pores, to a lower extent[23, 25] as given in Figure 3.11.

The specific capacitance, energy density, and power density of PAN/CNT sample (FK series) followed similar trend in $BMIMBF_4$/AC as samples tested with 6M KOH electrolyte. The activation temperature of 800 ºC (FK.82.8.6M) showed the highest energy density of ~ 22 Wh/Kg (Figure 3.12a). 6M, and 10M KOH activated samples showed significantly higher energy density than 1M and 3M samples due to higher surface area and pore volume (Figure 3.12b).

As for the composition effect (FK series), samples with lower nanotube content (PAN, PAN/CNT 90/10) show lower energy density compared to PAN/CNT 60/40, 40/60 and CNT buckypaper electrodes in $BMIMBF_4$/AC. This is an inverse trend in energy densities measured in 6M KOH electrolytes where higher energy densities are obtained for samples with lower CNT content (Figure 3.5c). These results are comparable to reports from C Zhou[24] where higher energy density and specific capacitance, than activated PAN/CNT films, were obtained for buckypaper electrodes with larger pore sizes when tested with ionic liquid electrolytes with larger ion sizes.

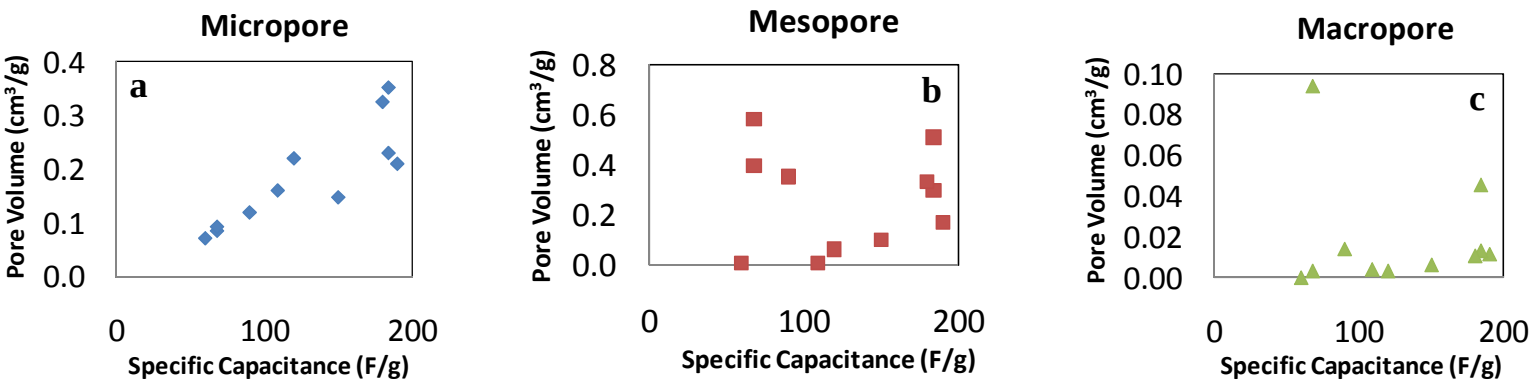

Figure 3.11. Correlation between specific capacitance measured in $BMIMBF_4$/AC electrolyte and pore sizes for PAN/CNT films (FK series) activated at different processing conditions (a) micropore, (b) mesopores and (c) macropore. All conditions from Table 3.1 are included.

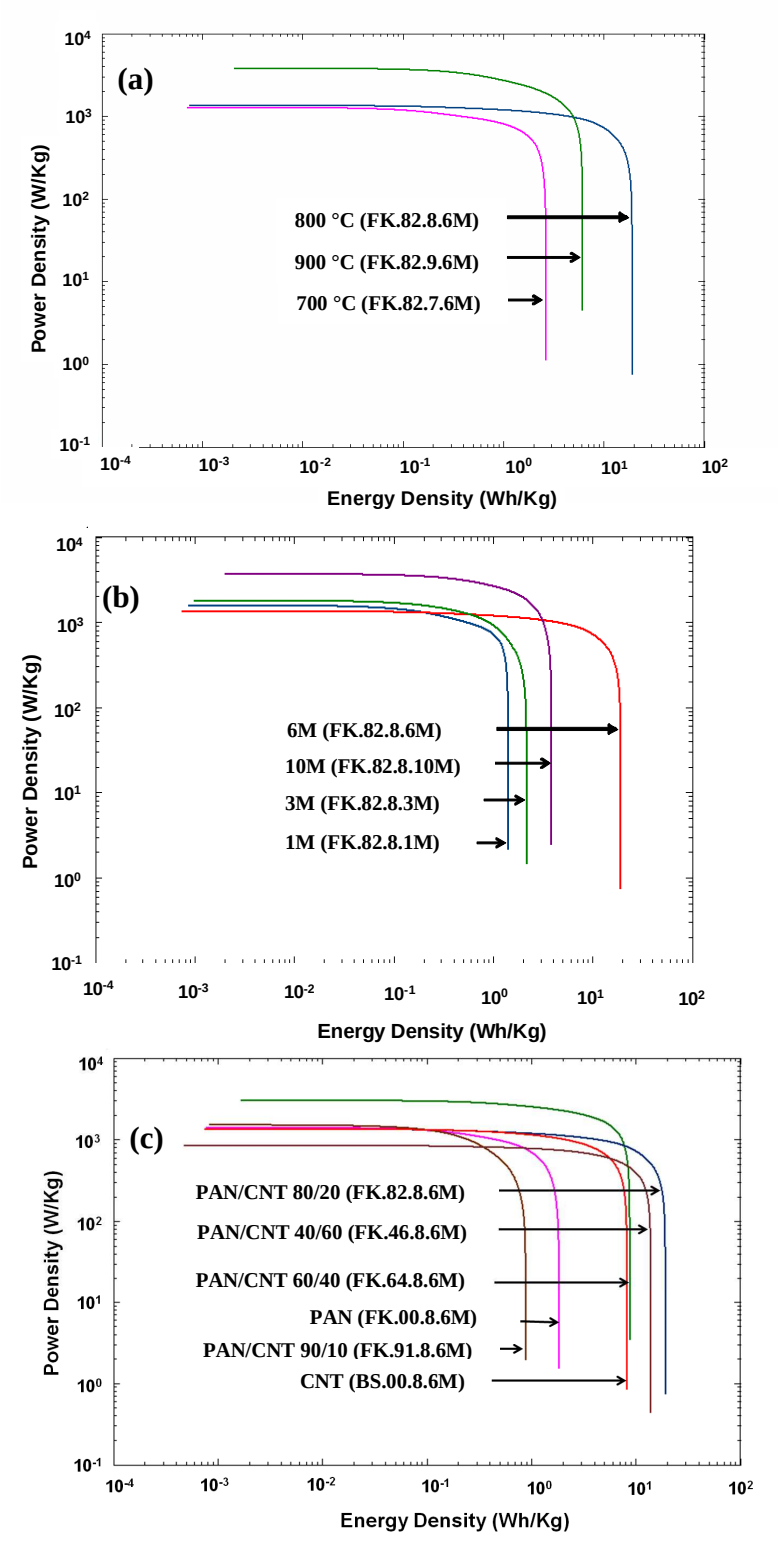

Figure 3.12 Power density and Energy density measured at 0.5 mA galvanostatic test measured in $BMIMBF_4$:AN(1:2) electrolyte for PAN/CNT films activated at different processing conditions to understand the effect of (a) activation temperature, (b) molarities of impregnating activating agent, and (c) composition of PAN/CNT film.

Conversely, CO_2 activated PAN/CNT samples with smaller pore sizes showed enhanced energy density and specific capacitance in 6M KOH[24]. Hence, higher energy density can be achieved by increasing the operating voltage to 3V and pore sizes in the electrode material can be changed by varying the CNT content in composite electrodes for specific applications.

From this study on KOH activated PAN/CNT films, 800 ºC is concluded to be the optimum activation temperature (FK.82.8.6M). Literature studies[4, 7] report collapse of additional pores created when the heat treatment temperature is increased above 800 ºC causing a decrease in surface area. Similar pores collapse was observed for PAN/CNT films in this chapter. A 6M KOH impregnation solution resulted in highest specific capacitance. The maximum uptake of potassium ions was observed for 6M and 10M KOH solutions showing that a saturation value reached beyond a molarity of 6M KOH. The PAN/CNT film with composition of 80/20 is concluded to have optimum balance between porosity and rigidity of electrode. The porosity decreases with increase in CNT content while the rigidity increases with increase in CNT content up to 60 wt%, both reaching a balance at 20 wt % concentration.

3.4 Conclusions

Polyacrylonitrile/carbon nanotube film based electrodes have been prepared by chemical activation with potassium hydroxide for electrochemical capacitors. The influence of activation temperature, molarity of activating agent, and composition of PAN/CNT precursor films on specific capacitance, pore distribution and surface area have been studied in 6M KOH and $BMIMBF_4$/AC electrolytes. PAN/CNT film (FK.82.8.6M) impregnated with 6M KOH and activated at 800 ºC is found to be the

optimum process condition and composition for PAN/CNT systems resulting in a maximum specific capacitance of ~ 302 F/g. When CNT content is increased in PAN/CNT films to understand the influence of composition, a bi-modal pore distribution is observed. The pores at 1.2 nm as well as 2.5-2.7 nm range were observed for KOH activated PAN films. With increase in CNT content, density of pores at 2.5-2.7 nm increased when compared to 1.2 nm pores.

PAN/CNT 80/20 ratio is found to be the optimum composition to achieve maximum specific capacitance of ~ 302 F/g. Molarity and impregnation time have influence on amount of KOH picked up during impregnation as well as resulting surface areas and specific capacitance. The specific capacitance, energy density, and power density of 6M, 10M samples were significantly higher than 1M and 3M. A significant increase of energy density ~ 2 Wh/Kg in 6M KOH to ~ 22 Wh/Kg in $BMIMBF_4$/AC was achieved by increasing the operating voltage from 0.8 V to 3.0 V respectively. The cycle life of activated PAN/CNT films increases with an increase in the CNT content. The specific capacitance of activated CNT buckypaper remained constant throughout 10,000 cycles while activated PAN based electrodes (FK.00.8.6M) reduced to negligible value after 7000 cycles. Micropores make a significant contribution to the capacitance performance of these materials in both 6M KOH as well as $BMIMBF_4$/acetonitrile electrolytes while correlating the specific capacitance with surface area, pore size, and pore size distribution.

3.5 References

[1] Ahmadpour A, Do DD. The preparation of active carbons from coal by chemical and physical activation. Carbon. 1996;34(4):471-9.

[2] Illan-Gomez MJ, Garcia-Garcia A, Salinas-Martinez de Lecea C, Linares-Solano A. Activated Carbons from Spanish Coals. 2. Chemical Activation. Energy Fuels. 1996;10(5):1108-14.

[3] Macia-Agullo JA, Moore BC, Cazorla-Amoros D, Linares-Solano A. Activation of coal tar pitch carbon fibres: Physical activation vs. chemical activation. Carbon. 2004;42(7):1367-70.

[4] Moon SY, Kim M-s, Hahm H-S, Lim Y-S. Preparation of activated carbon fibers by chemical activation method with hydroxides. Material Science Forum. 2006;510-511:750-3.

[5] Phan NH, Rio S, Faur C, Le Coq L, Le Cloirec P, Nguyen TH. Production of fibrous activated carbons from natural cellulose (jute, coconut) fibers for water treatment applications. Carbon. 2006;44(12):2569-77.

[6] Raymundo-Pinero E, Azais P, Cacciaguerra T, Cazorla-Amoros D, Linares-Solano A, Beguin F. KOH and NaOH activation mechanisms of multiwalled carbon nanotubes with different structural organisation. Carbon. 2005;43(4):786-95.

[7] Teng H, Hsu LY. High-Porosity Carbons Prepared from Bituminous Coal with Potassium Hydroxide Activation. Ind Eng Chem Res. 1999;38(8):2947-53.

[8] Xue R, Shen Z. Formation of graphite-potassium intercalation compounds during activation of MCMB with KOH. Carbon. 2003;41(9):1862-4.

[9] Lee J, Kim J, Kim S. Microtexture and electrical properties of PAN-ACF. Journal of Materials Science. 2007;42(7):2486-91.

[10] Lee J-G, Kim J-Y, Kim S-H. Effects of microporosity on the specific capacitance of polyacrylonitrile-based activated carbon fiber. Journal of Power Sources. 2006;160(2):1495-500.

[11] Xu B, Wu F, Chen R, Cao G, Chen S, Zhou Z, et al. Highly mesoporous and high surface area carbon: A high capacitance electrode material for EDLCs with various electrolytes. Electrochemistry Communications. 2008;10(5):795-7.

[12] Lozano-Castello D, Lillo-Rodenas MA, Cazorla-Amoros D, Linares-Solano A. Preparation of activated carbons from Spanish anthracite: I. Activation by KOH. Carbon. 2001;39(5):741-9.

[13] Teng H, Yeh TS. Preparation of Activated Carbons from Bituminous Coals with Zinc Chloride Activation. Ind Eng Chem Res. 1998;37(1):58-65.

[14] Lozano-Castello D, Macia-Agullo JA, Cazorla-Amoros D, Linares-Solano A, Muller M, Burghammer M, et al. Isotropic and anisotropic microporosity development upon chemical activation of carbon fibers, revealed by microbeam small-angle X-ray scattering. Carbon. 2006;44(7):1121-9.

[15] Bansal RC, Donnet J-B, Stoeckli F. Active carbon Marcel Dekker, Inc New York. 1988.

[16] Marsh H, Rodriguez-Reinoso F. Oxford: Activated Carbon, Elsevier Science Ltd 2006:322-65.

[17] Yu M-J, Bai Y-J, Wang C-G, Xu Y, Guo P-Z. A new method for the evaluation of stabilization index of polyacrylonitrile fibers. Materials Letters. 2007;61(11-12):2292-4.

[18] Lee Y-J, Kim J-H, Kim J, Lee DB, Lee J-C, Chung Y-J, et al. Fabrication of activated carbon fibers from stabilized PAN-based fibers by KOH. Materials Science forum. 2004;449-452:217-20.

[19] Kim J, Lee WI, Lafdi K. Numerical modeling of the carbonization process in the manufacture of carbon/carbon composites. Carbon. 2003;41(13):2625-34.

[20] Donnet J-B. Carbon Fibers. New York Marcel Dekker, Inc. 1998.

[21] Patrick JW. Porosity in Carbons. Halsted Press. 1995.

[22] Liu T, Sreekumar TV, Kumar S, Hauge RH, Smalley RE. SWNT/PAN composite film-based supercapacitors. Carbon. 2003;41(12):2440-2.

[23] Huang J, Sumpter Bobby G, Meunier V. A Universal Model for Nanoporous Carbon Supercapacitors Applicable to Diverse Pore Regimes, Carbon Materials, and Electrolytes. Chemistry - A European Journal. 2008;14(22):6614-26.

[24] Zhou C. Carbon nanotube based electrochemical supercapacitors. PhD Thesis, Georgia Institute of Technology. 2006:42.

[25] Arzhantsev S, Jin H, Baker GA, Maroncelli M. Measurements of the Complete Solvation Response in Ionic Liquids. The Journal of Physical Chemistry B. 2007;111(18):4978-89.

Chapter 4

EFFECT OF PROCESS VARIABLES ON SPECIFIC CAPACITANCE AND PORE STRUCTURE OF CO_2 ACTIVATED POLY(ACRYLONITRILE)/CARBON NANOTUBE FILMS

4.1 Introduction

The electrical conductivity, porous structure, accessibility of ions, electrode processability, and chemical stability are the important factors for the development of electrochemical capacitor electrode materials [1-3]. The characteristics of the porous structure, pore size, and its distribution and pore volume fraction enables the formation of a large surface area that can be used either for the development of the electrical double layer to store the static charge or for the reversible chemical redox reaction sites to provide faradaic capacitance[1, 4]. Earlier studies on the capacitance performance of porous electrodes show that electrolyte access to the smaller pores is limited by a cut-off pore size up to several nanometers, depending on the electrolyte concentration and the applied voltage [5-7]. Only those pores larger than the cut-off pore size can be accessed by the electrolyte to form an electrical double layer. However, there is a recent report of anomalous increase in specific capacitance for sub-nanometer pore sizes[8]. This significant effect of pore structure on the electrochemical capacitor performance necessitates good pore structure control for this application. The heat-treatment and activation conditions are the important parameters for controlling the surface morphology, pore size, and pore size distribution of the activated carbon materials[9, 10]. The effect of process variables on specific capacitance and pore structure of PAN/CNT

composite films (FC series) activated by carbon-di-oxide activation are explored in this chapter.

4.2 Experimental

CNTs were obtained from Carbon Nanotechnologies, Inc (Houston, TX) (Grade X012UA, 1% catalytic impurity). PAN used in this study, poly(acrylonitrile-co-methylacrylate) containing 6.7 mol% methylacrylate, was obtained from Exlan, Co. (Japan). DMF purchased from Sigma-Aldrich was used as received. Detailed description of film preparation method, heat treatment conditions as well as characterization methods are given in chapter 2.

4.3 Results and Discussion

4.3.1 Structure and morphology

The SEM images of the samples activated at different times and temperature are given in Figure 4.1. The PAN polymer was carbonized to a lower degree at 700 ºC. The complete carbonization and exposure of more CNT bundles was observed when the activation temperature was increased to 900 ºC. The diameter of as-received CNT bundles measured by averaging 30 randomly selected bundles from high resolution SEMs were 18 ± 2 nm while the diameter of CNT bundles after activation at 800 ºC and all activation times for 900 ºC varied from 30 to 50 nm. This increase in diameter of CNT bundles after activation is due to PAN wrapping the CNT bundles. The bundle size of CNTs decreases during the sonication process due to removal of individual tubes. The increase in bundle size is significant considering that individual tubes are lost from the CNT bundle during sonication. The presence of CNTs increases the rigidity of the films

and its interaction with PAN reduces weight loss during the activation process as given in Table 4.1.

4.3.2 Residual weight measurement

The average residual weight loss for PAN/CNT composite films that was carbonized in an inert atmosphere (argon) at 700 °C for 30 minutes for all the samples and activated with CO_2 at different times and temperature are reported in Table 4.1. The weight loss of the PAN/CNT (80/20) composite films increased with activation temperature as 52 wt% residue for 700 °C decreased to 42 wt% residue for 900 °C at fixed activation time of 30 minutes. A further increase in weight loss was observed by increasing the activation time from 30 minutes (42 wt%) to 90 minutes (22 wt%). The weight loss decreased when the ratio of CNTs increased in the film composition as expected due to higher thermal stability of CNTs. The residual weight increased from 42 wt % to 54 wt % when the CNT content is increased from 20 to 40 wt%.

4.3.3 Gas adsorption isotherms

The pore structures of activated PAN/CNT electrodes heat treated at different activation conditions are probed using nitrogen gas adsorption. The nitrogen adsorption isotherms for CO_2 activated PAN/CNT samples with different compositions and heat treatment conditions are given in Figure 4.2. The type I absorption isotherm based on the IUPAC classification is exhibited by ideal microporous absorbents, while type IV isotherm is exhibited by mesoporous materials[11-13]. The activated carbon typically contains pores over a wide range of pore sizes, including micro and meso pores.

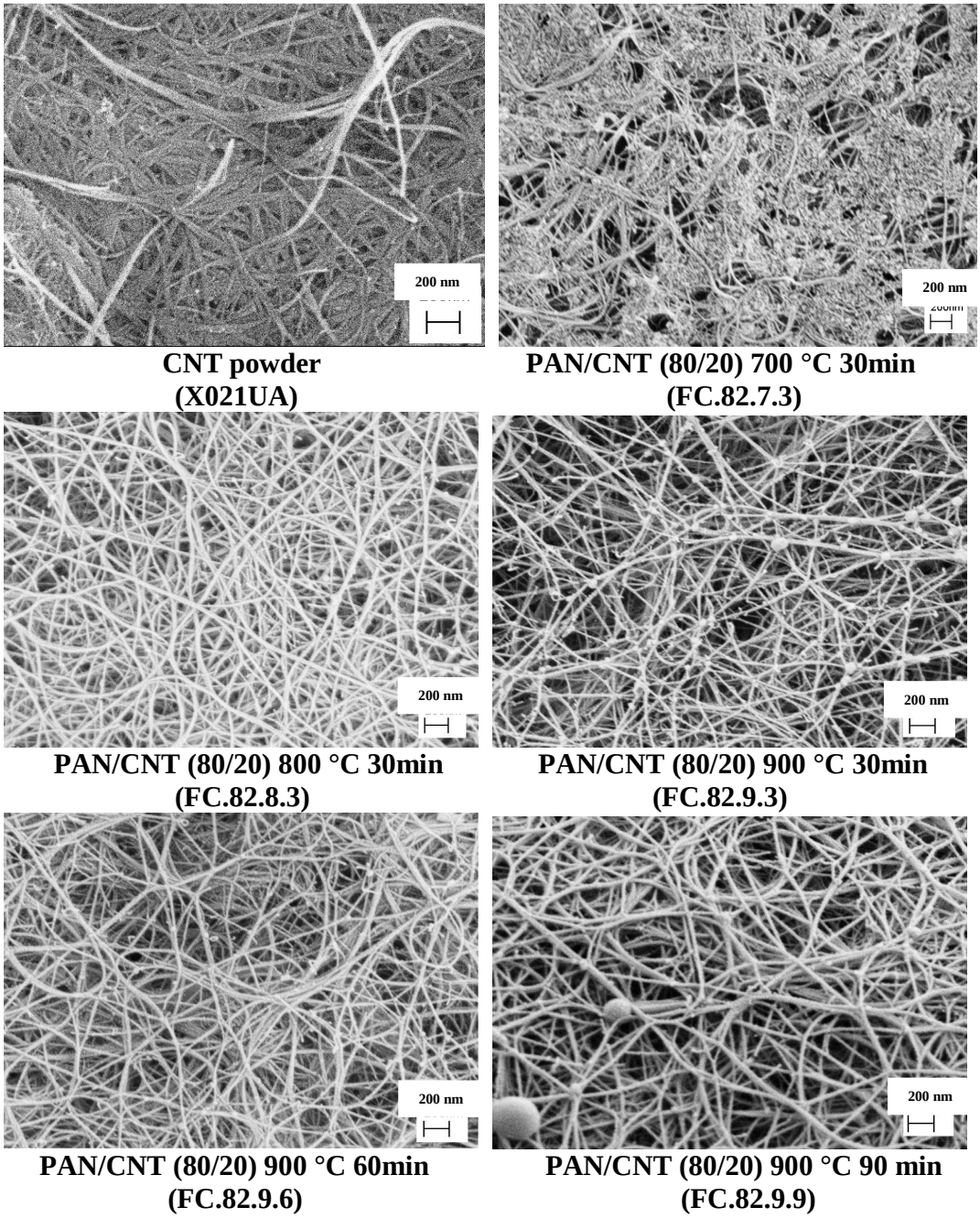

Figure 4.1 Scanning microscope images of CO_2 activated PAN/CNT (80/20) samples with different activation time and temperatures.

Table 4.1 Specific capacitance, surface area and pore volume distribution for CO_2 activated PAN/CNT films.

Label	Sample ratio	Acitvated film thickness	Activation Temperature	Activation Time	Residue	Specific capacitance	Surface (m^2/g) Area		Energy Density*	Power* Density	Double layer capacitance ($\mu F/cm^2$)**		Pore Volume
	%	μm	°C	Min	%	F/g	BET	DFT	Wh/Kg	W/Kg	BET	DFT	(cm3/g)
(a) Temperature effect													
FC.82.7.3	PAN/CNT (80/20)	20-23	700	30	54	6	9	3	0.29	192	67	181	0.0028
FC.82.8.3	PAN/CNT (80/20)	20-23	800	30	47	7	14	4	0.37	244	50	162	0.0075
FC.82.9.3	PAN/CNT (80/20)	15-20	900	30	42	72	256	58	1.68	190	28	125	0.0487
(b) Activation time effect													
FC.82.9.3	PAN/CNT (80/20)	15-20	900	30	42	72	256	58	1.07	194	28	125	0.0487
FC.82.9.6	PAN/CNT (80/20)	12-15	900	60	37	89	451	129	1.15	292	20	69	0.1016
FC.82.9.9	PAN/CNT (80/20)	12-15	900	90	22	96	638	190	1.68	294	15	51	0.1924
(c) Composition effect													
FC.82.9.3	PAN/CNT (80/20)	15-20	900	30	42	72	256	58	1.68	194	28	125	0.0487
FC.73.9.3	PAN/CNT (70/30)	20-23	900	30	52	77	314	78	1.06	248	25	99	0.0597
FC.64.9.3	PAN/CNT (60/40)	20-23	900	30	54	74	385	94	0.59	210	19	79	0.1371

*Energy and Power densities reported for galvanostatic test performed at 0.5 mA using KOH electrolyte.
**Double layer capacitance reported for 6M KOH electrolyte.

The PAN/CNT films activated at all temperatures, times and compositions show the hysteresis loop at higher relative pressures indicating the presence of mesoporosity while microporous type I behavior is observable by the jump in nitrogen absorption at lower relative pressures. The hysteresis loops observed in isotherms are widely believed to originate from the difference in condensation and evaporation mechanisms of adsorbate molecules on porous samples.

The type H2 hysteresis are often disordered carbon with a distribution of pore sizes or shape not well defined. The steep region in the desorption part for all the samples confirm the presence of disordered carbon with wide size pore distribution. Hence, the nitrogen adsorption isotherms for CO_2 activated PAN/CNT films show a disordered carbon or sample with wide pore size distribution which is further confirmed by the pore size distribution given in Figure 4.2.

4.3.4 Surface area and pore size distribution

The surface area and porosity analyzer was used to evaluate the surface area of the composite samples and to establish any correlation between the pore size distributions to the specific capacitance. The surface area of samples activated at different temperatures given in Table 4.1, appears to have a direct correlation to the specific capacitance.

The surface area for samples activated at 700 and 800 °C are lower than 15 m^2/g as listed in Table 4.1. The sample activated at 900 °C shows an improved BET surface area of 256 m^2/g due to increase in number of micro pores as observed by increase in amount of nitrogen adsorbed at specific partial pressures.

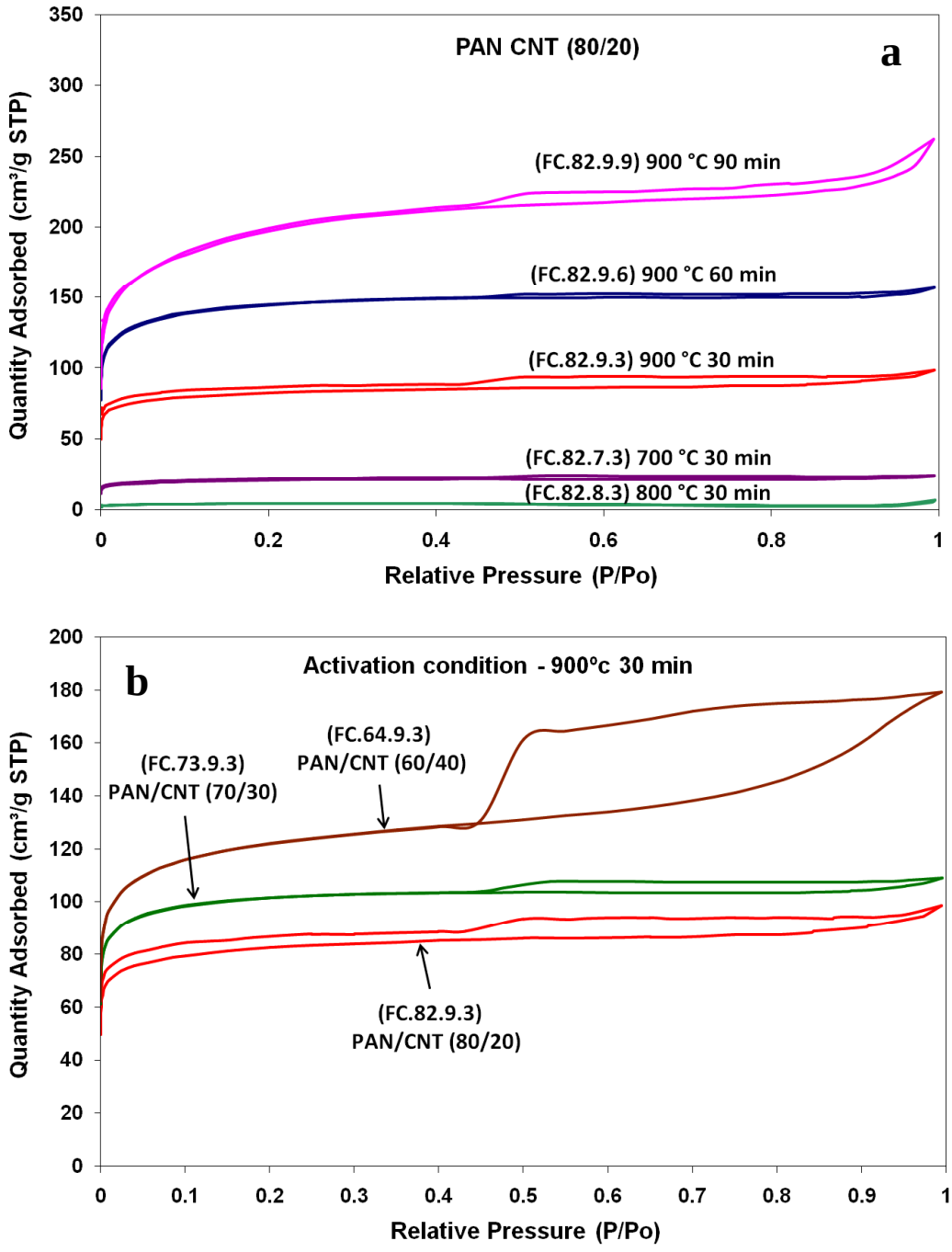

Figure 4.2 Nitrogen absorption isotherms for CO_2 activated PAN/CNT films activated at (a) different conditions - activation time and temperature effect and (b) Composition.

The surface area increases further up to 638 m^2/g with increasing the activation time from 30 to 90 minutes due to creation of more number of pores. An increased surface area was also observed with the increase in amount of nanotubes in the composite samples. The pore volume distribution of samples activated at different conditions given in Figure 4.3 shows no significant variation in pore size distribution even though pore volume increases with increasing activation time and temperature.

4.3.5 Electrochemical properties

The specific capacitance of PAN/CNT (80/20) films activated at 700 ºC and 800 ºC is lower than 10 F/g (Table 4.1) due to lower surface area developed at those activation temperatures. These values are consistent with earlier studies on PAN/CNT composites[9, 10]. However, Liu[14] achieved a specific capacitance value of ~ 380 F/g for PAN/CNT (60/40) films using CO_2 activation at 700 ºC. The capacitance value of an electrode depends upon the nature and the surface area of the carbon/electrolyte interface. A surface area characterized by increased micro and mesopores is required for the electrode material[5, 8, 15-17]. In addition, this surface area must also be electrochemically accessible for ions which make the presence of optimum pore size desirable. These lower values of specific capacitance for samples CO_2 activated at 700 and 800 ºC in our case can be due to lower degree of carbonization [18, 19]. Specific capacitance of 72 F/g was obtained when the activation temperature is increased to 900 ºC. This value further increased to 96 F/g when the activation time was increased from 30 to 90 minutes.

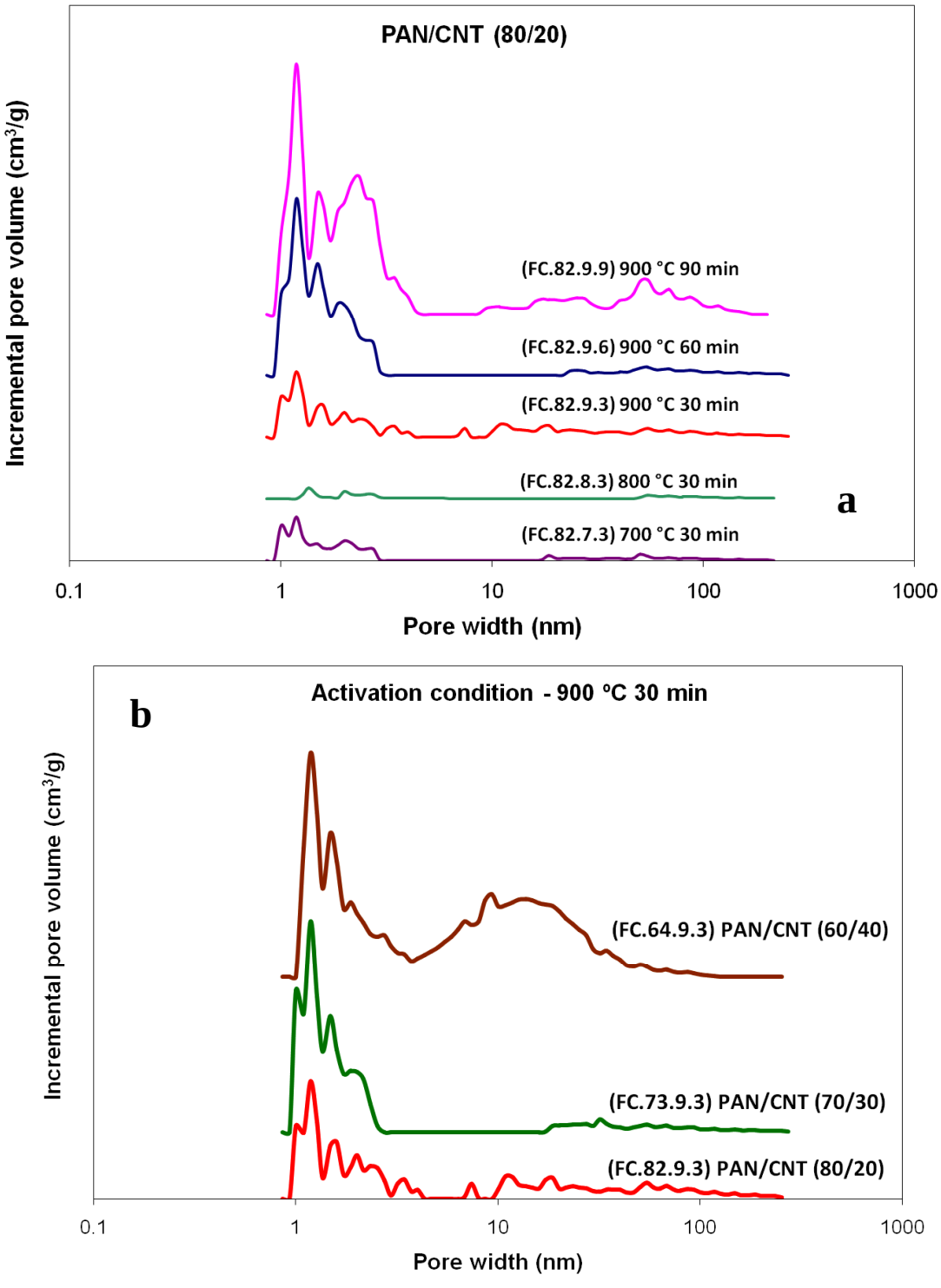

Figure 4.3 The pore size distribution of samples activated with CO_2 at (a) different conditions - temperature and time effect, and (b) Composition effect.

Specific capacitance values measured from galvanostatic test are plotted as a function of current densities in Figure 4.4. The pores larger than the cut-off pore size can be readily accessed by the electrolyte to form an electrical double layer. On the other hand, higher resistance of the electrolytes in smaller pores causes slower response to the applied voltage, preventing the electrical double layer formation. The smaller size pores thus lose their capacitance contribution at higher current density, resulting in lower capacitance. Therefore, the specific capacitance decreases with increasing current density as well as with decreasing scan rate when time available for ions to access the pores decreases (Figure 4.4). The samples activated for longer times (60 and 90 minutes) exhibited increased specific capacitance, and also were able to retain higher specific capacitance even at higher current densities (Figure 4.4a).

Different composition samples containing 20, 30, and 40 % CNTs did not show a significant change in specific capacitance values (72 -77 F/g) as given in Table 4.1. The samples with higher nanotube concentration were able to retain this specific capacitance at higher current densities (Figure 4.4b) than samples with lower CNT concentration. The power densities were between 200 to 300 Wh/kg for films with different compositions and activated at different conditions. Zhou[10] determined the contribution of pseudo capacitance to overall specific capacitance by plotting the current density values as a function of scan rate. The deviation of correlation coefficient R^2 value from unity was used to determine the contribution of pseudo capacitance to the overall specific capacitance.

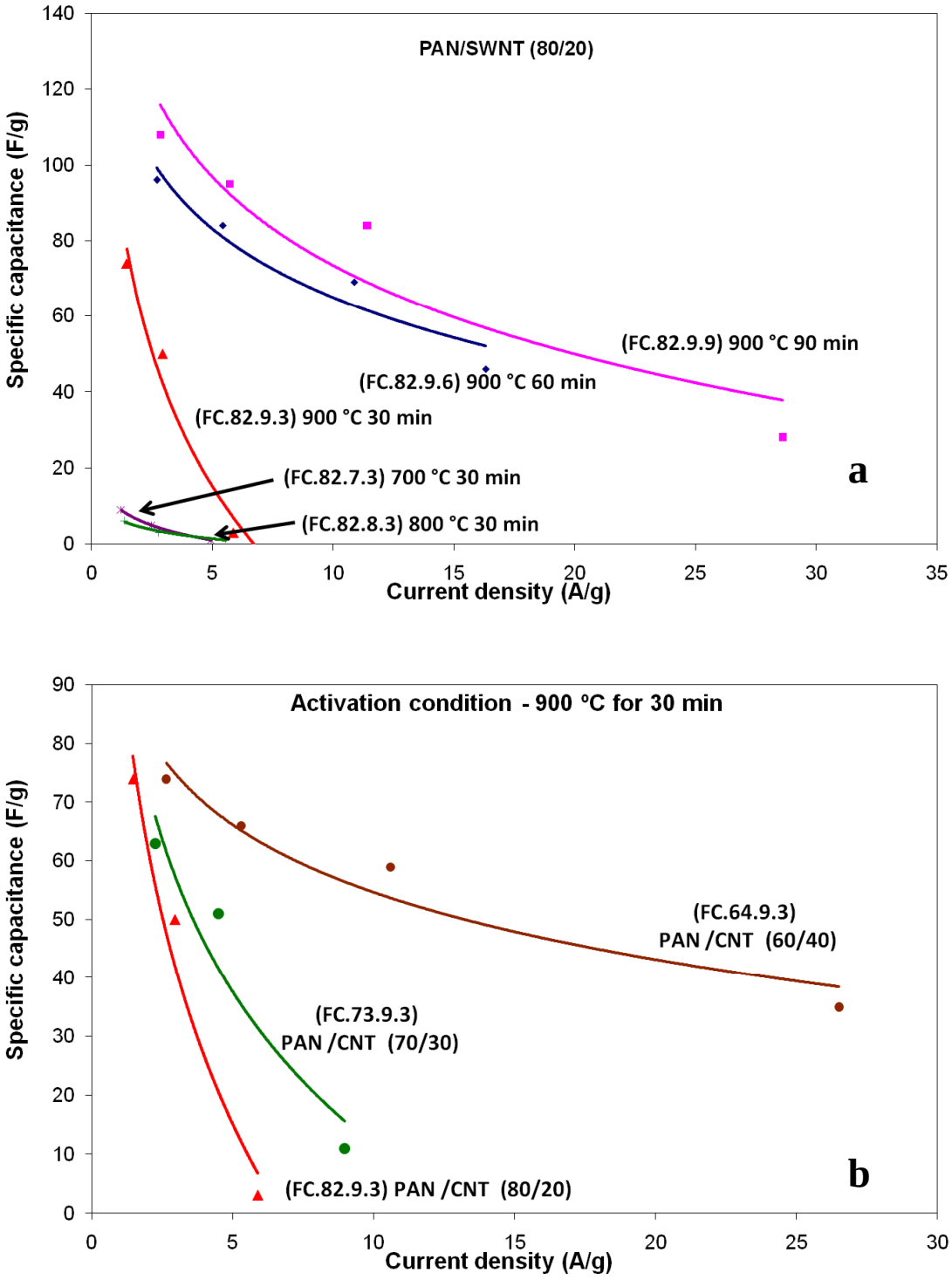

Figure 4.4 Specific capacitance as a function of current density measured in 6M KOH electrolyte for samples activated with CO_2 at (a)different conditions - activation time and temperature effect, and (b) Composition effect.

The current densities measured by cyclic voltammetry method are plotted against the scan rate of samples with different compositions or different activation conditions in Figure 4.5. The samples activated at 700 and 800 ºC showed a lower correlation coefficient (R^2) value due to lower degree of carbonization of the PAN polymer while the sample activated at 900 ºC showed R^2 value closer to unity. Hence, specific capacitance of the samples activated at 900 ºC has more contribution from double layer capacitance while there may be higher contribution from pseudocapacitance for samples activated at 700 and 800 ºC. Also, changes in activation times and film composition did not vary R^2 value significantly indicating negligible pseudocapacitance for all samples activated at 900 ºC.

The micro, meso, and macro pore volume of PAN/CNT films activated at all temperatures, times, and composition are plotted against specific capacitance in Figure 4.6. This is done to determine individual contribution to overall specific capacitance. There are reports in literature which argue that it is difficult to achieve a monolayer of nitrogen gas for pores less than 2 nm to calculate micropore surface areas accurately. IUPAC concluded that pore volume measurements are more accurate than surface area measurements if there are pores less than 2 nm[20, 21]. The results show that specific capacitance has direct correlation with pore volume of physically activated sample with all micro, meso and macro pores contributing to overall specific capacitance. A more linear fit was noticed for micro pore volumes when plotted against specific capacitance.

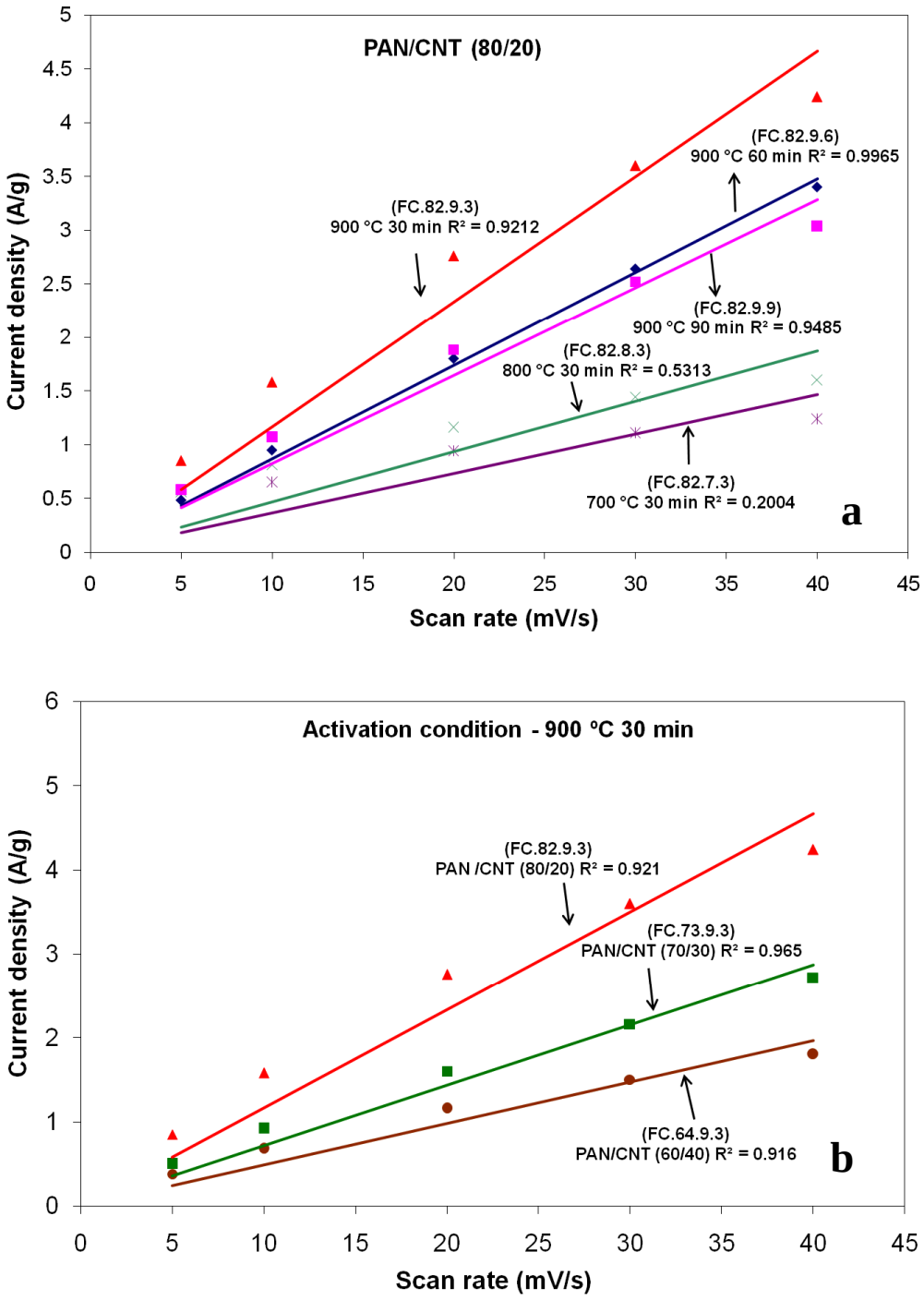

Figure 4.5 The current density as a function of scan rate to determine the role of pseudocapacitance for samples activated with CO_2 in 6M KOH electrolyte at (a) different conditions – activation temperature effect and time effect, and (b) composition effect.

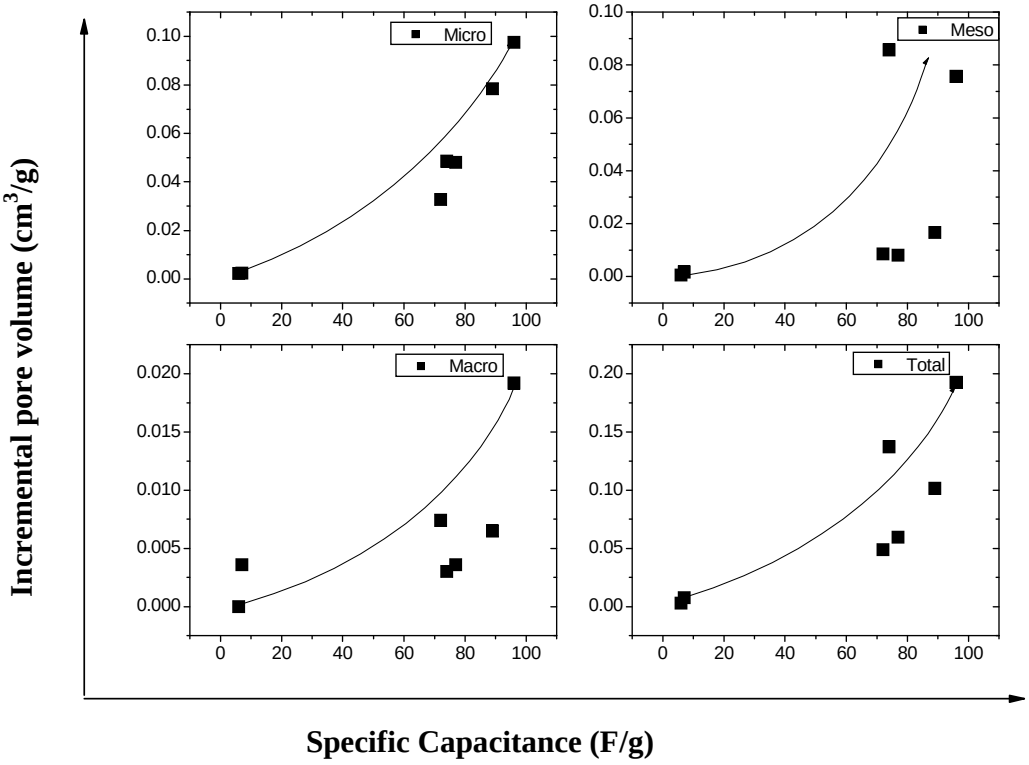

Figure 4.6 The correlation between the micro, meso and macro pore volume to specific capacitance of CO_2 activated PAN/CNT composite films (FC series) measured in 6M KOH electrolyte. All conditions from Table 4.1 are included.

The charge discharge curves from galvanostatic test and cyclic voltammograms from cyclic voltammetry tests are given in Figure 4.7 and 4.8 respectively. High ohmic drop observed in charge-discharge curves of all the samples are due to high internal resistance of micropores present in activated carbon samples. The cyclic voltammograms show more rectangular shape, and a characteristic of double layer capacitance for samples activated at 900 ºC than 700 ºC and 800 ºC samples. This rectangular shape is further tending towards ideal double layer capacitance shape when the activation temperature is increased to 60 and 90 minutes.

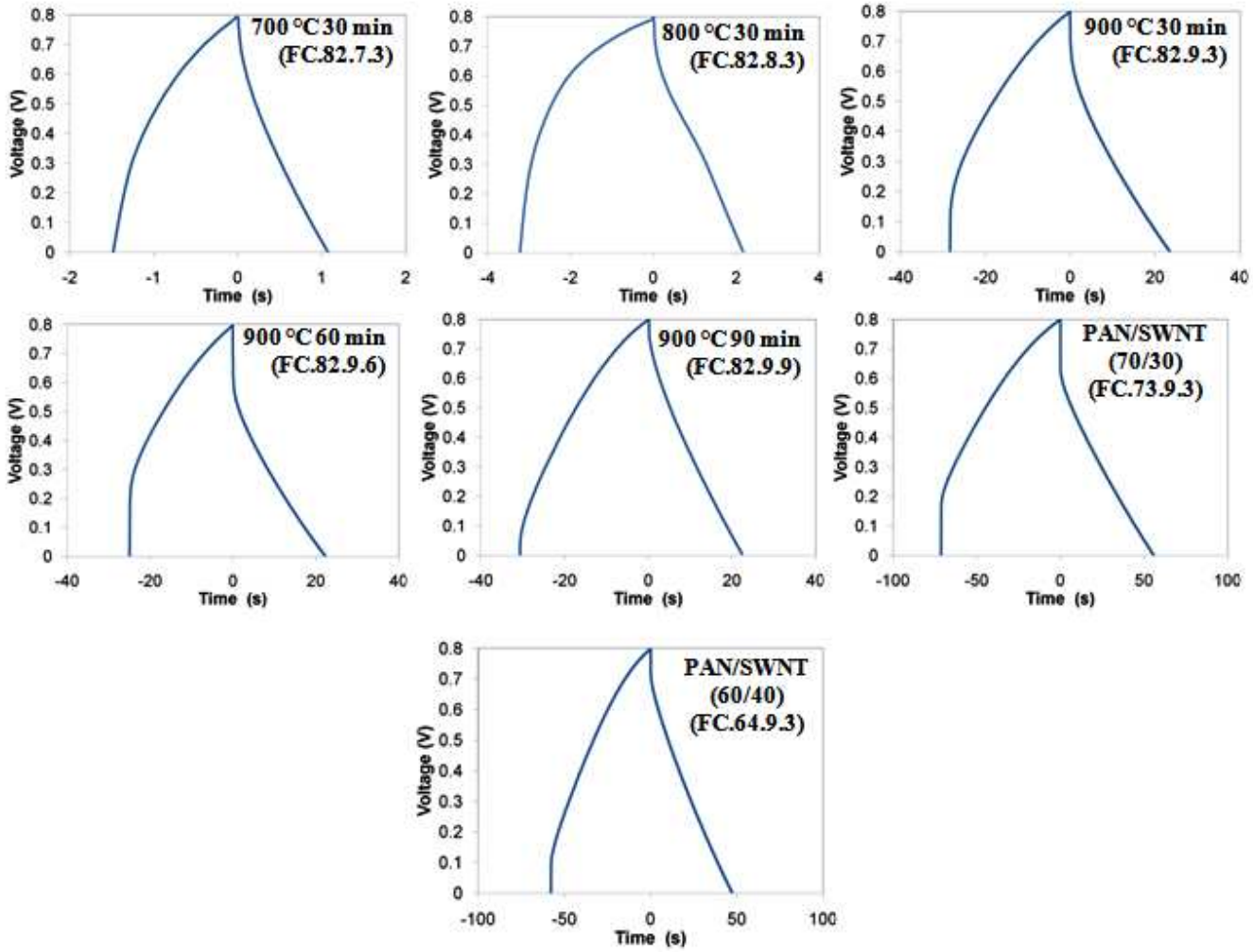

Figure 4.7 Charge discharge curves measured at 0.5 mA galvanostatic test performed in 6M KOH electrolyte for PAN/CNT films activated at different conditions.

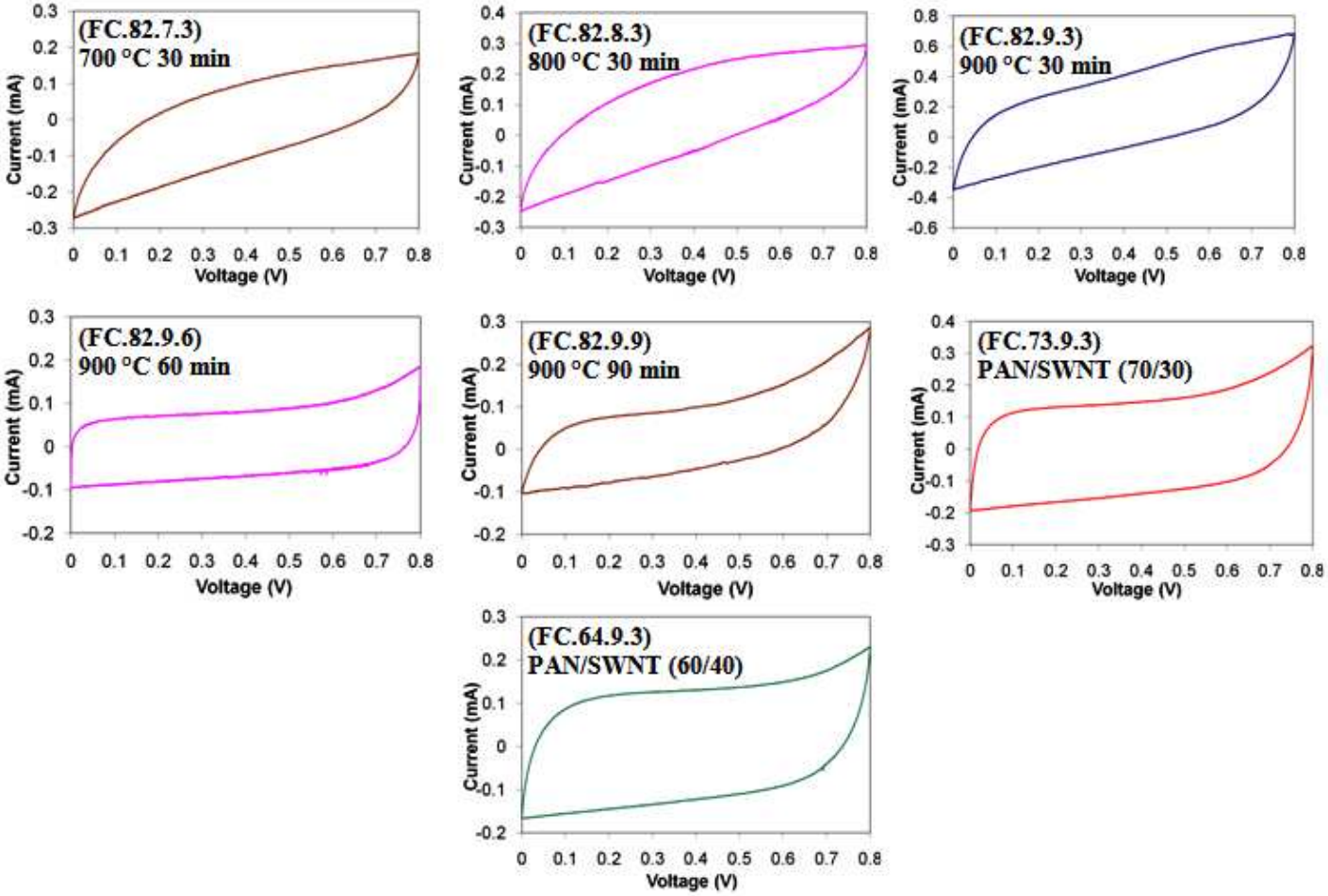

Figure 4.8 Cyclic voltammograms from 5 mV/s cyclic voltammetry test performed in 6M KOH electrolyte for PAN/CNT films activated at different conditions.

The samples with higher CNT contents also revealed rectangular shapes possibly due to increase in content of electrochemically inert CNTs.

Ragone plots with energy and power densities of electrodes plotted against each represent electrochemical capacitor's energy storage capabilities at different power levels. The ragone plots given in Figure 4.9 show a clear increase in energy density values for samples activated at 900 ºC when compared 700 ºC and 800 ºC samples due to increase in accessible surface area. A small increase in energy and power density is observed when the activation time was increased from 30 to 90 minutes due to creation of additional pores. The power density of the composite samples did not increase significantly as expected due to higher electrical conductivity of CNTs with higher content of CNTs (70/30 and 60/40 ratios). Hence, a higher energy density and specific capacitance is obtained for samples activated at 900 ºC due to increase in surface area and pore volume achieved at higher activation temperatures. These values are further increased when activation time is increased from 30 to 90 minutes. This study reveals that there is a correlation between specific capacitance, energy density, and pore volume for PAN/CNT samples activated by CO_2. Since the maximum specific capacitance for CO_2 activated samples were relatively low (less than 80 F/g), the samples with different compositions activated at higher activation times (60 and 90 min at 900 ºC) were not activated. The focus of research is shifted to more promising chemical activation process discussed in the subsequent chapters.

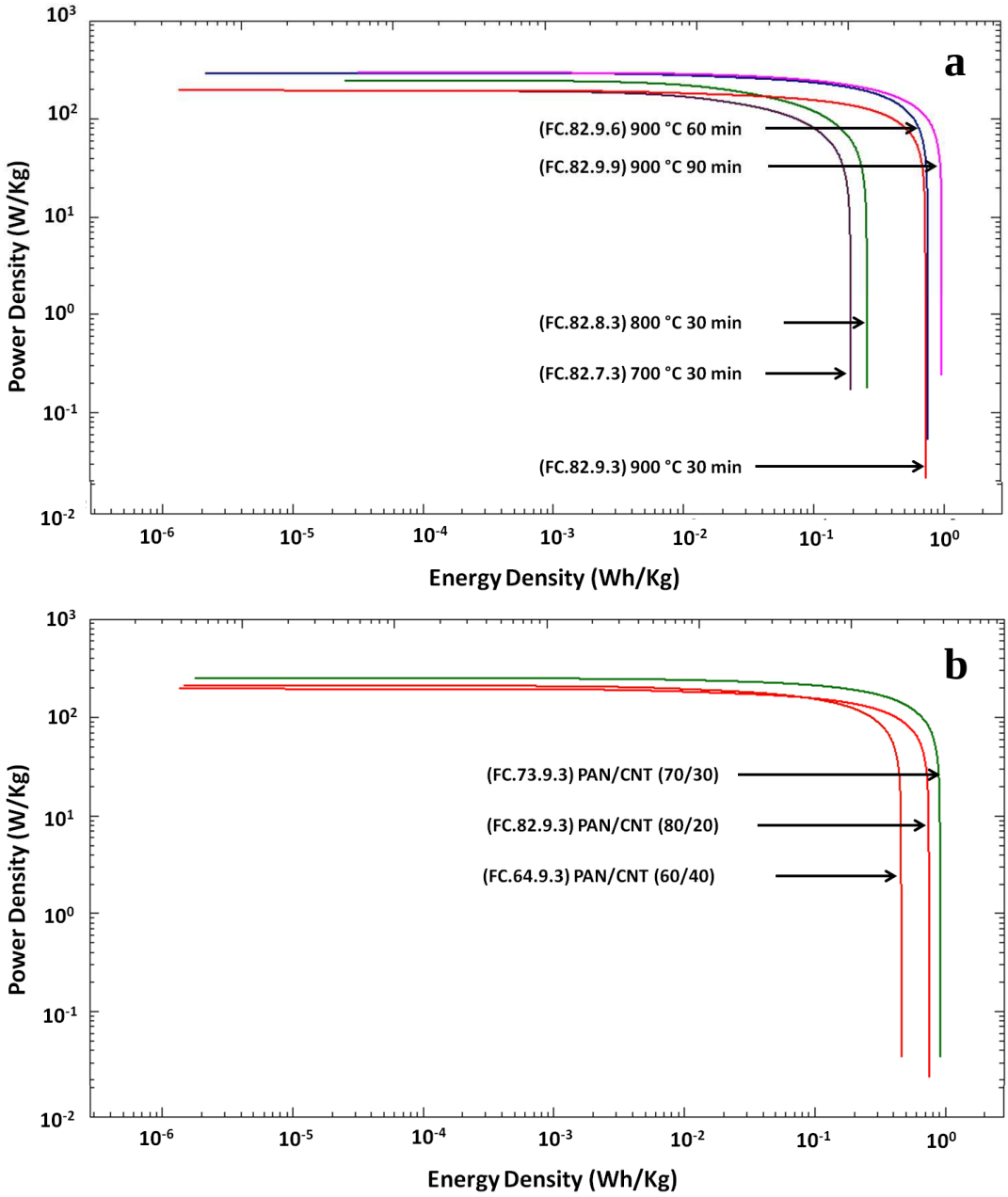

Figure 4.9 The power density and energy density measured at 0.5mA galvanostatic test in 6M electrolyte for CO_2 activated PAN/CNT films (FC series) treated at (a) different conditions – activation temperature effect and time effect (b) composition effect.

4.4 Conclusions

The effect of activation time, temperature, and composition of samples on the specific capacitance and pore structure of CO_2 activated poly(acrylonitrile)/carbon nanotube composite films (FC series) were evaluated. The conclusions from this study are given below:

- For CO_2 activated PAN/CNT films, sample with 80/20 PAN/CNT ratio activated at 900 °C for 90 minutes gave the highest surface area (638 m^2/g) and specific capacitance (96 F/g).
- Weight loss of the PAN/CNT composite film increased with activation temperature and time and declined when the CNT content is increased.
- A lower value of specific capacitance and surface area observed for samples activated at 700 and 800 ºC can be due to lower degree of carbonization leading to lower surface areas. An increase of activation temperature to 900 °C and activation time resulted in an increase specific capacitance due to higher surface area and pore volume caused due to creation of more number of pores at those conditions.
- The specific capacitance has direct positive correlation with surface area, specifically micropore area, for CO_2 activated PAN/CNT System.
- The samples with different composition of nanotubes and polymer show a small increase in surface area with the increase in concentration of nanotubes but no significant increase in specific capacitance.
- From cyclic voltammograms and plot of scan rate vs. current density for samples activated at different conditions, there may be contributions from pseudo capacitance

for samples activated at 700 and 800 ºC samples, while samples activated at 900 ºC at 30 - 90 minutes have more contributions from double layer capacitance.

4.5 References:

[1] Conway BE. Electrochemical supercapacitors : scientific fundamentals and technological applications, Plenum Press, New York. 1999.

[2] Kotz R, Carlen M. Principles and applications of electrochemical capacitors. Electrochimica Acta. 2000;45(15-16):2483-98.

[3] Burke A. Ultracapacitors: why, how, and where is the technology. Journal of Power Sources. 2000;91(1):37-50.

[4] Bard AJ, Faulkner LR. Electrochemical methods : fundamentals and applications New York : Wiley. 2001:833.

[5] Lee J-G, Kim J-Y, Kim S-H. Effects of microporosity on the specific capacitance of polyacrylonitrile-based activated carbon fiber. Journal of Power Sources. 2006;160(2):1495-500.

[6] Lozano-Castello D, Cazorla-Amoros D, Linares-Solano A, Quinn DF. Influence of pore size distribution on methane storage at relatively low pressure: preparation of activated carbon with optimum pore size. Carbon. 2002;40(7):989-1002.

[7] Wu F-C, Tseng R-L, Hu C-C, Wang C-C. Effects of pore structure and electrolyte on the capacitive characteristics of steam- and KOH-activated carbons for supercapacitors. Journal of Power Sources. 2005;144(1):302-9.

[8] Chmiola J, Yushin G, Gogotsi Y, Portet C, Simon P, Taberna PL. Anomalous Increase in Carbon Capacitance at Pore Sizes Less Than 1 Nanometer. Science. 2006 September 22, 2006;313(5794):1760-3.

[9] Wang T. Electrospun Carbon Nanofibers for Electrochemical Capacitor Electrodes. PhD Thesis, Georgia Institute of Technology. 2007.

[10] Zhou C. Carbon nanotube based electrochemical supercapacitors. PhD Thesis, Georgia Institute of Technology. 2006:42.

[11] Lowell S, Shields JE, Thomas MA, Thommes M. Characterization of porous solids and powders: Surface area, pore size and density. Kluwer Academic Publishers, Dordrecht/Boston/London. 2004.

[12] Sing KSW, Everett DH, Haul RAW, Moscou L, Pierotti RA, Rouquerol J, et al. Reporting physisorption data for gas/solid systems with special reference to the determination of surface area and porosity. Pure & Appl Chem. 1985;57(4):603.

[13] Webb PA, Orr C. Analytical methods in fine particle technology. Micromeritics Instruments Corp , Norcross, Georgia. 1997.

[14] Liu T, Sreekumar TV, Kumar S, Hauge RH, Smalley RE. SWNT/PAN composite film-based supercapacitors. Carbon. 2003;41(12):2440-2.

[15] Yamada H, Moriguchi I, Kudo T. Electric double layer capacitance on hierarchical porous carbons in an organic electrolyte. Journal of Power Sources. 2008;175(1):651-6.

[16] Fuertes AB, Lota G, Centeno TA, Frackowiak E. Templated mesoporous carbons for supercapacitor application. Electrochimica Acta. 2005;50(14):2799-805.

[17] Morishita T, Soneda Y, Tsumura T, Inagaki M. Preparation of porous carbons from thermoplastic precursors and their performance for electric double layer capacitors. Carbon. 2006;44(12):2360-7.

[18] Donnet J-B. Carbon Fibers. New York Marcel Dekker, Inc. 1998.

[19] Patrick JW. Porosity in Carbons. Halsted Press. 1995.

[20] Kaneko K, Ishii C. Superhigh surface area determination of microporous solids. Colloids and Surfaces. 1992;67:203-12.

[21] Sing KSW. The use of physisorption for the characterization of microporous carbons. Carbon. 1989;27(1):5-11.

Chapter 5

STRUCTURE AND ELECTROCHEMICAL PROPERTIES OF SOLUTION-SPUN POLYACRYLONITRILE/ CARBON NANOTUBE BASED FIBERS ACTIVATED BY PHYSICAL AND CHEMICAL METHODS

5.1 Introduction

In chapters 3 and 4, the processing conditions of physical and chemical activation are varied for PAN/CNT films to determine the optimum conditions to achieve maximum specific capacitance. A number of studies have been reported in literature on PAN/CNT films and fibers[1-12] used for electrochemical capacitor applications. Fibers have been spun by conventional solution spinning[2, 5], gel spinning[1], as well as electrospinning [6-8, 10]. However, no systematic study has been reported to understand the effect of polymer molecular orientation and orientation and exfoliation of carbon nanotubes. The polymer molecular chains and carbon nanotubes are randomly oriented in PAN/CNT films. In solution spun fibers, the polymer molecular chains are oriented along the direction of fibers in solution spun fibers, while the CNTs are still randomly oriented and exist as unexfoliated bundles. To the best of our knowledge, to date there are no activation studies in the literature on solution spun PAN/CNT fibers.

The stabilized PAN, PAN/MWNT (5%), and PAN/SWNT (5%) fibers are used as a precursor for the preparation of activated carbon fibers by CO_2 (SSC series) as well as KOH activation (SSK series). The optimum activation conditions based on conclusions from literature and results from our research group were used for activating the fibers. The present study reports improvement of specific capacitance of activated carbon

materials prepared by KOH activated carbon fiber over CO_2 activated samples. The effect of various activation conditions on morphology, pore size distribution and electro-chemical performance were investigated.

5.2. Experimental

SWNTs were obtained from Carbon Nanotechnologies, Inc (Houston, TX) (Grade PO247, 2.4% catalytic impurity) and MWNTs were from Iljin Nanotech, Co (Korea) (2.5% catalytic impurity). Poly(acrylonitrile-co-methylacrylate) containing 6.7 mol% methylacrylate, was obtained from Exlan, Co. (Japan). DMF purchased from Sigma-Aldrich was used as received. Detailed description of fiber processing method, heat treatment conditions as well as characterization methods are given in chapter 2.

5. 3. Results and Discussion

5.3.1 Stabilization studies

PAN and PAN/CNT fibers stabilized for various times were treated in DMF for 6 hours at 150 ºC to monitor stabilization. Under these conditions, fiber diameters for samples stabilized for 2 and 4 hours increased due to swelling of the unstabilized PAN, while fibers stabilized for 8 and 16 hours did not show a significant change in diameter. Fibers stabilized for 2 and 16 hours before and after boiling in DMF is shown in Figure 5.1. The cross-sections of 16 hour stabilized PAN and PAN/CNT fibers boiled in DMF for 6 hours do not show a hollow core, which is consistent with complete stabilization (Figure 5.2). Any unstabilized PAN remaining in the core would have been removed by DMF, leaving hollow core as stabilization is controlled by diffusion of oxygen[13-15].

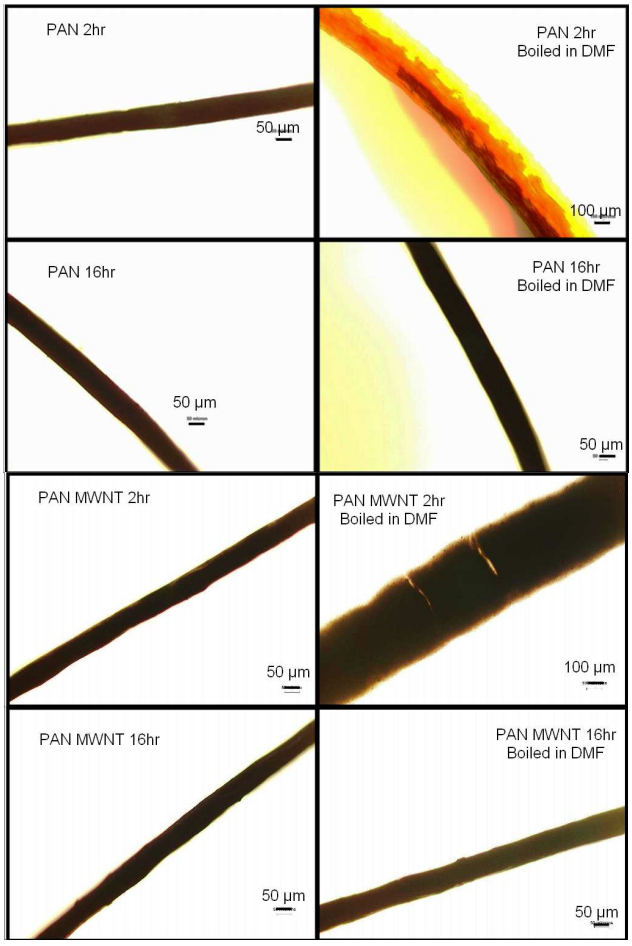

Figure 5.1 Optical microscopy images of stabilized PAN, PAN/MWNT samples boiled in DMF.

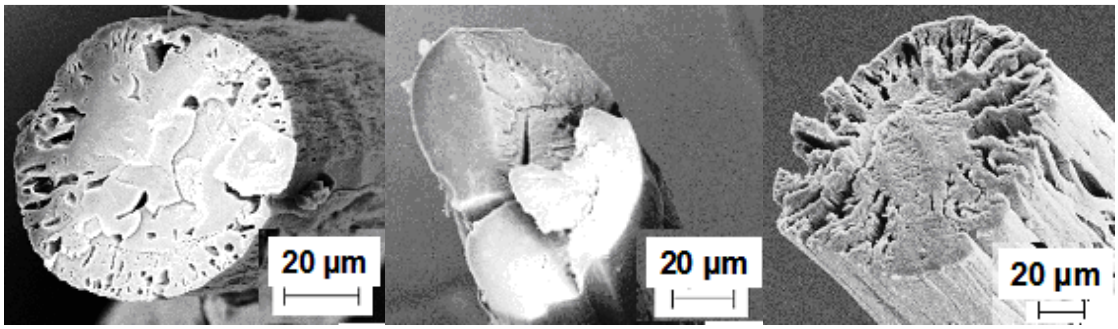

Figure 5.2 Scanning Electron Micrographs of (a) PAN, (b) PAN/MWNT and (c) PAN/SWNT fibers stabilized for 16 hours and boiled in DMF for 6 hours.

Stabilization progression in all samples was also monitored by WAXD [16]. Unstabilized and partially stabilized fibers show WAXD peak at 2θ ~ 17° due to (110) and (200) PAN reflections (Figure 5.3), while this peak was absent in the 16 hour stabilized samples. Based on these studies, it was concluded that only 16 hour samples were fully stabilized. Therefore, for subsequent studies all three fiber samples were stabilized for 16 hours. The potassium distribution in the stabilized and KOH impregnated samples was monitored by EDS, and was found to be uniform through the fiber cross section (Figure 5.4).

5.3.2 Structure and morphology

The SEM images of CO_2 (SSC series) and KOH (SSK series) activated PAN, PAN/MWNT, and PAN/SWNT fibers are given in Figures 5.5 and 5.6 respectively. The thermal activation process being controlled by diffusion of CO_2 into the carbon precursor is a surface phenomenon while the chemical activation depends on the ability of activating agents to diffuse into precursors during impregnation and activation during pyrolysis. The SEM images of the cross sections show that both activation processes are effective only up to a few microns from the surface of fiber samples causing a condensed core/porous surface structure for all the samples (Figure 5.5 and 5.6). The images also show a difference in physical structure for control PAN fibers (SSC.9.6) and composite samples (SSCS.9.6 and SSCM.9.6). The fibril structure observed for KOH activated PAN fibers (SSK.8.6M) are similar to the morphology reported by S. Y. Moon[17] and Y. J. Lee[18]. To best of our knowledge, the structures developed by chemical activation of PAN/CNT composite samples were not investigated in the literature.

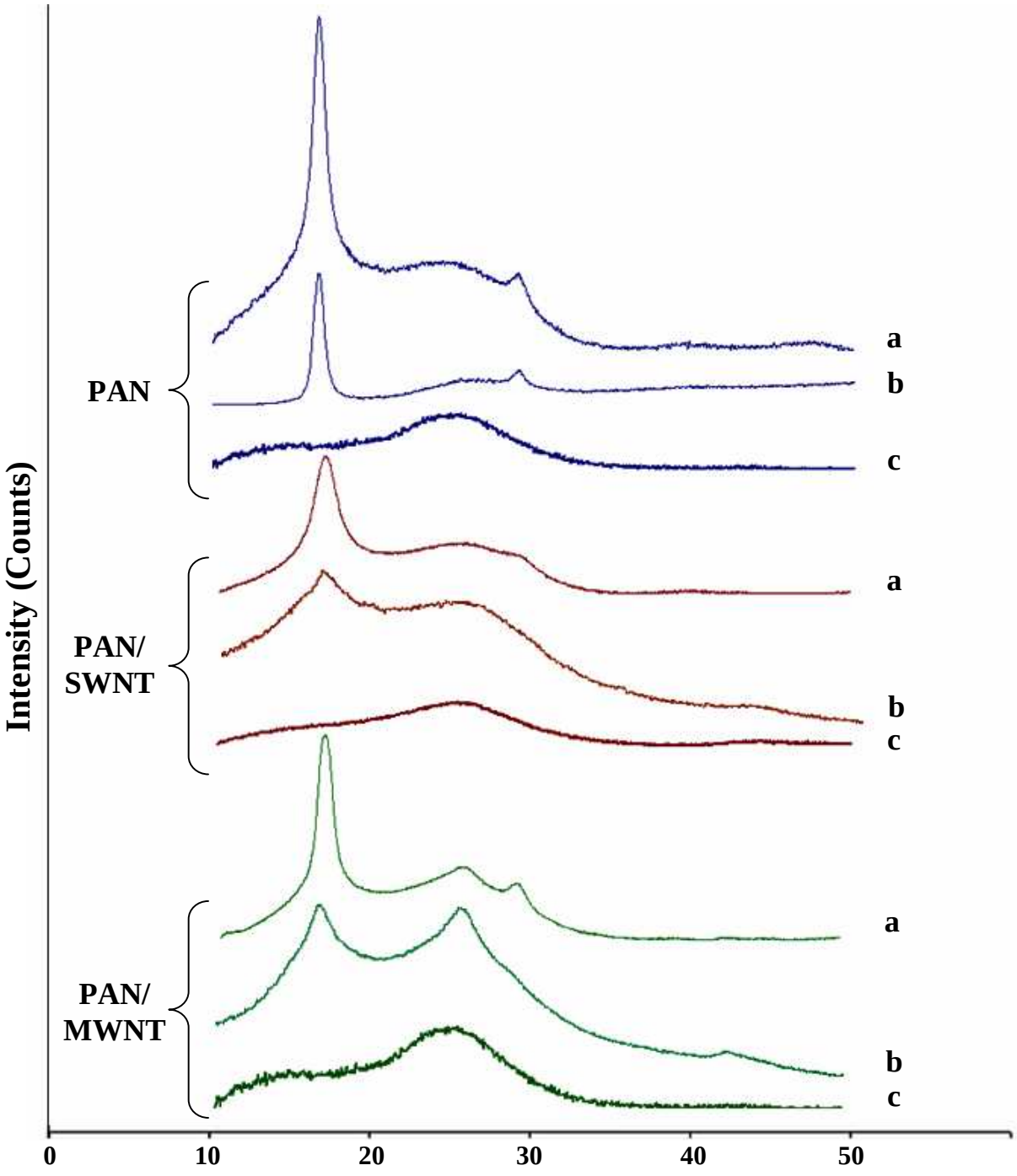

Figure 5.3 WAXD integrated scans for (a) precursor and (b and c) stabilized PAN, PAN/MWNT, and PAN/SWNT fibers (precursors for SSC and SSK series). Stabilization time is (b) 8 hours and (c) 16 hours.

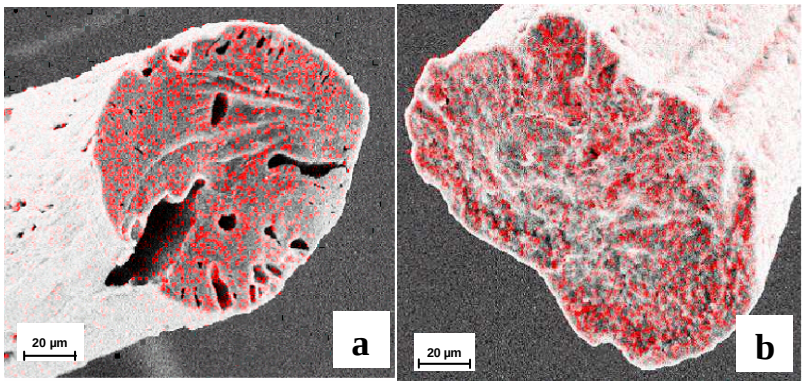

Figure 5.4. Distribution of potassium through the fiber cross-section as characterized by energy dispersive system after KOH impregnation of stabilized (a) PAN, and (b) PAN/MWNT fibers in 6M KOH for 24 hours. Red dots indicate the presence of potassium.

5.2.3 Surface area and pore size distribution

Surface area and pore size distribution of activated fibers are characterized by nitrogen gas adsorption. Based on the IUPAC classification, type I nitrogen gas adsorption isotherm is exhibited by micropores, while type IV isotherm is exhibited by mesoporous materials[19-21]. For CO_2 activated PAN (SSC.9.6) and PAN/SWNT (SSCS.9.6) fibers, the hysteresis loop at higher relative pressure indicate the presence of mesoporosity while microporous type I behavior is observed at low pressures (Figure 5.7). The type H2 hysteresis is often attributed to disordered carbon with a distribution of pore sizes or shape not well defined. Thus, the steep region in the desorption part of CO_2 activated PAN and PAN/SWNT fibers (Figure 5.7a inset) suggests the presence of disordered carbon or sample with wide pore size or shape distribution. The CO_2 activated PAN/MWNT (SSCM.9.6) sample show type II sorption isotherm typically obtained for non-porous or macroporous absorbent with negligible hysteresis of type H3 at relatively high pressure.

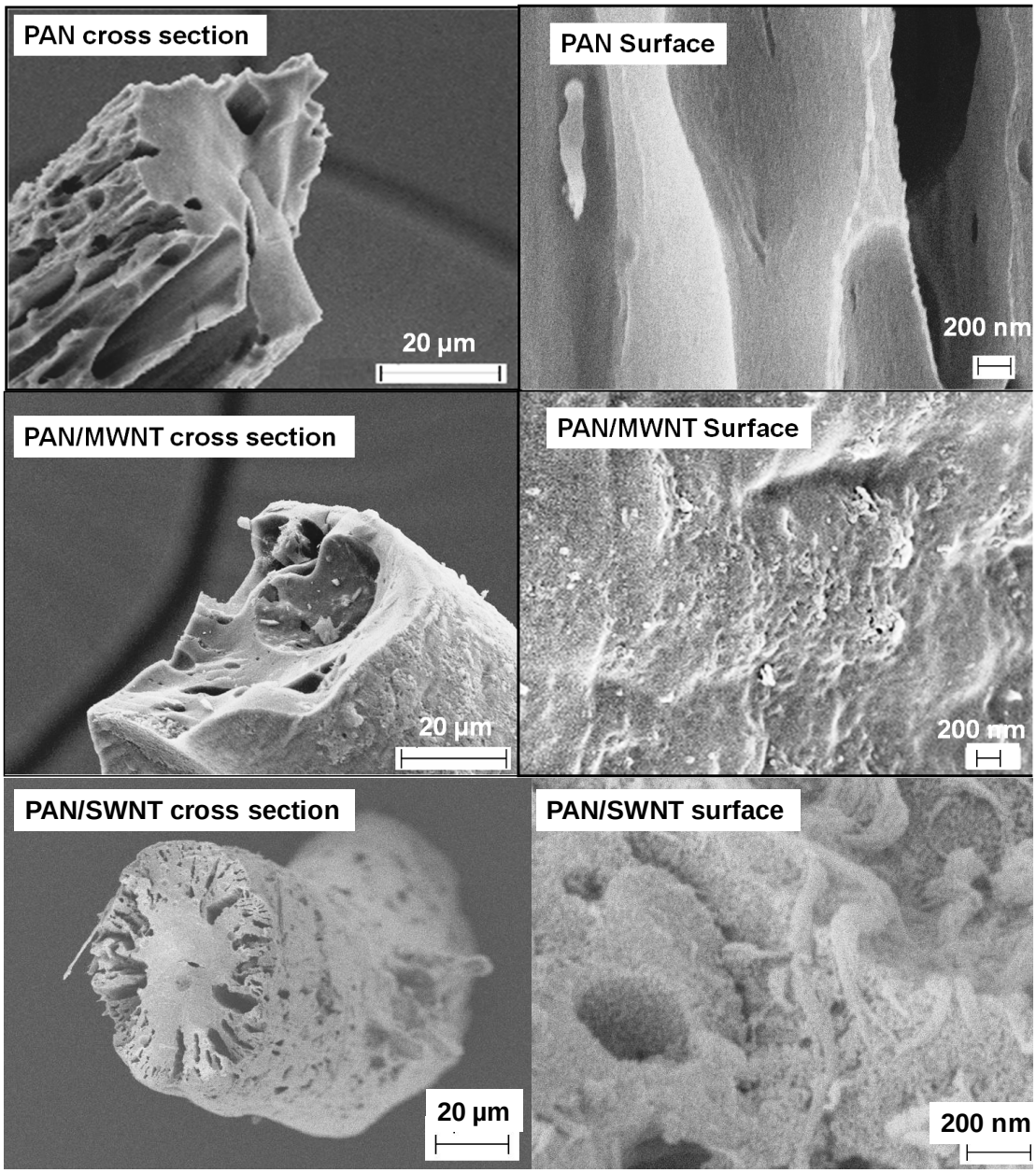

Figure 5.5 Scanning electron microscopy images of PAN (SSC.9.6), PAN/MWNT (SSCM.9.6) and PAN/SWNT fibers (SSCS.9.6) activated with CO_2 at 900 ºC for 1 hour.

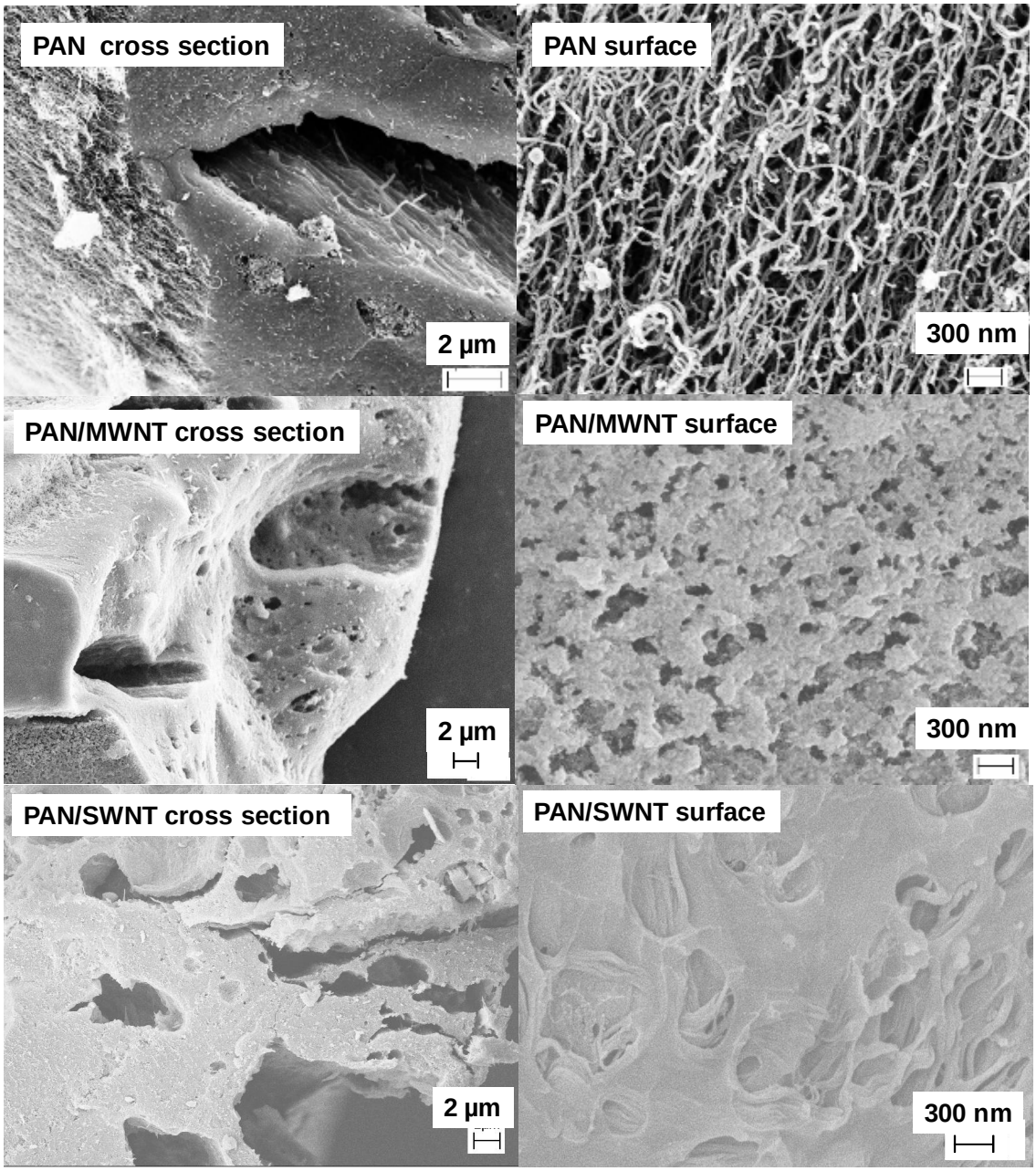

Figure 5.6 Scanning electron microscopy images of PAN (SSK.8.6M), PAN/MWNT (SSKM.8.6M) and PAN/SWNT fibers (SSKS.8.6M) activated with KOH at 800 ºC for 1 hour.

The KOH activated PAN (SSK.8.6M) and PAN/SWNT (SSKS.8.6M) fibers show type I isotherm (Figure 5.7b) with high nitrogen uptakes at relatively low pressures characteristic of micropores with small amount of type IV mesopores behavior presenting a hysteresis loop at relatively high pressures. The hysteresis loops obtained for KOH activated PAN and PAN/SWNT fibers are of type H4, which is typically attributed to narrow slit shaped pores including pores in the micropore region[19]. Similar type I isotherm is obtained for KOH activated PAN/MWNT (SSKM.8.6M) fibers with negligible hysteresis loop H4. All three KOH activated samples show pores predominantly in the 1-5 nm range, while somewhat broader pore size distribution can be seen for the CO_2 activated samples (Figure 5.7c). In fact for KOH activated PAN/MWNTs, the pore size distribution is predominantly in the 1 to 3 nm range. Surface area calculated by both BET and DFT methods for the KOH activated samples (SSK series) is an order of magnitude higher than for the corresponding CO_2 activated samples (SSC series) (Table 5.1).

5. 2.4 Electrochemical properties

Constant current charge-discharge as well as CV plots for samples tested in 6M KOH electrolyte are given in Figure 5.8, and the specific capacitance as a function of current density is plotted in Figure 5.9. Deviation from ideal rectangular shape at about 0.1 V in both CO_2 and KOH activated samples (Figure 5.8b) can be due to the presence of surface functional groups making a pseudo-capacitance contribution.

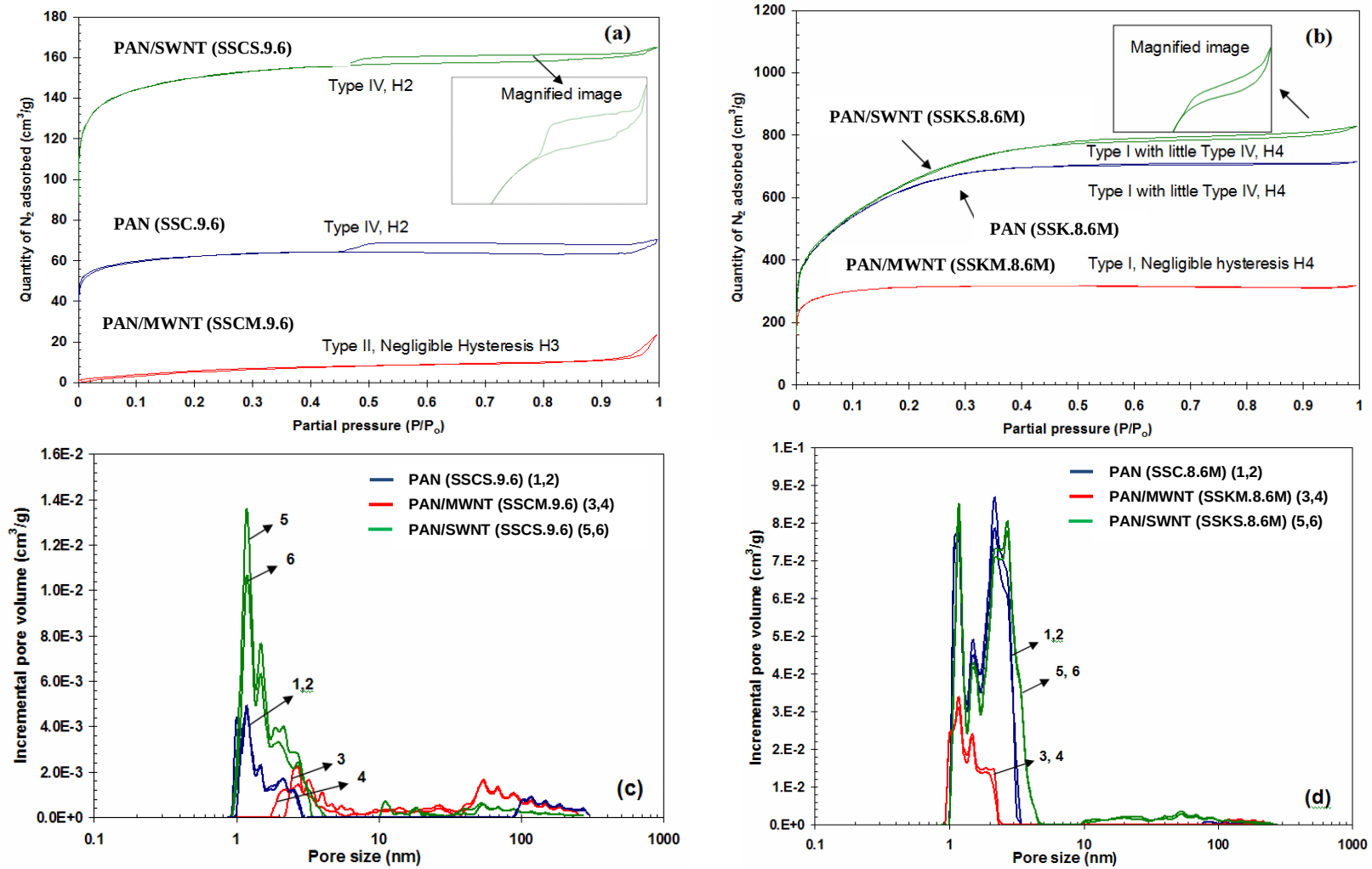

Figure 5.7 Nitrogen adsorption isotherms (a, b) and Pore size distribution measured by density functional theory method (c,d) for PAN, PAN/MWNT and PAN/SWNT fibers activated by (a,c) CO_2 and (b,d) KOH.

High ohmic drop observed in charge-discharge curves can be due to high internal resistance of the electrodes as well as due to the distributed resistance of the electrolyte in the pores of the electrode. KOH activated samples (SSK series) exhibit substantially higher capacitance over the CO_2 activated samples (SSC series) in 6M KOH as well as in ionic liquid electrolytes (Figure 5.9 and 5.10). In addition, in both types of activation, PAN/SWNT samples show higher capacitance than the PAN and PAN/MWNT samples.

Capacitance of PAN/SWNT samples (SSKS.8.6M) activated in KOH is as high as 250 F/g at low current density (0.01 A/g in 6M KOH). Energy density for KOH activated samples (SSK series) is also substantially higher than that for the CO_2 activated samples (SSC series) (Figure 5.11). Energy density for KOH activated PAN/SWNT (SSKS.8.6M) is about 50% higher than the corresponding PAN (SSK.8.6M) and PAN/MWNT (SSKM.8.6M). On the other hand, power density did not increase significantly even with the presence of conducting SWNTs and MWNTs. The energy density increased from 3 Wh/Kg for KOH electrolyte to 6.4 Wh/Kg in $BMIMBF_4$/acetonitrile electrolyte system for the chemically activated PAN/SWNT (SSKS.8.6M) (Figure 5.11). However the specific capacitance in ionic liquid is lower than KOH even at low current density (Figure 5.9 and 5.10). This is attributed to the relatively large ion size of the ionic liquid that cannot access small pores even at low current density. The bucky paper and carbonized PAN/CNT samples exhibit better wettability in ionic liquid than in KOH as determined by contact angle measurement[22].

The literature summary of activation conditions and capacitance performance for PAN based precursors is given in Table 1.3 in chapter 1.

Table 5.1. Specific capacitance, surface area, and double layer capacity for CO_2 and KOH activated solution spun fibers.

Label	Sample	Diameter	Precursor Crystal size	Specific capacitance (F/g) (0.1mA constant current test)		Surface Area (m^2/g)		Double layer capacitance (μF/cm^2)		Pore volume
		(μm)	(nm)	6M KOH	BMIMBF4: AC (1:2)	BET	DFT	BET	DFT	(cm^3/g)
CO_2 Activation										
SSC.9.6	PAN	55	3.7	26	15	212	40	12	65	0.034
SSCM.9.6	PAN/MWNT (95/5)	86	5.0	21	11	30	10	70	210	0.035
SSCS.9.6	PAN/SWNT (95/5)	70	5.0	113	36	358	98	32	115	0.076
KOH Activation										
SSK.8.6M	PAN	55	3.7	172	140	2133	925	8	19	0.778
SSKM.8.6M	PAN/MWNT (95/5)	86	5.0	134	80	970	316	14	42	0.234
SSKS.8.6M	PAN/SWNT (95/5)	70	5.0	236	190	2266	916	10	26	0.936

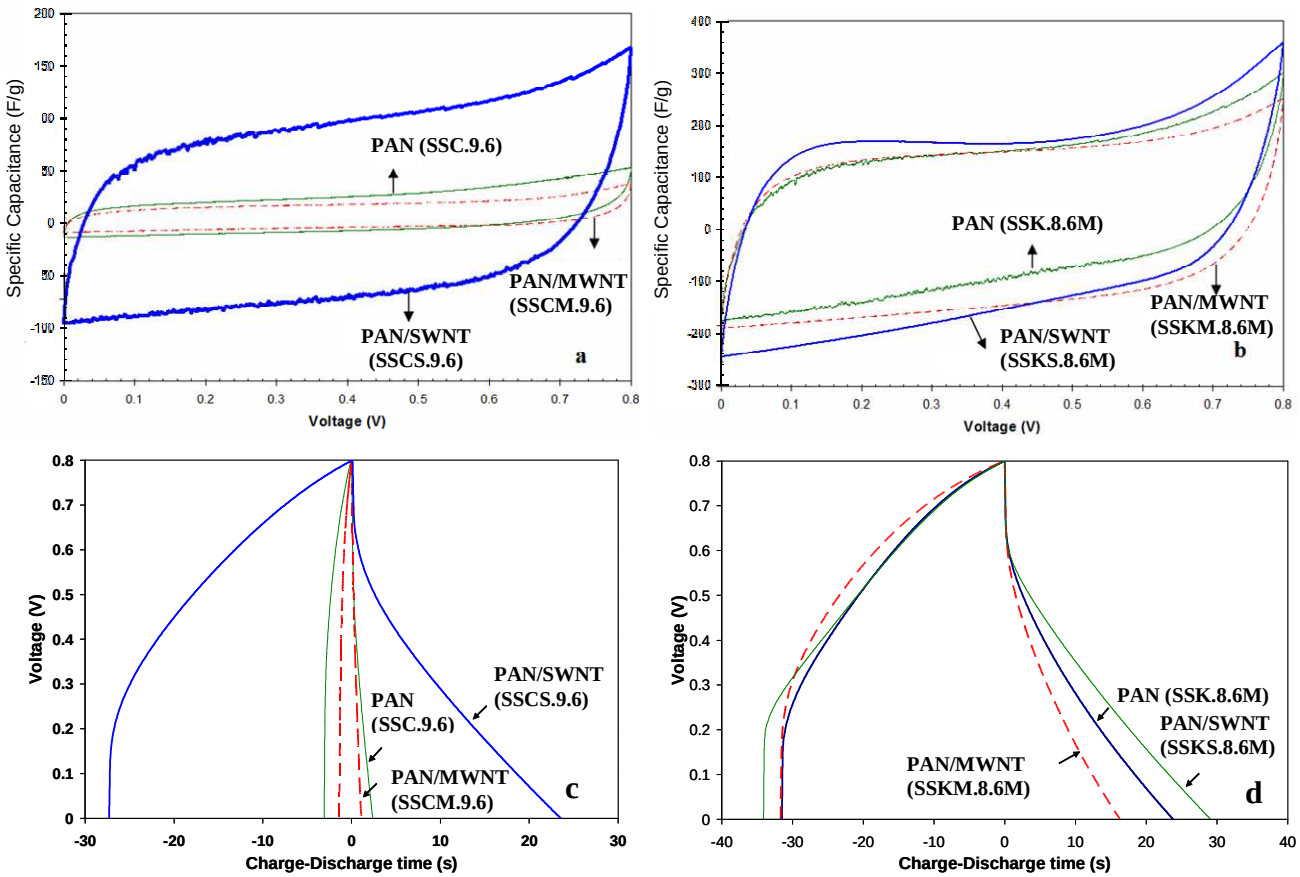

Figure 5.8 The cyclic voltammograms at 5 mV/s scan rate (a, b) and charge discharge curves at a constant current test of 0.5 mA (c,d) for PAN, PAN/MWNT and PAN/SWNT fibers activated by (a,c) CO_2 and (b,d) KOH. The electrolyte for this test was 6M KOH.

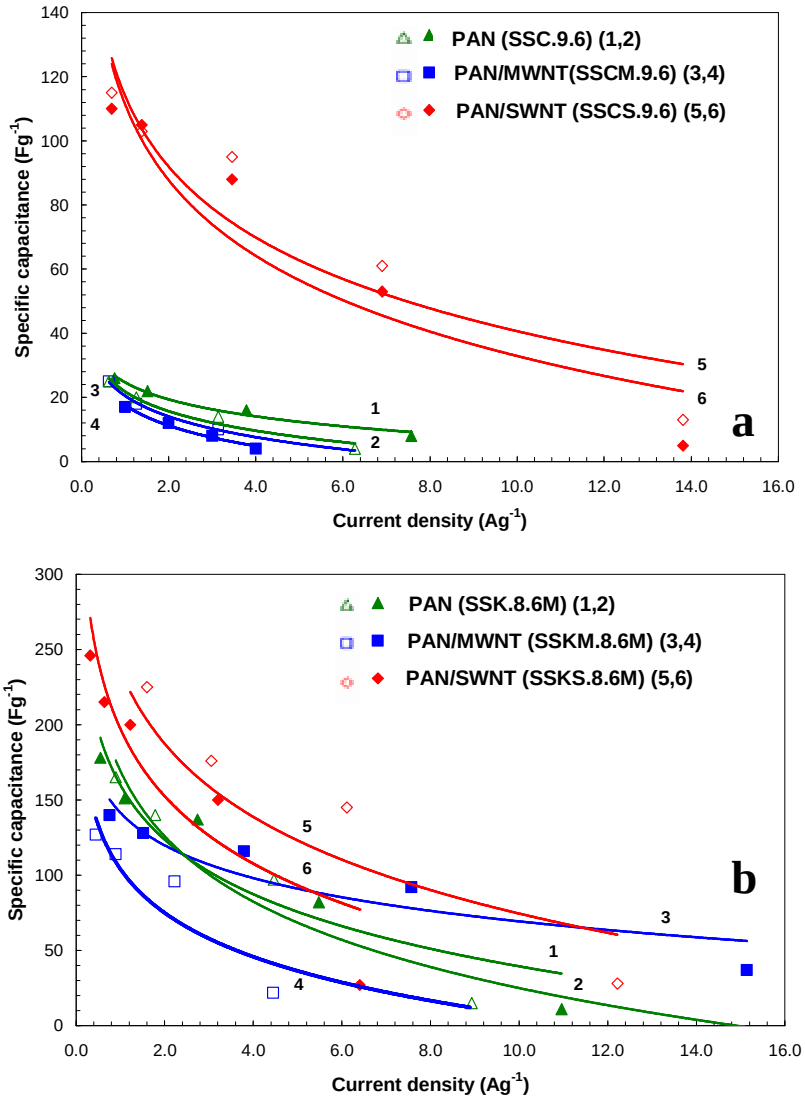

Figure 5.9. The specific capacitance as a function of current density measured from galvanostatic test for PAN, PAN/MWNT and PAN/SWNT fibers activated by (a) CO_2 and (b) KOH. 6M KOH was used as electrolyte. In each case, two samples were tested to assess reproducibility.

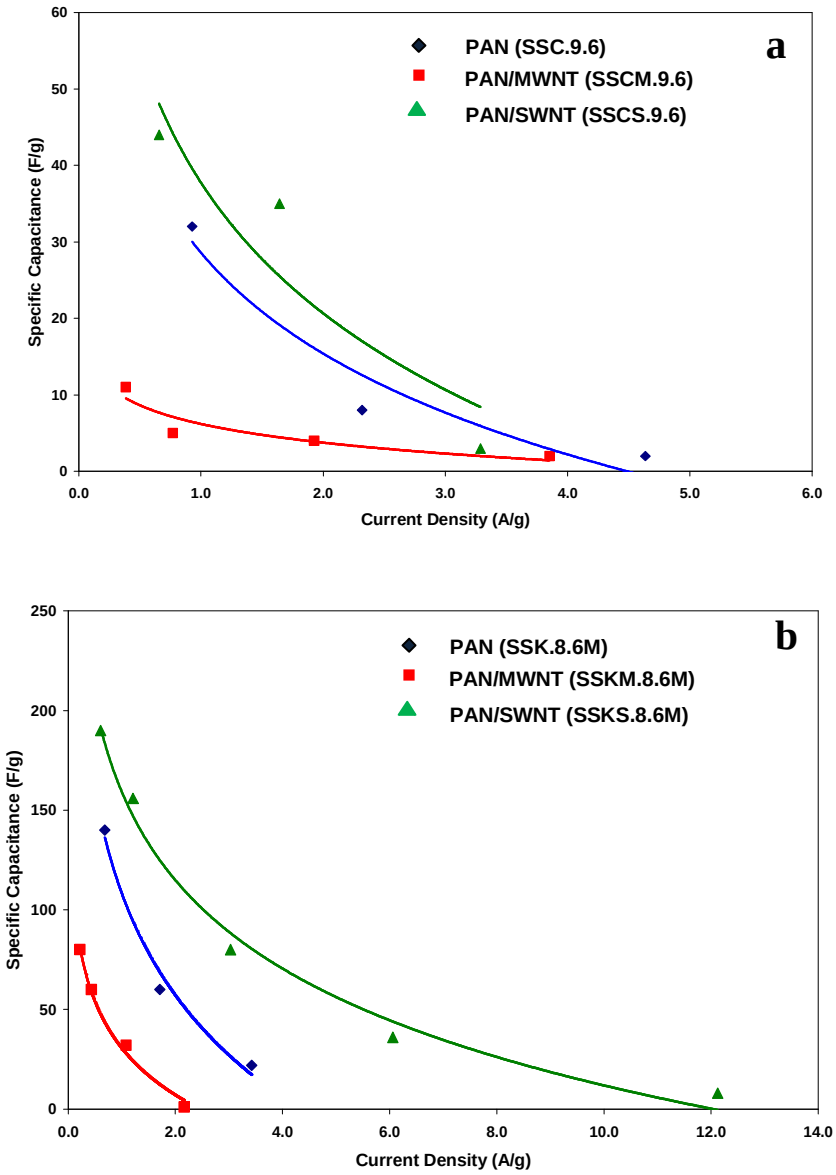

Figure 5.10. The specific capacitance as a function of current density measured from galvanostatic test for PAN, PAN/MWNT and PAN/SWNT fibers activated by (a) CO_2 and (b) KOH. $BMIMBF_4$/acetonitrile (1:2) was used as electrolyte.

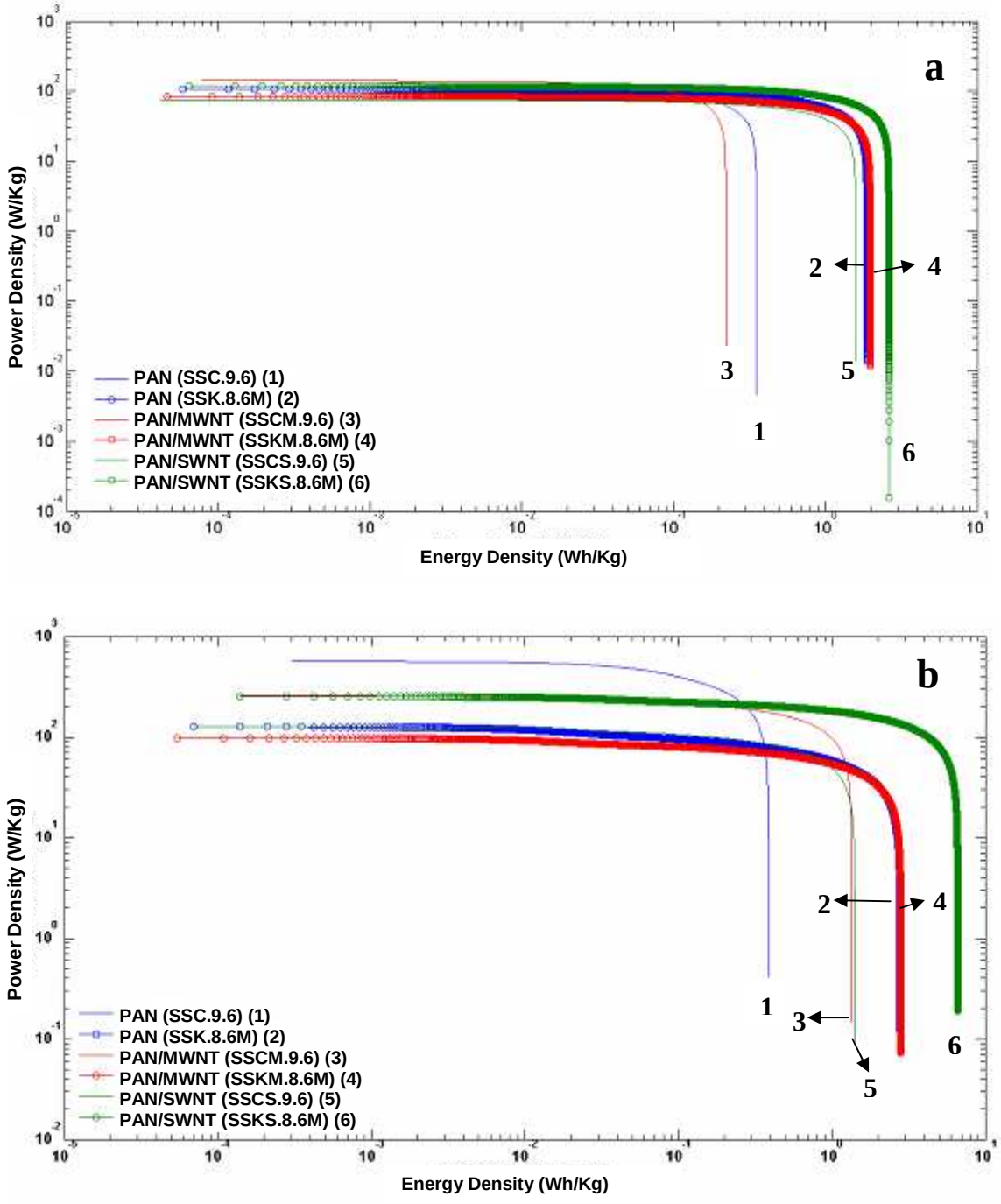

Figure 5.11. The power density and energy density measured at 0.1 mA galvanostatic test using 6M KOH(a) and $BMIMBF_4$/acetonitrile (1:2) as the electrolytes (b) for PAN, PAN/MWNT and PAN/SWNT fibers activated by CO_2 and KOH.

A surface area of 800 – 1000 m^2/g and specific capacitance of 100 – 200 F/g is typically reported for physically activated PAN films and fibers. A wide pore size distribution of 2 – 100 nm for films and nano fibers were reported. For chemically activated samples, surface area approaching 2500 m^2/g is often reported. The surface area differences between the physically and chemically activated current set of samples is consistent with the literature reports. Table 1.4 in chapter 1 summarizes capacitance data for other carbon materials, as well as for multi and single wall carbon nanotubes. The surface area differences between the CO_2 and KOH activated samples observed in the current work is consistent with the literature data that significantly higher surface area is obtained with chemical activation than from physical activation.

Capacitance of both MWNT and SWNT electrodes is consistently below 100 F/g, while higher values have been reported for functionalized MWNTs as well as for composites of carbon nanotubes with other systems (Tables 1.3 and 1.4). To the best of our knowledge, there are no literature reports on chemical activation of solution spun PAN/CNT fibers. Capacitance of 250 F/g in the current study for KOH activated solution spun PAN/CNT fibers (SSKS.8.6M) containing 5 wt% SWNTs in the precursor, is among the higher capacitance values reported to date. However, we do note that physically (CO_2) activated SWNT/PAN composite film containing 40% SWNTs showed capacitance in the range of 60 to 380 F/g, when the test cell was discharged from 0.7 to 0.2 V [3]. These studies show that the electrochemical capacitance of activated PAN/SWNT composites is higher than that of either SWNT bucky paper or activated PAN alone. Addition of just a few percent carbon nanotubes improves the capacitance performance significantly.

While there is no definite correlation established to date between the measured specific capacitance, electrolyte ion size, wettability, and electrode pore distribution, most literature reports suggest that meso-pores represents the ideal pore size for electrochemical capacitors[22-26]. However, there is a recent report of anomalously high capacitance at sub-nanometer pore size. The pore size obtained by KOH activation (SSK series) in the current work (1-5 nm) measured using nitrogen adsorption is on the high end of the micropore size and at the lower end of the mesopore size. Sub-nanometer size pores could not be measured in the samples studied in the current work due to our instrumental limitation, therefore we draw no conclusions on the anomalous mechanism.

5.2.5 Impedence spectroscopy

Figure 5.12 show impedance plots for CO_2 and KOH activated samples (SSC and SSK series). The knee frequency, transition point between kinetics controlled high-frequency impedance, and migration controlled low-frequency impedance is a measure of electrical and ionic conductivity of the cell. Specific capacitance as a function of knee frequency shows that for a given series (KOH or CO_2 activation), samples with higher knee frequency have lower specific capacitance (Figure 5.10c). However, it is noted that the CO_2 activated samples (SSC series) for a given knee frequency have lower specific capacitance than the KOH activated samples (SSK series). Keiser[27] derived relations for impedance as a function of frequency for various pore geometries using a transmission line equivalent circuit (figure 5.10 d). The impedance curves of CO_2 activated PAN (SSC.9.6) and PAN/MWNT (SSCM.9.6) samples exhibiting low specific capacitance is comparable in shape to the Keiser plots for type 5 pores.

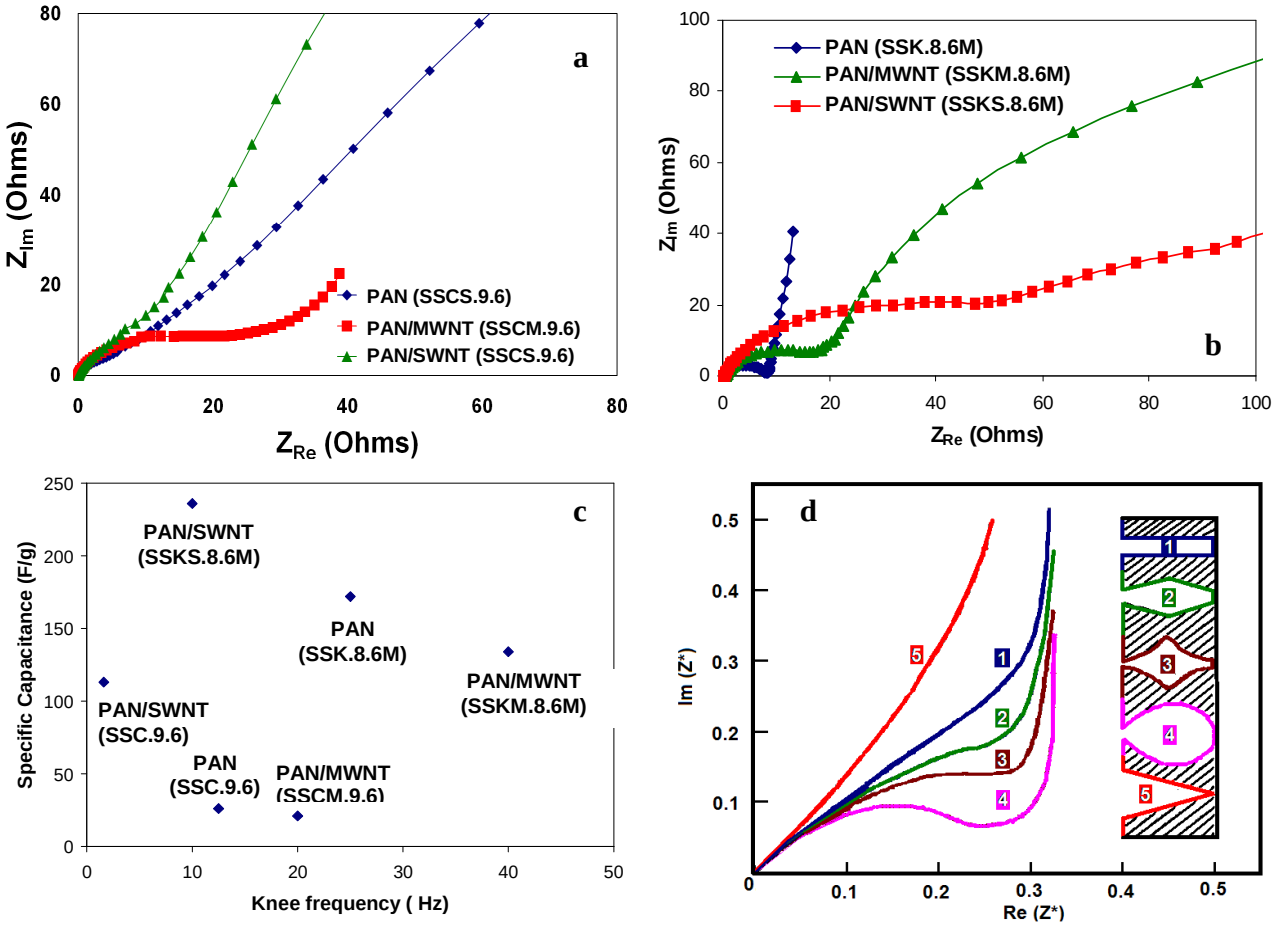

Figure 5.12. Impedance spectroscopy results for PAN, PAN/MWNT and PAN/SWNT samples activated by (a) CO_2 and (b) KOH. (c) Specific capacitance plotted against knee frequency (d) Pore shapes treated by Keiser [76] and corresponding complex-plane impedance plots. [Figure 9d. adapted from reference 76]. 6M KOH was used as electrolyte.

The type 5 pores in Keiser plot are wider at the surface with a decreasing width as they go deeper in the sample. However, a comparison of the observed impedance data to the Keiser derived impedance data suggests that KOH activated samples(SSK series) as well as CO_2 activated PAN/SWNT samples (SSCS.9.6) contain pores of the type 2, 3 or 4 with narrow entrance and wider body, which can act as an electrolyte reservoir.

In the case of CO_2 activation, pores are expected to be wider on the surface and narrow with depth. This is due to CO_2 diffusion along the sample thickness. In single and multi-wall carbon nanotube containing samples (SSCS.9.6 and SSCM.9.6), CO_2 can also diffuse through hollow tubes, as well as through tube interstices in the case of SWNT. In the case of SWNT, the single graphene layer would be easily damaged during CO_2 activation, providing pathways for CO_2 diffusion through the sample.

In the case of MWNTs, due to the presence of multiple graphene layers, damage under CO_2 activation may be limited to only few walls, while the other walls remain intact. Thus CO_2 diffusion through the bulk of the sample is very limited or non-existent in PAN/MWNT samples (SSCM.9.6), while it occurs in PAN/SWNT samples (SSCS.9.6). This is reflected in differences in surface area as well as in capacitance performance of the three CO_2 activated samples (Table 5.1). This also explains why impedance behavior and the pore shapes in PAN/SWNT (SSCS.9.6) are of different type than in PAN (SSC.9.6) and PAN/MWNT (SSCM.9.6).

Another question is why MWNT contribute in a negative way to the capacitance behavior under both types of activation, PAN/MWNT samples exhibit lower capacitance than the corresponding PAN. This can also be understood by multiple graphene layer stacking in MWNTs, which is not always penetrated by CO_2 activation as in the

surrounding matrix. Hence, we hypothesize that the presence of MWNTs limits activation, resulting in relatively low surface area and hence relatively low capacitance as compared to PAN and PAN/SWNT. Interaction differences between PAN-SWNT and PAN-MWNT may also be responsible for some of the observed differences. Based on the temperature dependence of dynamic mechanical tan δ plots, differences between PAN-SWNT and PAN-MWNT interactions have been reported[2]. Width of the tan δ vs temperature plot for the PAN/MWNT fibers is significantly reduced as compared to that of the control PAN due to polymer interaction with the nanotubes resulting in narrower spectrum of relaxation times. In the case of SWNT containing fibers, tan δ peak is broadened towards high temperature. We conjecture that PAN interactions with SWNT are stronger than with other larger diameter MWNTs and that PAN segments closer to the SWNT exhibit tan δ loss at higher temperature than the segments farther from it, leading to the broadening in the high temperature region. Intercalation of PAN in the SWNT bundle may also be partially responsible for the tan δ broadening behavior. Intercalated PAN on activation would enhance surface area leading to higher capacitance.

5.4 Conclusions

The structure and electrochemical properties of PAN, PAN/SWNT, and PAN/MWNT fibers activated by physical (CO_2) and chemical (KOH) methods are compared. High specific capacitance, surface area, and pore volume with narrow pore size distribution are achieved in PAN/SWNT (SSKS.8.6M) with chemical activation. The specific capacitance of KOH activated PAN/SWNT samples (SSKS.8.6M) was as high as 250 F/g in 6M KOH electrolyte. Under the comparable KOH activation conditions, PAN (SSK.8.6M) and PAN/SWNT fibers (SSKS.8.6M) had comparable surface areas (BET

surface area about 2200 m^2/g) with pore size predominantly in the range of 1 to 5 nm, while surface area of PAN/MWNT samples (SSKM.8.6M) was significantly lower (BET surface area 970 m^2/g). Energy density of activated fibers is improved when ionic liquid was used as an electrolyte instead of aqueous 6M KOH. The highest energy density (6.4 Wh/kg) was obtained for KOH activated PAN/SWNT (SSKS.8.6M) in ionic liquid.

5. 5 References

[1] Chae HG, Minus ML, Kumar S. Oriented and exfoliated single wall carbon nanotubes in polyacrylonitrile. Polymer. 2006;47(10):3494-504.

[2] Chae HG, Sreekumar TV, Uchida T, Kumar S. A comparison of reinforcement efficiency of various types of carbon nanotubes in polyacrylonitrile fiber. Polymer. 2005;46(24):10925-35.

[3] Liu T, Sreekumar TV, Kumar S, Hauge RH, Smalley RE. SWNT/PAN composite film-based supercapacitors. Carbon. 2003;41(12):2440-2.

[4] Sreekumar TV, Kumar S. Macroscopic fiber comprising single-wall carbon nanotubes and acrylonitrile-based polymer and process for making the same US Patent 6,852,410 2005.

[5] Sreekumar TV, Liu T, Min BG, Guo H, Kumar S, Hauge RH, et al. Polyacrylonitrile Single-Walled Carbon Nanotube Composite Fibers. Advanced Materials. 2004;16(1):58-61.

[6] Ko F, Gogotsi Y, Ali A, Naguib N, Ye H, Yang GL, et al. Electrospinning of Continuous Carbon Nanotube-Filled Nanofiber Yarns. Advanced Materials. 2003;15(14):1161-5.

[7] Ye H, Lam H, Titchenal N, Gogotsi Y, Ko F. Reinforcement and rupture behavior of carbon nanotubes--polymer nanofibers. Applied Physics Letters. 2004;85(10):1775-7.

[8] Prilutsky S, Zussman E, Cohen Y. The effect of embedded carbon nanotubes on the morphological evolution during the carbonization of poly(acrylonitrile) nanofibers. Nanotechnology. 2008;19(16):165603.

[9] Vaisman L, Wachtel E, Wagner HD, Marom G. Polymer-nanoinclusion interactions in carbon nanotube based polyacrylonitrile extruded and electrospun fibers. Polymer. 2007;48(23):6843-54.

[10] Kim D-K, Park SH, Kim BC, Chin BD, Jo SM, Kim DY. Electrospun Polyacrylonitrile-Based Carbon Nanofibers and Their Hydrogen Storages. Macromolecular Research. 2005;13(6):521-8.

[11] Béguin F, Szostak K, Lota G, Frackowiak E. A Self-Supporting Electrode for Supercapacitors Prepared by One-Step Pyrolysis of Carbon Nanotube/Polyacrylonitrile Blends. Advanced Materials. 2005;17(19):2380-4.

[12] Hou H, Ge JJ, Zeng J, Li Q, Reneker DH, Greiner A, et al. Electrospun Polyacrylonitrile Nanofibers Containing a High Concentration of Well-Aligned Multiwall Carbon Nanotubes. Chem Mater. 2005;17(5):967-73.

[13] Yu M-J, Wang C-G, Bai Y-J, Ji M-X, Xu Y. SEM and OM Study on the Microstructure of Oxidative Stabilized Polyacrylonitrile Fibers. Polymer Bulletin. 2007;58(5):933-40.

[14] Layden GK. Retrograde core formation during oxidation of polyacrylonitrile filaments. Carbon. 1972;10(1):59-60.

[15] Barnet FR, Norr MK. A three-dimensional structural model for a high modulus pan-based carbon fibre. Composites. 1976;7(2):93-9.

[16] Yu M-J, Bai Y-J, Wang C-G, Xu Y, Guo P-Z. A new method for the evaluation of stabilization index of polyacrylonitrile fibers. Materials Letters. 2007;61(11-12):2292-4.

[17] Moon SY, Kim M-s, Hahm H-S, Lim Y-S. Preparation of activated carbon fibers by chemical activation method with hydroxides. Material Science Forum. 2006;510-511:750-3.

[18] Lee Y-J, Kim J-H, Kim J, Lee DB, Lee J-C, Chung Y-J, et al. Fabrication of activated carbon fibers from stabilized PAN-based fibers by KOH. Materials Science forum. 2004;449-452:217-20.

[19] Sing KSW, Everett DH, Haul RAW, Moscou L, Pierotti RA, Rouquerol J, et al. REPORTING PHYSISORPTION DATA FOR GAS/SOLID SYSTEMS with Special Reference to the Determination of Surface Area and Porosity. Pure & Appl Chem. 1985;57(4):603.

[20] Lowell S, Shields JE, Thomas MA, Thommes M. Characterization of porous solids and powders: Surface area, pore size and density, Kluwer Academic Publishers, Dordrecht/Boston/London. 2004.

[21] Webb PA, Orr C. Analytical methods in fine particle technology, Micromeritics Instruments Corp , Norcross, Georgia. 1997.

[22] Zhou C. Carbon nanotube based electrochemical supercapacitors. PhD Thesis, Georgia Institute of Technology. 2006:42.

[23] Liu CG, Fang HT, Li F, Liu M, Cheng HM. Single-walled carbon nanotubes modified by electrochemical treatment for application in electrochemical capacitors. Journal of Power Sources. 2006;160(1):758-61.

[24] Fuertes AB, Lota G, Centeno TA, Frackowiak E. Templated mesoporous carbons for supercapacitor application. Electrochimica Acta. 2005;50(14):2799-805.

[25] Morishita T, Soneda Y, Tsumura T, Inagaki M. Preparation of porous carbons from thermoplastic precursors and their performance for electric double layer capacitors. Carbon. 2006;44(12):2360-7.

[26] Wang T. Electrospun Carbon Nanofibers for Electrochemical Capacitor Electrodes. PhD Thesis, Georgia Institute of Technology. 2007.

[27] Keiser H, Beccu KD, Gutjahr MA. Abschatzung der porenstruktur poroser elektroden aus impedanzmessungen. Electrochimica Acta. 1976;21(8):539-43.

Chapter 6

STRUCTURE AND ELECTROCHEMICAL PROPERTIES OF CHEMICALLY ACTIVATED GEL SPUN FIBERS CONTAINING NANOTUBES

6.1 Introduction

Gel spinning is developed to produce ultra high strength fibers with high polymer molecular orientation from high molecular weight polymers[1-6]. This process involves transformation of polymer solution into a gel, gel spinning and subsequent solvent removal, and drawing to orient the polymer chains. The as-spun fibers from gel spinning will retain most of the solvent to form a gel of polymer and solvent. These fibers on annealing can give additional pores due to solvent evaporation. Recently, PAN/SWNT composite fibers spun by gel spinning process and drawn to a draw ratio of 51 are reported to have exfoliated SWNTs[7]. These well dispersed exfoliated SWNTs in gel spun fibers can act as a template to create an ordered pore structure. Therefore, chemical activation of gel spun fibers is explored to achieve ordered pore structure with optimum electrochemical properties. These samples are chosen due to higher degree of polymer molecular orientation, CNT exfoliation, and orientation compared to films and solution spun fibers.

In chapter 5 on solution spun fibers, PAN/SWNT samples (SSCS.9.6 and SSKS.8.6M) exhibited higher specific capacitance than PAN (SSC.9.6 and SSK.8.6M) and PAN/MWNT (SSCM.9.6 and SSKM.8.6M) fibers. Microscopic studies reveal PAN/MWNT samples with more condensed structure while PAN and PAN/SWNT were highly porous. The electrochemical properties achieved by chemical activation of gel

spun PAN fibers containing two types of CNTs and the differences in values achieved for as-spun gel spun fibers and drawn gel spun fibers on activation are explored.

6.2 Experimental

SWNTs were obtained from Carbon Nanotechnologies, Inc. (Houston, TX) (Grade XO1PPP, 2.4% catalytic impurity) and MWNTs were from Iljin Nanotech, Co (Korea) (2.5% catalytic impurity). Poly(acrylonitrile) with viscosity average molecular weight ~ 250,000 g/mol from same supplier was used for preparing gel spun fibers. The solvent, DMF purchased from Sigma-Aldrich were used as received. Detailed description of fiber processing method, heat treatment conditions as well as characterization methods are given in chapter 2.

6.3 Results and discussion

6.3.1 Structure and morphology

PAN and PAN/CNT fibers were stabilized at conditions optimized by H.G. Chae et al.[8] used for preparing carbon fibers. The extent of stabilization was verified using WAXD as explained in chapter 4[9, 10]. The scanning electron microscopy images of activated PAN and PAN/CNT gel spun fiber (GSASK and GSDRK series) sample surfaces activated by KOH at 800 °C are given in Figure 6.1. The samples with diameters greater than 25 µm (all as-spun and PAN DR(draw ratio) 42) were able to retain the integrity as individual fibers after activation, while PAN/MWNT DR 45(GSDRKM.8.6M) and PAN/SWNT DR 45 (GSDRKM.8.6M) fibers with diameters less than 20 µm resulted in bulk carbon after KOH activation. The images also show a similarity in activated structure for both control PAN fibers and composite samples. The fibril structure observed for KOH activated solution spun PAN fibers(SSK.8.6M) in

chapter 4 as well as the ones reported in literature by S. Y. Moon[11] and Y. J. Lee[12] is not observed for as-spun and drawn gel spun fibers. However, these porous structures resemble chemically activated solution spun PAN/CNT composite fiber samples (SSKS.8.6M and SSKM.8.6M).

6.3.2 Surface area and pore size distribution

The BET surface areas given in Table 6.1 show an enhanced value for PAN and PAN/SWNT samples when compared to PAN/MWNT fibers for both as-spun (GSASK series) as well as drawn gel spun fibers (GSDRK series). MWNTs having relatively perfect graphite-like crystalline structure with stacked graphene sheets makes it hard to attack during the activation process. Hence, similar to the hypothesis made for solution spun fibers the presence of MWNTs limits activation resulting in relatively low surface area hence relatively low capacitance as compared to PAN (SSK.8.6M) and PAN/SWNT fibers (SSKS.8.6M). As explained in chapter 4, the interaction differences between PAN-SWNT and PAN-MWNT may also be responsible for some of the observed differences. Based on the temperature dependence of dynamic mechanical tan δ plots in reference[13], we conjecture that PAN interactions with SWNT are stronger than with other larger diameter MWNTs and that PAN segments closer to the SWNT exhibit tan δ loss at higher temperature than the segments farther from it, leading to the broadening in the high temperature region[13]. Intercalation of PAN in the SWNT bundle may also be partially responsible for the tan δ broadening behavior. Intercalated PAN on activation would enhance surface area leading to higher capacitance.

Table 6.1. Specific capacitance, surface area, and double layer capacity for gel spun spin-drawn and drawn fibers.

Label	Sample	Diameter	Precursor Crystal size	Specific capacitance (F/g) (0.1 mA constant current test)		Surface Area (m^{2}/g)		Energy Density*	Power Density*	Double layer capacitance (μF/cm^2)**		Pore volume (cm^3/g)
		(μm)	(nm)	6M KOH	BMIMBF4: AC (1:2)	BET	DFT	(Wh/kg)	(W/kg)	BET	DFT	
Spin-drawn fibers												
GSASK.8.6M	PAN SDR - 4	58	2.6	225	220	2026	812	2.41	590	11	28	0.81
GSASKM.8.6M	PAN/MWNT SDR - 3	49	3.0	196	150	956	442	1.73	250	21	44	0.36
GSASKS.8.6M	PAN/SWNT SDR - 3	26	2.5	212	196	2332	1011	1.86	800	9	21	0.94
Drawn fibers												
GSDRK.8.6M	PAN DR - 42	28	11.5	240	188	2724	1130	1.94	620	9	21	1.16
GSDRKM.8.6M	PAN/MWNT DR - 45	14	9.6	90	78	1213	621	1.02	730	7	14	0.66
GSDRKS.8.6M	PAN/SWNT DR - 45	19	11.5	140	160	2018	890	0.30	1230	7	16	1.10

*Energy density and Power density measured at galvanostatic test at 0.5 mA using KOH electrolyte.
**Double layer capacitance reported for 6M KOH electrolyte.

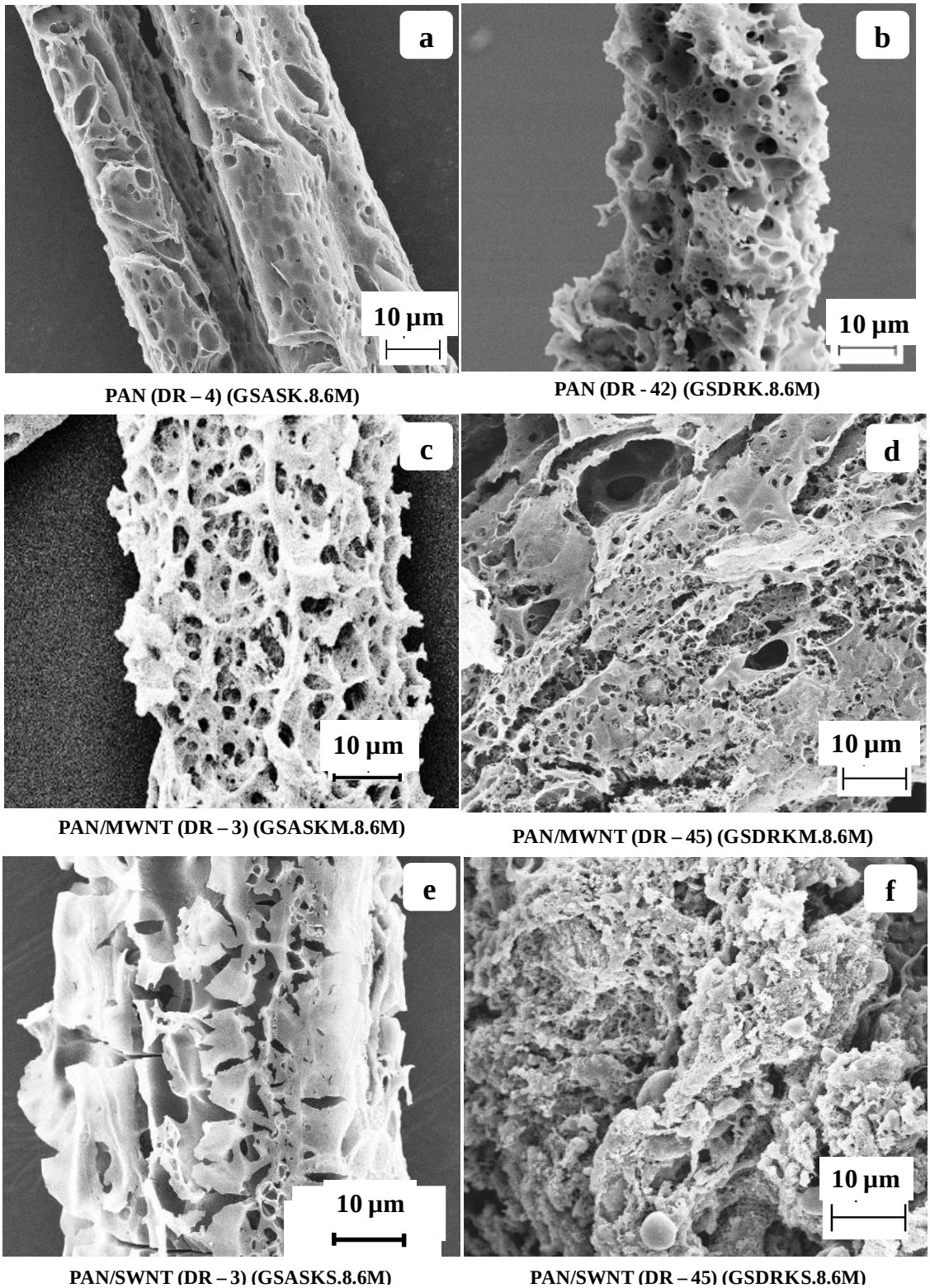

Figure 6.1 Scanning Electron Micrographs of as-spun (a, c, e) and drawn (b, d, f) PAN, (a, b), PAN/SWNT (c, d) and PAN/MWNT (e, f) fibers KOH activated at 800 ºC.

Surface area and pore size distribution of activated fibers are characterized by nitrogen gas adsorption. Based on the IUPAC classification, type I nitrogen gas adsorption isotherm is exhibited by micropores, while type IV isotherm is exhibited by mesoporous materials[13-15]. The KOH activated as-spun PAN and PAN/CNT fibers (GSAS series) show a mixture of type I isotherm (Figure 6.2a) with high nitrogen uptakes at relatively low pressures characteristic of micropores as well as type IV mesopores behavior presenting a hysteresis loop at relatively high pressures. The hysteresis loops obtained for KOH activated as-spun PAN and PAN/CNT fibers (GSASK series) are of type H4, which is typically attributed to narrow slit shaped pores including pores in the micropore region[13]. Similar type I and IV isotherms are obtained for drawn KOH activated PAN and PAN/CNT fibers (GSDRK series) with negligible hysteresis loop H2. The type H2 hysteresis is often attributed to disordered carbon with a distribution of pore sizes or shape not well defined. All six KOH activated gel spun samples show pores predominantly in the 1-5 nm range, with two prominent peaks at 1.2 and 2.5-2.7 nm range. The first peak is more prominent for as-spun fibers while the pore size distribution becomes wider for drawn gel spun fibers noted by the increase in intensity of second peak.

6.3.3 Electrochemical properties

KOH activated as-spun PAN (GSASK.8.6M) and drawn PAN (GSDRK.8.6M) gel spun fibers exhibit higher capacitance compared to respective PAN/CNT activated fiber samples in 6M KOH as well as in ionic liquid electrolytes (Figure 6.3).

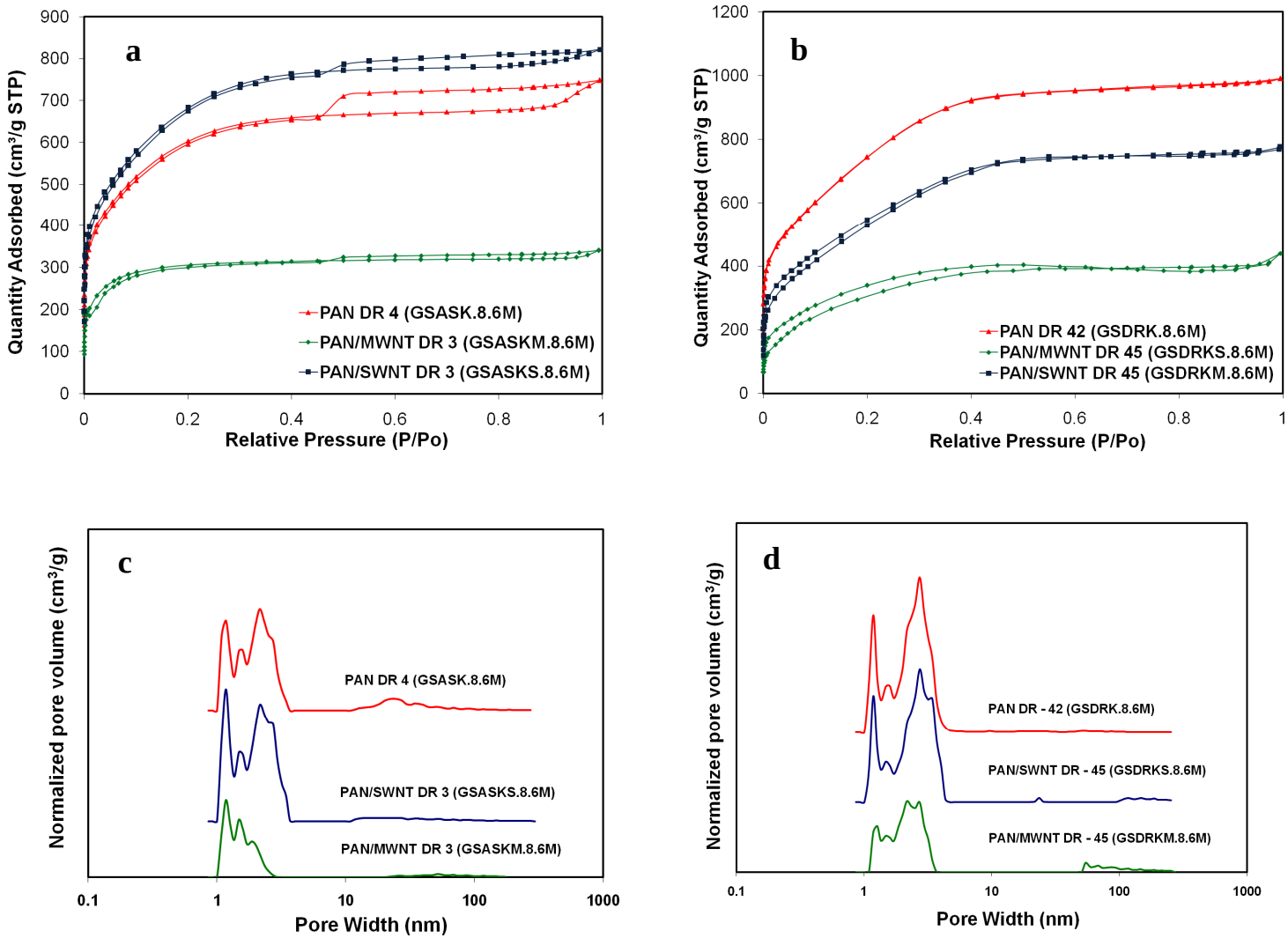

Figure 6.2 Nitrogen adsorption isotherms (a, b) and Pore size distribution measured by density functional theory method (c,d) for PAN, PAN/MWNT and PAN/SWNT (a,c) as-spun and (b,d) drawn gel spun fibers.

In addition, in both type of fibers, PAN (GSASK.8.6M and GSDRK.8.6M) and PAN/SWNT (GSASKS.8.6M and GSDRKS.8.6M) shows higher capacitance than PAN/MWNT samples (GSASKM.8.6M and GSDRKM.8.6M) similar to solution spun fibers.

A maximum capacitance for drawn PAN gel spun fibers is as high as 240 F/g at low current density (0.01 A/g in 6M KOH). The energy densities of fibers followed a similar trend as specific capacitance values. The energy density and specific capacitance for as-spun fibers were higher than drawn PAN possibly due to porous nature of precursor as-spun gel spun fibers. In drawn PAN/CNT fibers, the excellent interaction between polymer and nanotube cause break down of carbon structure at activation temperature more challenging leading to reduction in electrochemical properties. The enhancement of PAN-CNT interaction has been verified by comparing the mechanical properties of solution spun as well as gel spun fibers in previous publications[7, 8]. An enormous increase of energy density from ~2 Wh/Kg in 6M KOH to ~ 22 Wh/Kg in $BMIMBF_4$/AC was achieved at 0.1mA constant current for PAN as-spun fibers by increasing the operating voltage from 0.8 to 3.0 V respectively (Figure 6.4). The specific capacitance values measured in ionic liquid is lower than that in KOH at all current densities (Table 6.1 and Figure 6.3). This is attributed to the relatively large ion size of the ionic liquid that cannot access small pores even at low current density[16].

There was no significant increase in power density observed for activated PAN fibers with the addition of CNTs, possibly due to addition of polyvinylene di fluoride (PVDF) used for electrode preparation.

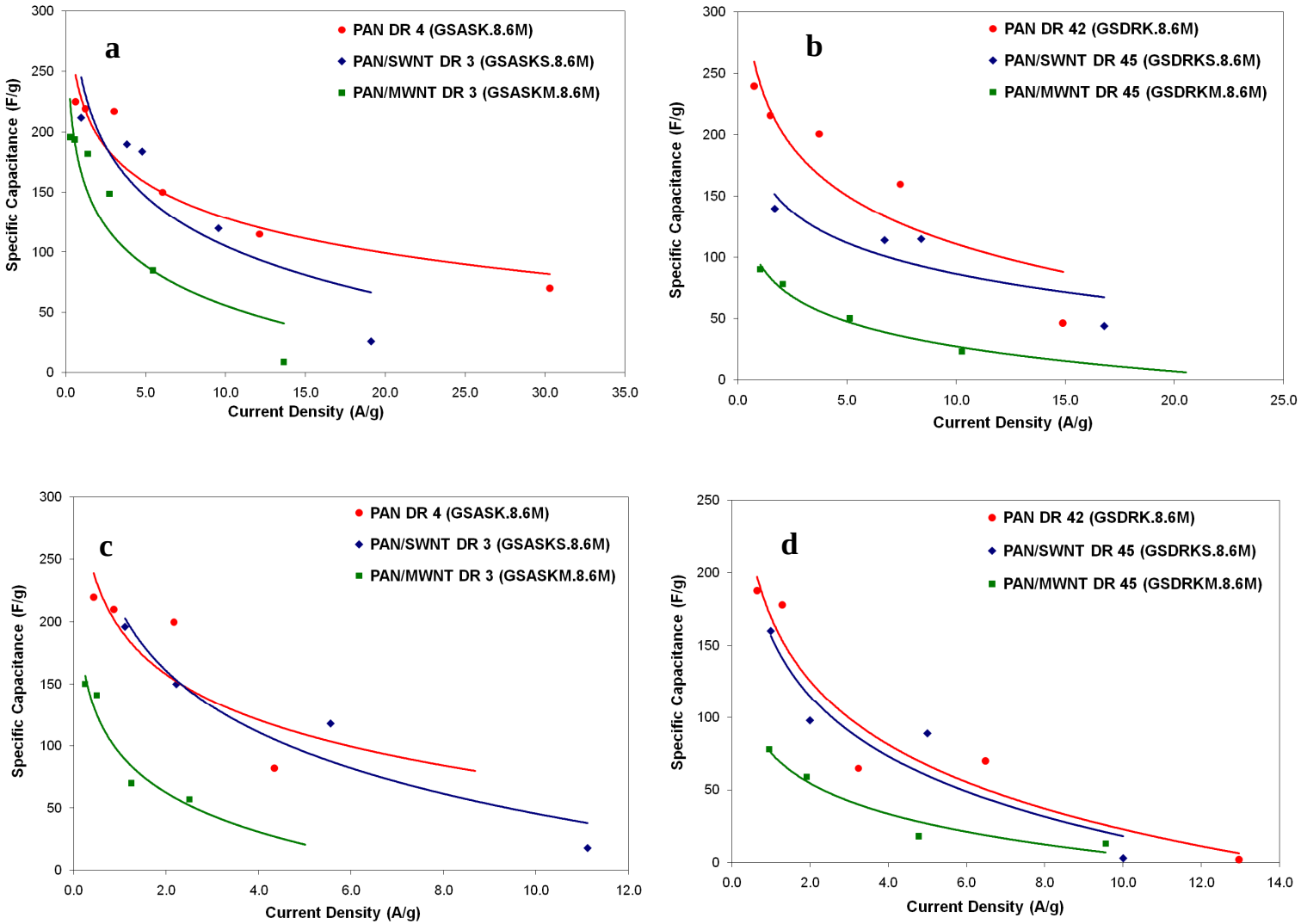

Figure 6.3 Specific capacitance as a function of current density for as-spun (a,c) and drawn gel spun PAN, PAN/SWNT and PAN/MWNT fibers tested in 6M KOH(a, b) as well as $BMIMBF_4$/AC (1:2) electrolytes (c, d).

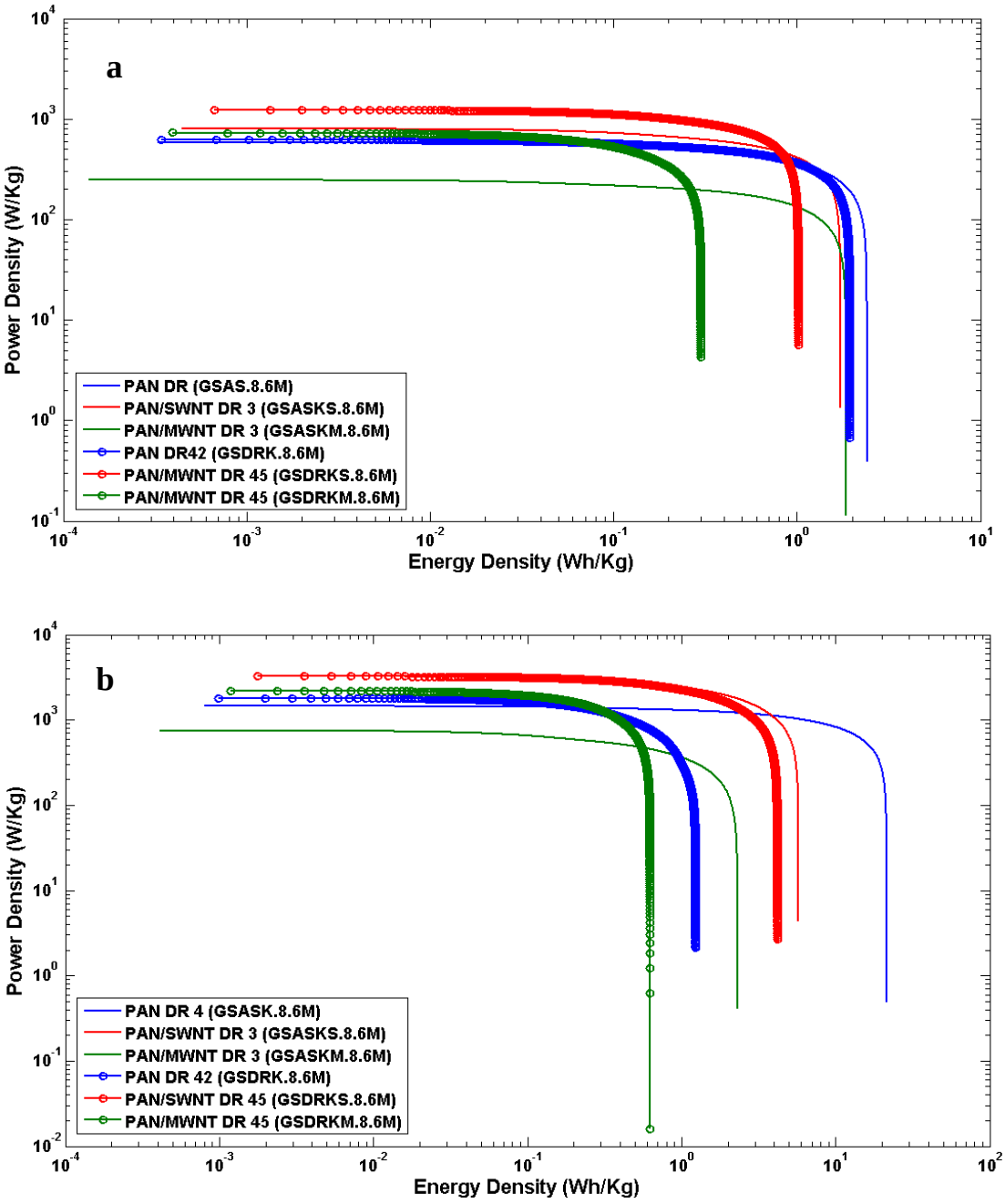

Figure 6.4 Power density and Energy density measured at 0.5 mA galvanostatic test measured in (a) 6M KOH and (b) $BMIMBF_4$:AC electrolytes for as-spun and drawn PAN, PAN/SWNT and PAN/MWNT gel spun fibers.

Use of insulating polymeric binder aggravates the power performance of the electrochemical capacitor by increasing the resistance of the electrode, since the energy delivery rate for a device is proportional to the product of its resistance and capacitance. Also, the binder materials could fill up or block the pores formed on activation process, so that the energy density of the electrode also deteriorates by using the binder materials. Hence, dependence of electrochemical properties on type of CNTs used, draw ratio, diameter of fibers and changes in power densities (Table 1) were not clearly understood when binder is used for electrode preparation.

6.4 Conclusions

The structure, and electrochemical properties of drawn and as-spun gel spun PAN, PAN/SWNT and PAN/MWNT fibers, with higher degree of polymer molecular orientation and CNT exfoliation and orientation activated by chemical (KOH) methods were investigated. The specific capacitance of KOH activated drawn PAN samples was as high as 240 F/g in 6M KOH electrolyte. Under the comparable KOH activation conditions, as-spun as well as drawn PAN and PAN/SWNT fibers resulted in higher BET surface areas with pore size predominantly in the range of 1 to 5 nm, while surface area of PAN/MWNT samples was significantly lower. Energy densities increased from ~2 Wh/Kg in 6M KOH to a maximum of ~ 22 Wh/Kg in $BMIMBF_4$/AC at 0.1mA constant current for PAN as-spun fibers by increasing the operating voltage from 0.8 to 3.0 V respectively.

6.5 References

[1] Smith P, Lemstra PJ. Tensile-Strength Of Highly Oriented Polyethylene. Journal of Polymer Science Part B-Polymer Physics. 1981;19(6):1007-9.

[2] Smith P, Lemstra PJ, Kalb B, Pennings AJ. Ultrahigh-Strength Polyethylene Filaments By Solution Spinning And Hot Drawing. Polymer Bulletin. 1979;1(11):733-6.

[3] Cha WI, Hyon SH, Ikada Y. Gel Spinning of Poly(vinyl alcohol) from Dimethyl Sulfoxide/Water Mixture. Journal of Polymer Science Part B-Polymer Physics. 1994 Jan 30 1994;32(2):297-304.

[4] Zhang X, Liu T, Sreekumar TV, Kumar S, Hu X, Smith K. Gel Spinning of PVA/SWNT Composite Fiber. Polymer. 2004;45:8801-7.

[5] Yamaura K, Kumakura R. Gel Spinning of Partially Saponificated Poly(vinly alcohol). Journal of Polymer Science. 2000;77:2872-6.

[6] Hoogsteen W, van der Hooft RJ, Postema AR, ten Brinke G, Pennings AJ. Gel Spun Polyethylene Fibres. Journal of Materials Science. 1988;23(5):3459-66.

[7] Chae HG, Minus ML, Kumar S. Oriented and exfoliated single wall carbon nanotubes in polyacrylonitrile. Polymer. 2006;47(10):3494-504.

[8] Chae HG, Minus ML, Rasheed A, Kumar S. Stabilization and carbonization of gel spun polyacrylonitrile/single wall carbon nanotube composite fibers. Polymer. 2007:1-9.

[9] Yu M-J, Bai Y-J, Wang C-G, Xu Y, Guo P-Z. A new method for the evaluation of stabilization index of polyacrylonitrile fibers. Materials Letters. 2007;61(11-12):2292-4.

[10] Jagannathan S, Chae H, Jain R, Kumar S. Structure and electrochemical properties of activated polyacrylonitrile based carbon fibers containing carbon nanotubes. Journal of Power Sources (Accepted, In Press). 2008;doi:10.1016/j.jpowsour.2008.08.093.

[11] Moon SY, Kim M-s, Hahm H-S, Lim Y-S. Preparation of activated carbon fibers by chemical activation method with hydroxides. Material Science Forum. 2006;510-511:750-3.

[12] Lee Y-J, Kim J-H, Kim J, Lee DB, Lee J-C, Chung Y-J, et al. Fabrication of activated carbon fibers from stabilized PAN-based fibers by KOH. Materials Science forum. 2004;449-452:217-20.

[13] Sing KSW, Everett DH, Haul RAW, Moscou L, Pierotti RA, Rouquerol J, et al. REPORTING PHYSISORPTION DATA FOR GAS/SOLID SYSTEMS with Special

Reference to the Determination of Surface Area and Porosity. Pure & Appl Chem. 1985;57(4):603.

[14] Lowell S, Shields JE, Thomas MA, Thommes M. Characterization of porous solids and powders: Surface area, pore size and density, Kluwer Academic Publishers, Dordrecht/Boston/London. 2004.

[15] Webb PA, Orr C. Analytical methods in fine particle technology, Micromeritics Instruments Corp , Norcross, Georgia. 1997.

[16] Zhou C. Carbon nanotube based electrochemical supercapacitors. PhD Thesis, Georgia Institute of Technology. 2006:42.

Chapter 7

CHEMICAL ACTIVATION OF CARBON NANOTUBE BUCKYPAPER ELECTRODES

7.1 Introduction

Literature reports on CNT based electrodes for electrochemical capacitors show a specific capacitance of 15 – 55 F/g for untreated CNT buckypapers in aqueous electrolytes[1-4] and 25 – 75 F/g in organic electrolytes[2, 5, 6]. The CNTs were treated with NH_3 plasma[1], HNO_3[7, 8], HCl[6, 9] or functionalized with aryl sulphonic acid[3, 4] to increase the specific capacitance to 100 – 365 F/g by increasing the pseudocapacitance of the electrodes. Chemical activation is presented as an alternate method to increase specific capacitance by increasing the accessible surface area of electrodes and by achieving narrow micropore distribution required for charge storage. Sodium hydroxide and potassium hydroxide, among all chemical activating agents, are the widely reported for activation of CNT electrodes[10-12].

Jiang et al.[12] reported increase in specific capacitance of carbon nanotubes from 25 to 50 F/g when activated with KOH at 850 ºC for 1h. Jiang[11] also measured the effect of nitrogen flow rate on specific capacitance of KOH activated carbon nanotubes at 850 ºC. The experiment with nitrogen flow rates varying form 0 – 1400 ml/min showed a maximum capacitance of 45 F/g for flow rate maintained at 400 ml/min. Similar observation was reported by Frackowiak [10] where the specific capacitance increased from 10-15 F/g for untreated sample in electrolytes 6M KOH, 1M H_2SO_4 and 1.4 M $TEABF_4$ in acetonitrile to 90 F/g in KOH, and up to 95 F/g in H_2SO_4, 65 F/g in $TEABF_4$ on activation of MWNTs with 4:1 (K:C) chemical ratio at 800 ºc in nitrogen atmosphere.

In previous chapters on solution spun (SSK series) and gel spun fibers (GSASK and GSDRK series), PAN and PAN/SWNT samples exhibited higher specific capacitance than PAN/MWNT fibers. Microscopic studies reveal that PAN/MWNT samples with more condensed structure while PAN and PAN/SWNT were highly porous. Hence, changes in physical structure of CNTs and formation of any chemical groups on the surface of CNTs are probed in this chapter for SWNT (BS.00.8.6M) and MWNT (BM.00.8.6M) buckypapers to understand any possible difference in interaction with PAN.

7.2 Experimental

CNTs (Grade X0671UA ~ 1% metal impurity) received from Carbon Nanotechnologies Inc., Houston, TX was used to prepare CNT buckypapers. MWNTs from Iljin Nanotech, Co (Korea) (2.5% catalytic impurity) were used for MWNT buckypapers. The solvent DMF purchased from Sigma-Aldrich were used as received. Detailed description of fiber processing method, heat treatment conditions as well as characterization methods are given in chapter 2.

7.3 Results and discussion

7.3.1 Structure and Morphology

SEM images given in Figure 7.1 for SWNTs (BS.00.8.6M) with show a change in morphology with visible etching of bundle structures by KOH during activation process. The presence of amorphous or disordered carbon was observed in MWNT buckypapers (BM.00.8.6M) which becomes more visible after activation.

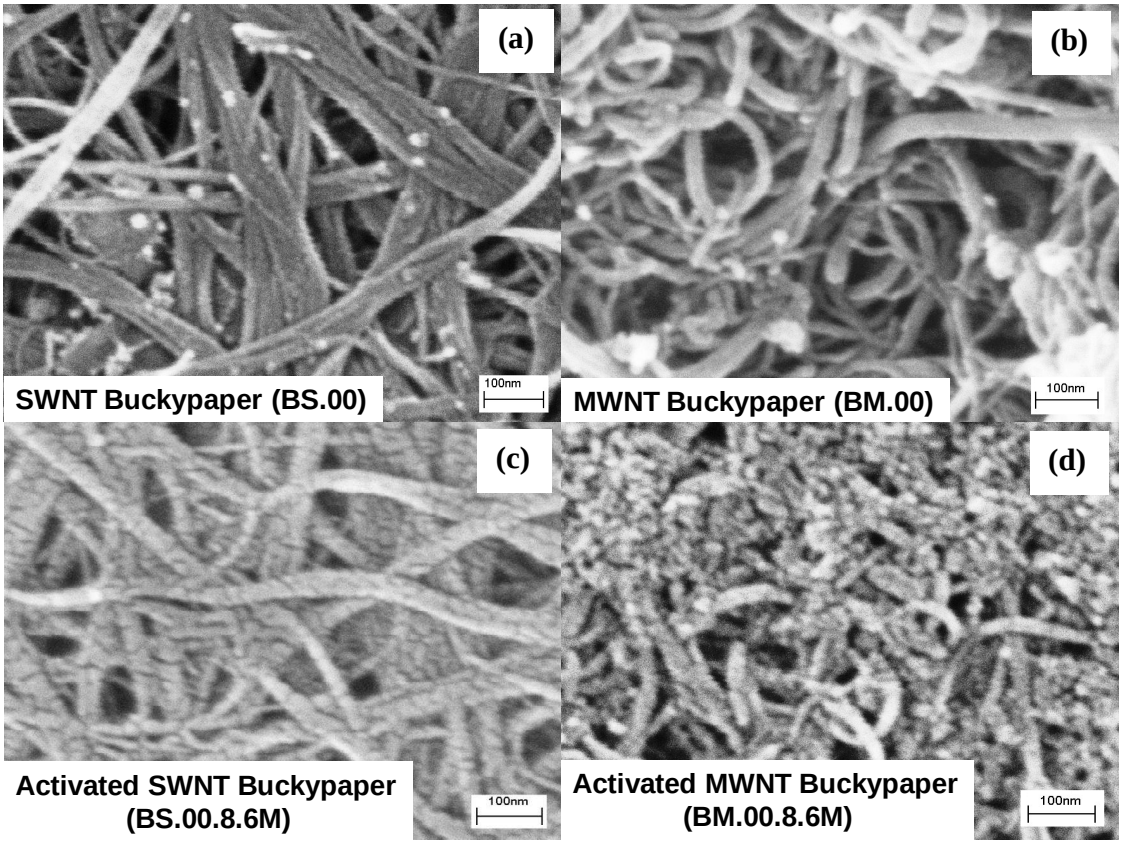

Figure 7.1 Scanning electron microscopy images of (a, c) SWNT and (b, d) MWNT buckypapers (a, b) as prepared and (c, d) activated at different resolutions.

Raman spectra for all the samples were collected as given in Figure 7.2 and the intensity in all cases is normalized to the intensity of the G band (1550-1605 cm^{-1}). The disorder induced D band appears at ~1300 cm^{-1} due to the presence of disordered carbon, and SWNTs with incomplete or modified wall structure [13, 14]. The intensity of this peak is referred to understand the degree of disorder in CNTs. Normalized intensity of D band for SWNT bucky paper (BS.00.8.6M) reduced from 0.1 to 0.08 during activation process denoting relatively undamaged CNTs structures for both as prepared as well as activated SWNT buckypapers. The intensity of D band of as prepared and activated MWNT bucky papers (BM.00.8.6M) were high (~2.9 and 2.3 respectively), indicating highly defective

graphitic structures present in these two samples. Decreases in D band intensities for activated samples are due to partial removal of amorphous carbon at activation temperature of 800 ºC.

7.3.2 Surface area and pore size distribution

The pore volume distribution and surface area results for CNT powder, as-prepared and activated buckypapers are given in Figure 7.3. BET surface area of SWNT powders reduces from 659 to 198 m^2/g during buckypaper preparation denoting formation of compact SWNT buckypaper film (BS.00) block good amount of micro and meso pores originally present in SWNT powders (Table 7.1). The CNT bundle diameter, measured from SEM images using digimizer software, increased from 18 to 21 nm during buckypaper formation. The total BET surface area increases to 626 m^2/g on chemical activation due to creation of more number of pores as seen in Figure 7.3a. BET surface area of MWNT powders reduces from 161 to 116 m^2/g on buckypaper film formation (BM.00). This decrease in surface area is lower compared to SWNT due to difficulty in preparing compact buckypaper films from MWNT. However, chemical activation process increases the BET surface area to 401 m^2/g which is about 2.5 times the value of MWNT powder. SWNT powders as well as buckypapers are predominantly mesoporous materials while MWNTs have combination of meso and macropores. With macropores not significantly contributing to total surface area, MWNTs exhibit much lower surface area compared to SWNTs. CNT film formation process as well as activation process did not vary the pore size distribution for both cases of SWNT and MWNT as seen in Figure 7.3(a, b).

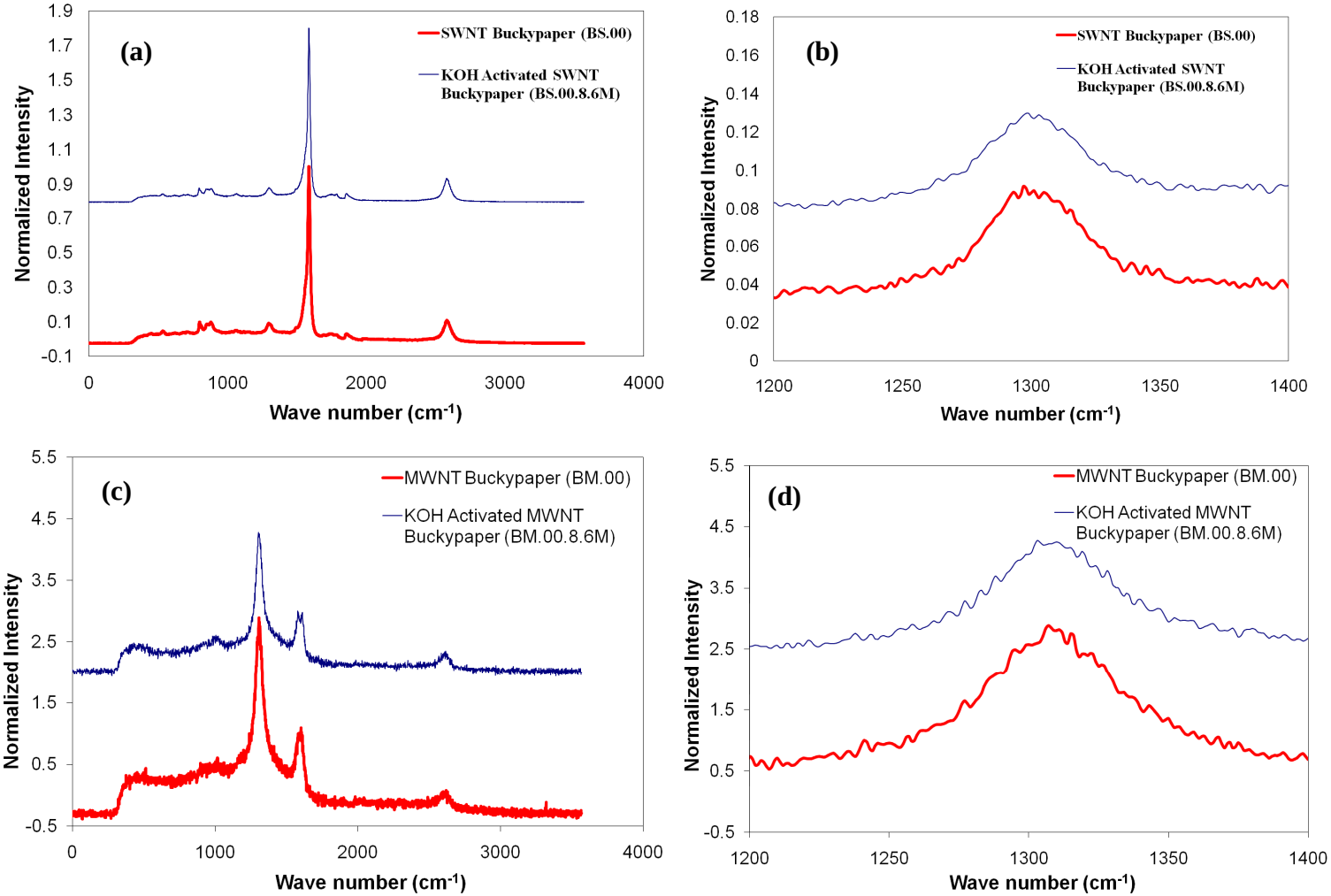

Figure 7.2 Raman Spectra (a, c) and D band intensities (b, d) for (a, b) SWNT and (c, d) MWNT as prepared and activated buckypapers. The spectra are normalized to G band intensity.

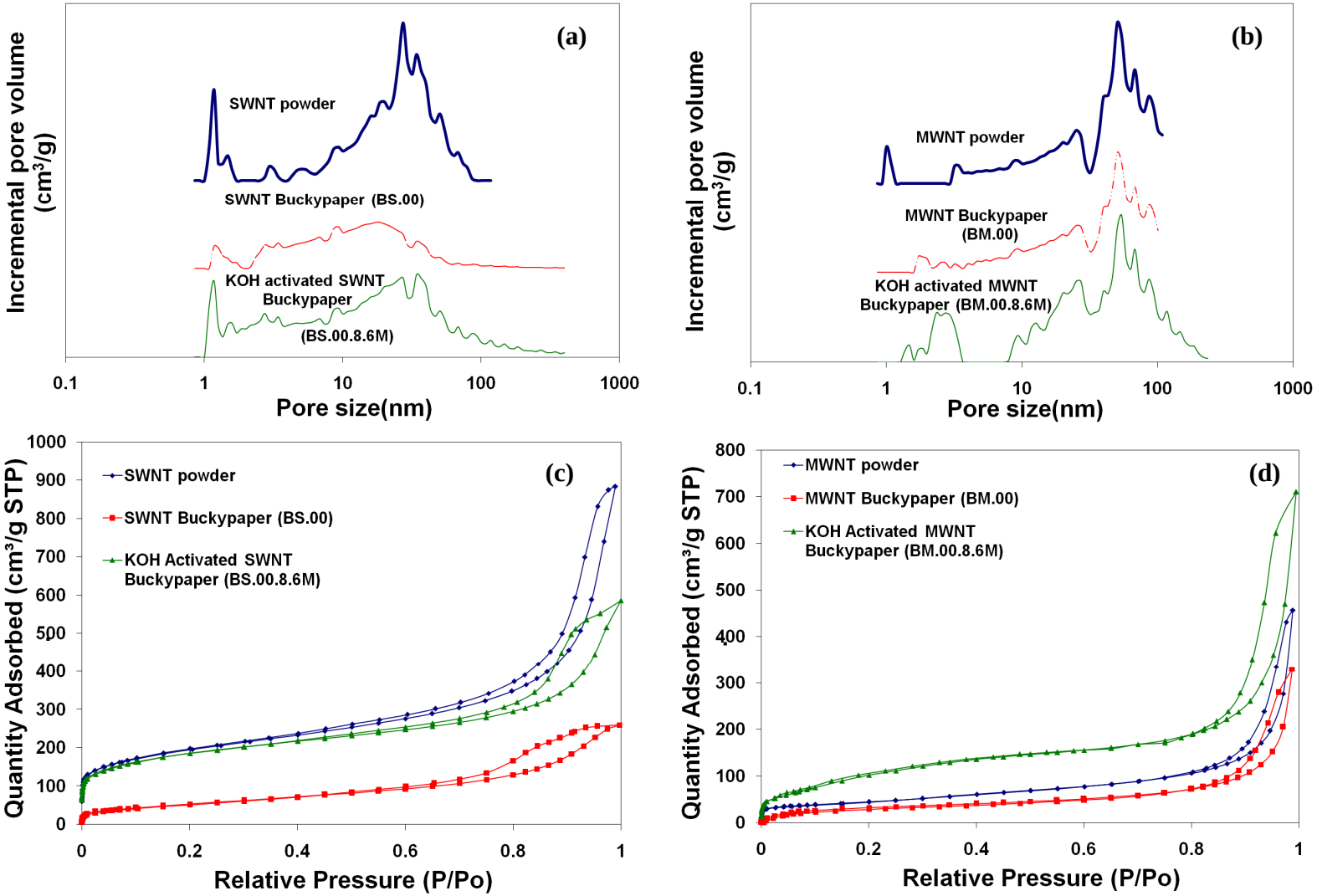

Figure 7.3 Pore volume distribution and nitrogen adsorption isotherms for (a,c) SWNT and (b,d) MWNT as prepared and activated buckypapers.

Table 7. 1. Surface area and pore volume distribution of CNT powders, as prepared and activated buckypapers.

Label	Sample	Specific capacitance (F/g) (0.1 mA constant current		Surface Area (m^2/g)		Energy Density*	Power Density*	Double layer capacitance ($\mu F/cm^2$)**		Pore volume
		6M KOH	BMIMBF4:AC (1:2)	BET	DFT	(W/kg)	(W/kg)	BET	DFT	(cm^3/g)
Powder										
SWNT	SWNT	-	-	659	152	-	-	-	-	0.64
MWNT	MWNT	-	-	161	82	-	-	-	-	0.60
As-prepared buckypaper										
BS.00	SWNT	31	60	198	116	0.36	110	16	27	0.39
BM.00	MWNT	2	30	118	64	0.02	210	2	3	0.50
KOH Activated buckypaper										
BS.00.8.6M	SWNT	48	72	626	272	0.62	320	8	18	0.78
BM.00.8.6M	MWNT	22	80	327	142	0.25	960	7	15	0.75

*Energy density and Power density measured at galvanostatic test at 0.5 mA using KOH electrolyte.
**Double layer capacitance reported for 6M KOH electrolyte.

The decrease in surface area on film formation is due to increase in bundle diameter of CNTs compared to CNT powders. The increase in surface area for activated sample is due to creation of more number of pores by rupture of outer walls of MWNTs or SWNT bundles. The type IV nitrogen adsorption isotherm for SWNT powder (Figure 7.3c) show agglomerates of SWNT bundles with micropore (1-2 nm) contributing to a jump at lower partial pressures and H1 hysteresis loop at higher partial pressures. The well-defined H1 hysteresis loop (almost vertical and nearly parallel over an appreciable range of gas uptake[15, 16]) at higher partial pressure is due to meso pores in the range of 10 – 100 nm. This porous structure is partially masked by the overlapping SWNT bundles in buckypaper film leading to a decrease in nitrogen adsorption and resulting in type H4 hysteresis loop for as prepared and activated SWNT buckypapers, which is characteristic of slit-shape pores or plate-like particles described by IUPAC[15]. MWNTs with predominantly meso and macropores show hysteresis loop at higher partial pressure similar to SWNTs (Figure 7.3d). However, the hysteresis loop retains its H1 hysteresis loop shape after film formation and activation due to difficulty to form films using MWNTs.

7.3.3 Functional groups and Crystallinity studies

As-prepared and activated CNT buckypapers were characterized with WAXD as well as by FTIR. The results from WAXD show two peaks at 2θ values at ~ 25 and 43º corresponding to (002) carbon interlayer spacing and asymmetric (100) peak for both as-prepared and activated SWNT and MWNT[17-19]. The FWHM (full width at half maximum) of (002) peak is a measure of degree of order in nanotube walls. Smaller FWHM for MWNT is indicative of more ordered structure compared to SWNT. The

(002) crystal size of as prepared and activated SWNT buckypapers were ~ 1.2 nm while for MWNTs were ~ 4.0 nm in both cases. Absence of any significant difference in x-ray diffraction results confirms presence of similar crystal structure and sizes for as-prepared and activated buckypapers in both cases and chemical activation process do not alter crystal structure of CNTs (Figure 7.4). Rather[20] observed an increase of interlayer spacing between walls of MWNT from 0.34 to 0.39 nm and a decrease of MWNT diameter from 13 to 8 nm representing a loss of outer walls during activation process. The KOH activation process did not change the interlayer spacing (0.35 nm in both cases) of MWNTs and the CNTs structures were undamaged as observed in TEM images (Figure 7.5). The FTIR spectrum of as-prepared and activated CNT buckypapers given in Figure 7.6 show two strong peaks at wave numbers 1098 and 1248 cm^{-1} and a weak peak at 801 cm^{-1}. Similarity of FTIR spectra for as-prepared and activated samples shows that the chemical activation process does not introduce any functional groups to the surface of CNT buckypapers. Hence, the possibility of functional groups contributing to specific capacitance in CNT buckypaper electrode is eliminated which can result in increase in cycle life of CNT based electrodes.

7.3.4 Electrochemical properties

The charge discharge curves from galvanostatic test and cyclic voltammograms from cyclic voltammetry tests are given in Figure 7.7. High ohmic drop observed in charge-discharge curves of as-prepared buckypapers can be due to high internal resistance of the electrodes.

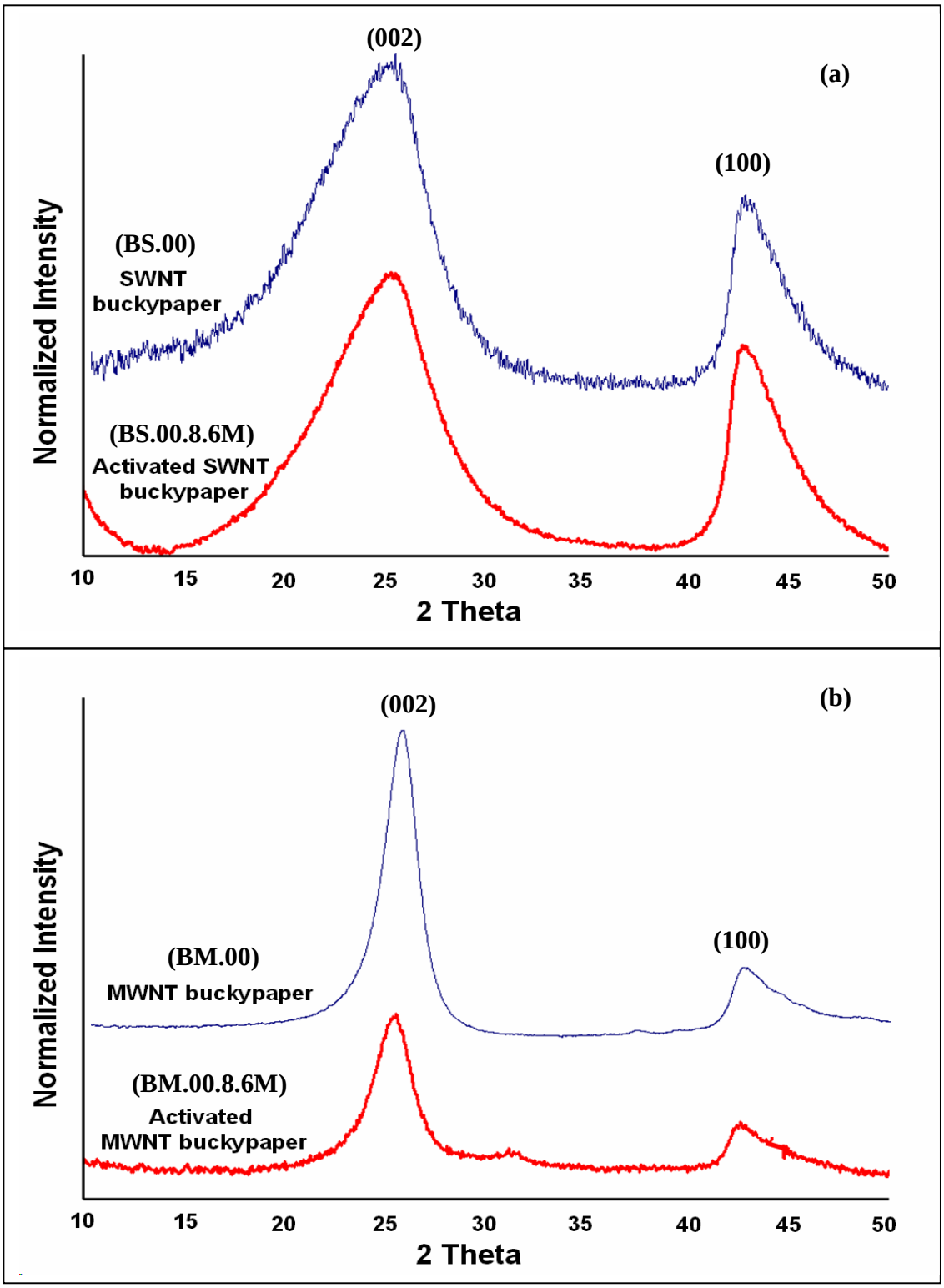

Figure 7.4 WAXD results for (a) SWNT and (b) MWNT as prepared and activated buckypapers.

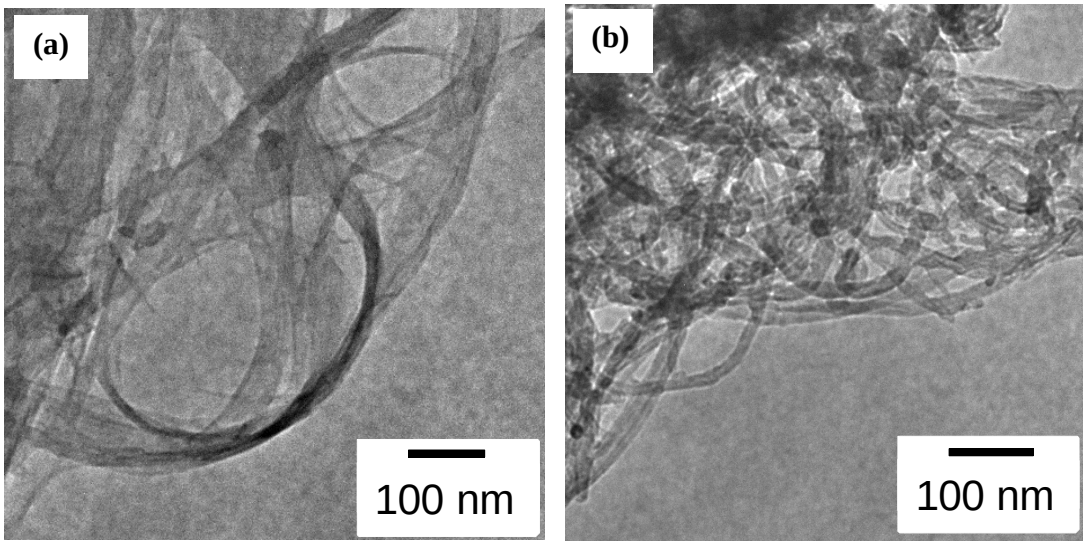

Figure 7.5 TEM images of activated (a) SWNT(BS.00.8.6M) and (b) MWNT (BM.00.8.6M) buckypapers.

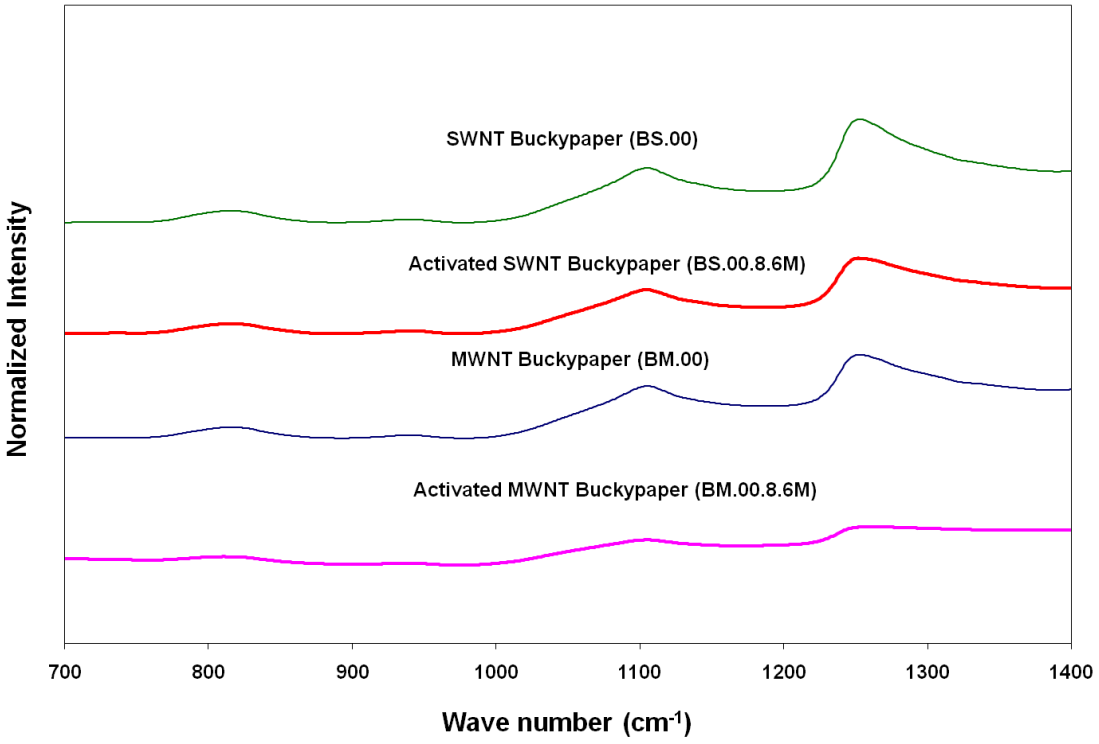

Figure 7.6 FTIR results for SWNT and MWNT as prepared and activated buckypapers.

Porous structure of SWNT powders is partially masked by the overlapping SWNT bundles during buckypaper film formation resulting in internal contact resistance for as-prepared buckypapers. The charge discharge curves for activated SWNT buckypaper negligible ohmic drop. This can be due to creation of more pores during activation process or exfoliation of individual SWNT tubes from bundles leading to increase in accessible pore volume. The ohmic drop observed for as-prepared MWNT buckypapers can be due to internal resistance created from defective graphitic structures detected by in increase in D band of Raman spectra compared to SWNTs (Figure 7.2). This ohmic drop reduces slightly after activation due to presence of defective graphitic or amorphous carbon structures in activated MWNT buckypapers. Similar results were obtained from cyclic voltammograms with SWNT buckypapers showing more rectangular shape corresponding to double layer capacitor, while MWNT buckypapers deviated from rectangular shape due to presence of defective graphitic or amorphous carbon structures.

The results of galvanostatic test performed at different current densities for as-prepared and activated buckypaper samples are given in Figure 7.8. The specific capacitance of activated SWNT buckypaper increased from 31 to 48 F/g, while for MWNT samples the increase is from 2 to 22 F/g when activated with KOH (Table 7.1). These lower specific capacitance values are comparable to values reported in literature for pristine buckypaper electrodes[1-4]. The specific capacitance values are measured for 10000 cycles to determine the cycle life of activated buckypaper electrodes. The results are compared to PAN/CNT(80/20)(FK.82.8.6M) film activated with KOH at 800 ºC for 1h shown in Figure 7.9.

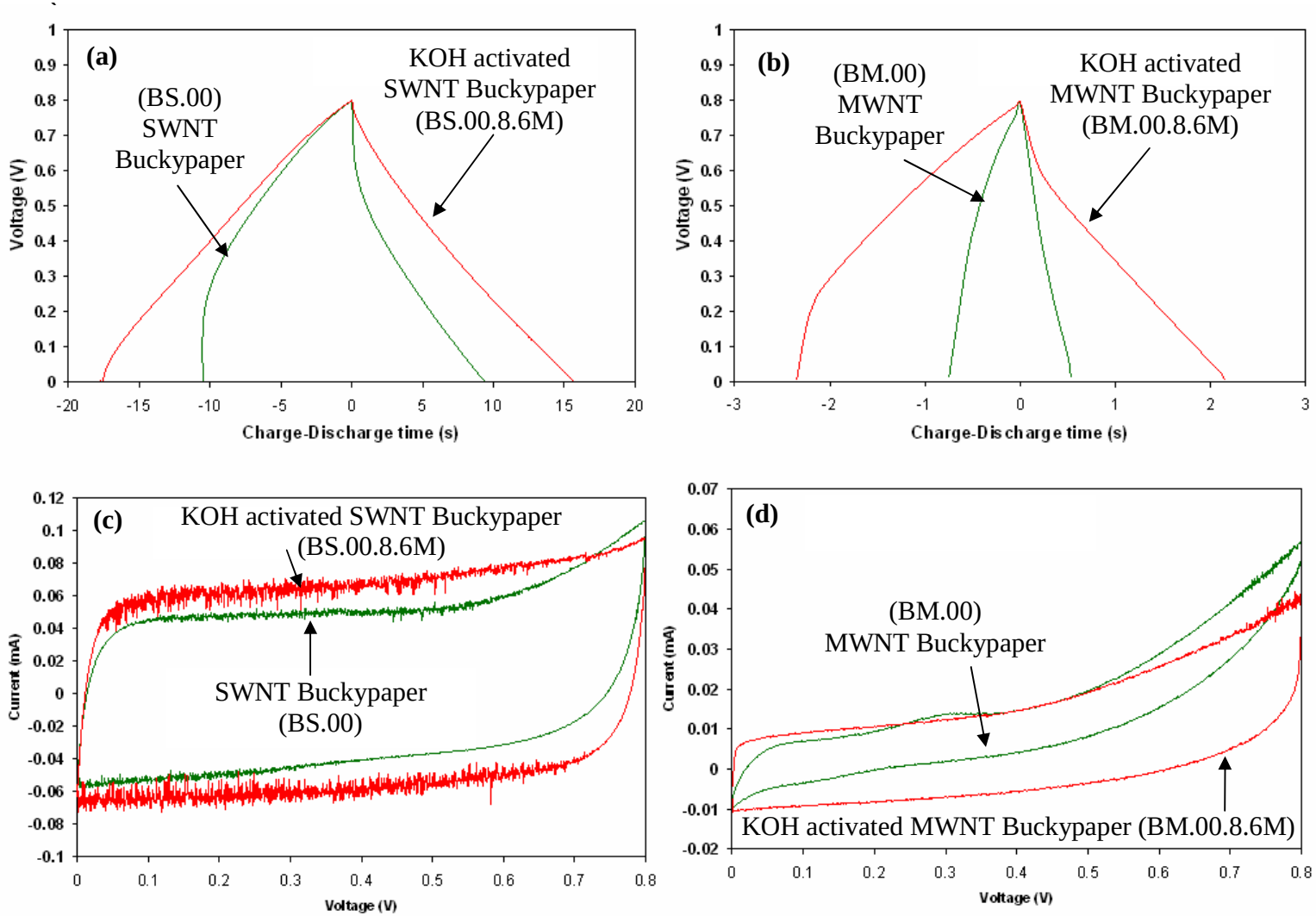

Figure 7.7. Charge discharge curves(a, b) at a constant current of 0.5 mA and cyclic voltammograms(c, d) at 5mV/s for as prepared and activated SWNT (a, c) and MWNT (b, d) buckypapers using 6M KOH as an electrolyte.

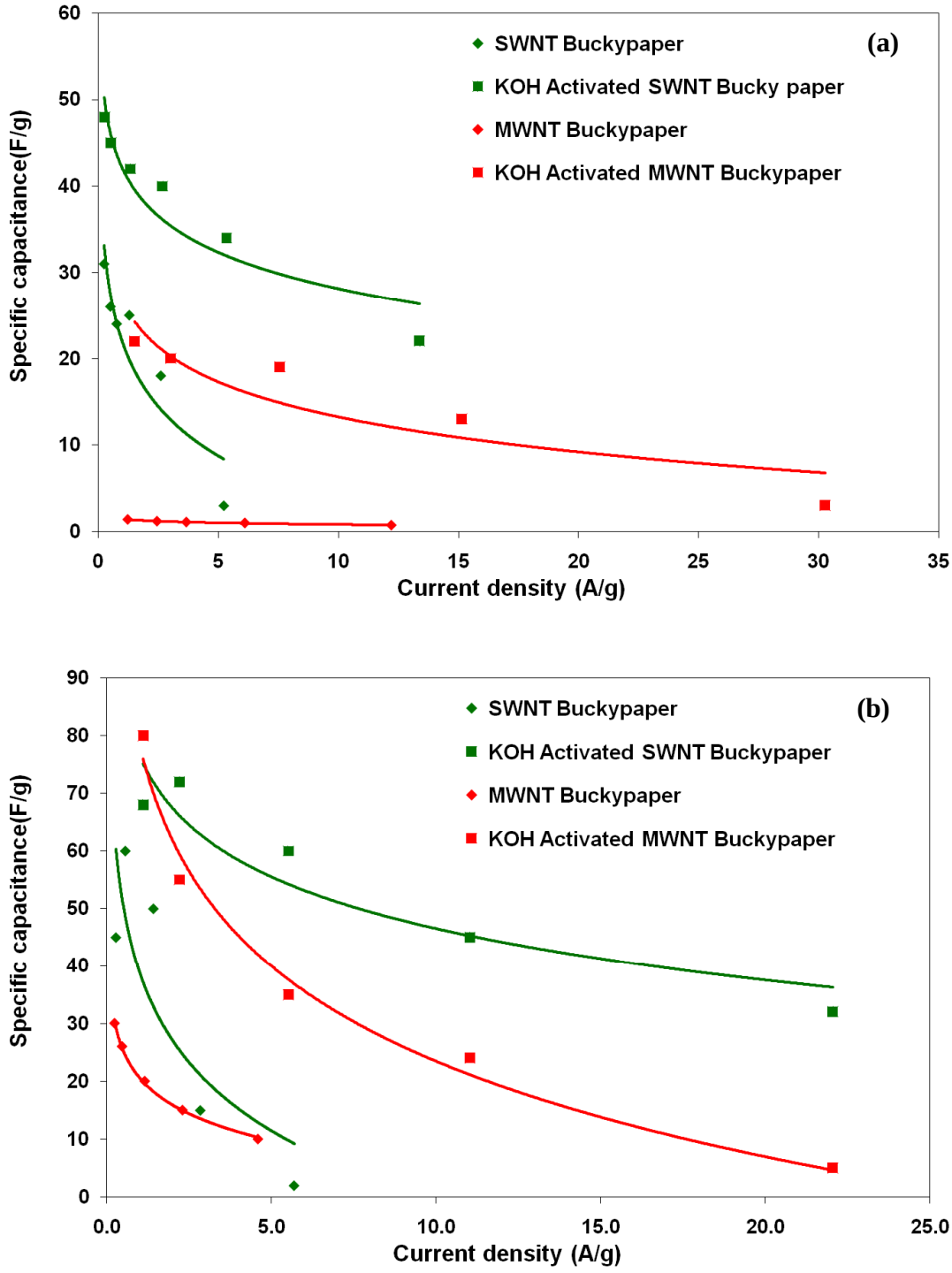

Figure 7.8 The specific capacitance as a function of current density measured for as-prepared and activated SWNT(BS.00 and BS.00.8.6M) and MWNT (BM.00 and BM.00.8.6M)buckypapers in (a) 6M KOH and (b) $BMIMBF_4$/AC(1:2) electrolytes.

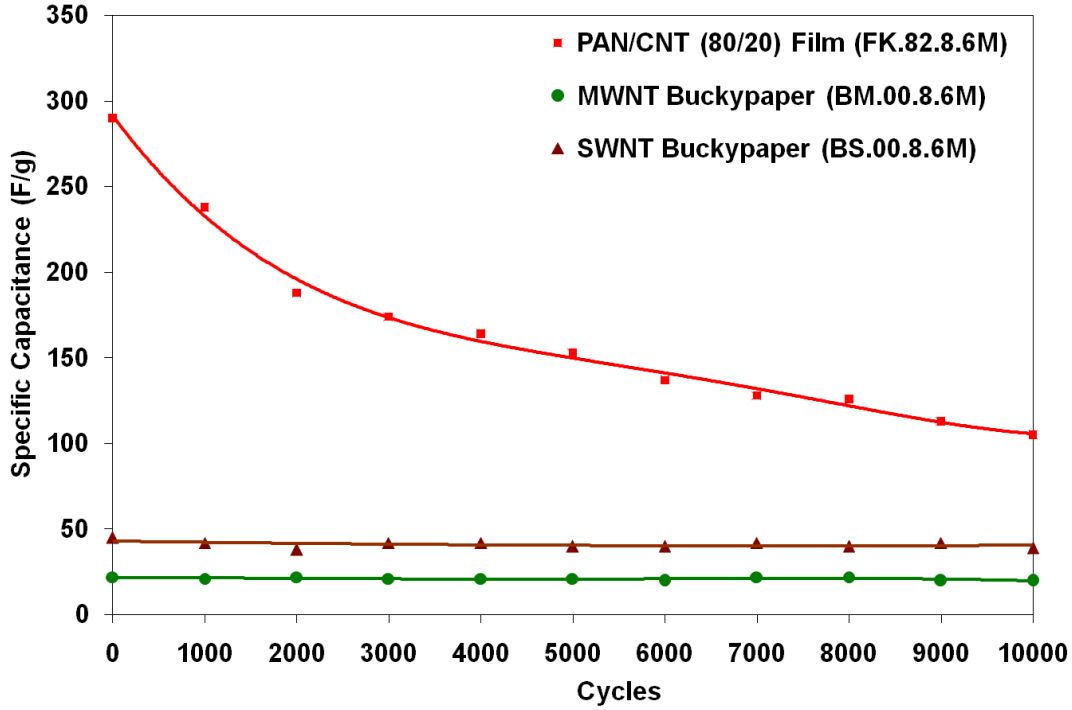

Figure 7.9. The specific capacitance measured for 10000 cycles for activated SWNT and MWNT buckypapers in 6M KOH electrolyte compared to KOH activated PAN/CNT (80/20) film).

The specific capacitance values remain constant for up to 10000 cycles for activated as well as pristine SWNT and MWNT electrodes. Activated PAN/CNT film with specific capacitance ~ 300 F/g initially loses its capacitance to about 39% of its original value after 10000 cycles. Hence, the increase in specific capacitance achieved for activated SWNT and MWNT buckypaper is sustained for 10000 cycles making it an attractive candidate for energy storage applications.

7.4 Conclusions

A study has been made to understand the changes in structures of SWNT and MWNT nanotubes on chemical activation using KOH activating agent. The chemical

activation increases the surface area, pore volume, specific capacitance and energy density of both SWNT and MWNT electrodes. The activation process do not alter the structure and crystal size of CNTs as verified by WAXD results and do not introduce any functional groups to the CNT surface as verified by FTIR results. Ohmic drop observed in as-prepared buckypapers is not observed for activated SWNT buckypapers. Such elimination was not observed in activated MWNT buckypapers due to inherently present disordered nanotube walls or amorphous carbon. The increase in specific capacitance achieved for activated SWNT and MWNT buckypaper is sustained for 10000 cycles making it an attractive candidate for energy storage applications. No significant difference was noticed between SWNT and MWNT structure and morphology due to chemical activation using KOH.

7. 5 References

[1] Yoon B-J, Jeong S-H, Lee K-H, Seok Kim H, Gyung Park C, Hun Han J. Electrical properties of electrical double layer capacitors with integrated carbon nanotube electrodes. Chemical Physics Letters. 2004;388(1-3):170-4.

[2] Zhang H, Cao G, Yang Y, Gu Z. Comparison Between Electrochemical Properties of Aligned Carbon Nanotube Array and Entangled Carbon Nanotube Electrodes. Journal of The Electrochemical Society. 2008;155(2):K19-K22.

[3] Zhou C, Kumar S, Doyle CD, Tour JM. Functionalized Single Wall Carbon Nanotubes Treated with Pyrrole for Electrochemical Supercapacitor Membranes. Chem Mater. 2005;17(8):1997-2002.

[4] Zhou C. Carbon nanotube based electrochemical supercapacitors. PhD Thesis, Georgia Institute of Technology. 2006:42.

[5] Futaba DN, Hata K, Yamada T, Hiraoka T, Hayamizu Y, Kakudate Y, et al. Shape-engineerable and highly densely packed single-walled carbon nanotubes and their application as super-capacitor electrodes. Nat Mater. 2006;5(12):987-94.

[6] Shiraishi S, Kurihara H, Okabe K, Hulicova D, Oya A. Electric double layer capacitance of highly pure single-walled carbon nanotubes (HiPco(TM) Buckytubes(TM)) in propylene carbonate electrolytes. Electrochemistry Communications. 2002;4(7):593-8.

[7] Niu C, Sichel EK, Hoch R, Moy D, Tennent H. High power electrochemical capacitors based on carbon nanotube electrodes. Applied Physics Letters. 1997;70(11):1480.

[8] Chen Q-L, Xue K-H, Shen W, Tao F-F, Yin S-Y, Xu W. Fabrication and electrochemical properties of carbon nanotube array electrode for supercapacitors. Electrochimica Acta. 2004;49(24):4157-61.

[9] Shiraishi S, Kibe M, Yokoyama T, Kurihara H, Patel N, Oya A, et al. Electric double layer capacitance of multi-walled carbon nanotubes and B-doping effect. Applied Physics A: Materials Science & Processing. 2006;82(4):585-91.

[10] Frackowiak E, Delpeux S, Jurewicz K, Szostak K, Cazorla-Amoros D, Beguin F. Enhanced capacitance of carbon nanotubes through chemical activation. Chemical Physics Letters. 2002;361(1-2):35-41.

[11] Jiang Q, Lu XY, Zhao Y. Effects of protection gas flow rate on the electrochemical capacitance of activated carbon nanotubes. Materials Chemistry and Physics. 2006;99(2-3):314-7.

[12] Jiang Q, Qu MZ, Zhou GM, Zhang BL, Yu ZL. A study of activated carbon nanotubes as electrochemical super capacitors electrode materials. Materials Letters. 2002;57(4):988-91.

[13] Duesberg GS, Loa I, Burghard M, Syassen K, Roth S. Polarized Raman spectroscopy on isolated single-wall carbon nanotubes. Physical Review Letters. 2000 Dec 18;85(25):5436-9.

[14] Zhang MF, Yudasaka M, Koshio A, Iijima S. Thermogravimetric analysis of single-wall carbon nanotubes ultrasonicated in monochlorobenzene. Chemical Physics Letters. 2002 Oct 4;364(3-4):420-6.

[15] Sing KSW, Everett DH, Haul RAW, Moscou L, Pierotti RA, Rouquerol J, et al. Reporting physisorption data for gas/solid systems with special reference to the determination of surface area and porosity. Pure & Appl Chem. 1985;57(4):603.

[16] Chiang Y-C, Chiang P-C, Chang EE. Evaluations of the physicochemical characterizations of activated carbons. Journal of Environmental Science and Health, Part A. 1998;33(7):1437 - 63.

[17] Andrews R, Jacques D, Qian D, Dickey EC. Purification and structural annealing of multiwalled carbon nanotubes at graphitization temperatures. Carbon. 2001;39(11):1681-7.

[18] Maniwa Y, Fujiwara R, Kira H, Tou H, Nishibori E, Takata M, et al. Multiwalled carbon nanotubes grown in hydrogen atmosphere: An x-ray diffraction study. Physical Review B. 2001;64(7):073105.

[19] Saito Y, Yoshikawa T, Bandow S, Tomita M, Hayashi T. Interlayer spacings in carbon nanotubes. Physical Review B. 1993;48(3):1907.

[20] Rather S-u, Zacharia R, Naik M-u-d, Hwang SW, Kim AR, Nahm KS. Surface adsorption and micropore filling of the hydrogen in activated MWCNTs. International Journal of Hydrogen Energy. 2008;33(22):6710-8.

Chapter 8

CONCLUSIONS AND RECOMMENDATIONS FOR FUTURE WORK

8.1 Conclusions

Structure and electrochemical properties of polyacrylonitrile (PAN)/carbon nanotube (CNT) composite film and fiber based electrodes developed for electrochemical capacitors are investigated in this thesis. Films are prepared by solution casting and fibers are spun by solution spinning, and gel spinning methods. The PAN/CNT film and fiber precursors are stabilized in air, carbonized in inert atmosphere (argon), and activated by physical (CO_2) and chemical (KOH) methods.

For CO_2 activated PAN/CNT films, sample with 80/20 PAN/CNT ratio activated at 900 °C resulted in highest surface area and specific capacitance. Specific capacitance increased with activation time and temperature and has direct correlation with micropore surface area. Wide pore size distributions of 1 – 250 nm were obtained for samples activated at all process conditions. Surface areas less than 700 m^2/g and pore volume less than 0.2 cm^3/g were obtained for physically activated PAN/CNT films.

The electrochemical properties and surface areas from physical and chemical activation processes were compared for solution spun PAN/CNT fibers. The surface areas as determined by nitrogen gas adsorption was an order of magnitude higher for KOH activated fibers as compared to the CO_2 activated fibers. Under the comparable KOH activation conditions, PAN and PAN/SWNT fibers had comparable surface areas (BET surface area about 2200 m^2/g) with pore size predominantly in the range of 1 to 5 nm, while surface area of PAN/MWNT samples was significantly lower (BET surface area

970 m^2/g). The highest capacitance and energy density was obtained for PAN/SWNT samples, suggesting SWNT advantage in charge storage. The capacitance behavior of these electrodes has also been tested in ionic liquids, and the energy density in ionic liquid is higher than the value obtained using KOH electrolyte.

The gel spun fibers with higher polymer molecular orientation, higher CNT orientation and exfoliation were activated using chemical activation process. The specific capacitance of KOH activated gel-spun PAN fiber samples was as high as high as 240 F/g in 6M KOH electrolyte. Under the comparable KOH activation conditions, spin drawn as well as drawn gel spun PAN and PAN/SWNT fibers resulted in higher BET surface areas with pore size predominantly in the range of 1 to 5 nm, while surface area of the comparably processed PAN/MWNT samples was significantly lower. Energy densities increased from ~2 Wh/Kg in 6M KOH to a maximum of ~ 22 Wh/Kg in $BMIMBF_4$/AC at 0.1mA constant current for as spun PAN fibers by increasing the operating voltage from 0.8 V to 3.0 V respectively.

The SWNT and MWNT buckypaper electrodes on chemical activation showed increased surface area, pore volume, specific capacitance, and energy density. The activation process does not alter the d-spacing of CNTs as verified by WAXD results and does not introduce any functional groups onto the CNT surface as verified by FTIR. The increase in specific capacitance achieved for activated SWNT and MWNT buckypaper is sustained for 10000 cycles making it an attractive candidate for energy storage application.

The chemical activation process variables like activation temperature, molarity of impregnating agent, and composition of PAN/CNT films were varied to determine

process condition to achieve highest electrochemical properties and surface areas. A specific capacitance of ~ 300 F/g was achieved by KOH activated PAN/CNT films as compared to less than 120 F/g achieved for CO_2 activated samples. The PAN/CNT (80/20) film impregnated with 6M KOH and activated at 800 °C resulted in maximum specific capacitance. Samples activated at all process conditions resulted in narrow pore size distribution of 1-5 nm. The specific capacitance measured from this study correlated to micropore surface areas. The energy density increased from ~ 2 Wh/Kg in 6M KOH to ~ 22 Wh/kg in $BMIMBF_4$/AC by increasing the operating voltage from 0.8 V to 3.0 V respectively. The energy density (~ 22Wh/kg) achieved from this study is in the range obtained for batteries as given in Figure 8.1. Capacitance of KOH activated PAN/CNT (80/20) films even after 10,000 charge/discharge cycles, was substantially higher than that for the KOH activated buckypapers.

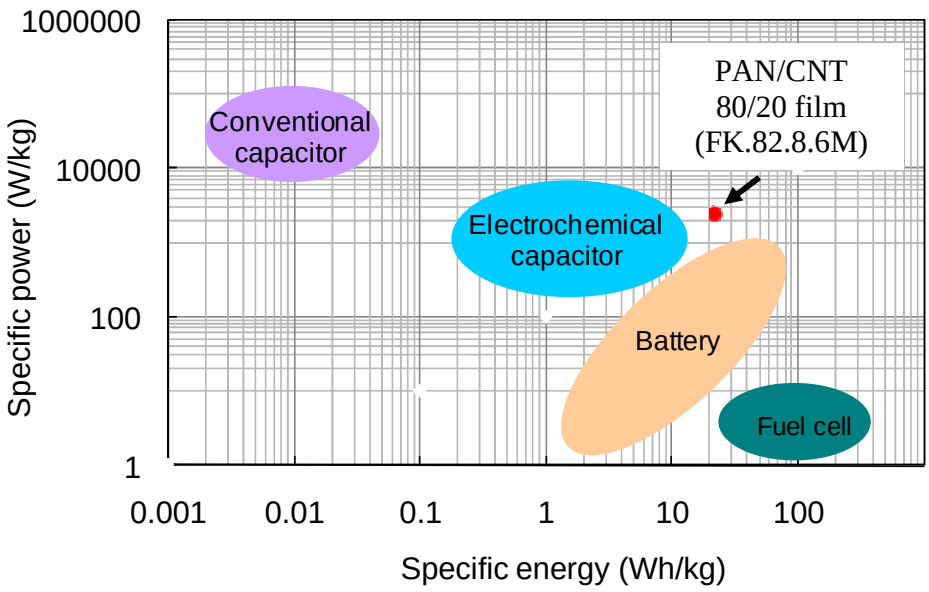

Figure 8.1. A comparison of maximum energy density and power density achieved in this thesis to typical values for energy storage devices [1].

A specific capacitance of 250 - 300 F/g and surface areas ~ 2500 m^2/g were consistently achieved by chemical activation of films, solution spun fibers and gel spun fibers as given in Table 8.1. The chemical activation process is therefore quite promising for developing next generation energy storage devices.

8.2 Recommendations for future work

8.2.1 Chemical activation of PAN/SAN/SWNT tertiary composite

If a polymer can be dispersed in the PAN/SWNT composite with the 1 to 100 nm domain size and if it can be subsequently burned out at low carbonization temperatures then it provides a mechanism for pore size control without activation. An approach explored in our laboratory for achieving pore structure control involving stabilization and carbonization of a composite film consists of single wall carbon nanotubes (SWNTs) and two polymer components, in which one is a carbonizing polymer (PAN) while the second polymer, poly(styrene-co-acrylonitrile) (SAN), is used as a sacrificial component for pore size control. Polymers such as SAN, polystyrene (PS), and poly(methyl methacrylate) (PMMA) are examples of polymers that completely burn out without leaving a residue. These polymers can also be processed in DMF, a solvent used for PAN/SWNT processing. However, films processed from blends of PAN with any one of these polymers exhibit phase separation on 2 to 10 µm scale. This is due to slow solvent evaporation, which provides sufficient time for phase separation. For example, carbonized PAN/SAN (80/20 weight ratio) film show pores with dimensions >2 µm. However, a carbonized PAN/SAN (80/20) electrospun nano fiber mat show predominant pores in the range of 10 to 100 nm. A specific capacitance of 210 F/g was obtained for

Table 8.1. Specific capacitance, surface area, and double layer capacity for KOH activated films and fibers.

Label	Sample	Thickness /Diameter (μm)	Precursor Crystal size (nm)	Specific capacitance (F/g) (0.1 mA constant current test) 6M KOH	Specific capacitance (F/g) (0.1 mA constant current test) BMIMBF4: AC (1:2)	Surface Area (m^2/g) BET	Surface Area (m^2/g) DFT	Energy Density* (Wh/kg)	Power Density* (W/kg)	Double layer capacitance (μF/cm^2)** BET	Double layer capacitance (μF/cm^2)** DFT	Pore volume (cm^3/g)
Films (KOH activated)												
FK.00.8.6M	PAN	25	5.0	167	150	880	273	1.30	315	19	61	0.26
FK.82.8.6M	PAN/CNT (80/20)	25	4.5	302	184	1740	715	1.32	1350	17	42	0.66
FK.64.8.6M	PAN/CNT (60/40)	25	2.9	83	90	820	349	1.30	315	19	61	0.26
Solution spun fibers (KOH Activated)												
SSK.8.6M	PAN	55	3.7	172	140	2133	925	1.15	450	8	19	0.78
SSKM.8.6M	PAN/MWNT (95/5)	86	5.0	134	80	970	316	1.21	358	14	42	0.23
SSKS.8.6M	PAN/SWNT (95/5)	70	5.0	236	190	2266	916	1.68	490	10	26	0.94
Gel spun as-spun fibers (KOH Activated)												
GSASK.8.6M	PAN DR - 4	58	2.6	225	220	2026	812	2.41	590	11	28	0.81
GSASKM.8.6M	PAN/MWNT (99/1) DR - 3	49	3.0	196	150	956	442	1.73	250	21	44	0.36
GSASKS.8.6M	PAN/SWNT (99/1) DR - 3	26	2.5	212	196	2332	1011	1.86	800	9	21	0.94
Gel spun drawn fibers (KOH Activated)												
GSDRK.8.6M	PAN DR - 42	28	11.5	240	188	2724	1130	1.94	620	9	21	1.16
GSDRKM.8.6M	PAN/MWNT (99/1) DR - 45	14	9.6	90	78	1213	621	1.02	730	7	14	0.66
GSDRKS.8.6M	PAN/SWNT (99/1) DR - 45	19	11.5	140	160	2018	890	0.30	1230	7	16	1.10
Buckypaper (KOH Activated)												
BM.00.8.6M	MWNT	100	9.3	22	80	327	142	0.25	960	7	15	0.75
BS.00.8.6M	SWNT	50	3.0	48	72	626	272	0.40	320	8	18	0.78

*Energy density and Power density measured at galvanostatic test at 0.5 mA using KOH electrolyte.
**Double layer capacitance reported for 6M KOH electrolyte.

carbonized PAN/SAN electrospun fiber mat[3] containing no carbon nanotubes. Hence, use of sacrificial component such as styrene acrylonitrile (SAN) with PAN/CNT system has exhibited enhanced specific capacitance and surface area [3-5]. This approach if used in combination with chemical activation, and the use of ionic liquid as electrolyte, can be a good route to develop electrochemical capacitor with enhanced energy densities.

8.2.2 Chemical activation of electrospun fiber mats

The electrospinning of two different polymers together were also reported to achieve intermediate properties of the two polymers [3]. A wide range of properties can be achieved by varying the type of polymer used. An interesting application of the electrospinning process proposed is the possibility of incorporating chemical activating agents like $ZnCl_2$ into carbonizing polymers like PAN in the solution stage. When PAN/$ZnCl_2$ solution is spun from a common solvent using this method, there is a possibility of phase separation like any other method used to produce polymer fibers. However the rapid evaporation of the solvent may prevent phase separation; making this method suitable to produce a homogeneous phase for almost any activating agent/ carbonizing polymer system that cannot be achieved from diffusion controlled impregnation; if they can be dissolved in a common solvent. The homogenous mixture can be annealed to allow phase separation to occur which can result in very fine nano-scale morphology, depending on the annealing conditions. This activating agent impregnated polymer can be further heat treated at higher temperatures to achieve activated carbon with optimum pore size distribution.

The preliminary studies performed on electrospun PAN fiber did not yield any significant specific capacitance values. The chemical activating agents – KOH and $ZnCl_2$

were used to activate PAN fibers. KOH, being a strong base, degrades the PAN when added in solution stage. KOH impregnation of stabilized electrospun PAN fibers resulted in destruction of fiber structure leading to a chunk of activated porous carbon due to severity of activation conditions. $ZnCl_2$ on the other hand dissolved completely in DMF and dispersed well in PAN on mechanical stirring at 80 °C. However, on activation, $ZnCl_2$ activated carbon showed negligible surface area and lower specific capacitance than KOH activation due to weaker activation of $ZnCl_2$. Hence, this study was not successful due to poor choice of activating agents. If a stronger activating agent that is soluble in DMF without degrading PAN molecules is chosen, activated carbon with high charge storage capability can be achieved. A list of possible intercalates for carbon precursors is given in Table 8.2.

Table 8.2 Possible intercalates for carbon precursors[6].

Bond nature	Electronic state of intercalate	Examples of intercalates
Ionic	Donor type	Li, Na, K, Rb, Cs Ca, Sr, Ba Mn, Fe, Ni, Co, Zn, Mo Sm, Eu, Yb K-Hg, Rb-Hg K-NH_3, Ca-NH_3, Eu-NH_3, Be-NH_3 K-H, K-D K-THF, K-C_6H_6, K-DMSO
Ionic	Acceptor type	F, Br, ICl, IBr, IF_5 $FeCl_2$, $FeCl_3$, $NiCl_2$, $AlCl_3$, $SbCl_5$ AsF_5, SbF_5, NbF_5, XeF_5 CrO_3, MoO_3 HNO_3, H_2SO_4, $HClO_4$, H_3PO_4
Covalent		F, O(OH)

In addition to the above recommendations for future work, following aspects of current study require further investigation.

- The minimum pore sizes measured using the nitrogen gas adsorption studies in surface area and pore size analyzer is about 8 Å. If the analysis is performed using CO_2 adsorbate at temperature close to 273 K, pore sizes less than 8 Å can be detected.
- Two different solvents - DMF and DMAc and two different PAN precursors – homopolymer (250K molecular weight) and a copolymer (100 k molecular weight with 6.7% Methyl acrylate comonomer) were used for study in this thesis. A study can be performed to understand the influence of type of solvent and type of polymer precursor on structure of resulting activated carbon and their electro chemical properties.
- The presence of pseudocapacitance was detected in this study as well as in literature from the shape of cyclic voltammograms. However, an improved method is required to quantify the contribution of pseudocapacitance and double layer capacitance to overall specific capacitance.
- Polyvinylidene difluoride (PVDF) binder is used in this thesis to prepare electrodes from fibers. A study can be undertaken to understand the influence of binder, solvent used for preparing carbon/PVDF slurry, and concentration of PVDF in the mixture on electrochemical properties.
- Completion of stabilization for all the precursors was verified using WAXD. A study can be carried out to understand the effect of over stabilization on surface area and electrochemical properties.

8.5 References

[1] Supercapacitors chart. [cited 2006 September]; Available from: www.maxwell.com/ultracapacitors/index.html

[2] Chae HG, Sreekumar TV, Uchida T, Kumar S. A comparison of reinforcement efficiency of various types of carbon nanotubes in polyacrylonitrile fiber. Polymer. 2005;46(24):10925-35.

[3] Wang T. Electrospun Carbon Nanofibers for Electrochemical Capacitor Electrodes. PhD Thesis, Georgia Institute of Technology. 2007.

[4] Zhou C. Carbon nanotube based electrochemical supercapacitors. PhD Thesis, Georgia Institute of Technology. 2006:42.

[5] Zhou C, Liu T, Wang T, Kumar S. PAN/SAN/SWNT ternary composite: Pore size control and electrochemical supercapacitor behavior. Polymer. 2006;47(16):5831-7.

[6] Inagaki M. New carbons : control of structure and functions. New York: Elsevier Science 2000.

Appendix A

Characterization of functionalized Buckypaper

A1. Introduction

Supercapacitors or electrochemical capacitors store the energy within the electrochemical double-layer at the electrode-electrolyte interface[1, 2]. The different types of materials used for electrode of supercapacitors include electrically conducting metal oxides, conducting polymers, activated carbon, and carbon nanotubes[2, 3]. For superior supercapacitor performance, the electrode should have a high electrical conductivity, a high surface area for charges accumulation, a sufficiently large pore diameter, and good pore connectivity for the electrolyte wetting and rapid ionic motion[4].

In this study, the electrode materials were prepared by treatment of single wall nanotubes with aniline (CDD II 124), chloro-aniline (CDD II 126), aryl sulphonic acid treated SWNTs/MWNTs(1:2) with pyrrole (CDD II 128). The functionalized bucky paper samples were prepared by Prof. James Tour group at Rice University as given in Figure A1. These samples were tested for specific capacitance using Cell Test, analyzed for crystalline structure using WAXD and surface morphology was studied using SEM.

A2. Experimental

The samples were tested for specific capacitance, power density and energy density using Solartron Cell Test 1470 using the procedure previously described in chapters 3-6 [5-7]. The galvanostatic tests, CV measurements, WAXD studies, SEM images were obtained using conditions explained in chapter 3-6.

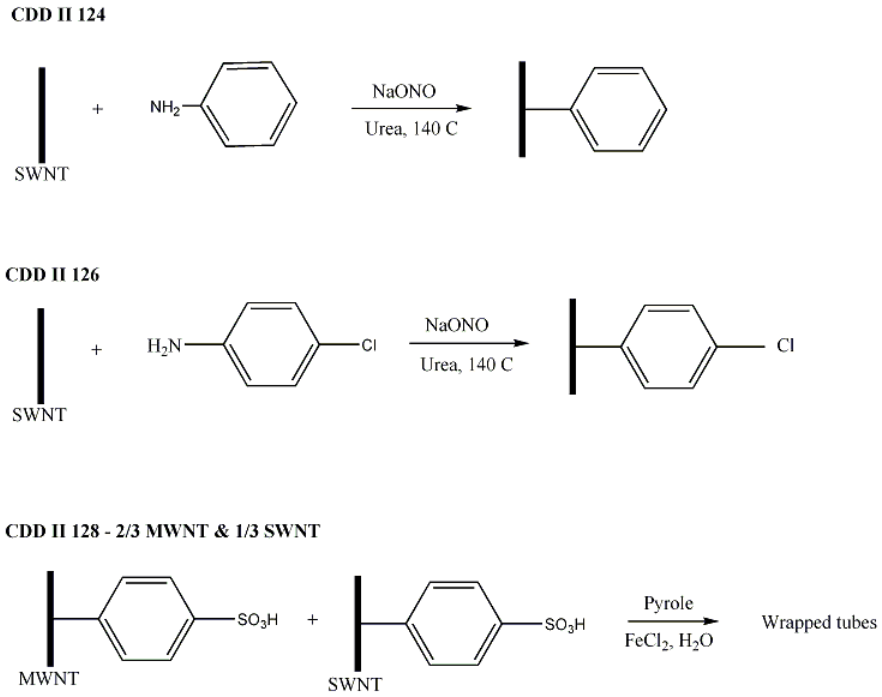

Figure A1. Scheme for electrode material preparation mechanism.

A3. Results and discussion

The performance of the supercapacitor depends on the amount of electrical charge that can be stored on the electrode-electrolyte interface due to (1) pure electrostatic attraction between ions and charged electrodes and (2) faradaic pseudocapacitance reactions[1, 8]. The capacitance due to double layer charge accumulation is proportional to the surface area (S) of the material, relative permittivity of the solution ε and inversely related to thickness d of the double layer.

$$\mathbf{C = S\,\varepsilon / d}$$

The contribution due to redox reaction, pseudocapacitance arises when the charge q required for progression of an electrode process changes continuously as a function of potential U. The capacitance C = dq/dU due to faradaic reactions strongly depend on the chemical affinity of carbon materials to the ions absorbed on the electrode surface.[2,6] An

ideal double layer capacitance behavior is characterized by a rectangular shape voltammetry plots. The electrode materials with pseudocapacitance properties shows a deviation of rectangular shape and reversible redox peaks due to pseudo faradaic reactions[1, 8].

A typical cyclic voltammetry plot for the functionalized bucky paper samples with a scan rate of 10 mV/s is given in Figure A2. The CV plots of samples CDD II 124 and CDD II 126 exhibited rectangular, exhibiting no pseudocapacitance of redox reaction. However the CV plot deviated from the ideal rectangular shape in the sample CDD II 128 at higher voltages (0.6 – 0.8V). Earlier studies on CNT-PPy systems show widely varying cyclic voltammograms with redox peaks appearing at different voltages depending on the electrolyte used[7, 9-11]. This deviation from rectangular shape needs further investigation to determine any role of psuedocapaitance arising from the pyrrole treatment.

The specific capacitance for the three functionalized bucky paper sample were between 80 to 120 F/g at 0.5mA constant current test (Figure A3a). The total amount of charge that is stored at the interface double layer is a function of time and current. The supercapacitance value decreases with the increase in current density as time is available for ions to access the pores decreases with increase in current. This decrease in capacitance is higher for pyrrole treated-functionalized nanotube samples CDD II 128 than other samples. This decrease may be due to inefficient accessibility of pores by electrolyte ions at higher current density, and larger internal resistance of the pyrrole moieties in comparison to nanotubes[7].

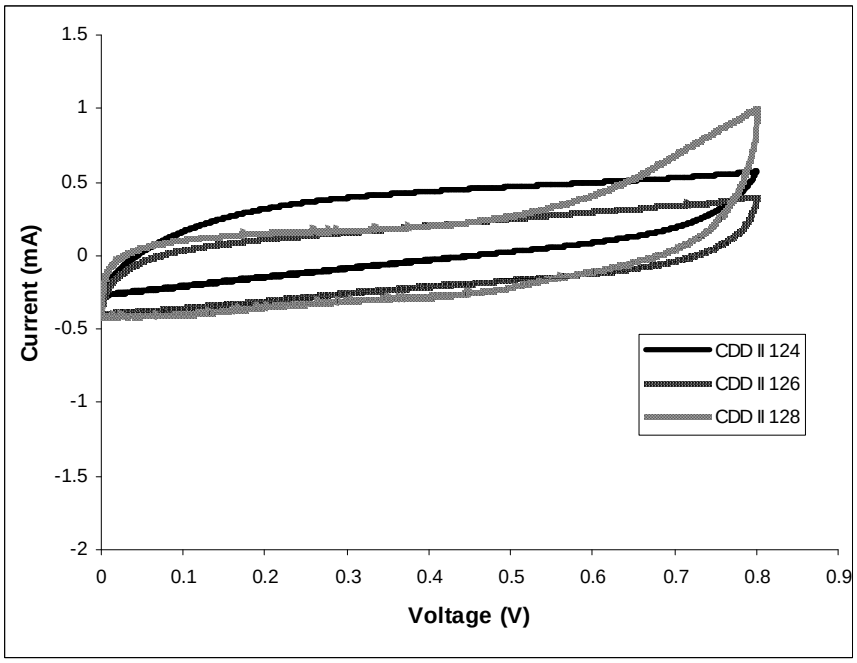

Figure A2. A typical cyclic voltammetry plot for the functionalized bucky paper samples with a scan rate of 10 mV/s

Power density and energy density of all three samples were comparable at lower current densities. However, a deviation in values is observed at higher current density due to difference in accessibility of pores by electrolyte ions. The values of specific capacitance, power and energy density are listed in Table B1.

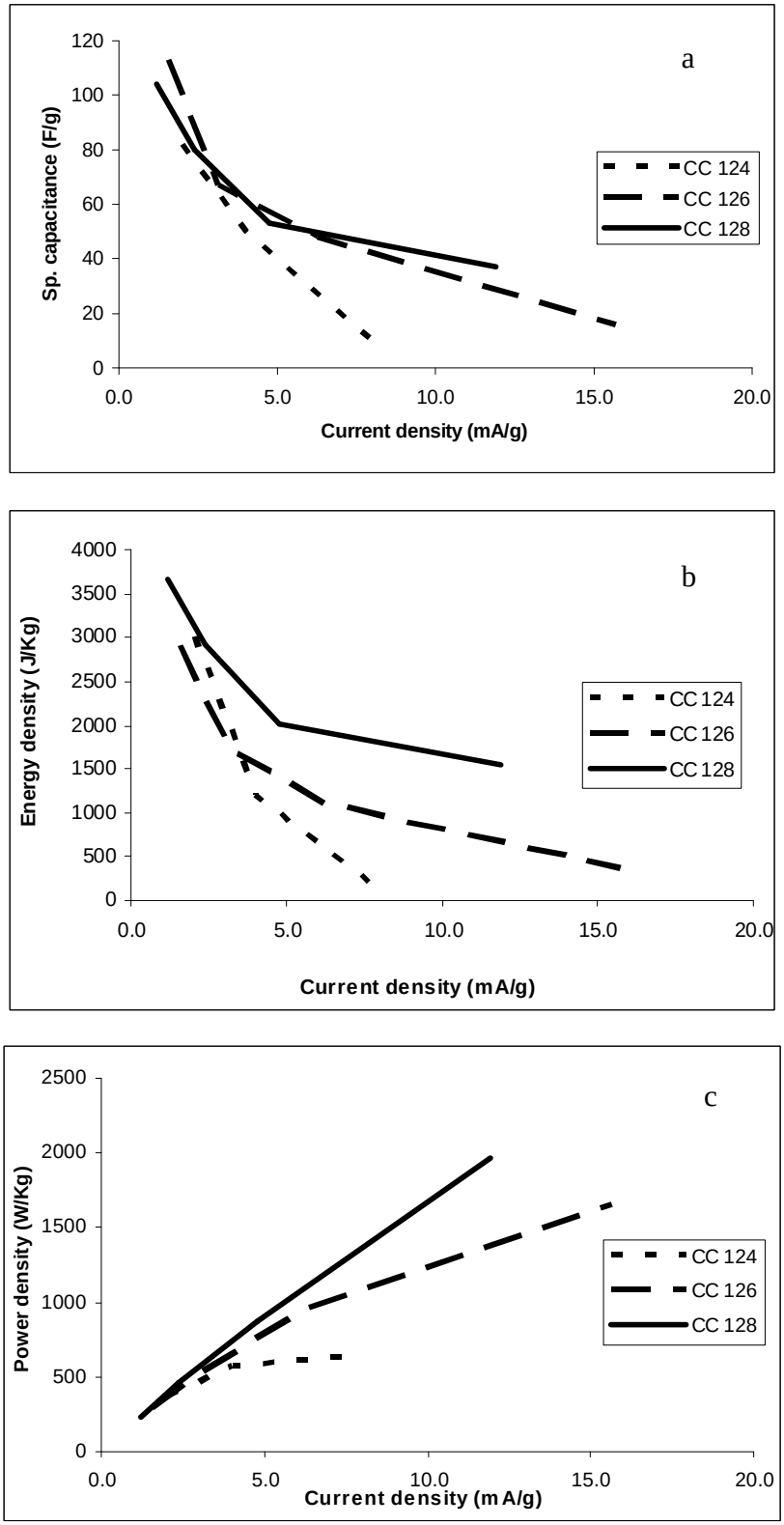

Figure A3. Specific capacitance, energy, and power density of functionalized buckypapers as a function of discharge current density at 0.5mA constant current test.

Table 1. Supercapacitance behavior of functionalized buckypapers

CDD II 124				
Constant current test	0.5 mA	1 mA	2mA	
Capacitance (F/g)	82	50	10	
Power Density (W/kg)	360	575	646	
Energy Density(J/Kg)	2998	1212	125	
Current density(mA/g)	2.0	4.0	8.0	
CDD - II - 126				
Constant current test	0.5 mA	1 mA	2mA	5mA
Capacitance (F/g)	113	67	48	16
Power Density (W/kg)	290	540	950	1650
Energy Density(J/Kg)	2890	1710	1090	358
Current density(mA/g)	1.6	3.1	6.3	15.7
CDD - II - 128				
Constant current test	0.5 mA	1 mA	2mA	5mA
Capacitance (F/g)	104	80	53	37
Power Density (W/kg)	235	460	870	1970
Energy Density(J/Kg)	3660	2920	2010	1550
Current density(mA/g)	1.2	2.4	4.8	11.9

The samples were analyzed for crystalline structure using WAXD. The diffraction results show several peaks which may be explained as follows:

a. The first two peaks peaks at 2θ values ~ 8.0º and 12.8º with d-spacings of ~ 11 and 6.9Å in samples CDD II 124 and CDD II 126 corresponds to (1 0) and (1 1) planes of the 2D hexagonal lattice of the ordered SWNT bundle. This suggests that SWNTs are not fully exfoliated. This gives a ratio d_{10}/d_{11} ~ 1.6 close to theoretical value of 1.732 for the trigonal symmetry[12].

b. The peak at 2-theta value 26.8º with d-spacing of 3.32Å in sample CDD II 128 is due to spacing between graphite layers within MWNTs.

c. The peaks at 2-theta values ~ 20º and 24.5º with d-spacing of ~ 4.5 and 3.6Å in samples CDD II 124 and CDD II 126 appears to be (100) and (110) polyaniline peaks. Polymerization of aniline when used with carbon nanotube electrodes and deposition of polyaniline films have been reported earlier[13-15].
d. The other prominent peaks ~ 22º and 24.3º for CDD II 126 and 18.4 and 43 for CDD II 128 are not identified. The diffraction results need further investigation to understand the components present and their structure.

The SEM pictures shows formation of uniform functionalized SWNT film for samples CDD II 124 and CDD 126. The sample CDD II 128 has pieces of SWNT films scattered in MWNTs possibly coated with pyrrole. The materials can be identified only if exact treatment condition and sample preparation method of each sample is known.

A4 Conclusions

The electrode materials were prepared by treatment of single wall nanotubes with aniline (CDD II 124), chloro-aniline (CDD II 126), aryl sulphonic acid treated SWNTs/MWNTs (1:2) with pyrrole (CDD II 128). The functionalized bucky paper samples were tested for specific capacitance using Cell Test, analyzed for crystalline structure using WAXD and surface morphology was studied using SEM.

CDD II 124

2-Theta	d(Å)	XS(A)
8.0	11.01	0.71
12.8	6.91	0.51
20.7	4.29	0.16
24.6	3.61	0.19
44.0	2.05	0.78
45.3	2.00	0.78

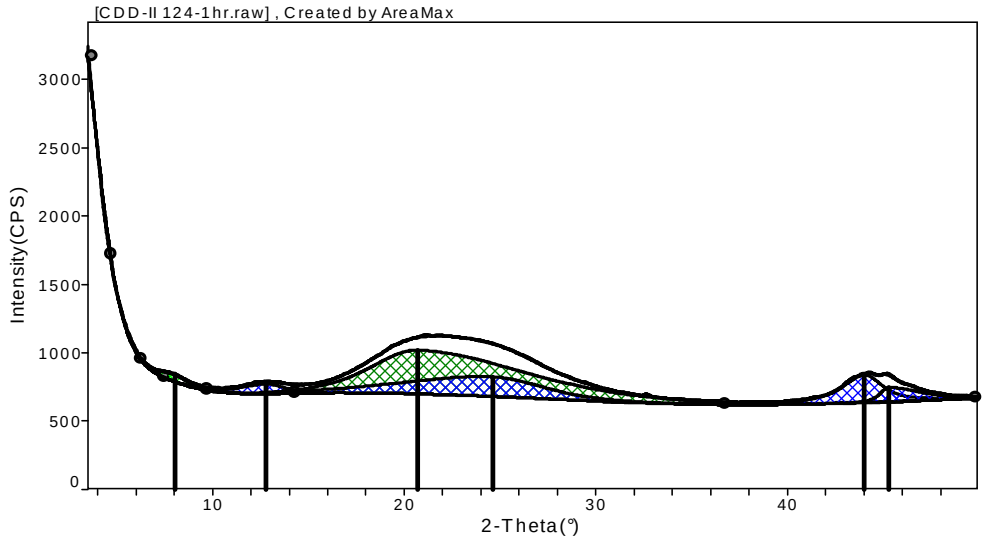

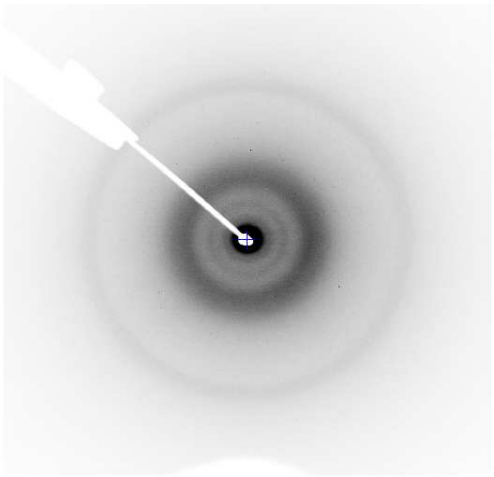

Figure A4. WAXD results for (a) CDD II 124

CDD II 126

2-Theta	d(A)	XS(A)
8.0	11.02	0.86
12.9	6.86	0.59
19.8	4.47	0.44
22.0	4.04	3.10
23.2	3.83	0.17
24.3	3.65	3.00
44.1	2.05	0.54
45.3	2.00	2.93

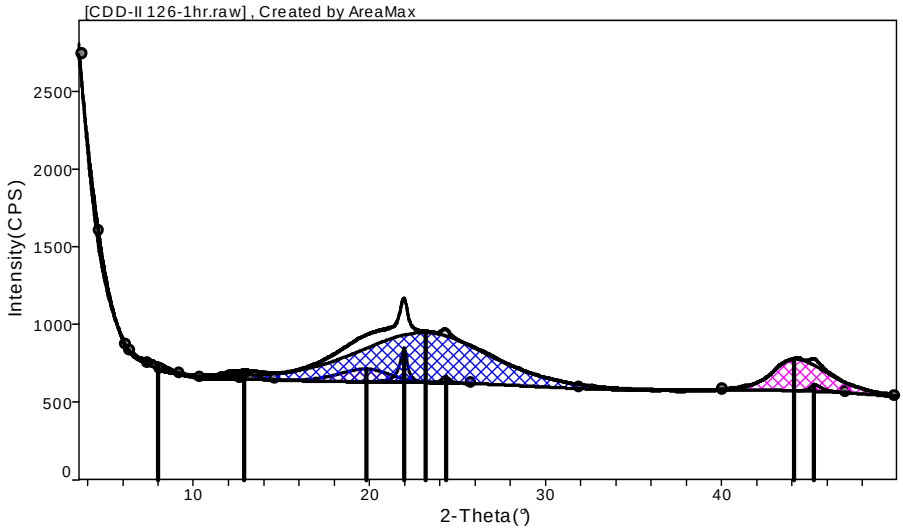

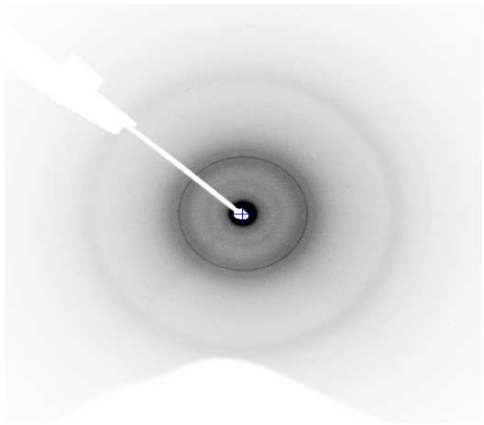

Figure A4. WAXD results for (b) CDD II 126

CDD II 128

2-Theta	d(A)	XS(A)
18.5	4.80	3.07
24.5	3.63	0.19
26.8	3.32	1.28
35.7	2.51	0.87
43.2	2.09	1.56
44.9	2.02	0.69

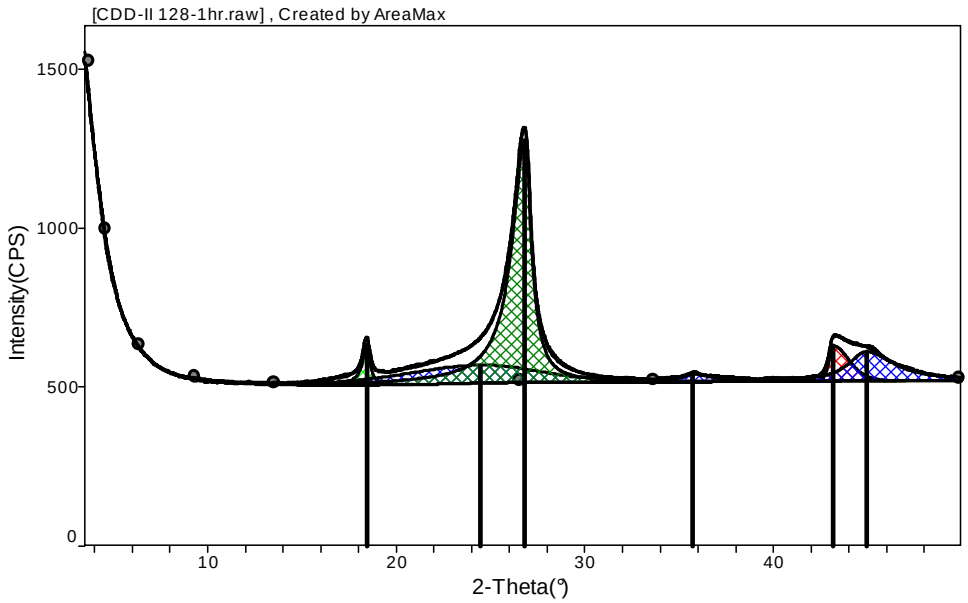

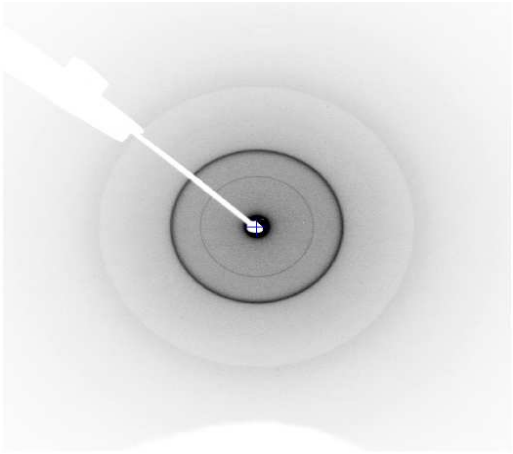

Figure A4. WAXD results for (c) CDD II 128

CDD II 124

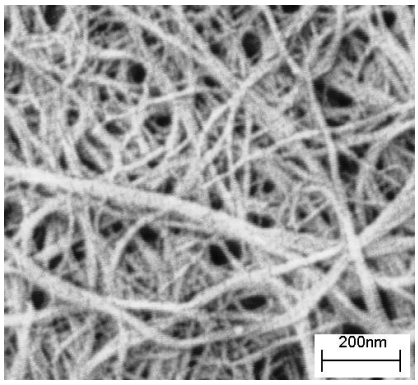

CDD II 126

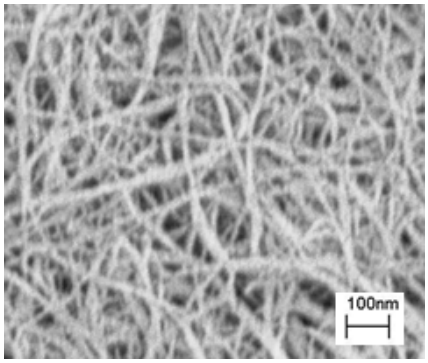

CDD II 128

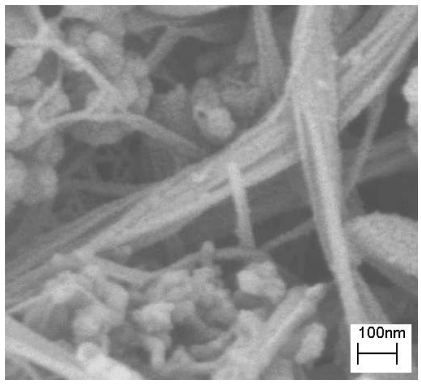

Figure A5. Scanning electron microscopy images for functionalized CNT buckypapers.

A5 References:

[1] Conway BE. Electrochemical supercapacitors : scientific fundamentals and technological applications Plenum Press, New York. 1999:xxviii, 698 p.

[2] Kotz R, Carlen M. Principles and applications of electrochemical capacitors. Electrochimica Acta. 2000;45(15-16):2483-98.

[3] Burke A. Ultracapacitors: why, how, and where is the technology. Journal of Power Sources. 2000;91(1):37-50.

[4] Vix-Guterl C, Saadallah S, Jurewicz K, Frackowiak E, Reda M, Parmentier J, et al. Supercapacitor electrodes from new ordered porous carbon materials obtained by a templating procedure. Materials Science and Engineering B. 2004;108(1-2):148-55.

[5] Liu T, Sreekumar TV, Kumar S, Hauge RH, Smalley RE. SWNT/PAN composite film-based supercapacitors. Carbon. 2003;41(12):2440-2.

[6] Zhou C, Liu T, Wang T, Kumar S. PAN/SAN/SWNT ternary composite: Pore size control and electrochemical supercapacitor behavior. Polymer. 2006;47(16):5831-7.

[7] Zhou C, Kumar S, Doyle CD, Tour JM. Functionalized Single Wall Carbon Nanotubes Treated with Pyrrole for Electrochemical Supercapacitor Membranes. Chem Mater. 2005;17(8):1997-2002.

[8] Frackowiak E, Beguin F. Carbon materials for the electrochemical storage of energy in capacitors. Carbon. 2001;39(6):937-50.

[9] An KH, Jeon KK, Heo JK, Lim SC, Bae DJ, Lee YH. High-Capacitance Supercapacitor Using a Nanocomposite Electrode of Single-Walled Carbon Nanotube and Polypyrrole. Journal of the Electrochemical Society. 2002;149:A1058-A62.

[10] Hughes M, Chen GZ, Shaffer MSP, Fray DJ, Windle AH. Electrochemical Capacitance of a Nanoporous Composite of Carbon Nanotubes and Polypyrrole. Chem Mater. 2002 April 15, 2002;14(4):1610-3.

[11] Jurewicz K, Delpeux S, Bertagna V, Béguin F, Frackowiak E. Supercapacitors from nanotubes/polypyrrole composites. Chemical Physics Letters. 2001;347(1-3):36-40.

[12] Thess A, Lee R, Nikolaev P, Dai H, Petit P, Robert J, et al. Crystalline Ropes of Metallic Carbon Nanotubes. Science. 1996 July 26, 1996;273(5274):483-7.

[13] Dan A, Sengupta PK. Synthesis and characterization of polyaniline prepared in formic acid medium. Journal of Applied Polymer Science. 2004;91(2):991-9.

[14] Downs C, Nugent J, Ajayan PM, Duquette DJ, Santhanam KSV. Efficient Polymerization of Aniline at Carbon Nanotube Electrodes. Advanced Materials. 1999;11(12):1028-31.

[15] Pouget JP, Jozefowicz ME, Epstein AJ, Tang X, MacDiarmid AG. X-ray structure of polyaniline. Macromolecules. 1991;24(3):779-89.

Appendix B

Electrochemical Capacitors from Electrospun PAN Fibers

B1. Introduction

The process of electrospinning uses a high potential difference to produce fibers of nanometer diameters. The procedure setup consists of a grounded collector target, a high voltage power source, and a syringe. When polymer solution is delivered to the syringe surface tension forces will cause a droplet to form at the needle tip. With the applied voltage, electrostatic attractive forces form between the grounded collector and the polymer droplet. When the applied voltage is sufficiently high enough to overcome the surface tension forces an electrified jet of polymer sample is pulled from the syringe to the collector plate. This sample is elongated and stretched forming fibers of very small diameter [1].

The significance of electrospun fibers is their nano-scale diameter, their small pore sizes between fibers, and large surface area per unit mass. The increase in surface area of the polymer fibers in relation to the reduction in fiber diameter is demonstrated in Figure B1 [2]. The electrospinning of two different polymers together were also reported to achieve intermediate properties of the two polymers [3]. A wide range of properties can be achieved by varying the type of polymer spun. Small insoluble particles, soluble drugs, and anti-bacterial agents can also be incorporated into the fiber to achieve the desired end properties [4].

An interesting application of the electrospinning process proposed is the possibility of incorporating chemical activating agents like $ZnCl_2$ into carbonizing

polymers like PAN in the solution stage. When PAN/$ZnCl_2$ solution is spun from a common solvent using this method, there is a possibility of phase separation like any other method used to produce polymer fibers. However the rapid evaporation of the solvent may prevent phase separation; making this method suitable to produce a homogeneous phase for almost any activating agent/ carbonizing polymer system that cannot be achieved from diffusion controlled impregnation; if they can be dissolved in a common solvent. The homogenous mixture can be annealed to allow phase separation to occur which can result in very fine nano-scale morphology, depending on the annealing conditions. This activating agent impregnated polymer can be further heat treated at higher temperatures to achieve activated carbon with optimum pore size distribution. The electospinning and heat treatment process conditions will be optimized to achieve superior electrochemical properties.

Kim et al[5] used chemically activated PAN/$ZnCl_2$ nanofibers for energy storage in an electrochemical capacitor. PAN and $ZnCl_2$ were directly dissolved in DMF to electrospin fibers from 200 to 350 nm diameter. Increase of salt concentration for 1 to 5 wt. % increased the specific capacitance from 120 to 140 F/g as given in Figure B1 [5]. Im et al[6] activated electrospun PAN fibers using $ZnCl_2$ and KOH salts for hydrogen storage. $ZnCl_2$ was directly added to PAN/DMF solution while KOH was incorporated into PAN nanofibers by immersion overnight. The surface area, pore volume and hydrogen absorption capacity increased with increase of molarity of both the salts as given in Table B1. KOH immersion method showed higher surface area and pore volume than direct addition of $ZnCl_2$. However, nanofibers activated with 6M $ZnCl_2$ displayed higher hydrogen storage capability than samples activated with 8M KOH.

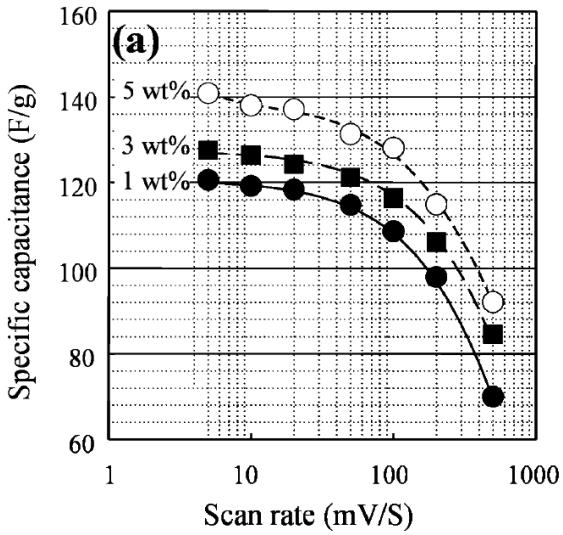

Figure B1. Specific capacitance measured by cyclic voltammetry for electrospun nanofibers from PAN/$ZnCl_2$/DMF system with different salt contents [1]

Table B1. Summary of surface area, pore volume, and hydrogen absorption of chemically activated PAN based nanofibers. The activation agents were added by direct addition (ZC- molarity 2-6 M) and immersion (PH- molarity 4-8 M [5].

	As-received	ZC-W2	ZC-W4	ZC-W6	PH-M4	PH-M6	PH-M8
S_{BET}[a] (m^2/g)	17	334	777	944	1410	2006	2420
V_T[b] (cc/g)	0.03	0.43	0.53	0.96	0.75	1.88	2.39
V_M[c] (cc/g)	0.02	0.24	0.32	0.47	0.57	0.86	1.04
$F_{M/V}$[d] (%)	67	56	60	49	76	46	44
V_H[e] (cc/g)	0.001	0.015	0.057	0.084	0.009	0.018	0.035
A_H[f] ($\sum$wt%)	0.02	0.53	0.71	1.54	0.67	0.91	1.03

[a] S_{BET}: BET specific surface area.
[b] V_T: total pore volume.
[c] V_M: HK micropore volume.
[d] $F_{M/V}$: fraction of micropore.
[e] V_H: pore volume (in the range of pore width from 0.6 to 0.7 nm).
[f] A_H: amount of hydrogen adsorption.

The challenge in carbon based electrochemical capacitor industry is to produce long life time, low self discharging electrochemical capacitor with optimum specific capacitance, energy density, and power density with wide operating voltage/temperature range that can be useful for wide range of applications. Using common electrode materials such as carbon nanotubes and the electrospinning process allows for the production of nano-scale diameter fibers with large surface areas per unit mass. As well

as the possibility of incorporating chemical activating agents such as $ZnCl_2$ and KOH into the fiber in order to achieve uniformly distribute pores throughout. Our objective in this study is to develop electrode material for electrochemical capacitors with these qualities as well minimal weight loss and relatively high yield.

B2. Experimental

The PAN (molecular weight ~ 250,000 with 6.7 mol % methylacrylate from Exlan Co, Japan) and PAN/$ZnCl_2$ fibers containing 5 wt% and 20 wt% $ZnCl_2$ were electrospun from dimethyl formamide solution. The process parameters used were a target distance of 10 cm and voltage of 22 V at a flow rate of 2 mL/hr , using a 18 gauge needle and syringe with 30 mL capacity. SEM photographs of each sample were analyzed using Digimizer to determine distribution of the diameters for thirty random fiber samples. All samples were stabilized without tension in a ceramic crucible in air by heating at 1 ºC/min to 285 ºC and by holding at that temperature for 2, 4, 8, and 16 hours. Stabilized samples were examined by scanning electron microscopy and the structure was studied by WAXD. For KOH activation, 16 hour stabilized samples were immersed in 6 M KOH for 5 minutes and 12 hours at room temperature. KOH impregnated fibers were dried at 90 ºC for 24 hours. With KOH impregnation, fiber weight increased by a factor of about ten. KOH impregnated fibers were heated at 5 ºC/min to 800 ºC and held at that temperature for one hour in argon. KOH activated samples were cooled down to room temperature and repeatedly washed with hot distilled water to remove excess KOH. The stabilized $ZnCl_2$ containing fibers were heated at 5 ºC/min to 800 ºC and held at that

temperature for one hour in argon. The activated samples were cooled down to room temperature and repeatedly washed with hot distilled water to remove excess $ZnCl_2$.

The samples were tested for specific capacitance, power density and energy density using Solartron Cell Test 1470. The thickness of electrodes (diameter ~ 0.8 mm) varied between 30-50 µm. The electrolyte used for both galvanostatic and cyclic voltammetry tests was 6 M KOH. The surface area and pore size distribution of the activated fibers were measured using Micromeritics ASAP 2020. WAXD studies were performed on a Rigaku Micromax-002 WAXS/SAXS system operated at 45 kV and 0.66 mA equipped with a Rigaku R-axis IV++ 2-D detection system. The optical microscopy and SEM images were obtained on Polarized light LEICA Microscope and LEO SEM 1530, respectively.

B3. Results and Discussion

PAN and PAN/$ZnCl_2$ electrospun fibers produced using the process conditions outlined in the experimental did not show a significant change in diameter after activation. Analysis from SEM images of the fiber samples showed a diameter distribution of 0.5 – 1.0 µm. Diameter distributions and SEM images for PAN and PAN/ZnCl2 samples are given in Figure B2 (a – c). The stabilization studies of sample fibers were analyzed by WAXD. Stabilization by heat treatment causes the PAN based fibers to partially cyclize and form a more stable ladder structure. Unstabilized and partially stabilized fiber samples show a WAXD peak at a $2\theta \sim 17^{o}$, while the peak disappears when the sample is fully stabilized.

(a) PAN average - 1.0 μm standard deviation - 0.3

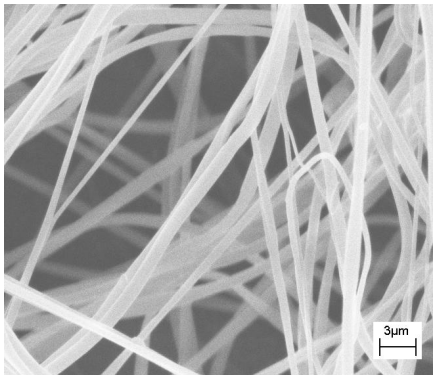

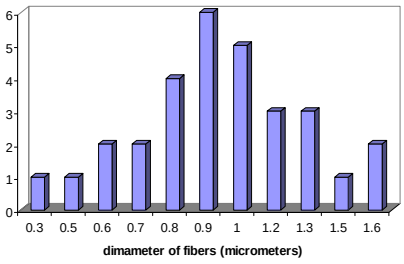

(b) PAN/$ZnCl_2$ 5 wt. % average - 0.5 μm standard deviation - 0.1

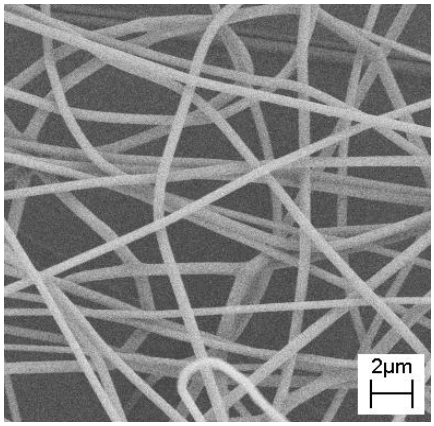

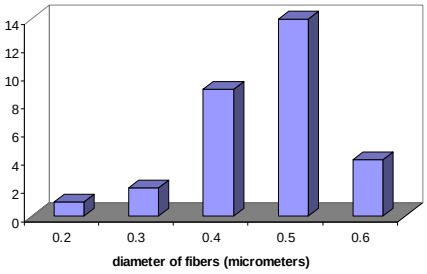

(c)Activated PAN/$ZnCl_2$ 20 wt. % average – 0.8 μm standard deviation – 0.2

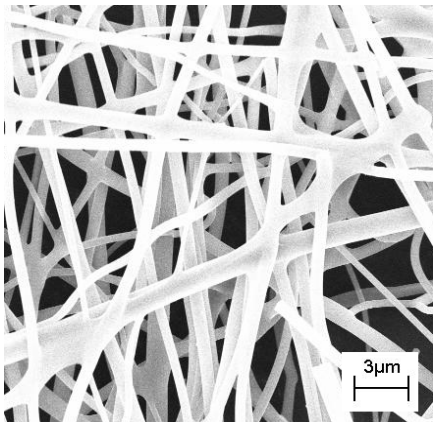

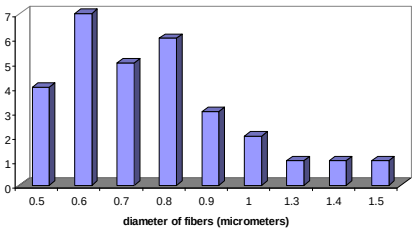

Figure B2. SEM images and diameter distributions of PAN (a) and PAN/$ZnCl_2$ ((b) 5 wt % $ZnCl_2$ and (c) 20 wt % ZnCl) electrospun fibers

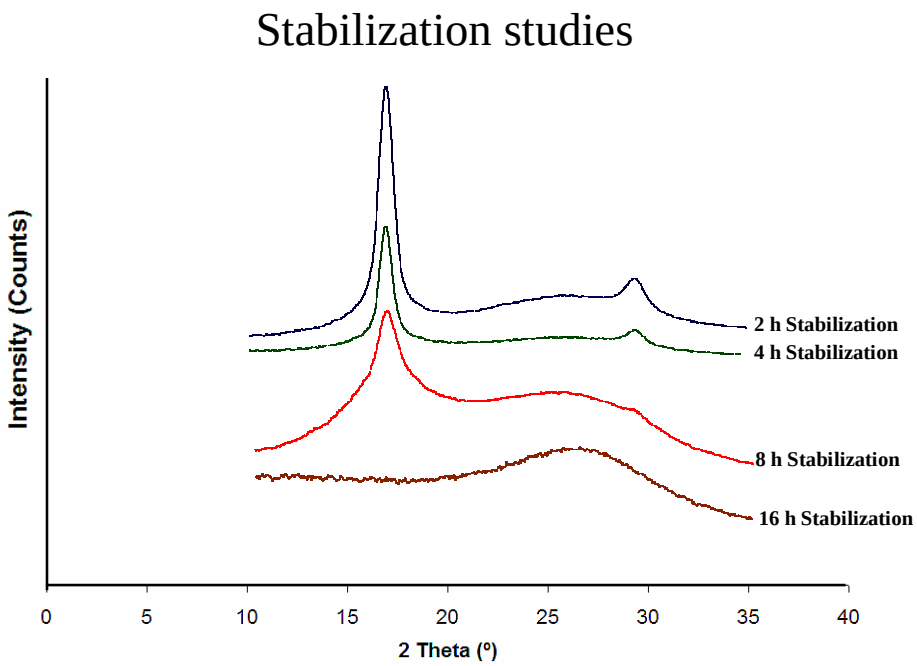

Figure B3. Stabilization progression using WAXD for PAN electrospun fibers

Possible reasons for longer stabilization time observed for 1 µm fibers could be either greater thickness (~ 100 µm) of the non-woven PAN fiber mat restricting the diffusion of air during stabilization stage or limited quantity of beads that were formed at the electrospun process conditions. The progression of the stabilization studies is shown in Figure B3. Based on these studies, all samples were stabilized for 16 hours to ensure complete stabilization. The chemical activating agents – KOH and $ZnCl_2$ were used to activate PAN fibers. KOH, being a strong base, degrades the PAN when added in solution stage. KOH impregation of stabilized electrospun PAN fibers resulted in destruction of fiber structure leading to a chunk of activated porous carbon due to severity of activation conditions. Both the samples impregnated in 6M KOH for 5 minutes as well as 16 h resulted in similar morphology as given in Figure B4. This KOH activated electrospun PAN fibers when tested for electrochemical properties, showed negligible specific capacitance values.

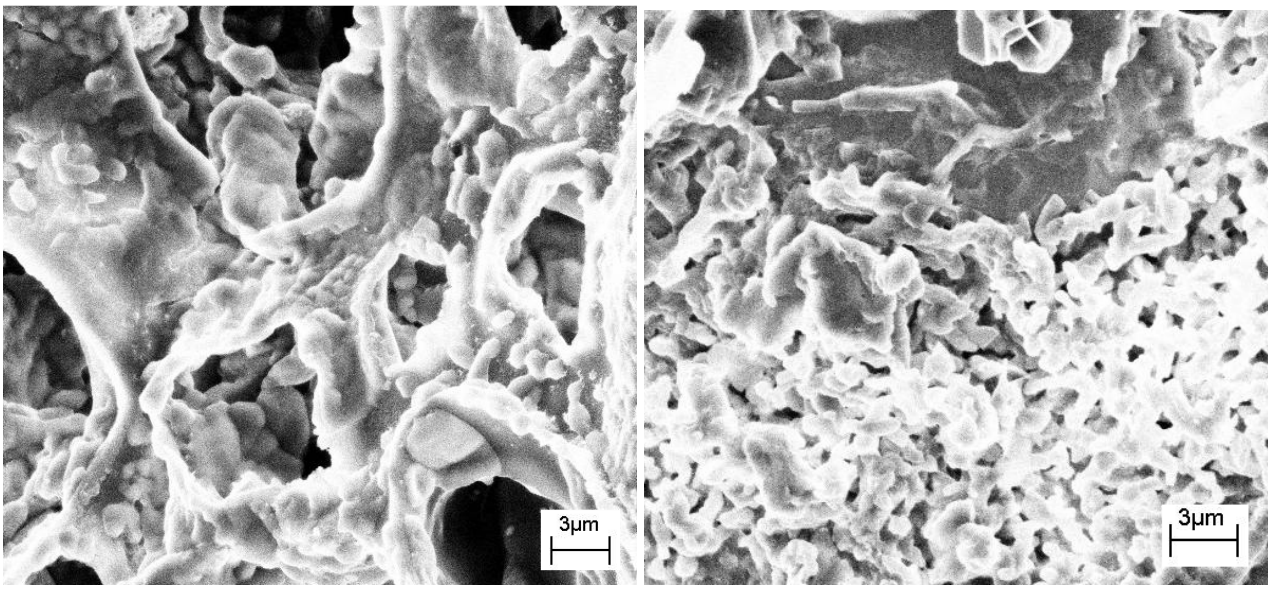

Figure B4. Scanning Electron Micrographs of electrospun PAN fibers impregnated in 6M KOH for (a) 5 minutes and (b) 12 hours and activated at 800 ºC for 1h.

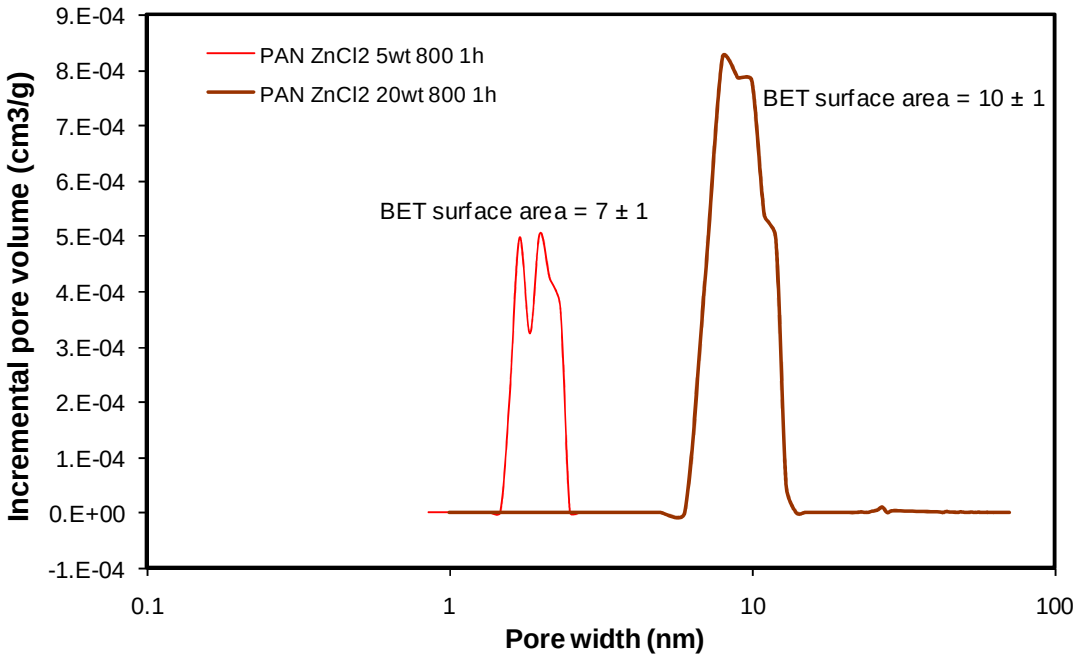

Figure B5. Pore Size Distribution Analysis of PAN/$ZnCl_2$ electrospun fibers.

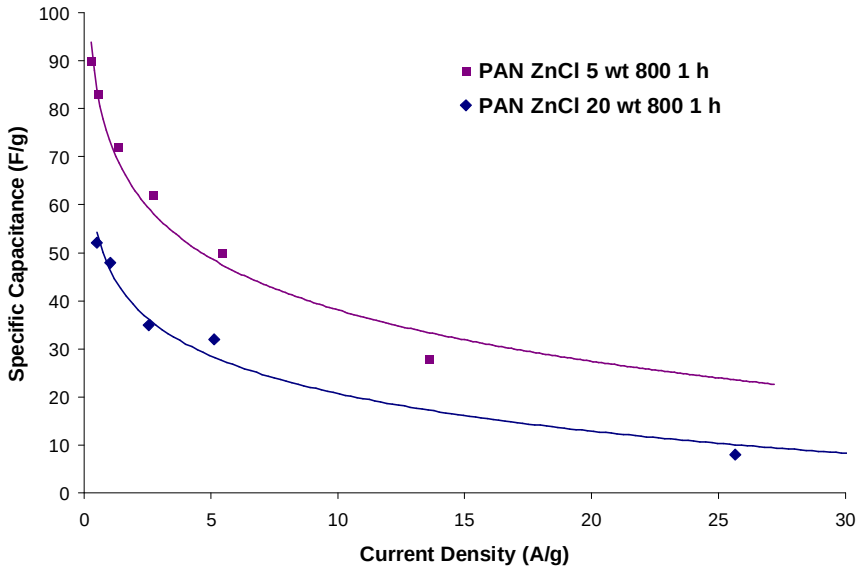

Figure B6. Specific capacitance as a function of current density measurements for PAN/$ZnCl_2$ activated fibers

Surface area and pore size distribution of activated fibers showed a relatively narrow distribution of pore size. Also as demonstrated in Figure B5, with an increase in the concentration of the activating agent, $ZnCl_2$, there was an increase in pore width and volume. 5 wt.% PAN/$ZnCl_2$ had a BET surface area measurement of 7 ± 1 m^2/g with a pore width distribution of 1.5 – 2.5 nm, while the 20 wt.% PAN/$ZnCl_2$ sample had a BET surface area measurement of 10 ± 1 m^2/g with a pore width that varied from 6.0 – 15.0 nm. As shown in Figure B6 specific capacity measurements of the activated fibers showed a drop in the capacitance from 90 F/g for the 5 wt. % PAN/$ZnCl_2$ to 52 F/g for the higher concentration 20 wt. %. A comparison of our results with Kim[5] as discussed in the preceding sections and as found in Table B1 show a substantially lower BET surface area as well as lower specific capacitance measurements for the chemically activated PAN fibers samples.

B4 Conclusions

Using the electrospinning process conditions, PAN based fibers with and without activating agent were electrospun to the desired diameter of approximately 1μm. Activation of the PAN fibers using direct addition of $ZnCl_2$ to PAN/DMF solution produced fibers of the desired integrity and diameter, however the method for immersion of the PAN electrospun fibers in KOH failed to produce satisfactory results. Trials using different concentrations of KOH and varying times periods of immersion showed similar results. Specific capacity measurements of the activated fibers showed a drop in the capacitance from 90 F/g for the 5 wt% PAN/$ZnCl_2$ to 52 F/g for the higher concentration of 20 wt%. Surface area measurements of the fiber samples revealed that for 5 wt% PAN/$ZnCl_2$ a BET surface area measurement of 7 ± 1 m^2/g with a pore width distribution of 1.5 – 2.5 nm, while the 20 wt% PAN/$ZnCl_2$ sample had a BET surface area measurement of 10 ± 1 m^2/g with a pore width that varied from 6.0 – 15.0 nm.

B5 References

[1] Wong T. PhD Thesis, Georgia Institute of Technology 2006.

[2] Gibson P, Schreuder-Gibson H, and Rivin D. Colloids and Surfaces A: Physicochemical and Engineering Aspects 2001;187-188:469-481.

[3] Jagannathan S. MS Thesis, University of Tennessee, Knoxville 2003.

[4] Frenot A and Chronakis IS. Current Opinion in Colloid & Interface Science 2003;8(1):64-75.

[5] Kim C, Yang K-S, Lee W-J. Electrochemical and Solid-State Letters 2004;7(A397).

[6] Im JS, Park S-J, Kim TJ, Kim YH, and Lee Y-S. Journal of Colloid and Interface Science 2008;318(1):42-49.

VITA

Sudhakar Jagannathan was born in Madras (now Chennai), India on 24th August 1978 to J. Kasthuri and J. Jagannathan. He received his Bachelor of Technology degree in Polymer Technology with overall rank II from University of Madras, India in the year 2000. He worked for one year (2000-01) in MK Electric (India) Ltd. as Plastics Engineer. He joined Polymer Engineering program in Department of Material Science and Engineering at University of Tennessee, Knoxville in August 2001 and received the degree of Masters of Science in 2003. He joined School of Polymer, Textile and Fiber Engineering at Georgia institute of Technology in August 2004 and completed his PhD degree in May 2009. During his study at Georgia Tech, he worked as graduate engineering Co-op with Invista SARL at Dalton, GA during the semester Spring 2007. He will work for Exide Technologies in Alpharetta, GA as senior material scientist from May 2009.